uOttawa

L'Université canadienne
Canada's university

FACULTÉ DES ÉTUDES SUPÉRIEURES ET POSTOCTORALES

uOttawa

L'Université canadienne
Canada's university

FACULTY OF GRADUATE AND POSDOCTORAL STUDIES

Tahirou Assane Oumarou
AUTEUR DE LA THÈSE / AUTHOR OF THESIS

M.A.Sc. (Civil Engineering)
GRADE / DEGREE

Department of Civil Engineering
FACULTÉ, ÉCOLE, DÉPARTEMENT / FACULTY, SCHOOL, DEPARTMENT

Cyclic Behaviour of Sand-Steel Interfaces : Experimental Investigation and Numerical Simulation with a Bounding Surface Model

TITRE DE LA THÈSE / TITLE OF THESIS

E. Evgin
DIRECTEUR (DIRECTRICE) DE LA THÈSE / THESIS SUPERVISOR

CO-DIRECTEUR (CO-DIRECTRICE) DE LA THÈSE / THESIS CO-SUPERVISOR

EXAMINATEURS (EXAMINATRICES) DE LA THÈSE / THESIS EXAMINERS

M. Mohareb

S. Sivathayalan

S. Vanapalli

Gary W. Slater
LE DOYEN DE LA FACULTÉ DES ÉTUDES SUPÉRIEURES ET POSTDOCTORALES /
DEAN OF THE FACULTY OF GRADUATE AND POSTDOCORAL STUDIES

CYCLIC BEHAVIOUR OF SAND-STEEL INTERFACES: EXPERIMENTAL INVESTIGATION AND NUMERICAL SIMULATION WITH A BOUNDING SURFACE MODEL

Tahirou ASSANE OUMAROU, B.A.Sc., B.Sc.

A Thesis
Submitted to the School of Graduate Studies
under the supervision of

Dr. Erman Evgin

In partial fulfillment of the requirements for the degree of
Master in Applied Science in Civil Engineering

Department of Civil Engineering
University of Ottawa
Ottawa, Ontario
Canada K1N 6N5

October 2005

The Master in Applied Science in Civil Engineering is a joint program between Carleton University and the University of Ottawa, which is administered by the Ottawa-Carleton Institute for Civil Engineering

Your file Votre référence
ISBN: 0-494-11208-5
Our file Notre référence
ISBN: 0-494-11208-5

ACKNOWLEDGEMENTS

I would like to sincerely thank my supervisor Dr. Erman Evgin for his help, encouragement, academic and financial support, and advice during this research program. It has always been an honour and a pleasure to work with Dr. Evgin.

I want to thank Dr. Sivathayalan for allowing me to use his triaxial test equipment. I extend my thanks to Drs. Garga, Khoo, Mohareb, Redekop, Sivathayalan, and Vanapalli for sharing their expertise through graduate courses I attended. I would like to want also to credit and thank Mr. Moore for his technical assistance.

I wish to express my gratitude to my love Mariame for her love, support, motivation, and patience.

Finally, I am most grateful to my parents to whom I dedicate this thesis. They have always believed in me and taught me values which were behind the successful completion of this thesis. I could not end this section without thanking my brothers, my sisters, my extended family, and my friends. They have always been on my side.

ABSTRACT

The first objective of this research program was to investigate the cyclic behaviour of sand-structure interfaces. To achieve this objective a series of monotonic and cyclic tests were performed using a simple shear type interface apparatus. The influence of the initial sand density, the number of cycles, the initial normal stress, and the amplitude of displacement on the shear stress mobilized at the interface, the normal displacement, and the amount of slip taking place at the interface were determined.

The second objective of this research program was to model the behaviour of interfaces with a bounding surface plasticity model. The model formulated by Dafalias and Manzari (2004) for the behaviour of sand was used to simulate the behaviour of interfaces. A parametric study was conducted to analyze the sensitivity of the model simulations to changes in the model constants. In addition, the model predictions and the experimental results were compared.

TABLE OF CONTENTS

LIST OF TABLES

LIST OF FIGURES

CHAPTER 1

INTRODUCTION

1.1 Statement of problem

Many geotechnical problems involve the interaction of soil and structures. The design of foundations, retaining walls, and tunnels typically deal with soil-structure interaction problems. The solution of these problems requires the knowledge of the loads transferred between the soil medium and the structure. The load transfer takes place at the interface, which is a thin layer of soil in the contact area between soil and structures. The mechanical behaviour of interfaces, characterized by strong displacement gradient and significant amount of grain rotations (Kishida and Usuegi, 1987; Boulon, 1989), influences significantly the magnitude of the transferred loads.

Due to its importance, the behaviour of interfaces has been the subject of many experimental and numerical studies. The majority of earlier studies, pioneered by Potyondy (1961), dealt primarily with the behaviour of interfaces subjected to monotonic loading conditions. Uesugi and Kishida (1986a, 1986b) listed several factors that influence the monotonic behaviour of interfaces. However, in geotechnical engineering, monotonic loading is recognized as the simplest loading condition that a structure has to withstand. In reality, many geotechnical structures must also endure cyclic loading conditions where the magnitude and direction of loads change frequently. Cyclic loads on soil-structure interfaces may result from many sources including wave action, machinery operation, and earthquakes which are known for their destructive impact on geotechnical

structures. Therefore, it is necessary to develop a sound understanding of the cyclic behaviour of interfaces for the design of safe and economical structures.

Several investigations were conducted on the cyclic behaviour of interfaces (Desai et al. 1985, Uesugi et al. 1989, 1990; Al-Douri and Poulos 1992; Fakharian and Evgin 1996; Shahrour and Rezaie 1997; DeJong et al. 2003). The influence of several factors on the cyclic behaviour of interface was studied. However, a study which addressed all together the influence of the initial sand density, number of cycles, magnitude of normal stress, and amplitude of horizontal (tangential) displacement on the shear stress mobilized at the interface, vertical (normal) displacement and sliding displacement (slip) at the interface has yet to be undertaken.

Beside the experimental studies on interfaces, some models were developed to predict the behaviour of interfaces subjected to cyclic loading condition (Desai et al. 1985; Desai and Nagaraj 1988; Aubry et al. 1990; Navayogarajah et al. 1992; Shahrour and Rezaie 1997; Mortara et al. 2002; Tejchman and Bauer 2004). However, when compared with the development of a cyclic model for the behaviour of soils, the development of cyclic models for the behaviour of interfaces has evolved at a slower rate. In fact, during the last four decades, the development of cyclic models for soil behaviour has experienced a rapid growth and a significant progress has been made (i.e. multi-surface plasticity, bounding surface plasticity, and hypoplasticity models). Despite the successful use of the cyclic soil models to solve various geotechnical problems and the similarities reported by Boulon and Nova (1990) between the behaviour of interfaces and the behaviour of soils, the cyclic models developed for soils have barely been extended to model the cyclic response of interfaces. Therefore, it is of interest to investigate how a cyclic model primarily developed for sand mass simulates the behaviour of interfaces.

1.2 Objectives

The objectives of this thesis are:

1. To determine experimentally the influence of the initial sand density, number of cycles, magnitude of normal stress, and amplitude of tangential displacement on the cyclic response of soil-structure interfaces.
2. To determine the suitability of an existing bounding surface plasticity model for the prediction of the behaviour of sand-structure interfaces subjected to cyclic loading.

1.3 Scope of research

The objectives of the current research are achieved as summarized below:

1. An experimental study on sand-structure interfaces is conducted using a Cyclic 3 Dimensional Simple Shear testing apparatus for Interfaces (C3DSSI). The study includes: 12 monotonic tests, of which 6 were conducted under constant normal stress conditions and the other 6 were conducted under constant volume conditions, and 18 two-way cyclic tests performed under constant normal stress conditions.
2. The bounding surface plasticity model developed for sand by Dafalias and Manzari (2004) is used to predict the behaviour of sand-structure interfaces subjected to cyclic loading condition. The model parameters are derived from experimental results.

1.4 Outline of the thesis

Excluding Chapter 1, which is an introductory chapter, and Chapter 8, which summarizes the thesis, presents the conclusions of the thesis, and gives some recommendations for future work, the thesis is divided into two parts. The first part (Part 1) comprises the Chapters 2 to 4 and deals with the experimental investigation on interfaces.

Chapter 2 presents the experimental apparatus (C3DSSI), the interface material, the sample preparation, and the testing procedure.

The results of a series of 12 monotonic tests and 18 cyclic tests performed on sand-structure interfaces with the C3DSSI and the interpretation of the test results are presented in Chapter 3. The results are interpreted by taking into consideration the influence of initial density of sand, number of cycles, amplitude of displacement, and magnitude of normal stress.

Chapter 4 provides first a review of techniques used for the determination of the thickness of the interface layer. Then the visualization technique presented by Li (2001) was used to observe the movement of the stack of plates during cyclic tests.

The second part (Part 2) comprises Chapter 5 to 7 and deals with the numerical simulation of the behaviour of soils and soil-structure interfaces.

Chapter 5 presents the main constituents (i.e. yield surface, flow and hardening rules) of the plasticity theory. Afterward, some cyclic models developed for soils were reviewed. The review includes the multi-surface model, the bounding surface model, and some other cyclic models reported in the literature. The chapter ends with a review of cyclic models developed for interfaces.

In Chapter 6, the model developed for sand by Dafalias and Manzari (2004) is described in detail. The model is integrated using a forward Euler algorithm with a return to the yield surface and validated by comparing its predictions with those made by Dafalias and Manzari (2004). A parametric study is done to analyze the sensitivity of the model to changes in the model constants. The chapter ends with the predictions of six conventional triaxial tests. The predictions are compared with the experimental results.

In Chapter 7, the model presented in Chapter 5 is used to predict the behaviour of interfaces subjected to cyclic loading conditions. The predictions of the model and the experimental results are compared.

In Appendix A, the procedures used to determine the model constants from triaxial test data are explained.

PART 1

EXPERIMENTAL INVESTIGATION

CHAPTERS 2-4

CHAPTER 2

TEST APPARATUS AND PROCEDURES

2.1 Introduction

Different types of apparatus were used by various investigators to study the behaviour of interfaces. Potyondy (1961), Yoshimi and Kishida (1981), Uesugi and Kishida (1986a, 1986b), Paikowsky et al. (1995) used a direct shear type, a ring torsion, a simple shear type, and a dual interface apparatus, respectively. The advantages and disadvantages of different types of apparatus were summarized by Kishida and Uesugi (1987), Paikowsky et al. (1995), and Fakharian (1996). In this study, the investigation was conducted with a simple shear type interface apparatus which is referred to as **C**yclic **3** **D**imensional **S**imple **S**hear testing of **I**nterface (C3DSSI). The experimental apparatus, the interface materials, the soil container, and the testing procedures are described in the following sections of this chapter.

2.2 Description of the testing apparatus

The C3DSSI, shown in Figure 2.1, was built by Fakharian and Evgin (1993). A detailed description of the C3DSSI was provided by Fakharian (1996). Therefore, only a brief description of the apparatus is provided here.

The apparatus may be used to conduct 2-D and 3-D tests, monotonic tests at various loading rates, displacement or load controlled cyclic tests, and circular or elliptical

shearing tests on interfaces. The tests may be conducted under constant normal stress, constant volume, and constant normal stiffness conditions.

The C3DSSI has three major parts: a reaction frame, a loading system, and a data acquisition and computer control system. The reaction frame, shown in Figure 2.2, is formed by three horizontal 600 x 600 mm aluminum plates supported by four vertical steel bars. Each aluminum plate can support a vertical load of 25 kN.

The loading system consists of a pneumatic actuator used to apply vertical load and two stepper motors used to apply tangential displacement in the horizontal X-Y plane. The pneumatic actuator can transfer a maximum load of 6.6 kN to the soil sample through a square loading platen (Figure 2.1). The loading platen is restrained from moving in the horizontal direction. However, it can move in the vertical direction for tests conducted under constant normal stress and constant normal stiffness conditions, but, it is restrained from moving in the vertical direction for tests conducted under constant volume conditions. The amount of normal displacement (change in sample height), positive for dilation and negative for contraction, is measured with an LVDT mounted beside the pneumatic actuator.

Each stepper motor can apply a maximum load of 9 kN in the horizontal plane. For 2-D tests only one stepper motor is used either in the X or Y horizontal direction. For 3-D tests, two stepper motors are used in concert to apply tangential displacement simultaneously in the X and Y directions. Owing to the three dimensional testing capabilities of the apparatus, it is possible to follow several stress paths in a test. The rate of displacement in the horizontal plane is selected in the range between 0.01 and 20 mm/min. The horizontal displacements are measured with two LVDTs for 2-D tests, but, with four LVDTs (i.e. two in each horizontal direction) for 3-D tests.

The data acquisition and computer control system allows the operation of the apparatus. The data acquisition system collects and records information related to horizontal and vertical displacements, normal stress applied on top of the loading platen, and shear stresses mobilized at the interface. The computer control system is used to specify the type of test, the rate of loading, the maximum horizontal displacement, the initial normal stress, and the initial values of the LVDTs.

2.3 Interface materials

The interface materials consist of dry quartz sand placed in a container and a steel plate. The sand grains have a sub-angular shape, an effective size (D_{10}) of 0.86 mm, and a mean diameter (D_{50}) of 1.36 mm. The grain size distribution is shown in Figure 2.3. The minimum and maximum void ratios of this sand are e_{min}=0.673 and e_{max}=1.014 as determined according to the ASTM Standards D 4253-93 and D 4254-93.

The steel plate, which has an area of 300x300 mm, plays the role of the structural member; it is characterized by its roughness. The behaviour of different types of soil-structure interfaces can be studied by simply varying the roughness of the steel plate or by replacing the steel plate with a concrete or a wooden plate. Uesugi and Kishida (1986a, 1986b) listed the roughness of the structural member as an influential factor of the behaviour of interfaces. However, in this study, the roughness of the steel plate is maintained constant by sand blasting the surface of the steel plate. The normalized roughness (Kishida and Uesugi 1987) of the steel plate is 0.018. During a test the steel plate is displaced in the horizontal directions using the stepper motors.

2.4 Soil container

The soil container (Figure 2.4) is formed from a stack of anodized, Teflon coated, aluminum plates (Figure 2.5). The aluminum plates have the overall dimensions of

150x150x1.0 (or 2.0) mm. A total of fifteen aluminum plates are used. Of the fifteen plates eleven are 1 mm thick, and four are 2 mm thick. The 1 mm thick plates are placed near the contact surface. A square section of 100x100 mm is removed from the middle of each plate to create room for the placement of soil. The area of the steel plate (300x300 mm) is much larger than the inside surface of the aluminum plates; therefore, the area of contact (100x100 mm) between soil and steel plate remains constant.

The aluminum plates are free to move in the horizontal plane because they are not fixed to each other. This freedom of movement makes the use of the stack of plates very advantageous because it is possible to make a distinction between the sliding displacement and the displacement due to the deformation of soil at the interface. This distinction could not be made in a direct shear type container.

In each horizontal direction, the first LVDT measures the total displacement due to the movement of the steel plate (δ_{steel}), while the second LVDT measures the displacement due to the deformation of soil (δ_{soil}) at the interface (Figure 2.4). The slip displacement (δ_{slip}) is calculated by subtracting δ_{soil} from δ_{steel} (Equation 2.1).

$$\delta_{slip} = \delta_{steel} - \delta_{soil} \qquad 2.1$$

In simple shear type interface tests, it is also possible to determine the movement of the individual aluminum plates. This information may be used to determine the thickness of the interface layer (Li 2001).

2.5 Test procedures

The test procedures consist in three main steps: 1) Positioning of the soil container in the loading units, 2) Sample preparation, 3) Configuration of test conditions.

Positioning of the soil container in the loading units

The objective of the first step is to position the soil container in the loading unit so that it fits the loading platen. The achievement of this objective requires the use of a dummy sample. The dummy sample acts just like the real sample with the difference that its role ends after the proper positioning of the soil container. For the positioning of the soil container in the loading unit, first, the aluminum plates are stacked on the dummy sample. Then, the stack of plates and the dummy sample are placed on top of the structural member (steel plate) and brought in the loading unit. The loading platen is slowly lowered; at the same time the position of the dummy sample is adjusted continuously until it fits the loading platen. Subsequently, the loading platen is lowered until it touches the upper surface of the dummy sample. Afterward, four clamps are used to fix the stack of aluminum plates to the steel plate. At this stage, the dummy sample, the steel plate, and the stack of plates form altogether a single component. This component is removed from the loading unit after moving up the loading platen. The dummy sample is withdrawn to create room for the placement of sand. At this stage, one may proceed with the sample preparation.

Sample preparation

The sample preparation depends on density. For loose samples, sand particles are gently spooned in the soil container. For dense samples, the sand particles are air-pluviated in the soil container from a rainer. When the container is full of sand, a suction device is used to level the top of the sample.

Configuration of testing conditions

After the sample preparation, the steel plate and the soil container filled with sand are returned to the loading unit. Then, the loading platen is lowered. The type of interface test

is selected from the computer control system. The LVDTs for measuring the horizontal and vertical displacements are mounted. The desired normal load is applied and the measurements of the LVDTs are initialized to zero. The four clamps used to fix the soil container to the steel plate are released to allow the free movement of the aluminum plates. At this point the sand sample is ready for testing.

In this study, only the stepper motor which applies displacement in the horizontal X direction is used. Therefore, only the measurements of three LVDTs are recorded. The first two LVDTs measure the displacement of the steel plate and the displacement of soil at the interface, respectively. The third LVDT measures the normal displacement of the sand samples. In addition to the measurements of the three LVDTs, the shear stress mobilized at the interface and the normal stress acting on top of the sand samples are recorded.

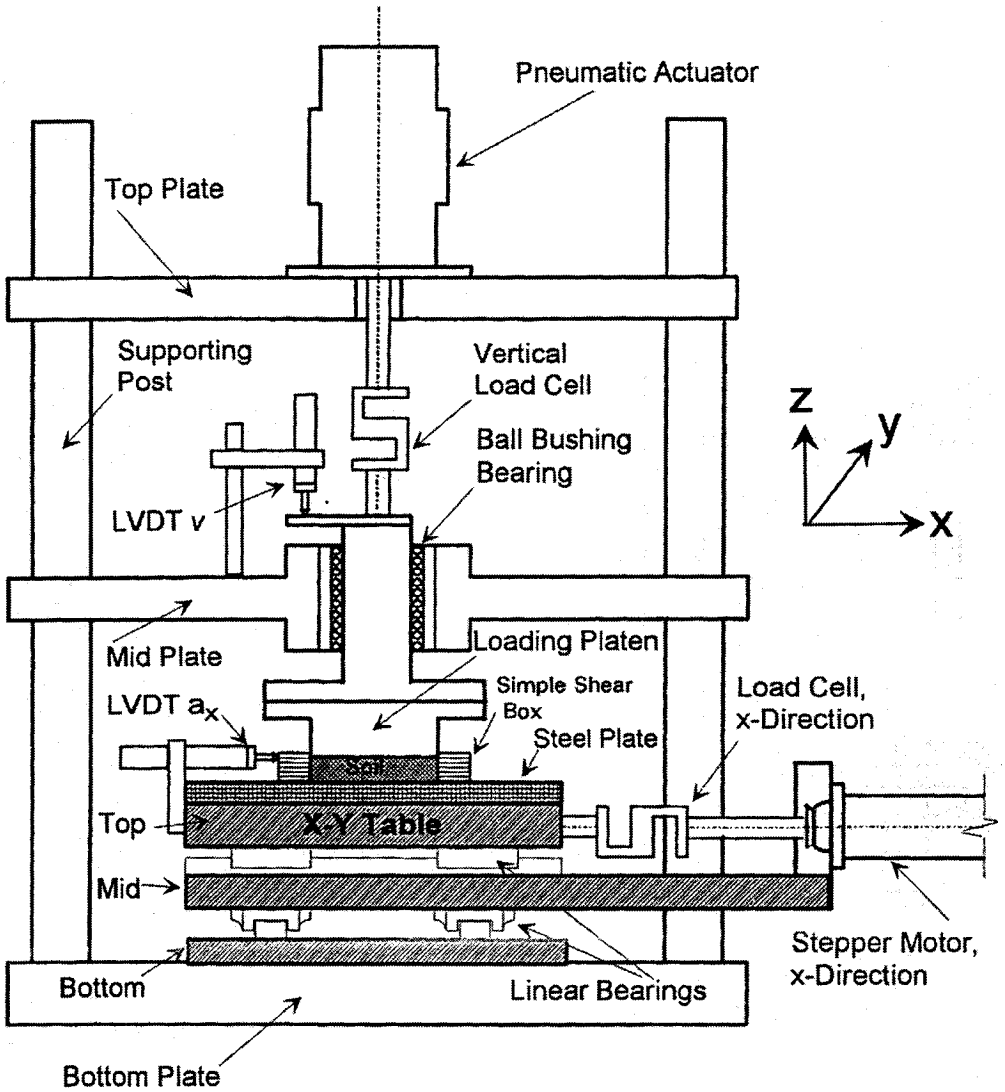

Figure 2.1 Schematic view of C3DSSI (after Fakharian 1996)

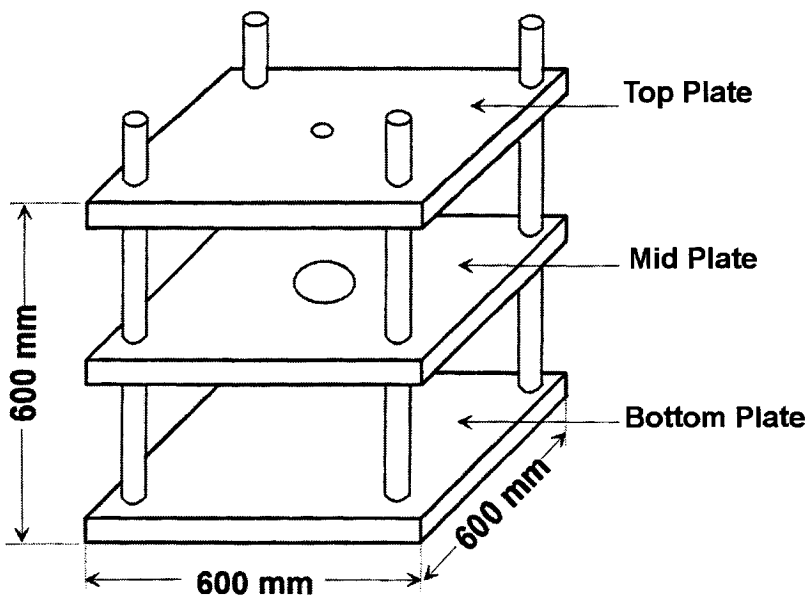

Figure 2.2 Reaction frame (after Fakharian 1996)

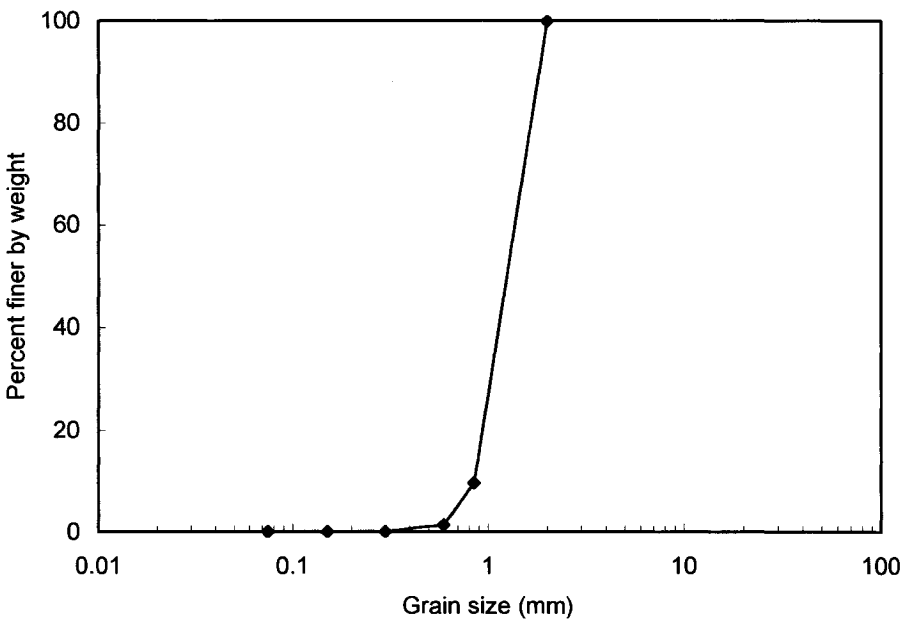

Figure 2.3 Grain size distribution

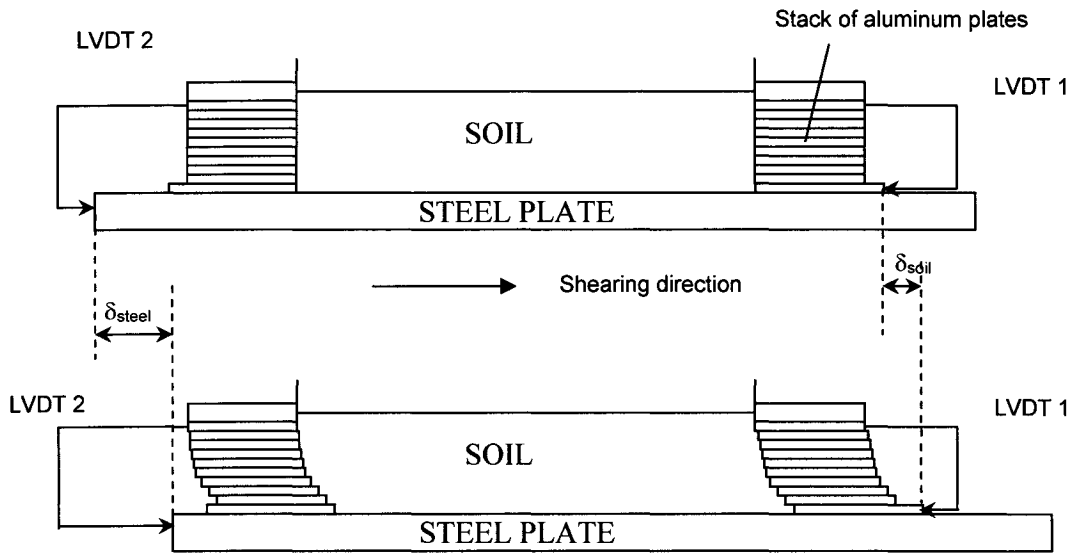

Figure 2.4 Simple shear container

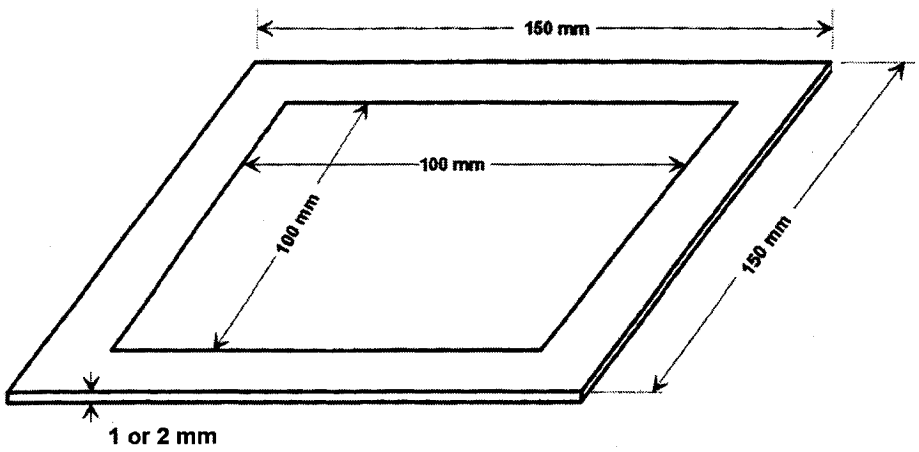

Figure 2.5 Teflon coated aluminum plate used to form the simple shear container

CHAPTER 3

EXPERIMENTAL PROGRAM, TEST RESULTS AND INTERPRETATION

3.1 Literature review

Experimental studies on the cyclic behaviour of interfaces were conducted by various investigators such as Desai et al. (1985), Uesugi et al. (1989, 1990), Al-Douri and Poulos (1992), Airey et al. (1992), Tabucanon et al. (1995), Fakharian and Evgin (1996, 1997), Shahrour and Rezaie (1997), Mortara et al. (2002), Porcino et al. (2003), and DeJong et al. (2003). These investigations were carried out with several types of apparatus (i.e. direct shear, simple shear, and ring torsion).

Desai et al. (1985) observed that the cyclic behaviour of interfaces is influenced by the amplitude of tangential displacement, normal stress, density of sand and the number of loading cycles. The study dealt mainly with the evolution of the mobilized shear stress. No information was provided about the volume change (i.e. normal displacement) in the samples. In addition, given the use of a direct shear type container, it was not possible to distinguish slip from the displacement at the interface resulting from soil deformation.

Uesugi et al. (1989, 1990) used a simple shear type soil container to investigate the cyclic behaviour of sand-steel and sand-concrete interfaces. The components of tangential displacement: slip (sliding displacement) and the displacement at the interface resulting from soil deformation were measured separately. The cyclic tests were conducted on dense sand samples (i.e. D_r=87-108%). These authors concluded that soil deformation was the major contributor to tangential displacement before the maximum stress ratio was

reached at the interface. Slip, however, became the main component of tangential displacement after the maximum stress ratio was experienced. They also reported that the residual coefficient of friction under a two-way cyclic test was close to that of the sand mass.

Al-Douri and Poulos (1992) studied the influence of density, normal stress and amplitude of tangential displacement on the shear stress mobilized at the interface and the change in sample height. However, the influence of these factors on slip taking place at the interface was not investigated. Shahrour and Rezaie (1997) conducted similar studies.

DeJong et al. (2003) conducted cyclic CNS tests with a direct shear type apparatus. Measurements obtained from Particle Image Velocimetry (PIV) were used to determine the percentage of slip occurring at the interface. They reported an increase in the percentage of slip with the number of cycles. A similar observation could be inferred from the results presented by Uesugi et al. (1989, 1990) and Fakharian (1996). These studies reporting the evolution of slip in cyclic tests did not fully address the influence of normal stress and density on the amount of slip. The specimens used by DeJong et al. (2003) were all in a relative density range of 60~65% and were tested with an initial normal stress of 100 kPa.

Porcino et al. (2003), who studied the influence of density on the response of interfaces, concluded that density was relatively uninfluential. This conclusion was reached perhaps because the authors looked principally into the influence of density on the mobilized shear stress. The influence of density on the change in sample height and the sliding displacement at the interface was not analyzed. Thus, as mentioned by these investigators, additional studies were necessary to confirm their conclusion.

In summary, the literature review shows that an investigation which addresses altogether the influence of sand density, number of cycles, magnitude of normal stress and

amplitude of displacement on the shear stress mobilized at the interface, sliding displacement and change in sample height has yet to be undertaken. Such an investigation is conducted in the present study.

3.2 Experimental program

The experimental program includes a series of 12 monotonic tests and 18 two-way cyclic tests performed on sand-structure interfaces with the C3DSSI. Of the 12 monotonic tests, 6 were conducted under constant normal stress conditions the other 6 were conducted under constant volume conditions. All cyclic tests were conducted under constant normal stress conditions. Although the focus of the research was on the cyclic behaviour of interfaces, the monotonic tests were also conducted because an understanding of the cyclic behaviour of interfaces requires a prior understanding of the monotonic behaviour. In addition, the results of the monotonic tests may be compared with those of the cyclic tests in order to highlight the similarities and differences.

The effects of selected factors (density, normal stress, amplitude of displacement, number of cycles) on the behaviour of interfaces were investigated. The effect of initial density of sand was analyzed by testing loose and dense sand samples. The samples were prepared according to the procedure described in Chapter 2. The loose samples used in the tests had a relative density of 22 % and a void ratio of 0.94. For the dense samples, the relative density was 92% and the void ratio was 0.70. The effect of the initial state of stress on the behaviour of interfaces was investigated by performing tests with different normal stress values (i.e. 100 kPa, 200 kPa, and 300 kPa).

For the cyclic tests, the effect of the amplitude of tangential displacement was investigated by conducting tests with three different amplitudes of tangential displacement (i.e. 1.0 mm, 2.0 mm, and 3.0 mm). In addition, the effect of the number of cycles was studied by subjecting the samples to ten displacement cycles. After the tenth

displacement cycle, the samples were subjected to an additional displacement cycle where they were sheared to failure.

3.3 Monotonic test results

This section reports the results of monotonic tests conducted under either constant normal stress condition or constant volume condition.

3.3.1 Constant normal stress tests on loose sand interfaces

The results of three monotonic tests conducted on loose sand interfaces under constant normal stress values of 100 kPa, 200 kPa, and 300 kPa, are shown in Figure 3.1. The results show the relationship between the shear stress and the tangential displacement of the steel plate (Figure 3.1a), the relationship between the change in sample height and the tangential displacement of the steel plate (Figure 3.1b), the relationship between the shear stress and the soil displacement at the interface (Figure 3.1c), the relationship between the shear stress and slip at the interface (Figure 3.1d), and the relationship between slip at the interface and soil displacement at the interface (Figure 3.1e).

Figure 3.1a shows that the shear stress mobilized at the interfaces increases with the tangential displacement of the steel plate before reaching a maximum value where it stabilizes. The amount of horizontal displacement required for the mobilization of the maximum shear stress increases with the magnitude of normal stress. In addition, the maximum shear stress mobilized at the interface increases as expected with the magnitude of normal stress. For example, it reaches the values 44.7 kPa, 96.9 kPa, and 147.8 kPa in the tests conducted with a normal stress of 100 kPa, 200 kPa, and 300 kPa, respectively. The stress ratios (shear stress divided by normal stress) computed based on the maximum shear stresses mobilized in the three tests are 0.45, 0.48, and 0.49,

respectively. These values indicate that the stress ratio increases with the magnitude of normal stress.

The magnitude of normal stress influences also the normal displacement (change in sample height) of the samples as shown in Figure 3.1b. In the tests conducted with normal stress values of 200 kPa and 300 kPa, the sand samples contract first and reach a state where they deformed without significant volume change. However, in the test conducted with a normal stress of 100 kPa, the contraction of the sample was followed by significant dilation. These observations imply that the magnitude of normal stress is an indicator of the dilative and contractive behaviour of interfaces.

Figures 3.1d shows that the amount of slip before the mobilization of the maximum shear stress is small, but, it becomes large afterward. Although, the amount of slip at the end of the test is less than the soil displacement (Figures 3.1c and 3.1d), Figure 3.1e shows that for any additional soil displacement the corresponding amount of slip is much larger. The logical implication of this observation is the reduction of the portion of soil displacement in the total displacement of the steel plate. In other words, the portion of slip that takes place at the interface increases with the tangential displacement of the steel plate.

At the end of the three tests, the portion of slip at the interface represents 27%, 30%, and 32% of the tangential displacement of the steel plate. These values show that the percentage of slip increases slightly with the magnitude of normal stress.

3.3.2 Constant normal stress tests on dense sand interfaces

The results of three monotonic tests conducted on dense sand interfaces under normal stress values of 100 kPa, 200 kPa, and 300 kPa are shown in Figure 3.2. In contrast to the loose sand interface, the shear stress mobilized in the dense sand interfaces increases to a peak value after which it decreases and eventually reaches nearly a constant value (Figure

3.2a). The peak shear stresses mobilized in the three tests are 56.3 kPa, 121.4 kPa and 185.1 kPa, respectively. The stress ratio corresponding to these shear stresses are 0.56, 0.61, and 0.62, respectively. Hence, similarly to the loose sand interfaces, the stress ratio recorded in dense sand interfaces increases with the magnitude of normal stress.

Figure 3.2b shows contraction of the samples followed by dilation. The amount of dilation decreases with increasing normal stress. For example, the amount of dilation is 0.419 mm, 0.292, and 0.159 mm at the end of the tests with a normal stress of 100 kPa, 200 kPa, and 300 kPa, respectively.

Figure 3.2d shows that slip is negligible before the peak stress is reached. However, after the peak stress the amount of slip increases substantially and becomes larger than the amount of soil displacement (Figure 3.2e). For example, the portion of slip represents 73%, 79%, and 77% of the tangential displacement of the steel plate for the tests conducted with a normal stress of 100 kPa, 200 kPa, and 300 kPa, respectively.

3.3.3 Constant volume tests on loose sand interfaces

Three monotonic tests were performed on loose sand under constant volume condition. The results in Figure 3.3 show the relation of normal stress versus the tangential displacement of the steel plate (Figure 3.3a), the relation of shear stress versus the tangential displacement of the steel plate (Figure 3.3b), the relation of shear stress versus normal stress (Figure 3.3c), and the relation of soil displacement at the interface versus slip at the interface (Figure 3.3d).

Figure 3.3a shows that the normal stress decreases until it reaches a minimum value then it starts increasing. Figure 3.3b shows the shear stress mobilized at the interface increases to a peak values, then it decreases, and finally increases. This behaviour resembles that of loose sand in undrained triaxial tests.

Figure 3.3c indicates that the relation of shear stress versus normal stress can be divided in three distinct parts. The first part of the relation has an elliptic shape for all tests. In this first part, the shear stress increases while the normal stress decreases. In the second part of the relation, both the normal stress and the shear stress decrease. Finally, in the third part of the relation, the shear stress increases linearly with the normal stress. The lines resulting from the relation in this third part were identical for all tests.

It is important to mention that the three parts observed in the relation of shear stress versus normal stress are also reported in undrained triaxial tests (Ishihara et al. 1975). The transition point between the second part of the relation and the third part of the relation is often referred to as the phase transformation point. It represents the transition from tendencies of contractive behaviour to dilative behaviour. A straight line linking the phase transformation points of tests conducted with different initial normal stress is called phase transformation line or dilatancy line.

Similar to the tests conducted under constant normal stress conditions, the amount of slip represents a small portion of the tangential displacement of the steel plate in the earlier stages of the tests, but, it increases with the tangential displacement of the steel plate. The percentage of slip is 32%, 30%, and 32% for the tests conducted with an initial normal stress of 100 kPa, 200 kPa, and 300 kPa. These percentages suggest that the initial normal stress has almost no influence on the percentage of slip.

3.3.4 Constant volume tests on dense sand interfaces

The results of three tests conducted on dense sand under constant volume condition with initial normal stress of 100 kPa, 200 kPa, and 300 kPa are shown in Figure 3.4. As shown in Figure 3.4a, the normal stress decreases until it reaches a minimum value then it increases. Figure 3.4b shows that the shear stress mobilized at the interface increases continuously. The relation of shear stress versus normal stress can be split in two distinct

parts (Figure 3.4c). The first part is characterized by an increase in shear stress and a decrease in normal stress. The shape of the relation is not elliptic as it was the case with the loose sand interface. In the second part the shear stress increases linearly with the normal stress.

Figure 3.4d shows the evolution of slip and soil displacement at the interface. As it was the case in the tests conducted on dense sand interfaces under constant normal stress (Figure 3.2e), the amount of slip in the tests conducted on dense sand interfaces under constant volume condition is larger than the amount of soil displacement at the interface (Figure 3.4d).

The test results presented in Figures 3.3c and 3.4c are re-plotted in Figure 3.5 for comparison. This figure shows a nearly overlapping of the regions where the shear stress increases with the normal stress. This overlapping occurs independently from the initial normal stress and the density of sand samples.

3.4 Cyclic test results

A total of eighteen two-way cyclic tests were performed under constant normal stress conditions. Nine tests were conducted on loose sand interfaces and the other nine tests were performed on dense sand interfaces. In addition to the density of soil, the magnitude of normal stress and the amplitude of tangential displacement are used to identify each test. The influence of normal stress is studied by subjecting the samples to a normal stress with three different magnitudes (i.e. 100 kPa, 200 kPa and 300 kPa). In the same manner, the effect of the amplitude of tangential displacement is investigated by using three different displacement amplitudes (i.e. 1 mm, 2 mm, and 3 mm). Each sample was subjected to 10 two-way displacement cycles followed by an additional displacement cycle where the soil was sheared to failure. The term initial loading or cycle "IL" is used to refer to the initial part of the shear stress versus tangential displacement curves starting

from the rest position (zero displacement) to a displacement of 1, 2 or 3 mm depending on the tangential displacement amplitude of a particular test.

3.4.1 Cyclic tests on loose sand interfaces

The results of the nine tests conducted on loose sand interfaces are shown in Figures 3.6 to 3.14. Figures 3.6, 3.7, and 3.8 show the results of tests conducted with a normal stress (σ_n) of 100 kPa. The tangential displacement amplitude in these tests was 1, 2, and 3 mm, respectively. Similarly, Figures 3.9 to 3.11 and Figures 3.12 to 3.14 show the results of the tests conducted with a normal stress of 200 kPa and 300 kPa, respectively. The measurements related to the displacement cycles in all experiments on loose sand samples are summarized in Table 3.1. The measurements in this table are also presented in graphical form in order to highlight the influences of the number of cycles, magnitude of normal stress, and amplitude of displacement (Figures 3.15 to 3.20).

3.4.1.1 Influence of number of cycles

In general, the shear stress mobilized at the end of each displacement cycle increases with an increase in the number of cycles (Figure 3.6a – 3.14a). The sand sample becomes stiffer as the cyclic displacement continues. The rate of increase in mobilized shear stress diminishes with increasing number of cycles (Figure 3.15). For illustration purposes, the measurements taken in three tests conducted with a constant normal stress of σ_n=200 kPa and the amplitudes of tangential displacement A=1 mm, 2 mm, and 3 mm are considered (Figure 3.15b). The curve corresponding to A=1 mm shows that the shear stress increases from 75.3 kPa at the end of the initial loading (i.e. cycle number = IL) to 91.6 kPa at the end of the first cycle. The shear stress is 100.7 kPa at the end of second cycle. Hence, the rate of increase in shear stress in these two displacement cycles has changed from 21.6% to 9.9%. The other two curves labeled as A=2 mm and A=3 mm indicate that the mobilized shear stress increases to a maximum value at the end of 2~3 cycles.

Subsequently, the mobilized shear stress decreases slightly with increasing number of cycles. The rate of change in the mobilized shear stress eventually becomes small in the experiments with loose sand. The number of cycles has, as illustrated in Figures 3.15a and 3.15c, a similar effect on the mobilized shear stress in the tests conducted with normal stress of 100 kPa and 300 kPa.

With respect to the influence of number of cycles on the shear stress mobilized in loose-sand interface tests, comparable results have been reported in the literature. For instance, laboratory tests performed on sand-concrete interfaces by Desai et al. (1985) showed an increase in the mobilized shear stress with an increase in the number of cycles. Shahrour and Rezaie (1997) also reported similar observations while performing cyclic direct shear type interface tests on loose sand.

In the present study, the changes that occur in sample height during cyclic tangential displacement of the steel plate are determined from LVDT readings taken at the top of the loading platen. Sample compression, which is indicated as negative normal displacement in the figures representing experimental data, increases with the number of cycles. The increase in sample compression occurs at a diminishing rate and indicates that the sand sample, which was initially loose, becomes denser (Figures 3.6b – 3.14b). Figure 3.16 shows that the same trend is observed in all tests conducted with loose sand. Several investigators (Al-Douri and Poulos (1992), Shahrour and Rezaie (1997, 1999)) have also reported an increase in compression with number of cycles.

The experimental results given in Figures 3.6d to 3.14d suggest that during the initial loading only a small amount of slip is experienced before the peak stress is reached. However, after the peak shear stress is mobilized, the amount of slip increases substantially. These observations are similar to those made by Uesugi et al. (1986a, 1989) but differ from those made by DeJong et al. (2003) who reported a relatively constant percentage of slip during monotonic loading.

The slip measured at the interface increases with the number of cycles. This trend is illustrated in Figure 3.17 by plotting the percentage of slip (i.e. the slip portion of the total tangential displacement) versus the number of cycles. For example, in the test with σ_n=200 kPa and A=2 mm, the percentage of slip increased from 11% at the end of the initial loading part to 69% at the end of the 10^{th} cycle. DeJong et al. (2003) have also reported that the percentage of slip is increasing with the number of cycles; this increase was attributed to particle crushing.

3.4.1.2 Influence of normal stress

The tests conducted with the same amplitude of tangential displacement but with different values of constant normal stress show that the shear stress mobilized at a given tangential displacement is, as expected, larger for higher normal stress values. The ratio of mobilized shear stress to normal stress (stress ratio) is used in the presentation of results. Figure 3.18 shows that the maximum stress ratio is reached in all tests although it required more displacement cycles when the displacement amplitude was 1mm. These test results also show that the stress ratio depends on the magnitude of the applied normal stress. For example, as indicated in Figure 18a, the maximum stress ratio has a value of 0.55, 0.58 and 0.60 in the experiments where σ_n=100 kPa, 200 kPa, and 300 kPa, respectively. Experimental results indicate that the stress ratio slightly increases with increasing normal stress.

The magnitude of normal stress influences the amount of normal displacement during shearing (Figure 3.19). For larger normal stress values, the change in sample height becomes larger. This observation is in agreement with the results published by Al-Douri and Poulos (1992). It is important however to add that, as shown in Figure 3.19, the effect of normal stress on the normal displacement is more pronounced for a smaller amplitude of tangential displacement. For example, considering the end of 10^{th} cycle when A=1mm (Figure 3.19a), the measured values of normal displacement are -1.809 mm for σ_n=100

kPa and -2.168 mm for σ_n=300 kPa. The difference between these two normal displacement values is about 20%. This difference reduces to 6% when A=3.0 mm (Figure 3.19c).

The experimental results summarized in Table 3.1 also show that the soil displacement portion of the tangential displacement at the interface tends to decrease with an increase in the normal stress value. In other words, the amount of slip has a tendency to increase as the normal stress becomes larger.

3.4.1.3 Influence of tangential displacement amplitude

The experimental results (Figures 3.9a, 3.10a, and 3.11a) suggest that the amplitude of tangential displacement influences the magnitude of shear stress developed during displacement cycles. There is a positive relation between the shear stress and the amplitude of tangential displacement, A, during the initial cycles. The shear stress mobilized at a given number of cycles and normal stress value is larger for larger values of A for the first few cycles. However, the nature of this relation is reversed during the remaining cycles as illustrated in Figure 3.15.

In addition, the amplitude of tangential displacement influences the rate of increase in shear stress. For example, considering the test with A=1 mm and σ_n=100 kPa (Figure 3.15a), the shear stress increases from 31.2 kPa at the end of the initial loading part of the test to 41.7 kPa at the end of the first cycle. This represents an increase in shear stress of 33.7%. For the test conducted under the same normal stress with A=3 mm, the shear stress increases from 44.7 kPa at the end of the initial loading part to 47.5 kPa at the end of the first cycle. The corresponding increase in shear stress is 6.3%. These results indicate that the rate of increase in shear stress is larger for smaller values of tangential displacement amplitudes.

As mentioned previously, the magnitude of cumulative normal displacement at the end of each cycle increases with the number of cycles. But, it is important to point out that the soil sample may both contract and dilate within any displacement cycle. For A=1 mm (Figures 3.9b), the sand sample contracts continuously with little dilation. However, for A=2 mm and A=3 mm (Figure 3.10b and 3.11b), the sample contracts in cycle IL, but in the subsequent cycles, it displays an initial contraction followed by dilation. These observations suggest that the tangential displacement amplitude affects the normal displacement behaviour of a sample.

The sample height changes more with larger tangential displacement amplitudes (Figure 3.16). Similar results were reported by Al-Douri and Poulos (1992). Considering the end of last cycle, the changes taking place in sample height in the experiments conducted with A=2 mm are in average 23% larger than that of tests with A=1 mm. The recorded changes in sample height when A=3 mm are, in average, 4% higher than those recorded in the experiments with A=2 mm. Although the change in sample height becomes larger with increasing values of tangential displacement amplitude, the overall difference between the results of tests with A=2 mm and A=3 mm is small. This observation suggests that there is a limiting value of amplitude after which increasing the amplitude of tangential displacement would not affect significantly the change in sample height. This type of behaviour can be attributed to the fact that the soil sample cannot compress indefinitely with increasing number of cycles.

The percentage of slip taking place at the interface increases as the amplitude of tangential displacement increases (Figure 3.17). The amount of slip at the end of the initial loading for A=1 mm, 2 mm and 3 mm when σ_n=100 kPa, represents 6%, 14%, and 16% of the total tangential displacement of the steel plate, respectively. These percentages increase to 38%, 58%, and 68%, respectively, at the end of the 10^{th} cycle.

3.4.2 Cyclic tests on dense sand interfaces

The results of the nine tests performed on dense sand interfaces are shown in Figures 3.21 to 3.29. Figures 3.21 to 3.23, Figures 3.24 to 3.26, and Figures 3.27 to 3.29 show the results of tests conducted with a normal stress of 100 kPa, 200 kPa, and 300 kPa. The measurements related to all ten displacement cycles in all experiments on dense sand samples are summarized in Table 3.2. The measurements in this table are also presented in graphical form in order to highlight the influences of the number of cycles, magnitude of normal stress, and amplitude of displacement (Figures 3.30 to 3.35).

3.4.2.1 Influence of number of cycles

In general, the mobilized shear stress on interfaces with dense sand decreases (at a diminishing rate) with an increase of the number of cycles (Figure 3.30). However, the amount of decrease in the mobilized shear stress is a function of the amplitude of tangential displacement and is discussed in the section related to the influence of tangential displacement amplitude.

During the initial loading part of the tests with dense sand, the maximum shear stress is, as expected, higher than that recorded for loose sand. For the test conducted with σ_n=100 kPa and A=3 mm, the maximum shear stress is 60.3 kPa for dense sand (Table 3.2) and 44.7 kPa for loose sand (Table 3.2). The difference in the shear stress values decreases with the number of cycles. At the end of the 10^{th} cycle, the shear stress for this particular test is 46.8 kPa for dense sand and 47.5 kPa for loose sand. These observations suggest that the mobilized shear stress reaches almost a constant value, which is independent of the initial density of sand samples.

In each cycle, the normal displacement shown in Figures 3.21b to 3.29b indicates contraction first and then dilation. During the initial cycles of some tests, the overall

normal displacement was positive, meaning that the volume of sample has increased (Figure 3.31 and Table 3.2). However, each displacement reversal is characterized by a contraction of the soil sample and the overall normal displacement becomes negative (contraction in the subsequent cycles). The change in normal displacement occurs at a decreasing rate.

The values of normal displacement at the end of each cycle show that loose sand undergoes greater contraction than dense sand (Tables 3.1 and 3.2). In fact, the normal displacement measured at the top of loose sand samples is 4 to 17 times larger than that of dense sand samples.

The percentage of slip in the experiments with dense sand increases with the number of cycles (Figure 3.32). The amount of slip is larger for dense sand when compared to that of loose sand (Table 3.1 and 3.2). For example, in the test performed with σ_n=100 kPa and A=1 mm, the slip portion of the total tangential displacement for dense sand is 32% and 64% at the end of initial loading and at the end of the 10^{th} cycle, respectively. The corresponding portions of slip for loose sand are 6.0% and 38%. Therefore, it can be stated that slip is influenced by sand density and constitutes an important part of the total tangential displacement.

In most cases the amount of slip at the end of 10^{th} cycle is the main component of the total tangential displacement (i.e. percentage of slip > 50%). Accordingly, not making a distinction between the slip and the displacement at the interface resulting from soil deformation, as is done when direct shear type interface equipment is used (Desai et al. 1985, Al-Douri and Poulos 1992, Shahrour and Rezaie 1997), will result in incomplete information on soil-structure interface behaviour.

3.4.2.2 Influence of normal stress

Similar to the observation made in tests with loose sand, the magnitude of normal stress influences the stress ratio in the experiments with dense sand (Figure 3.33). For example, the stress ratio at the end of the initial loading part of the tests conducted with A=1 mm and normal stress values of 100 kPa, 200 kPa, and 300 kPa is 0.56, 0.59 and 0.61, respectively. For large values of tangential displacement amplitude (i.e. 2 mm and 3 mm), the stress ratios in the tests with σ_n=200 kPa and 300kPa are nearly the same (Figure 3.33b and 3.33c), but they remain higher than the stress ratio in the test with σ_n=100 kPa. The normal stress also influences the amount of normal displacement. As shown in Figure 3.34, the amount of compression increases with increasing normal stress values. In addition, as is the case for loose sand, the magnitude of sliding displacement at the interface increases in most of the tests with increasing values of normal stress (Figure 3.35 and Table 3.2).

3.4.2.3 Influence of tangential displacement amplitude

The relationship between the mobilized shear stress and tangential displacement of the steel plate in the experiments with dense sand can be divided into two parts: 1) before the peak shear stress and 2) after the peak shear stress. If the tangential displacement amplitude, A, in a cyclic test is less than the amount of displacement required for the peak shear stress to develop in a monotonic loading test, the peak shear stress will not be reached in a cyclic test with dense sand, such is the case when A=1 mm. In this case, there is only a small amount of change in the mobilized shear stress recorded during the cycles (Figure 3.30a). However, if the peak shear stress is already mobilized (i.e. A=2 mm and A=3 mm) during the initial loading branch of an experiment, the peak shear stress decreases in the subsequent displacement cycles at a decreasing rate (Figures 3.30b, and 3.30c).

There is an inverse relation between the normal displacement measured at the top of the soil sample and the amplitude of tangential displacement (Figure 3.31). Larger amplitudes of tangential displacement are associated with smaller compression of the soil specimen during cyclic loading. This is due to the fact that when the amplitude of displacement is large, the sand sample dilates more. Therefore, the total amount of compression reduces. It is important to note that this is opposite to the observation made in tests with loose sand where the normal displacement increases with increasing values of tangential displacement amplitude. Although, Al-Douri and Poulos (1992) reported that the change in sample height increases with increasing values of tangential displacement amplitude, the results of the current investigation indicate that this observation is applicable only to soil-structure interfaces in loose sand.

The amplitude of tangential displacement, as in the case of loose sand, influences the amount of slip at the interface. The percentage of slip increases with increasing values of tangential displacement amplitude (Figure 3.32).

Table 3.1 Summary of experimental results for loose sand-steel plate interfaces.

Cycle Number	σ_n= 100 kPa Displacement amplitude			σ_n= 200 kPa Displacement amplitude			σ_n= 300 kPa Displacement amplitude		
	1 mm	2 mm	3 mm	1 mm	2 mm	3 mm	1 mm	2 mm	3 mm
				Shear Stress (kPa)					
0	31.2	39.3	44.7	75.3	84.1	93.6	114.6	135.6	142.4
1	41.7	47.8	49.5	91.6	104.7	107.8	139.7	159.0	164.5
2	46.4	50.9	50.5	100.7	110.5	111.6	155.0	170.2	167.1
3	50.1	52.6	50.2	106.5	111.5	110.2	161.4	173.9	168.5
4	51.6	51.9	50.2	109.2	112.2	108.5	167.8	176.6	167.1
5	52.5	51.6	48.8	110.2	109.5	107.8	171.9	175.3	166.8
6	53.2	51.6	48.9	115.3	110.2	107.5	176.3	174.2	165.8
7	53.6	52.6	47.5	115.6	108.5	106.8	176.0	172.9	165.1
8	53.6	52.5	49.2	114.3	107.2	104.8	177.3	173.2	163.7
9	55.3	51.2	46.8	116.0	108.8	105.8	179.3	173.3	165.5
10	55.3	50.5	47.5	117.0	108.1	105.4	179.7	174.6	164.8
				Normal displacement (mm)					
0	-0.173	-0.267	-0.279	-0.264	-0.314	-0.325	-0.307	-0.321	-0.329
1	-0.497	-0.798	-0.841	-0.621	-0.778	-0.879	-0.690	-0.872	-0.899
2	-0.838	-1.286	-1.343	-0.997	-1.235	-1.461	-1.083	-1.383	-1.468
3	-1.072	-1.591	-1.677	-1.239	-1.569	-1.773	-1.341	-1.710	-1.811
4	-1.255	-1.809	-1.895	-1.417	-1.794	-1.975	-1.529	-1.953	-2.026
5	-1.394	-1.970	-2.066	-1.567	-1.966	-2.143	-1.682	-2.112	-2.164
6	-1.524	-2.067	-2.181	-1.691	-2.081	-2.249	-1.795	-2.244	-2.289
7	-1.619	-2.157	-2.286	-1.798	-2.186	-2.350	-1.921	-2.357	-2.407
8	-1.685	-2.256	-2.345	-1.888	-2.267	-2.410	-2.020	-2.453	-2.484
9	-1.748	-2.323	-2.414	-1.962	-2.347	-2.497	-2.096	-2.540	-2.569
10	-1.809	-2.381	-2.465	-2.040	-2.392	-2.560	-2.168	-2.612	-2.614
				Soil displacement at the interface (mm)					
0	0.940	1.721	2.534	1.005	1.775	2.784	0.897	1.768	2.538
1	0.891	1.584	2.155	0.917	1.529	2.142	0.808	1.651	2.077
2	0.853	1.408	1.806	0.848	1.374	1.746	0.745	1.430	1.594
3	0.832	1.302	1.611	0.806	1.162	1.412	0.725	1.249	1.327
4	0.787	1.137	1.387	0.759	1.002	1.215	0.674	1.148	1.121
5	0.742	1.067	1.284	0.738	0.901	1.085	0.651	1.004	1.092
6	0.702	1.034	1.157	0.736	0.810	1.027	0.635	0.886	0.942
7	0.682	0.978	1.103	0.705	0.760	0.993	0.593	0.839	0.877
8	0.669	0.908	1.060	0.647	0.709	0.924	0.575	0.747	0.812
9	0.640	0.912	1.033	0.624	0.635	0.848	0.541	0.736	0.806
10	0.622	0.834	0.967	0.604	0.629	0.805	0.510	0.645	0.751

Table 3.2 Summary of experimental results for dense sand-steel plate interfaces.

Cycle Number	σ_n= 100 kPa Displacement amplitude			σ_n= 200 kPa Displacement amplitude			σ_n= 300 kPa Displacement amplitude		
	1 mm	2 mm	3 mm	1 mm	2 mm	3 mm	1 mm	2 mm	3 mm
				Shear Stress (kPa)					
0	56.3	60.3	60.3	118.0	126.8	129.5	183.7	192.5	189.1
1	56.7	56.0	55.0	119.0	125.4	118.7	184.8	187.5	176.6
2	57.3	53.6	52.6	116.3	120.0	113.3	184.7	175.6	171.6
3	56.0	52.6	50.2	114.9	118.0	112.2	183.8	174.6	166.8
4	55.6	50.2	49.2	112.2	116.0	110.2	184.4	173.6	165.8
5	55.0	50.9	48.8	112.9	114.3	109.8	185.1	170.9	163.7
6	55.6	51.2	48.8	111.9	114.6	108.8	184.4	170.5	164.8
7	53.6	50.5	47.5	111.6	112.5	107.5	183.1	168.2	163.1
8	54.9	49.2	48.2	112.2	112.2	106.1	185.1	168.5	162.7
9	54.6	48.8	47.8	112.9	111.9	107.2	185.1	171.2	161.4
10	53.2	48.2	46.8	111.5	111.2	106.8	183.4	168.1	162.1
				Normal displacement (mm)					
0	0.083	0.188	0.404	-0.018	0.094	0.170	0.000	0.112	0.177
1	0.074	0.233	0.471	-0.056	0.137	0.260	-0.118	0.076	0.157
2	-0.013	0.139	0.388	-0.163	0.013	0.123	-0.268	-0.091	0.008
3	-0.076	0.089	0.330	-0.246	-0.091	0.026	-0.358	-0.197	-0.132
4	-0.132	0.054	0.280	-0.320	-0.154	-0.062	-0.421	-0.278	-0.213
5	-0.163	0.007	0.246	-0.358	-0.202	-0.136	-0.473	-0.358	-0.300
6	-0.192	-0.018	0.202	-0.359	-0.260	-0.172	-0.513	-0.388	-0.347
7	-0.221	-0.054	0.165	-0.386	-0.296	-0.222	-0.554	-0.432	-0.377
8	-0.248	-0.091	0.148	-0.417	-0.327	-0.255	-0.581	-0.470	-0.434
9	-0.255	-0.103	0.125	-0.446	-0.365	-0.296	-0.605	-0.497	-0.459
10	-0.273	-0.134	0.112	-0.468	-0.421	-0.313	-0.625	-0.527	-0.509
				Soil displacement at the interface (mm)					
0	0.680	1.001	1.262	0.857	1.171	1.341	0.857	1.132	1.345
1	0.564	0.799	1.144	0.606	1.056	1.327	0.680	0.917	1.042
2	0.546	0.747	1.003	0.526	0.899	1.003	0.606	0.756	0.846
3	0.483	0.701	0.948	0.461	0.781	0.902	0.553	0.694	0.740
4	0.448	0.656	0.933	0.412	0.734	0.850	0.533	0.644	0.691
5	0.449	0.622	0.881	0.405	0.714	0.821	0.512	0.559	0.599
6	0.430	0.649	0.848	0.364	0.649	0.750	0.483	0.591	0.584
7	0.398	0.593	0.779	0.340	0.621	0.700	0.470	0.534	0.546
8	0.383	0.570	0.803	0.331	0.564	0.682	0.470	0.506	0.515
9	0.398	0.570	0.770	0.337	0.566	0.646	0.457	0.503	0.528
10	0.364	0.550	0.709	0.308	0.530	0.663	0.442	0.501	0.499

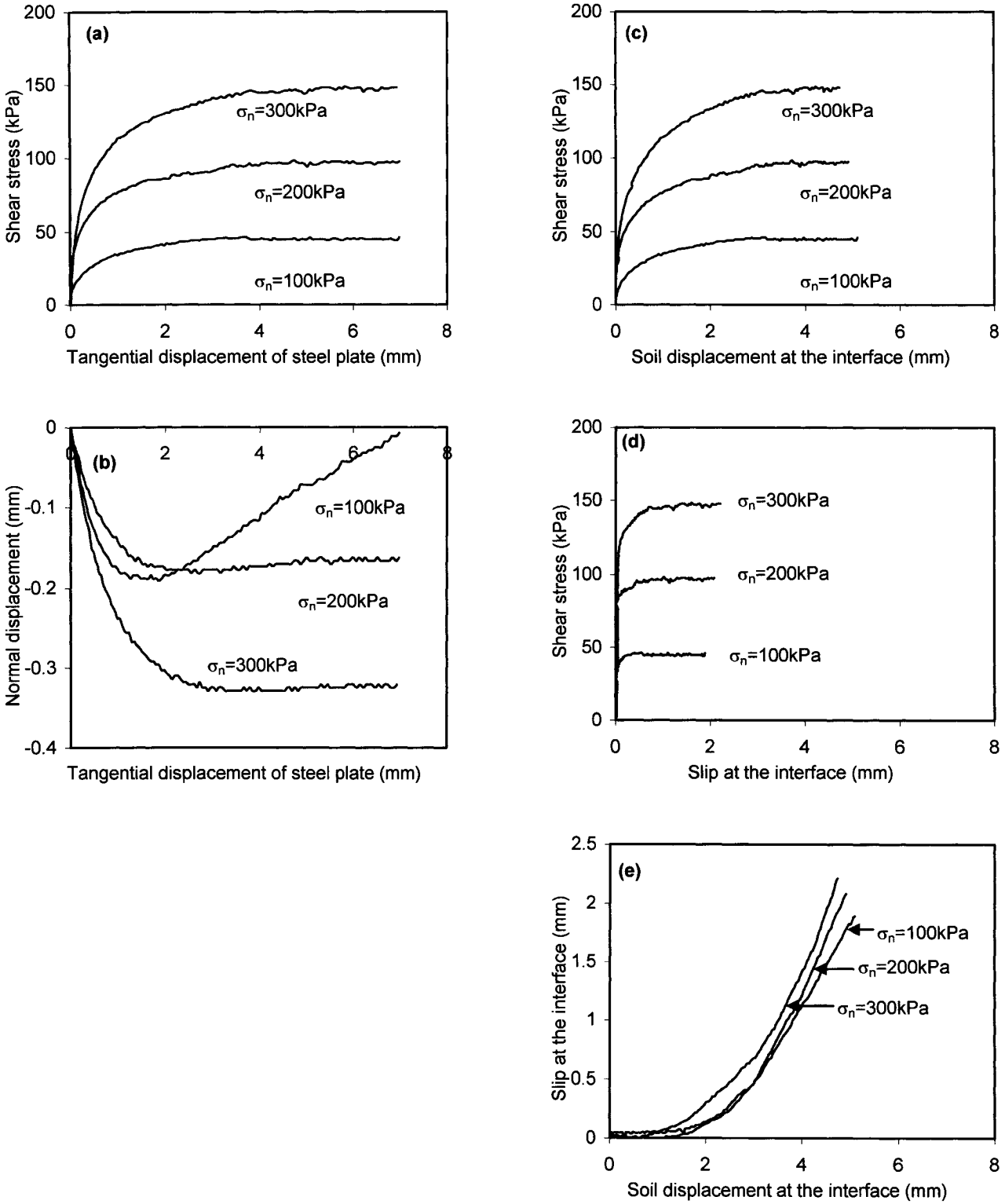

Figure 3.1. Results of monotonic tests conducted on loose sand interfaces under constant normal stress

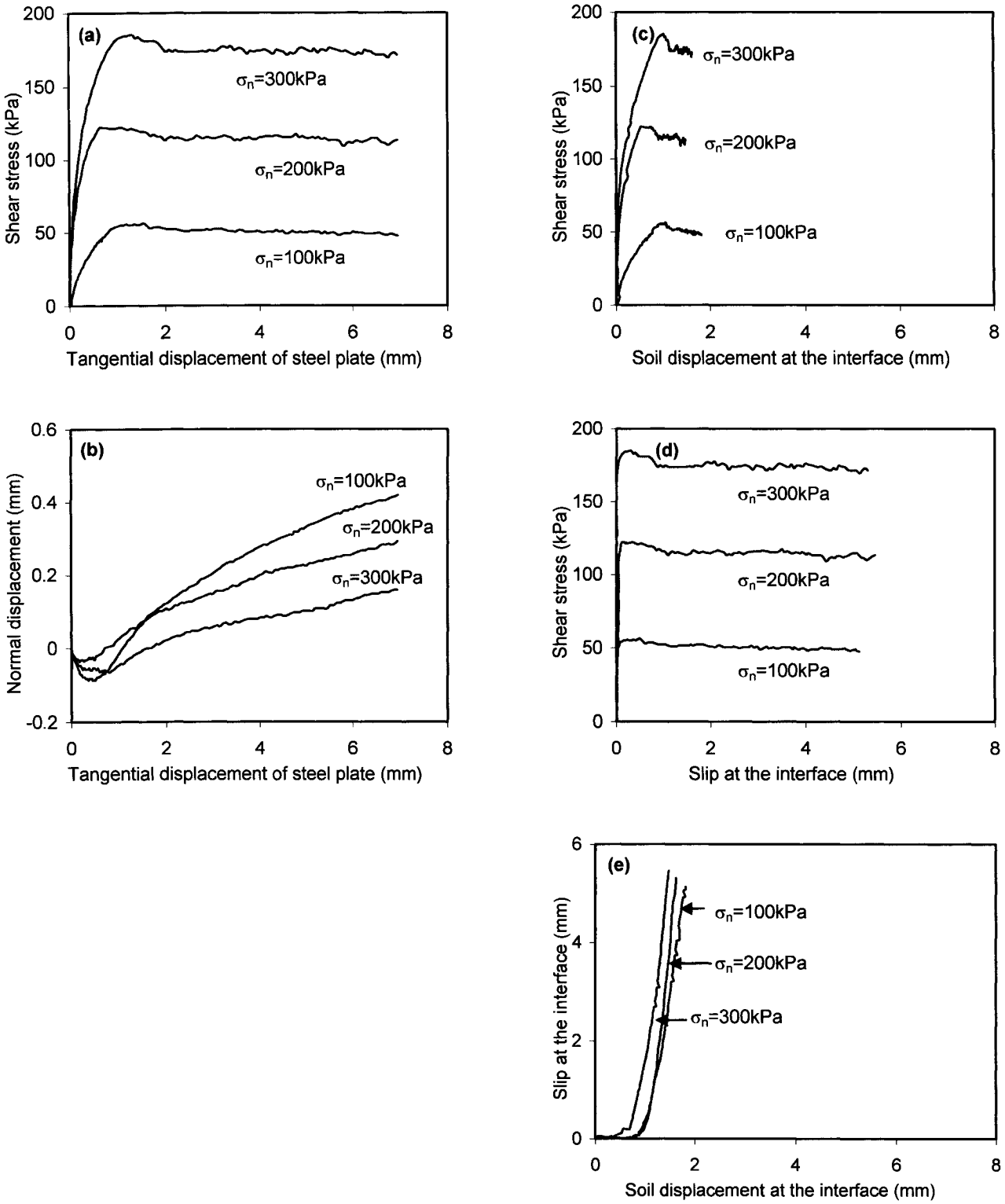

Figure 3.2. Results of monotonic tests conducted on dense sand interfaces under constant normal stress

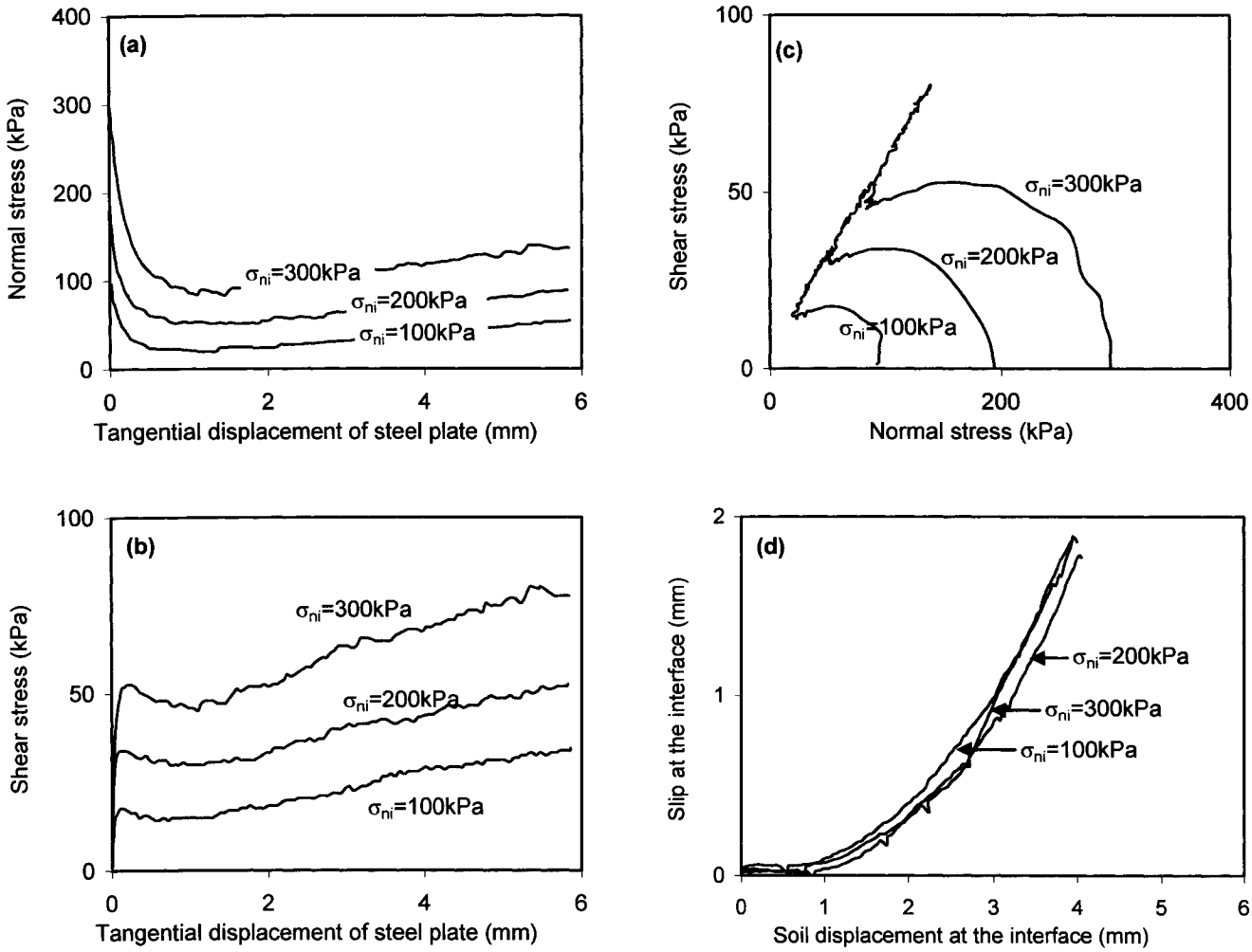

Figure 3.3 Results of monotonic tests conducted on loose sand interfaces under constant volume test condition

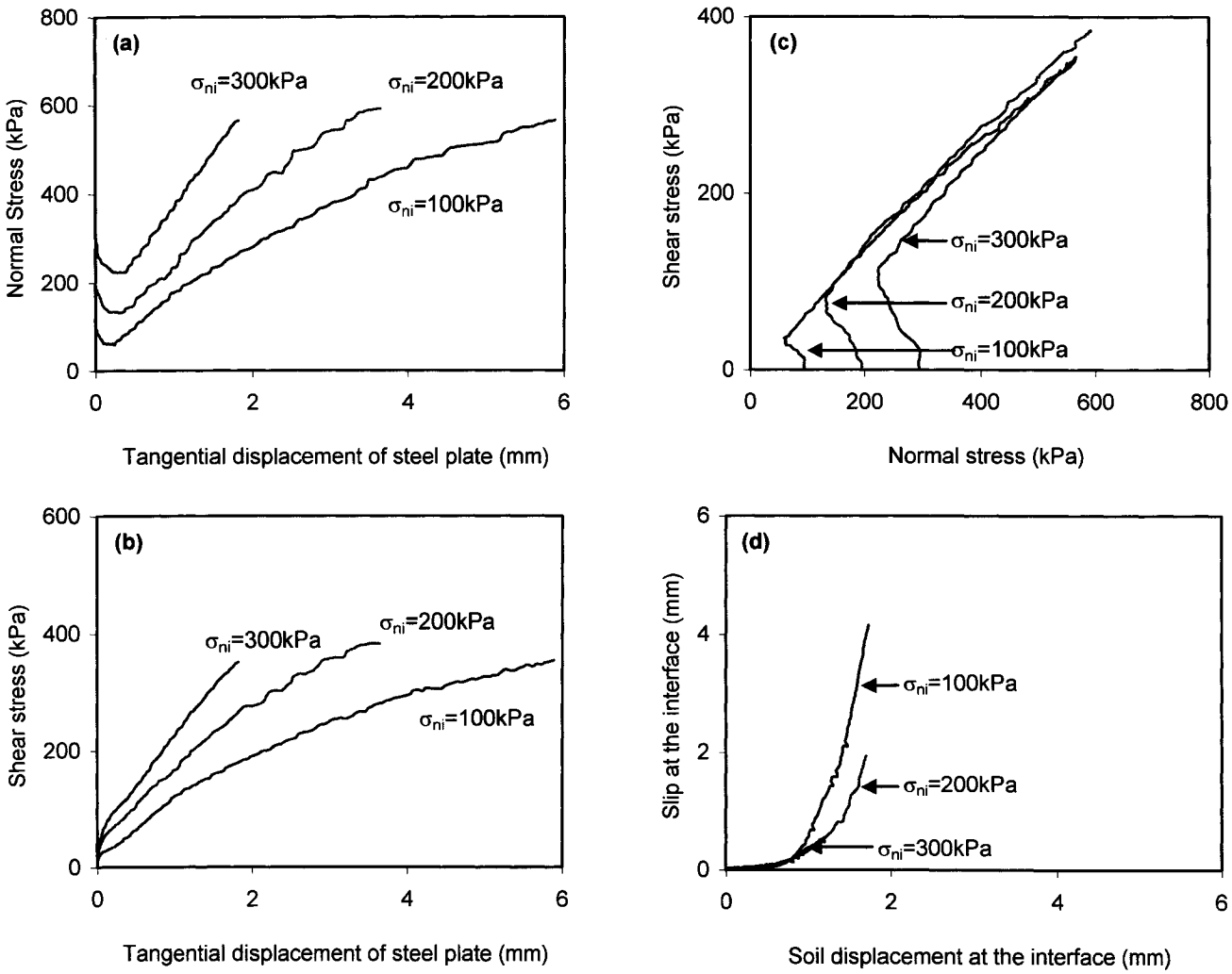

Figure 3.4 Results of monotonic tests conducted on dense sand interfaces under constant volume test condition

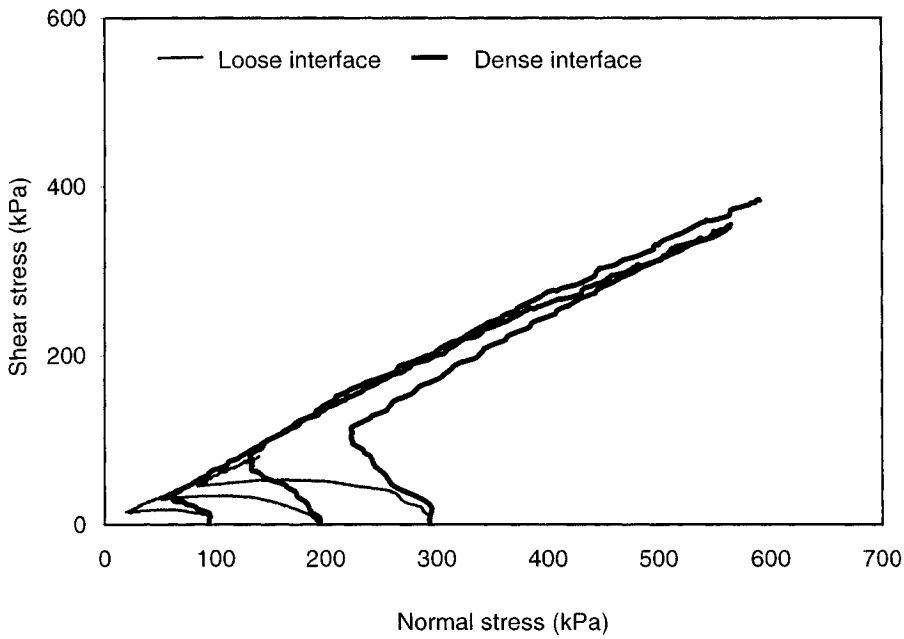

Figure 3.5 Shear stress versus normal stress relation for tests conducted under constant volume conditions on loose sand and dense sand interfaces

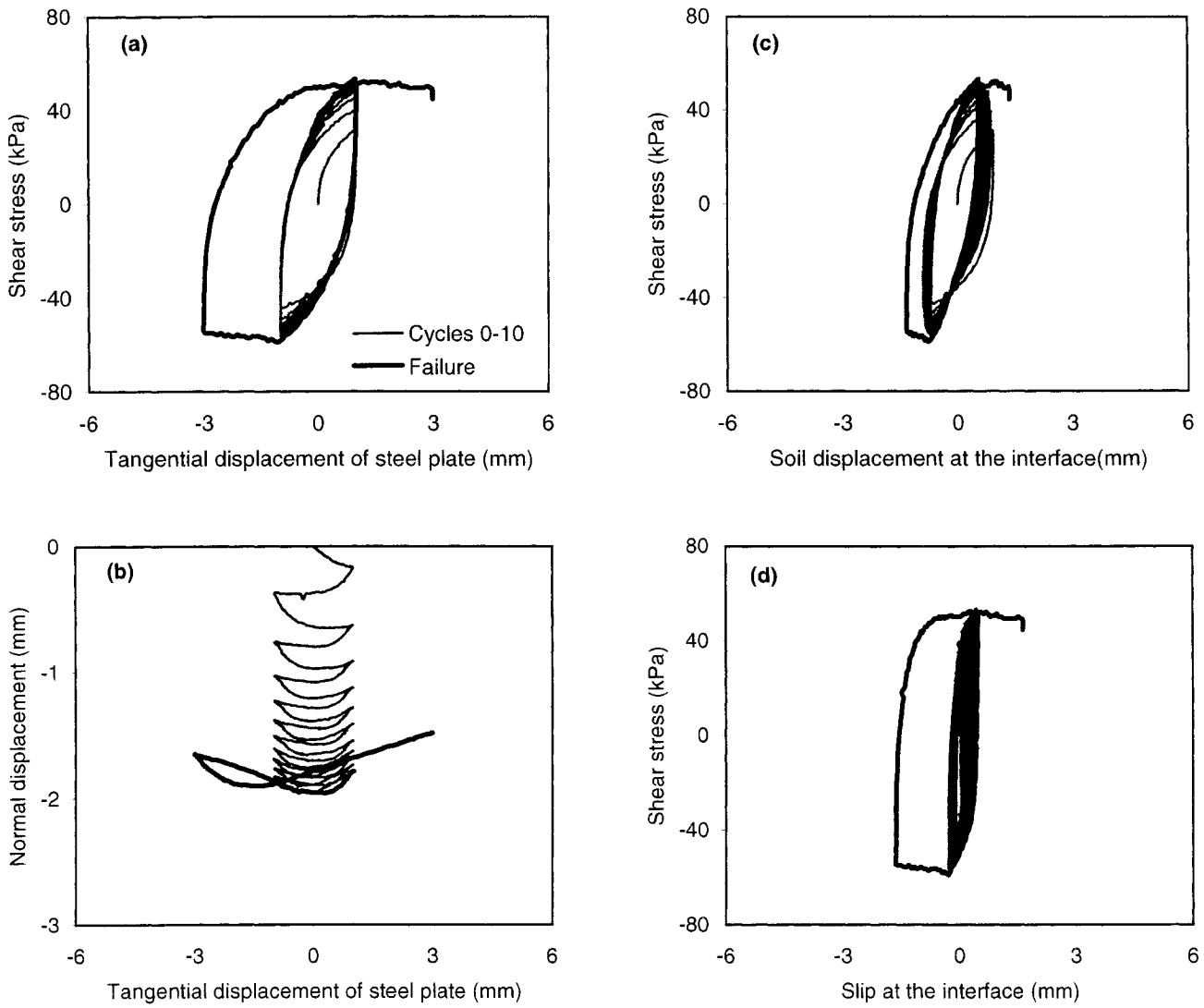

Figure 3.6 Results of the test conducted on loose sand interface with σ_n=100 kPa and A=1mm

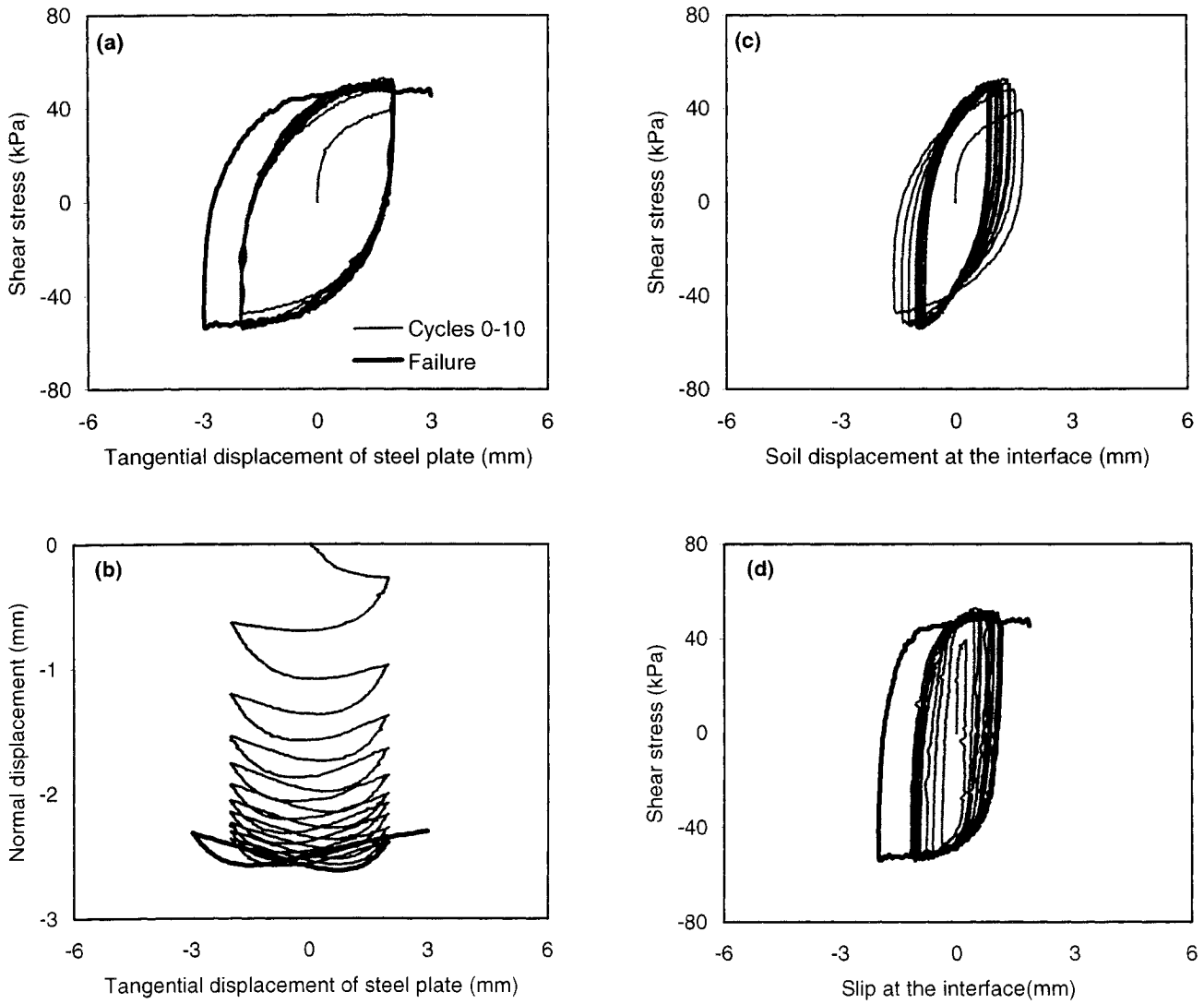

Figure 3.7 Results of the test conducted on loose sand interface with σ_n=100 kPa and A=2 mm

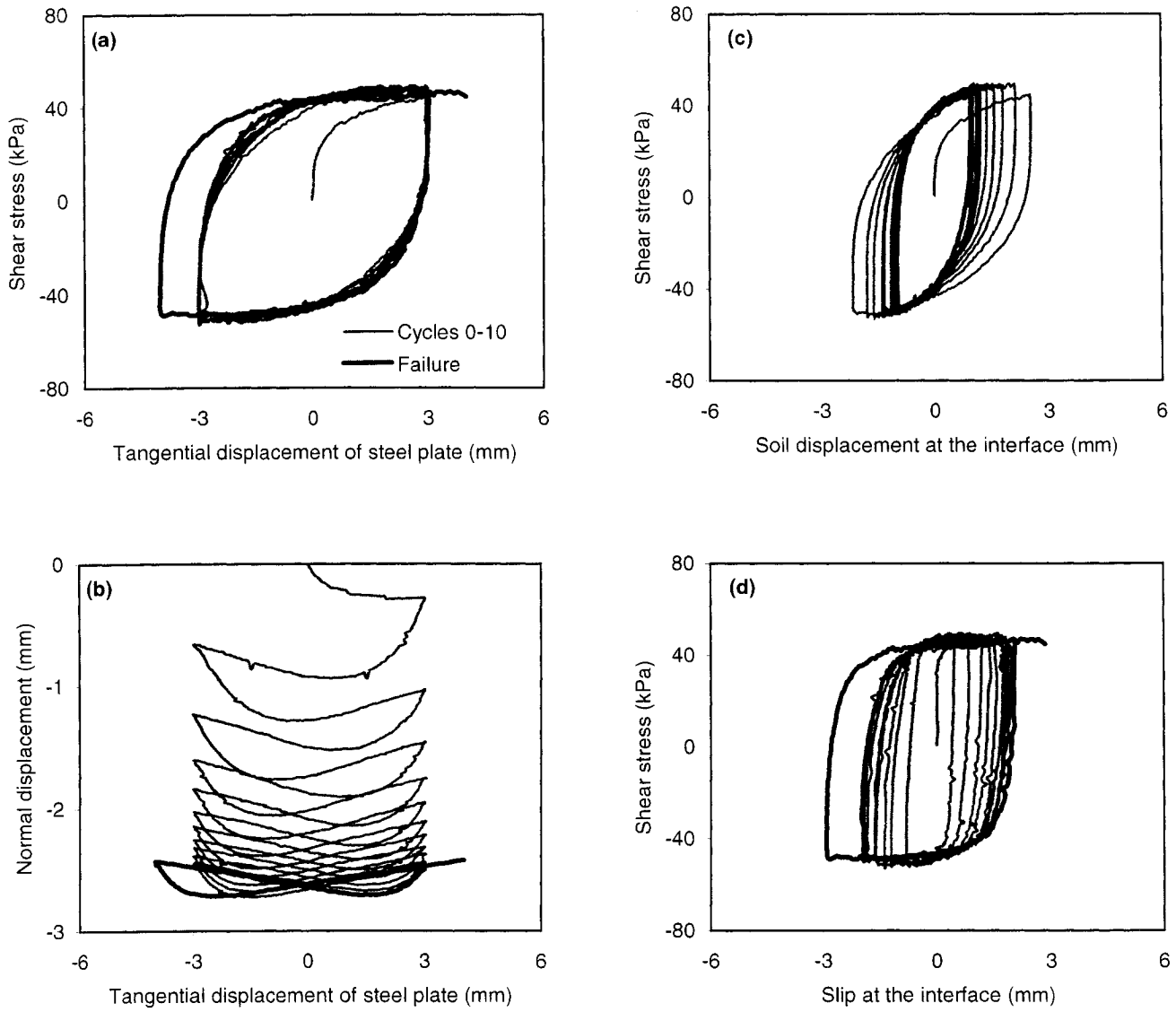

Figure 3.8 Results of the test conducted on loose sand interface with σ_n=100 kPa and A=3 mm

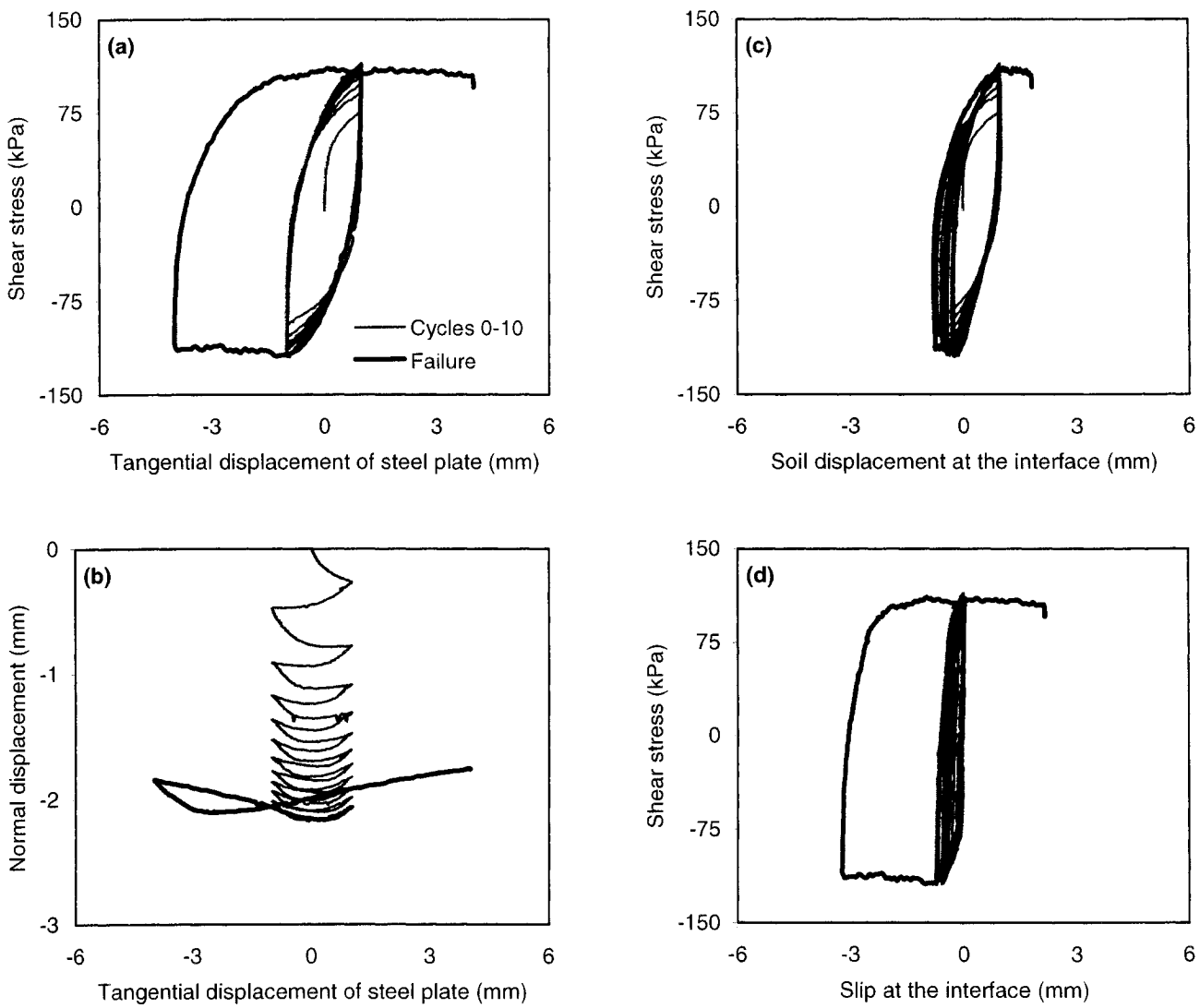

Figure 3.9 Results of the test conducted on loose sand interface with σ_n=200 kPa and A=1 mm

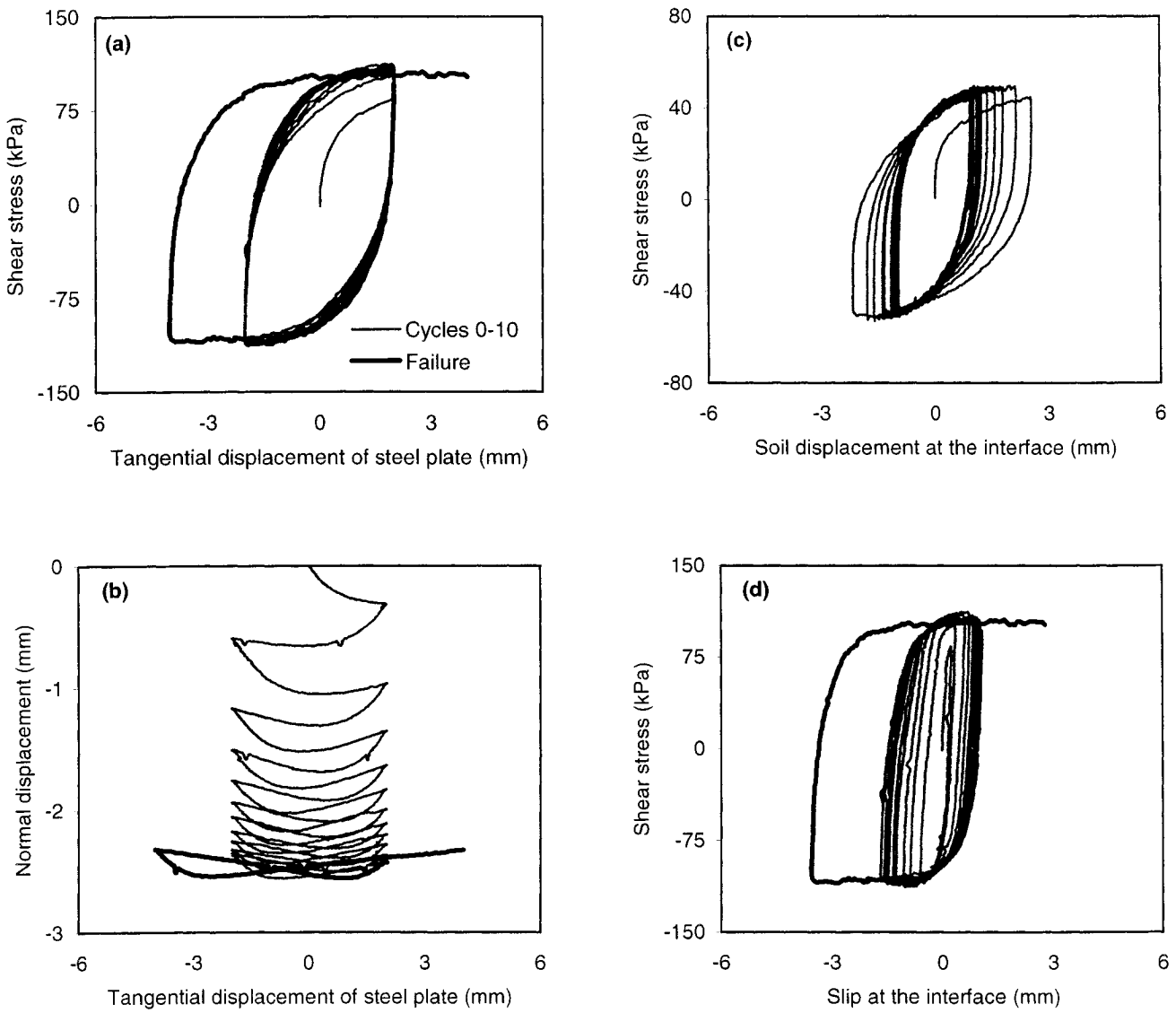

Figure 3.10 Results of the test conducted on loose sand interface with σ_n=200 kPa and A=2 mm

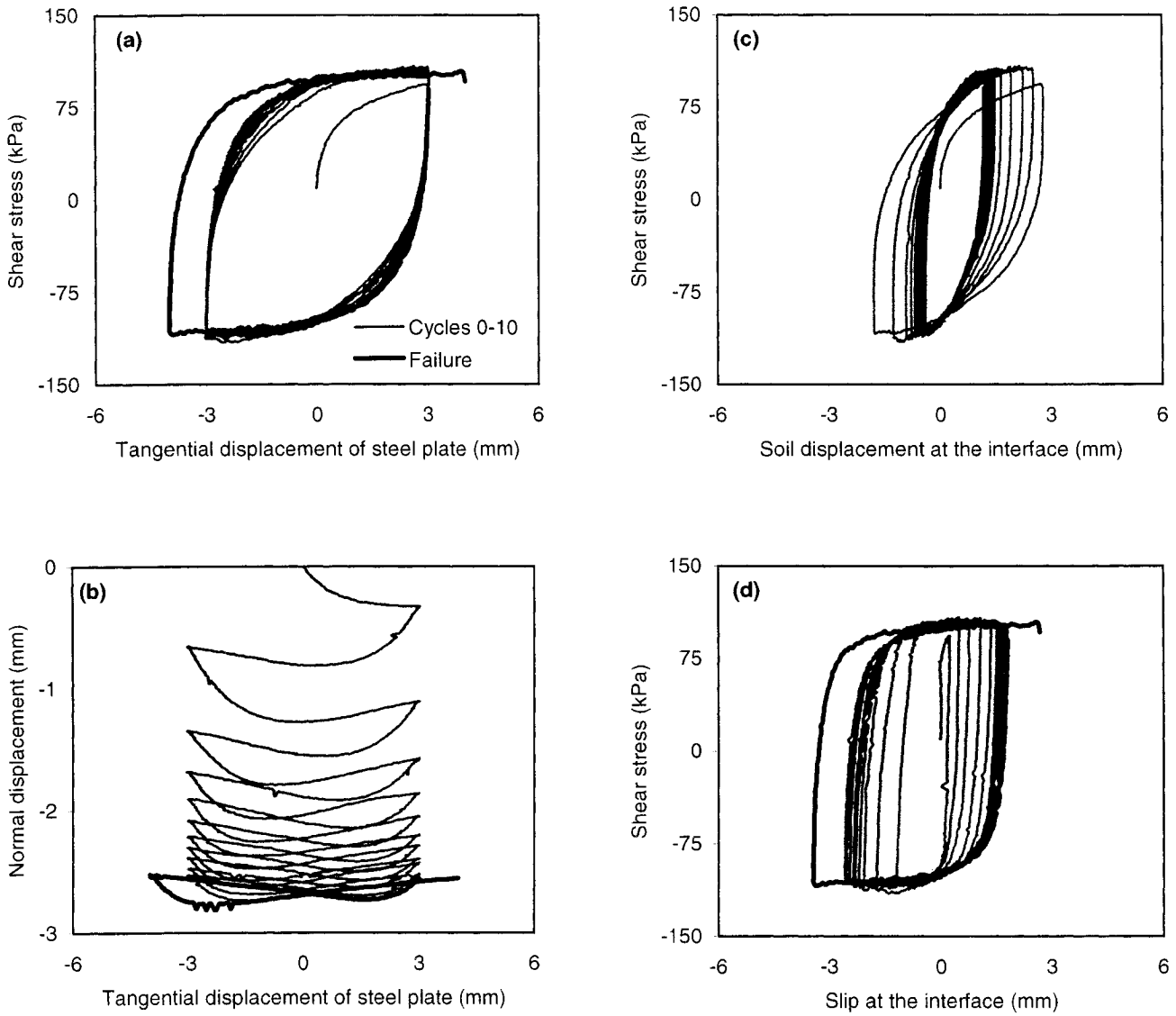

Figure 3.11 Results of the test conducted on loose sand interface with σ_n=200 kPa and A=3 mm

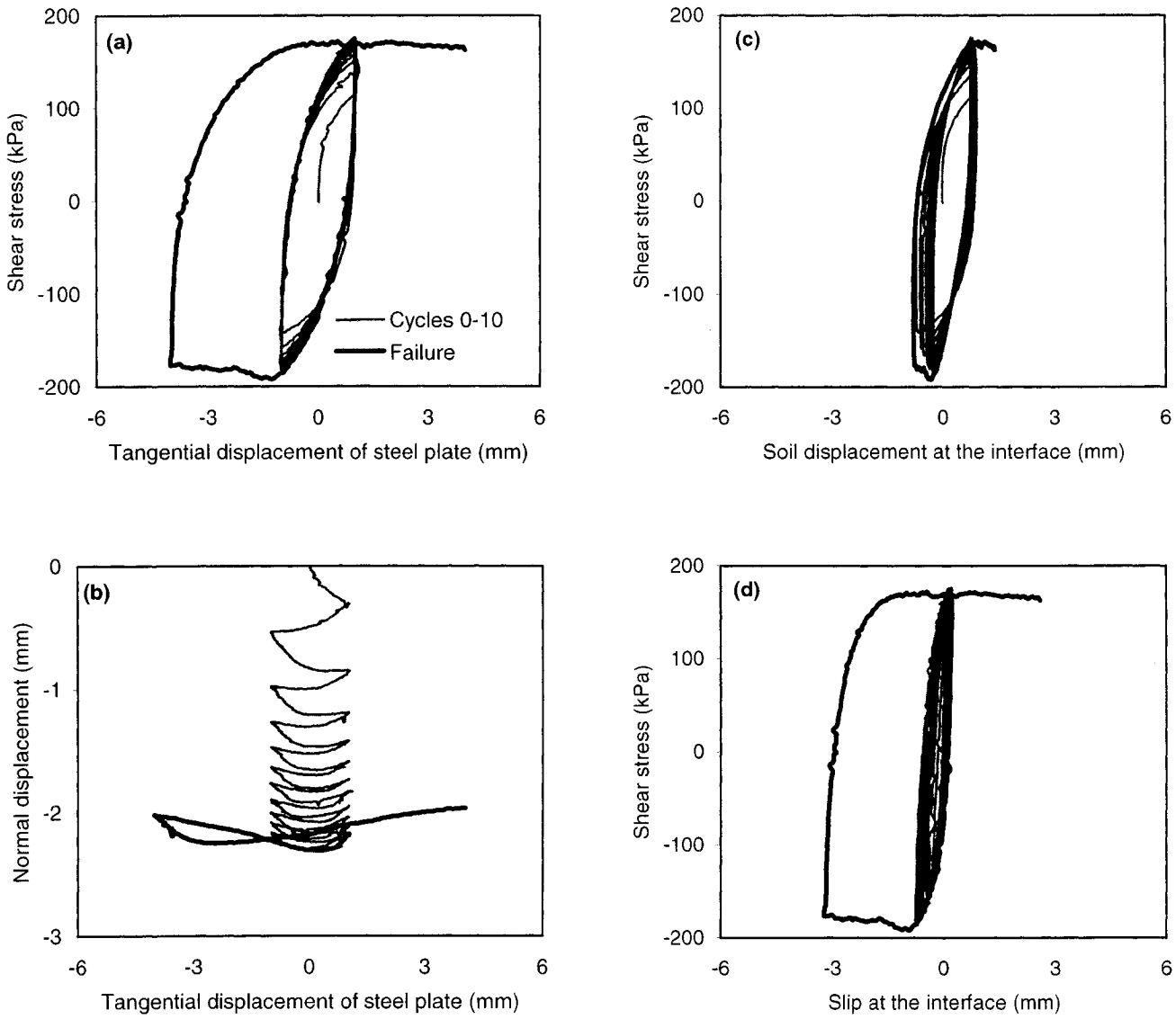

Figure 3.12 Results of the test conducted on loose sand interface with σ_n=300 kPa and A=1 mm

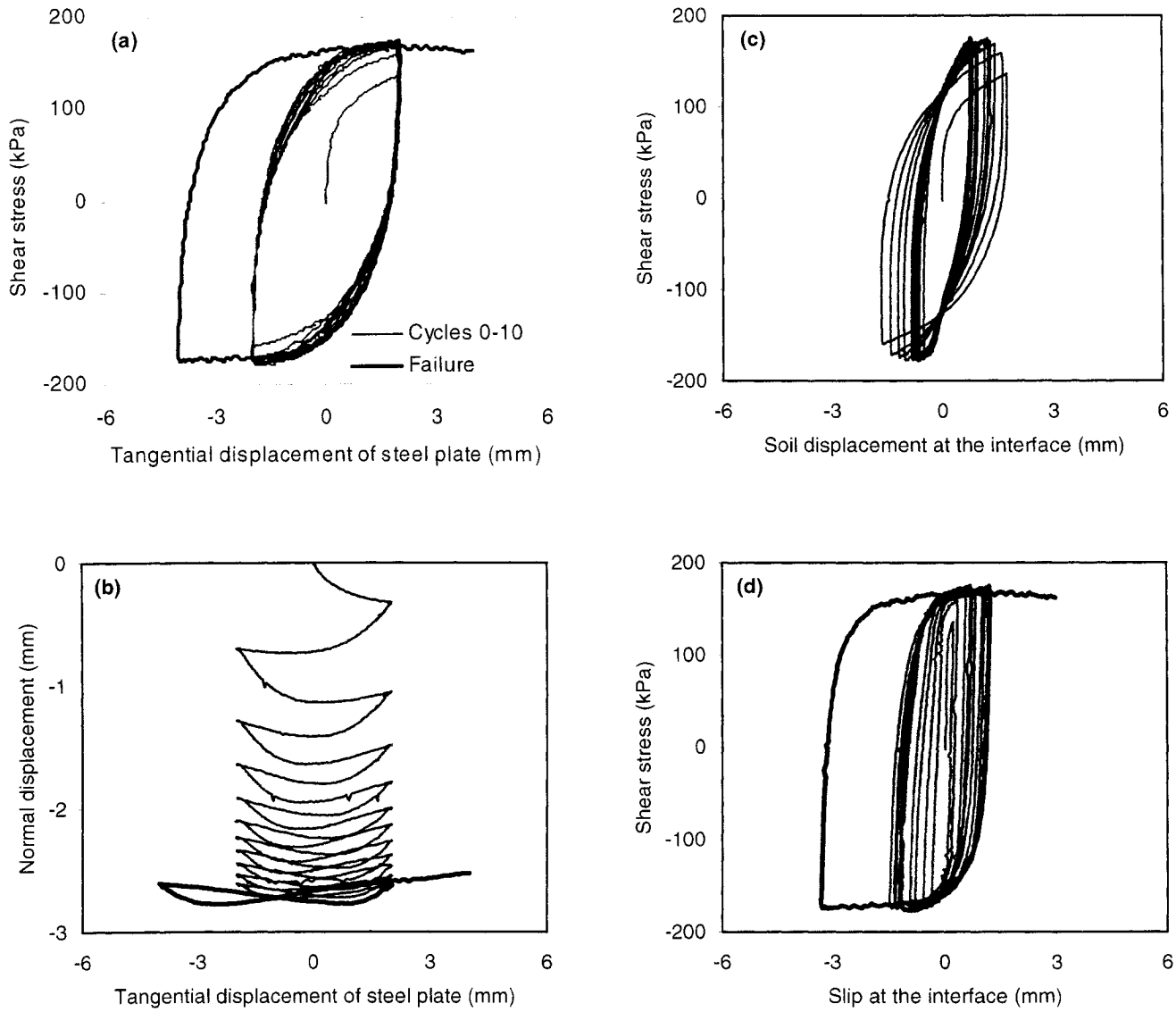

Figure 3.13 Results of the test conducted on loose sand interface with σ_n=300 kPa and A=2 mm

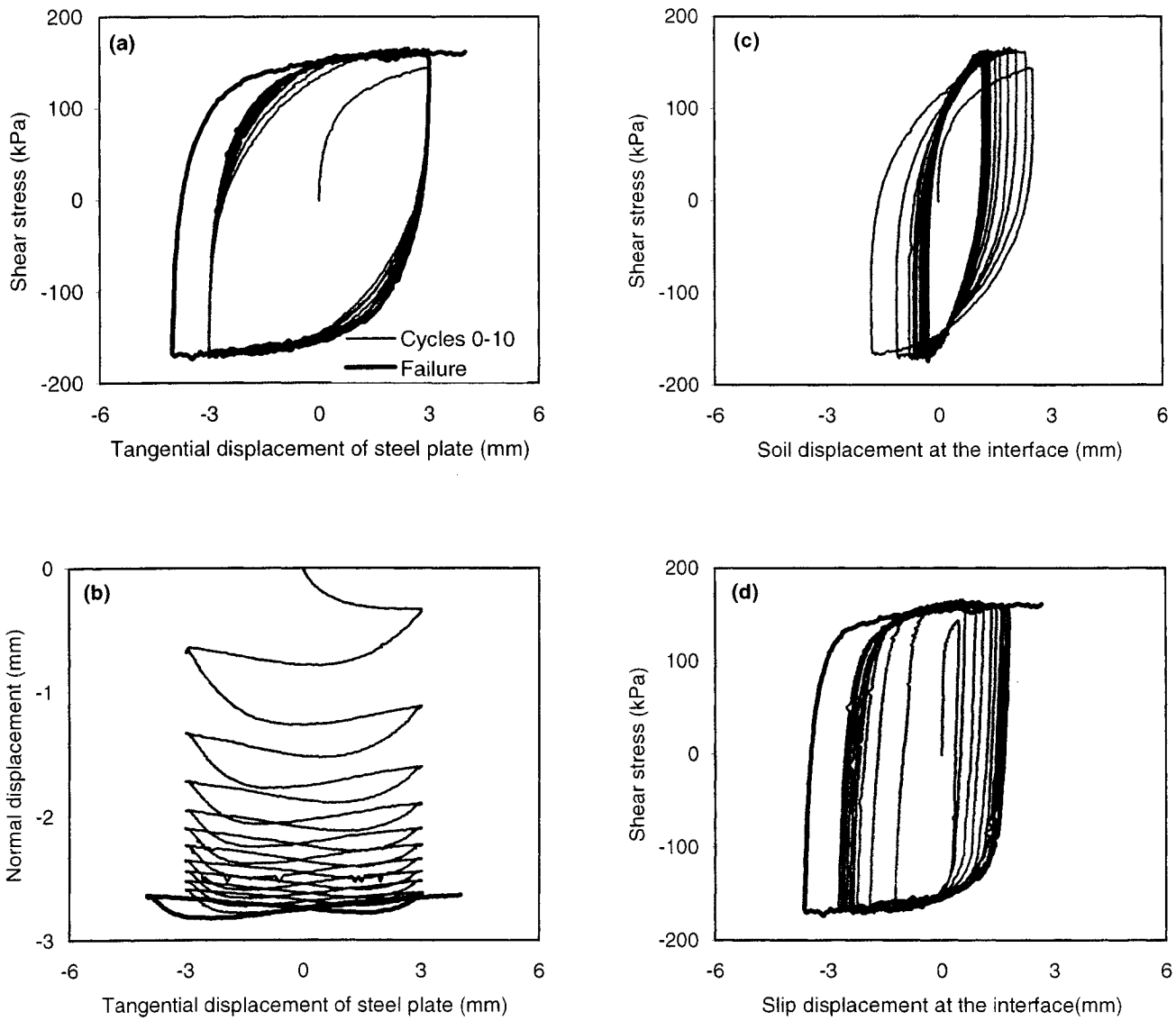

Figure 3.14 Results of the test conducted on loose sand interface with σ_n=300 kPa and A=3 mm

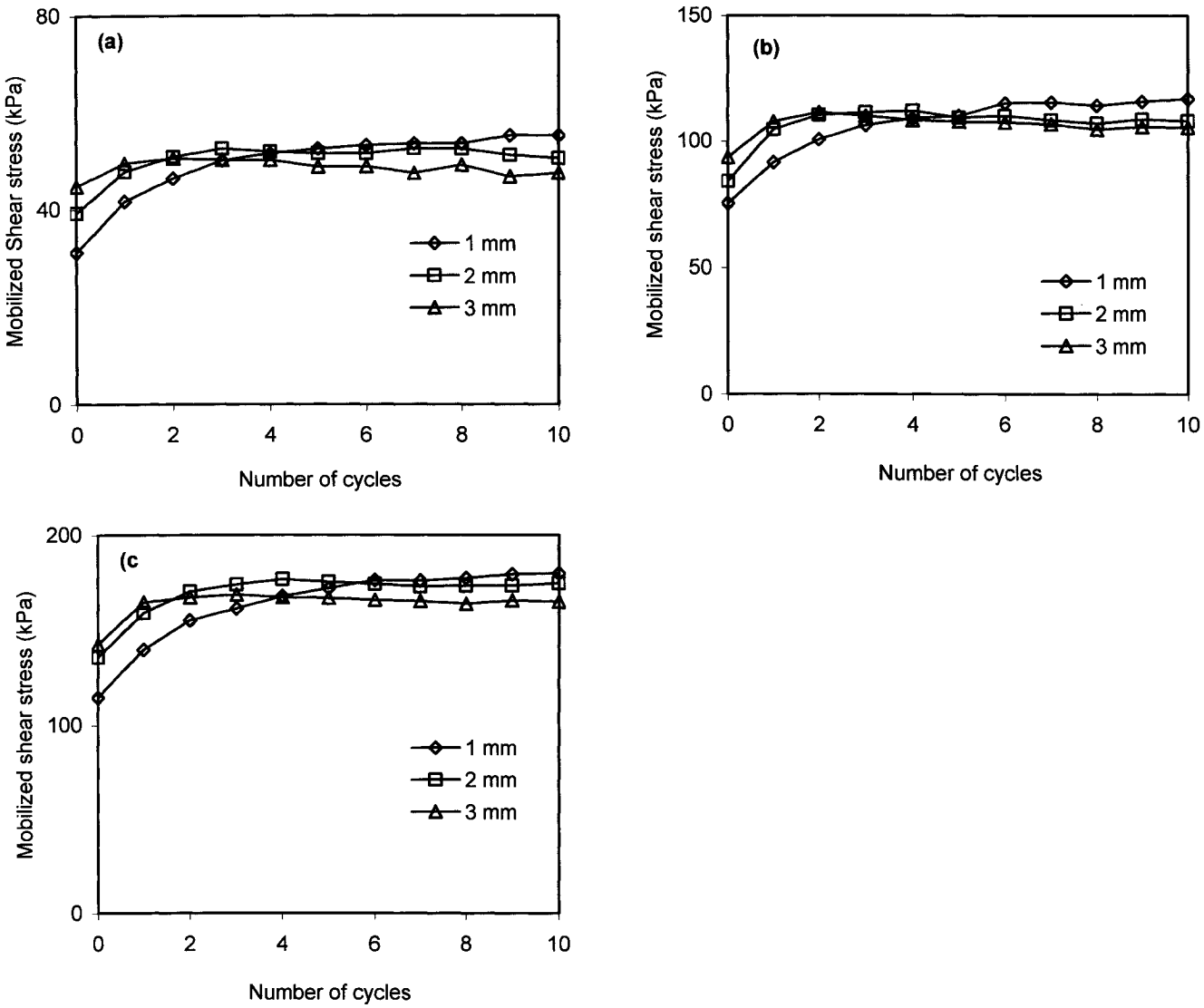

Figure 3.15 Effect of amplitude of tangential displacement and number of cycle on mobilized shear stress for the loose sand-steel plate interface: (a) σ_n=100 kPa, (b) σ_n=200 kPa, (c) σ_n=300 kPa

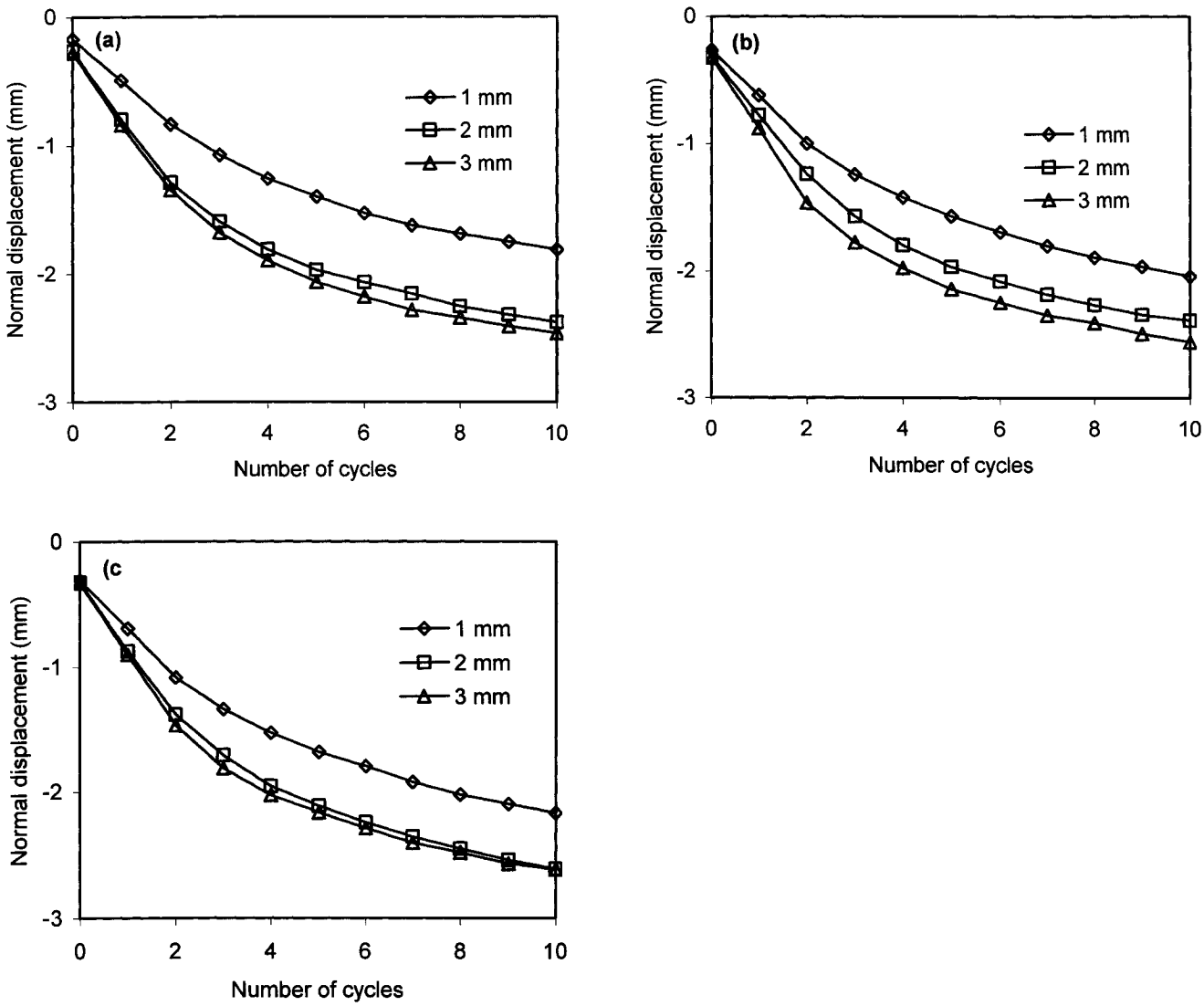

Figure 3.16 Effect of amplitude of tangential displacement and number of cycle on the normal displacement for the loose sand-steel plate interface: (a) σ_n=100 kPa, (b) σ_n=200 kPa, (c) σ_n=300 kPa

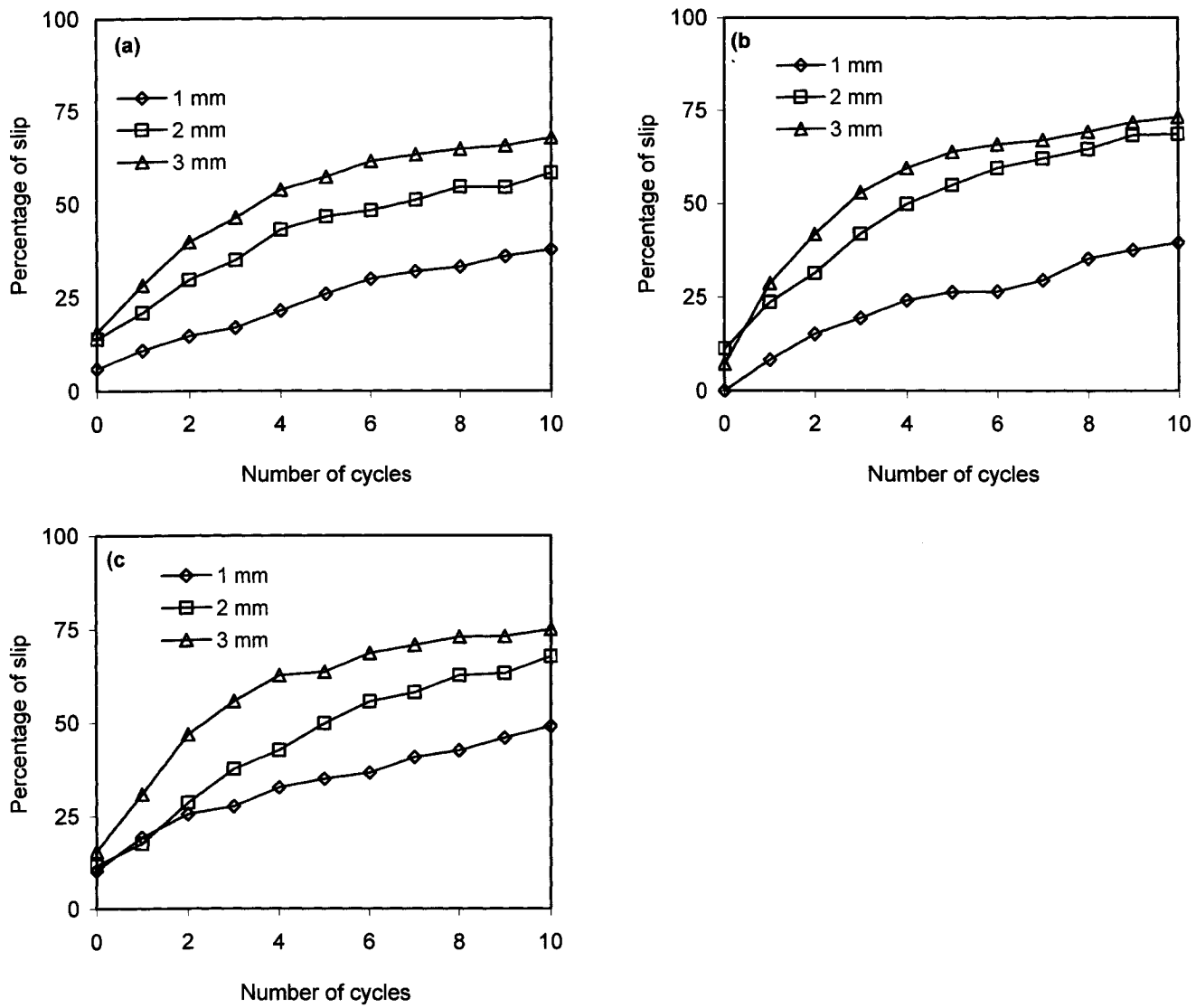

Figure 3.17 Effect of amplitude of tangential displacement and number of cycles on the percentage of slip for the loose sand-steel plate interface: (a) σ_n=100 kPa, (b) σ_n=200 kPa, (c) σ_n=300 kPa

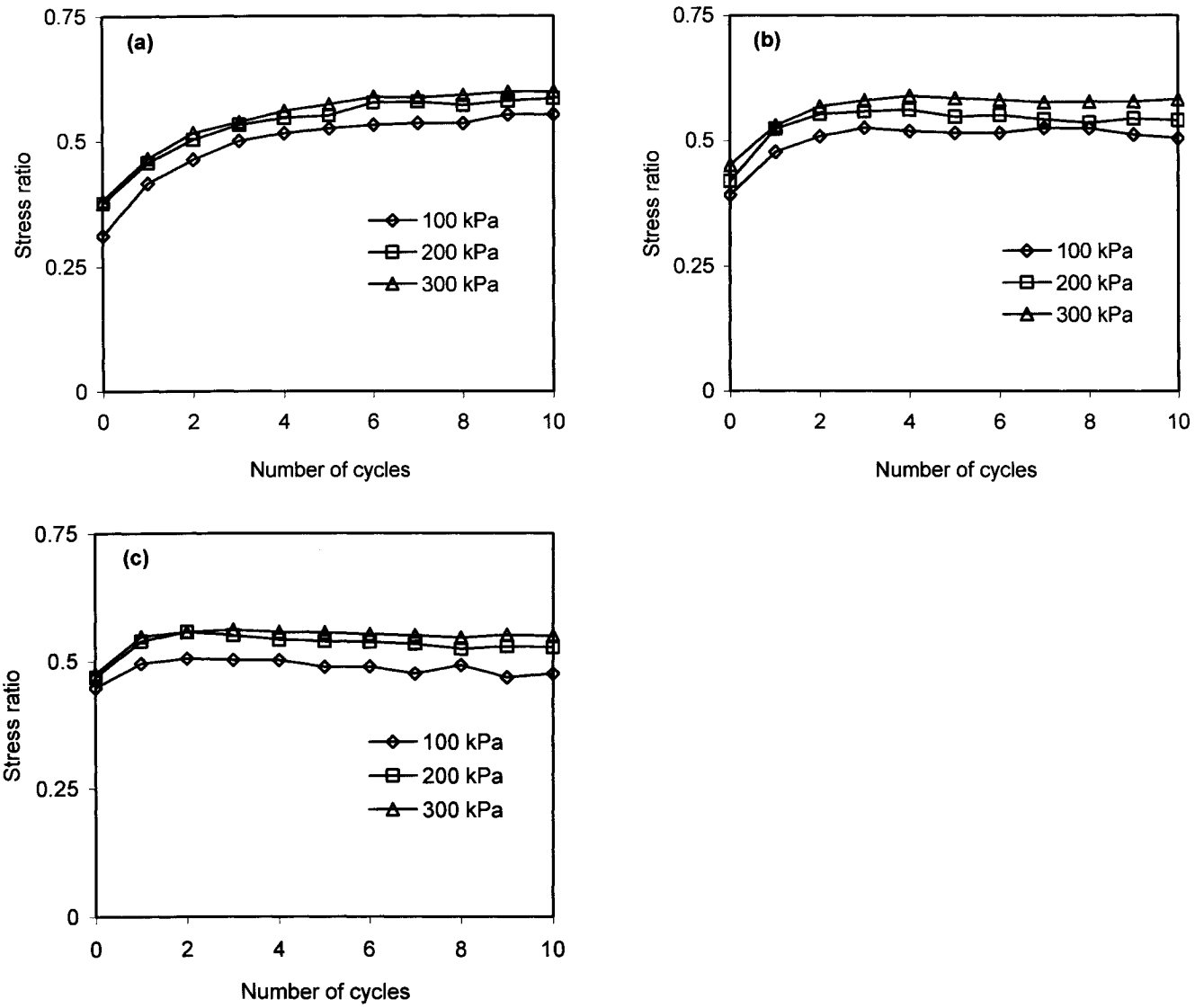

Figure 3.18 Effect of magnitude of normal stress and number of cycles on the stress ratio for the loose sand-steel plate interface: (a) A=1 mm, (b) A=2 mm, (c) A=3 mm

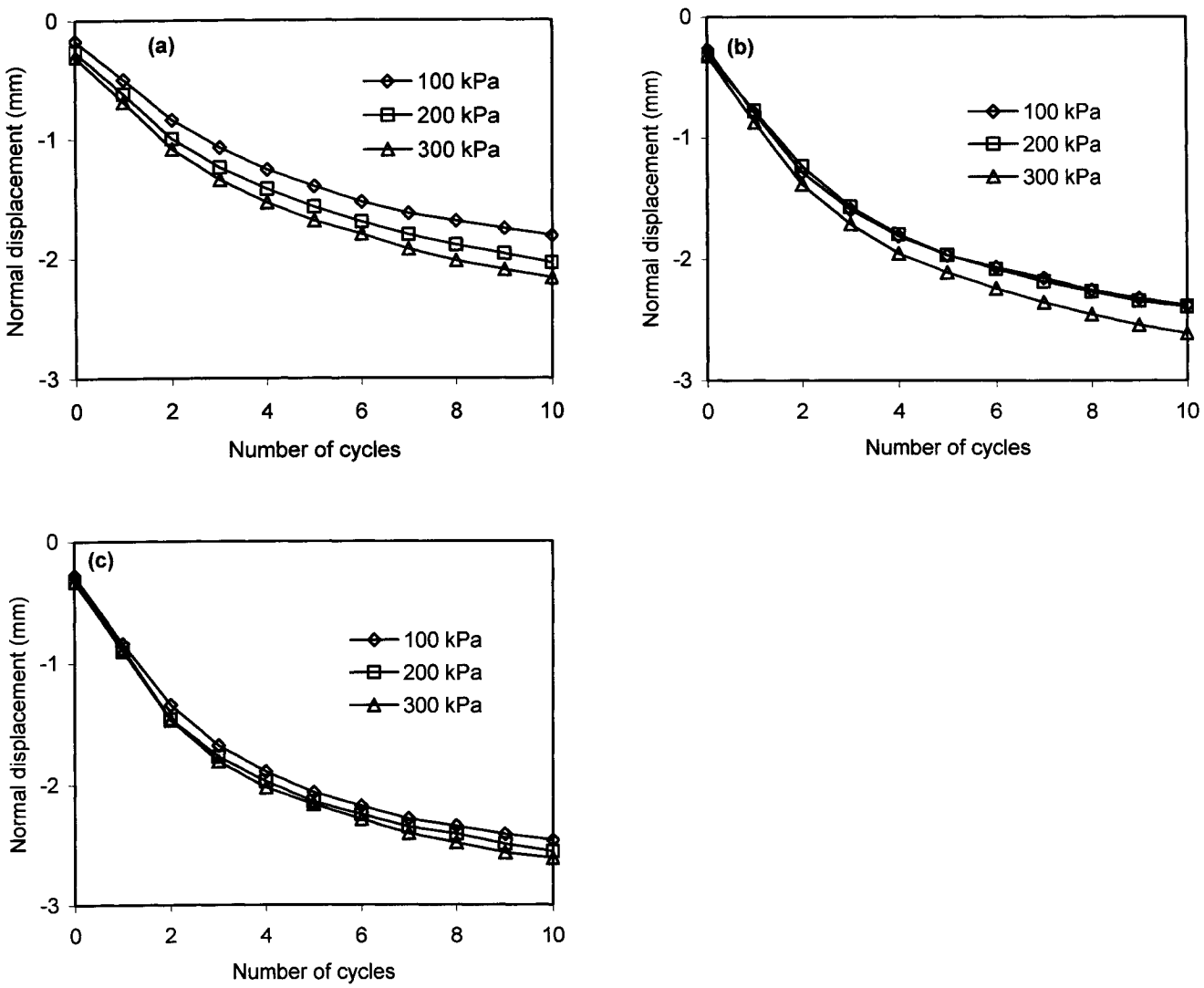

Figure 3.19 Effect of magnitude of normal stress and number of cycles on the normal displacement for the loose sand-steel plate interface: (a) A=1 mm, (b) A=2 mm, (c) A=3 mm

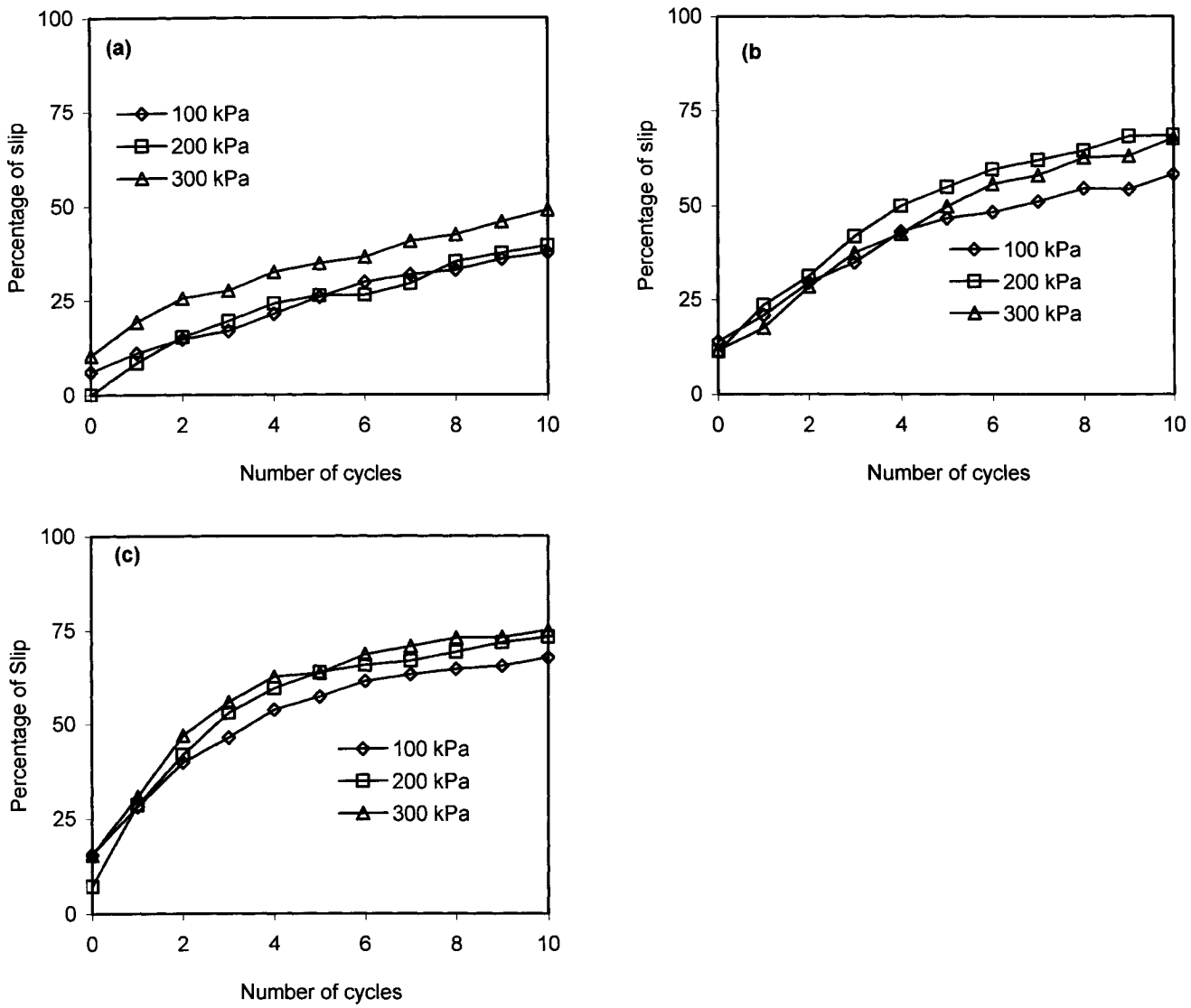

Figure 3.20 Effect of magnitude of normal stress and number of cycles on the normal displacement for the loose sand-steel plate interface: (a) A=1 mm, (b) A=2 mm, (c) A=3 mm

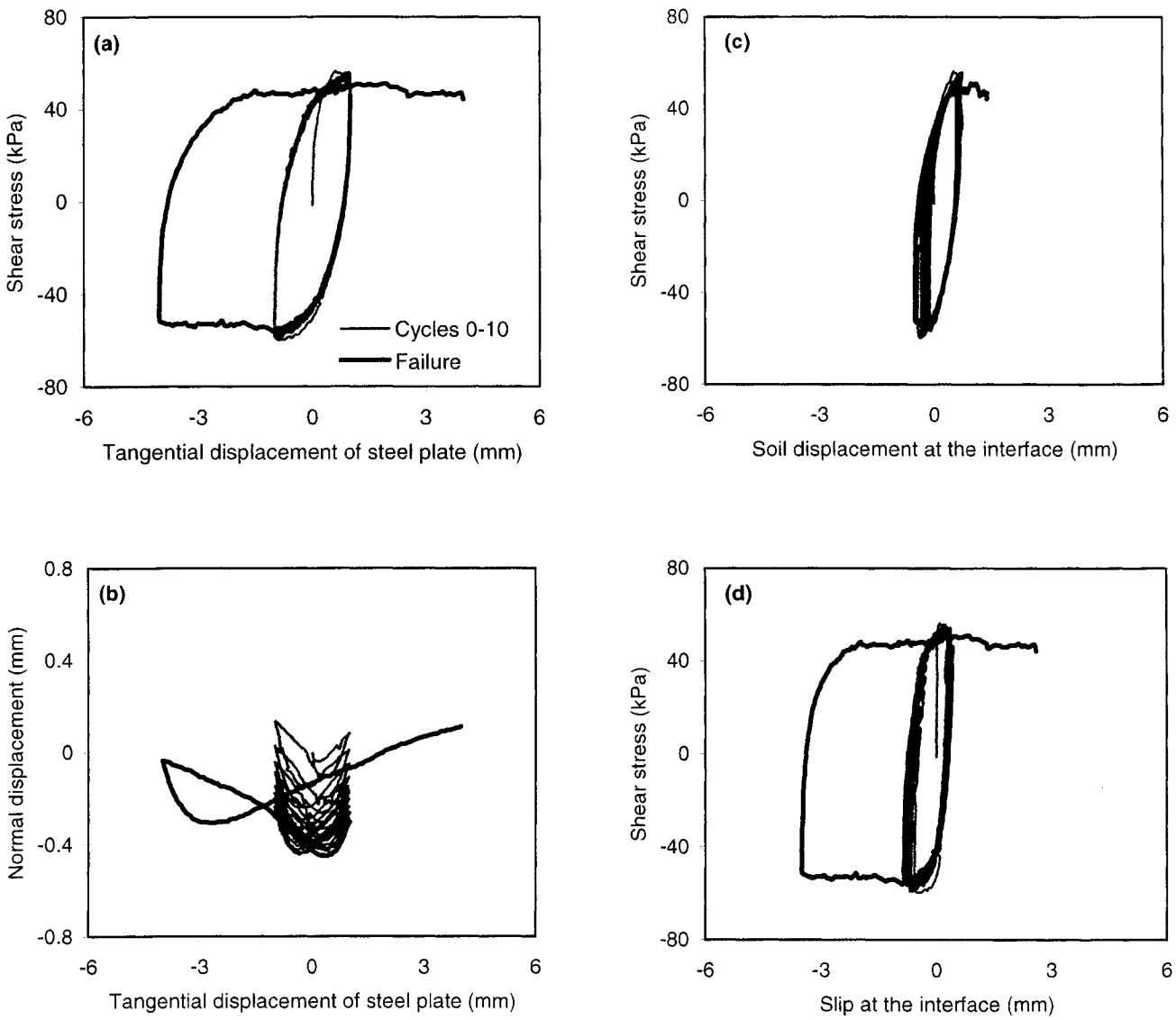

Figure 3.21 Results of the test conducted on dense sand interface with σ_n=100 kPa and A=1mm

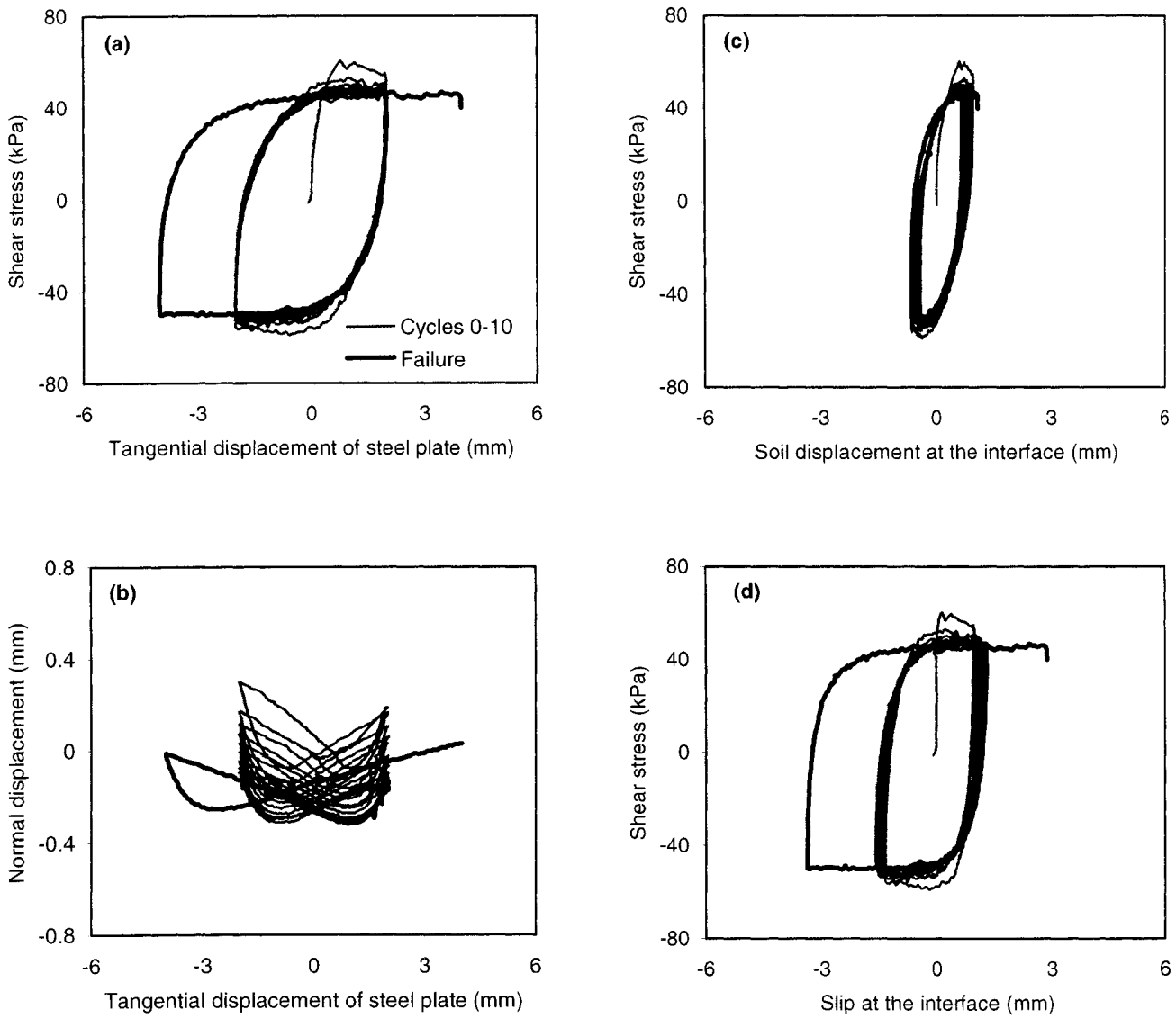

Figure 3.22 Results of the test conducted on dense sand interface with σ_n=100 kPa and A=2 mm

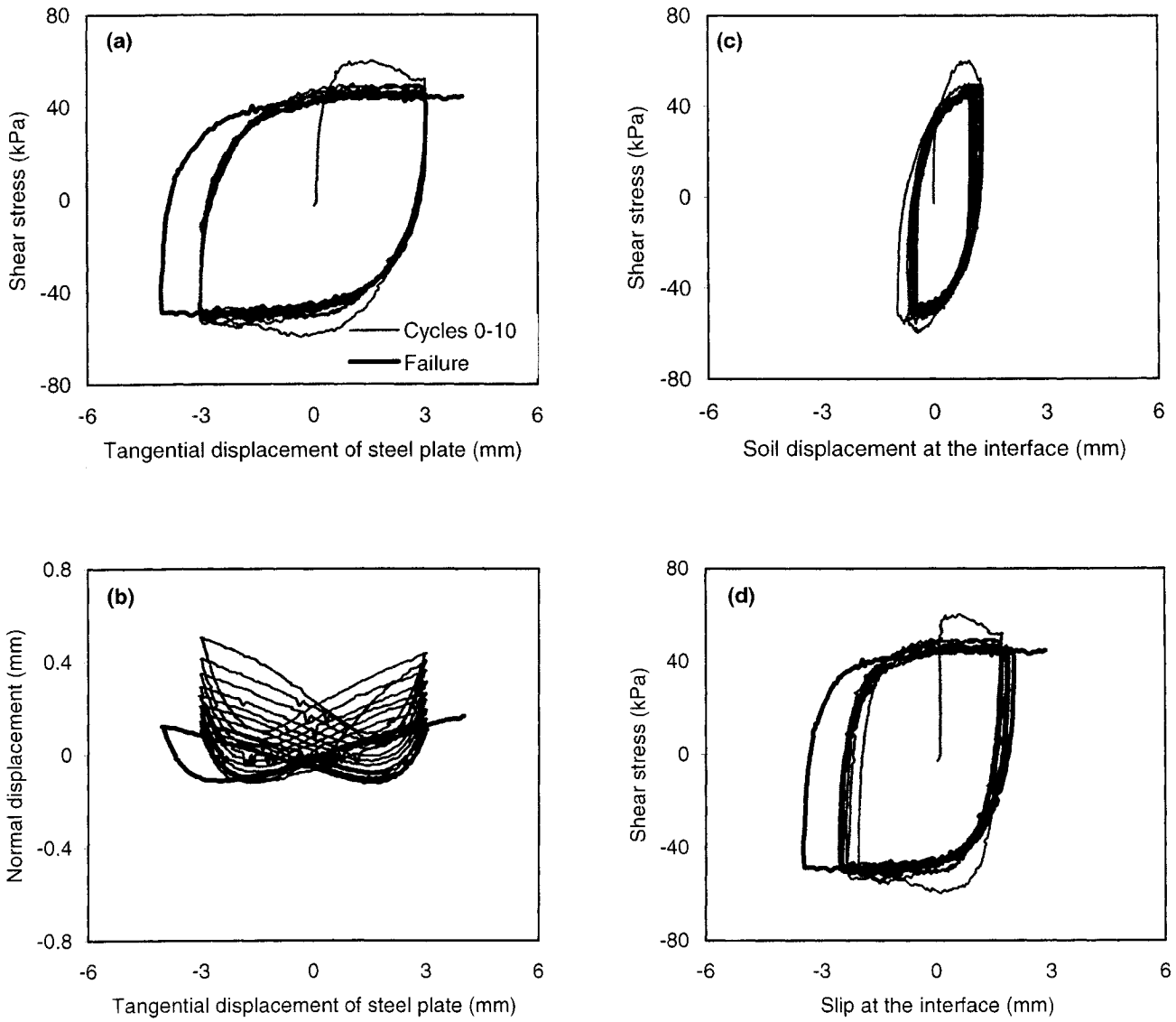

Figure 3.23 Results of the test conducted on dense sand interface with σ_n=100 kPa and A=3 mm

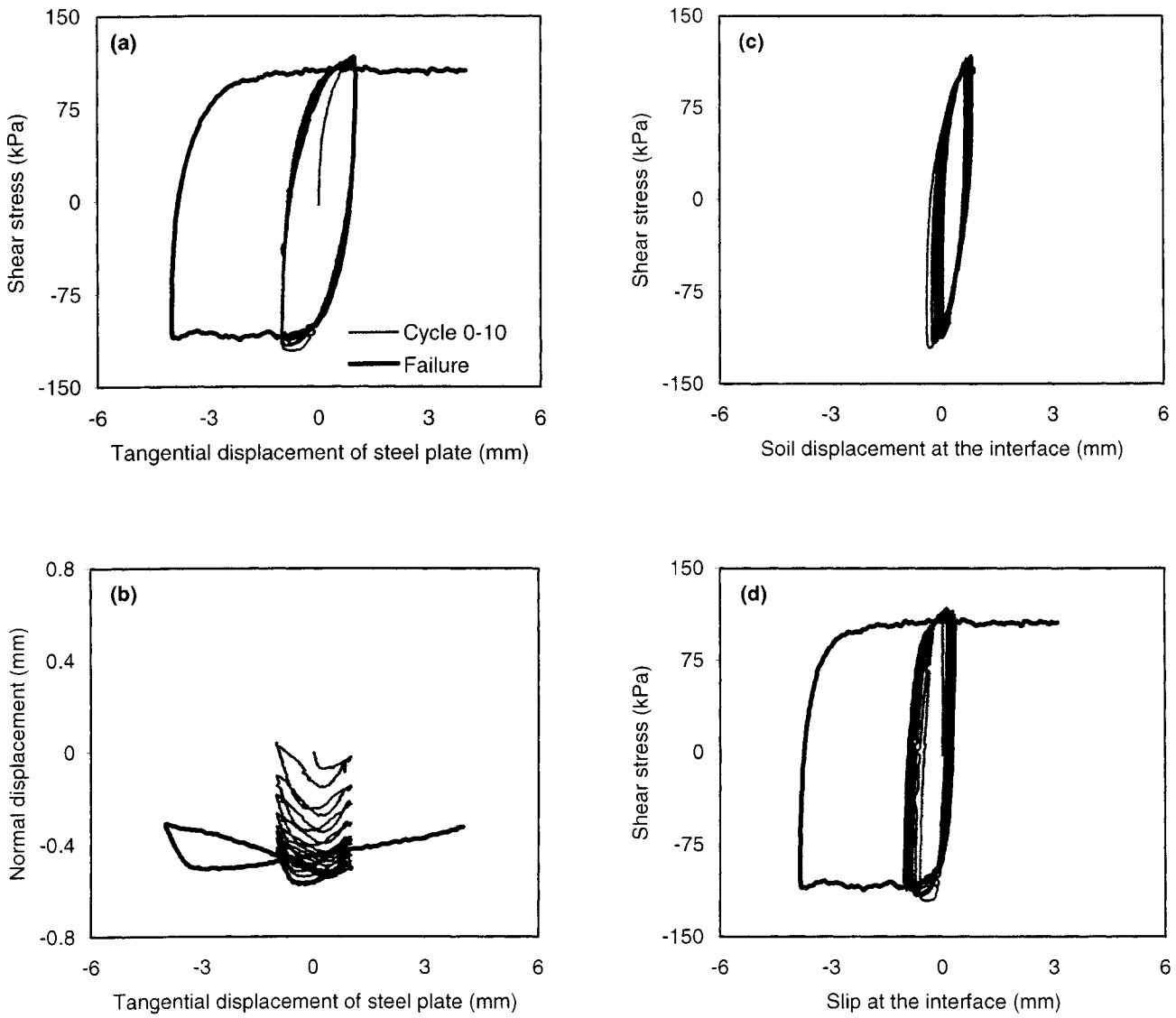

Figure 3.24 Results of the test conducted on dense sand interface with σ_n=200 kPa and A=1 mm

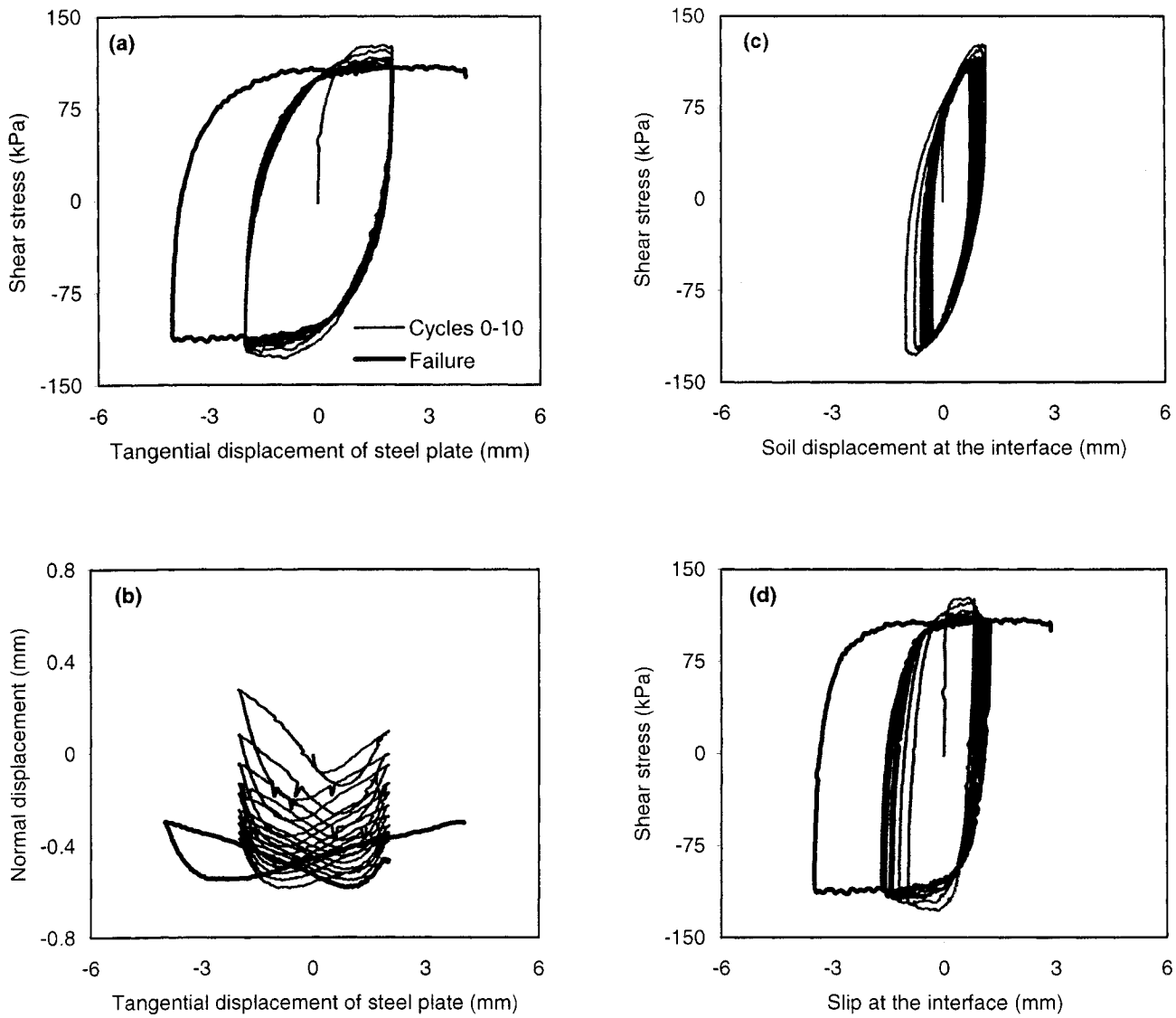

Figure 3.25 Results of the test conducted on dense sand interface with σ_n=200 kPa and A=2 mm

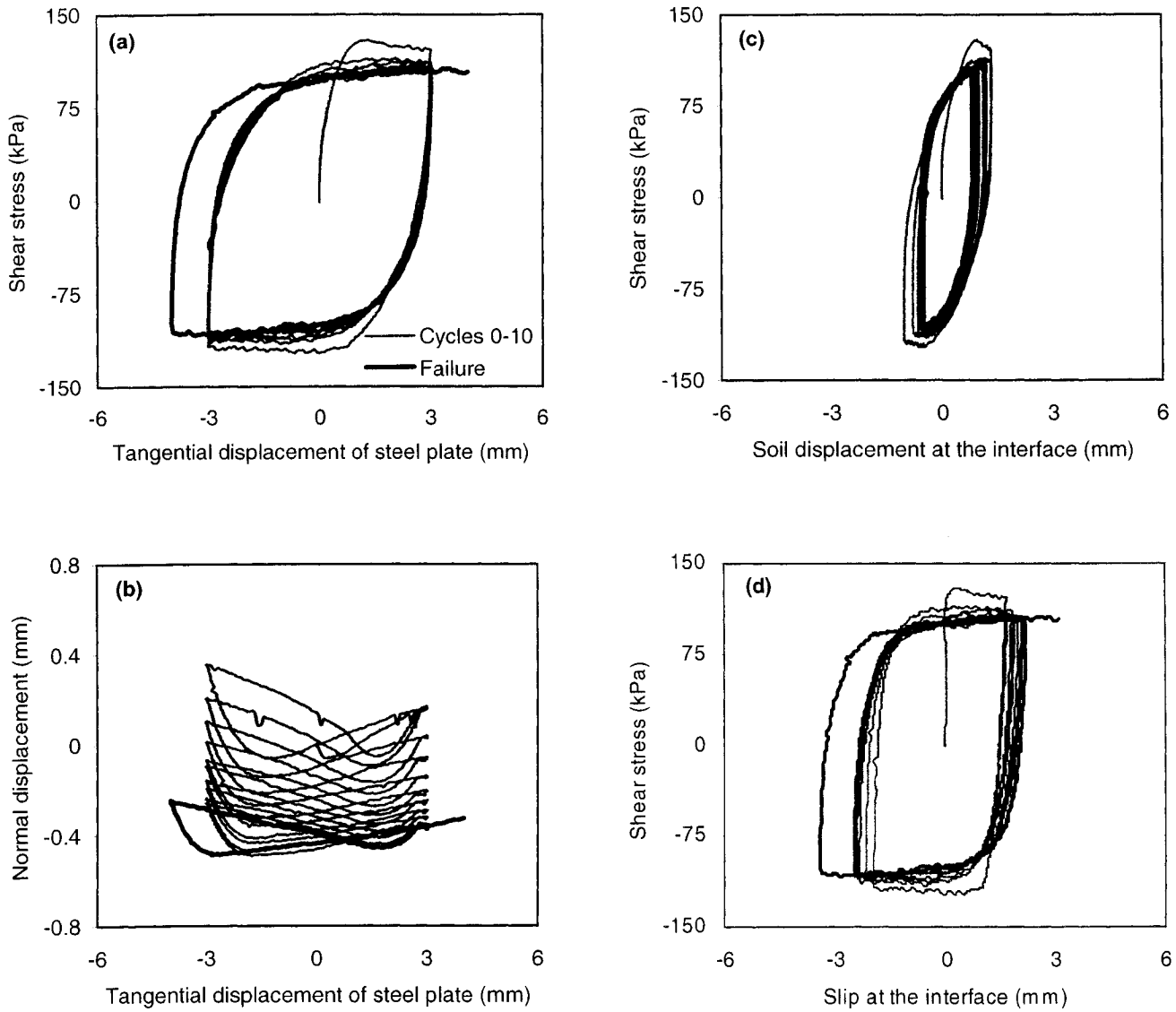

Figure 3.26 Results of the test conducted on dense sand interface with σ_n=200 kPa and A=3 mm

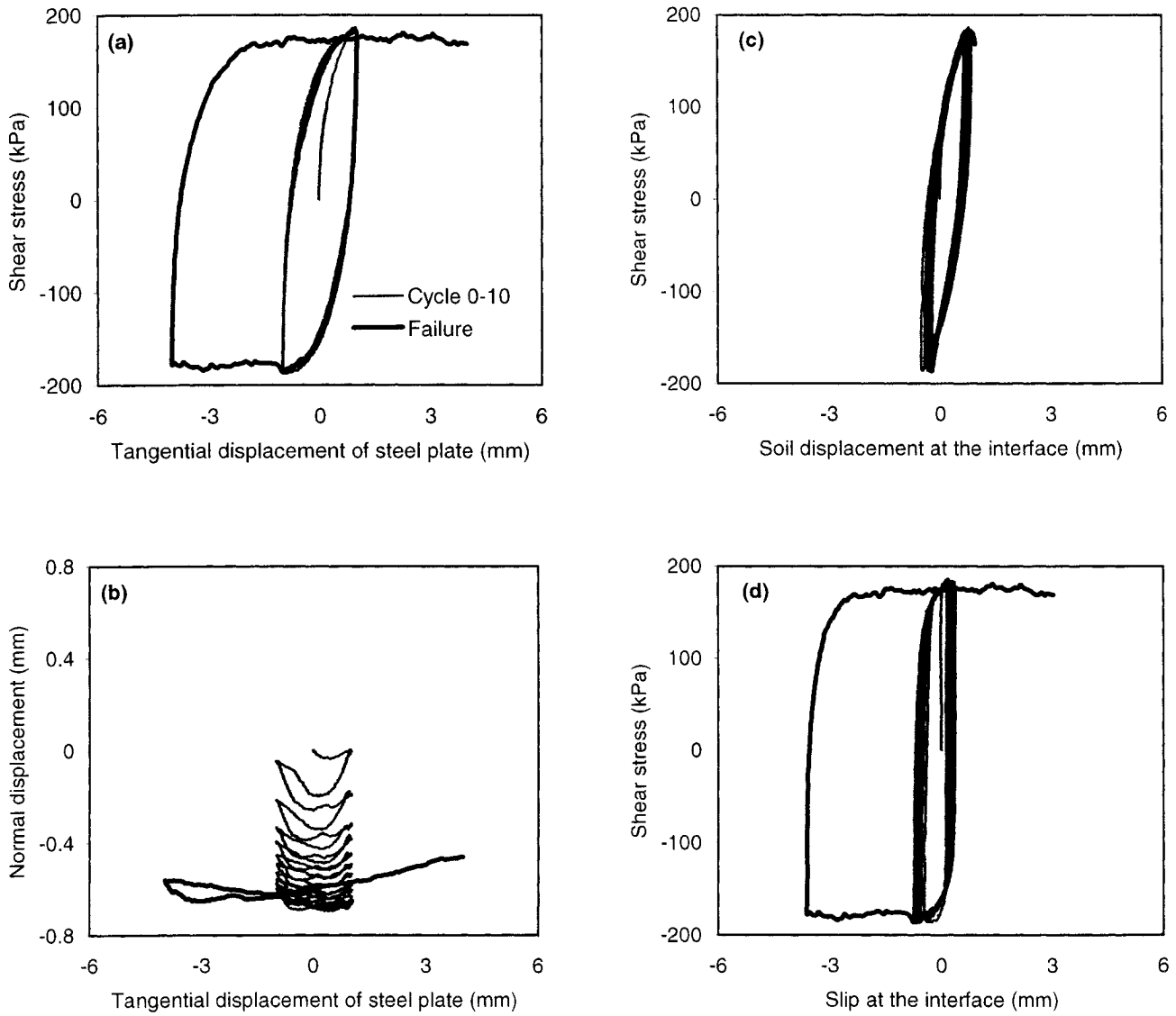

Figure 3.27 Results of the test conducted on dense sand interface with σ_n=300 kPa and A=1 mm

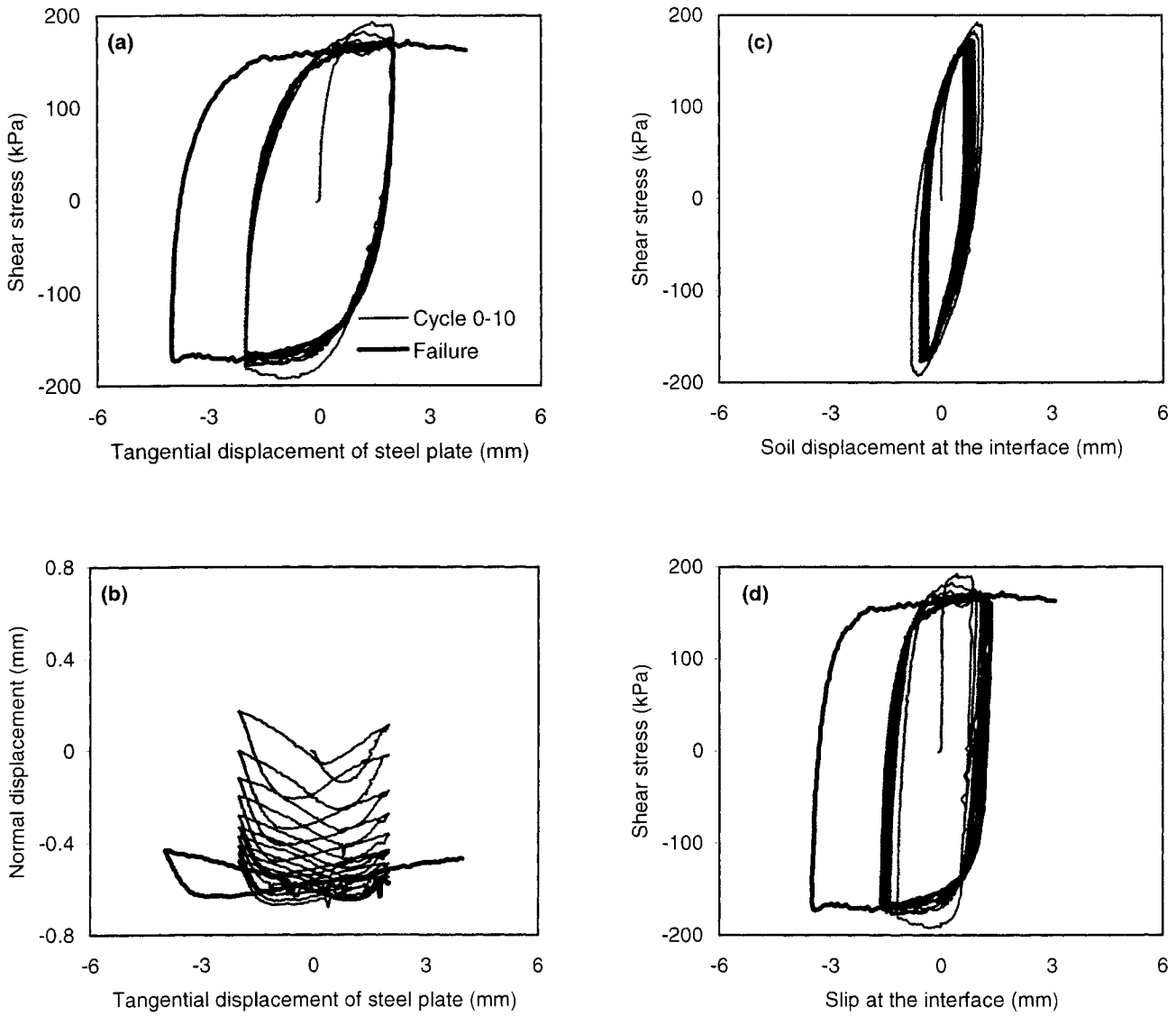

Figure 3.28 Results of the test conducted on dense sand interface with σ_n=300 kPa and A=2 mm

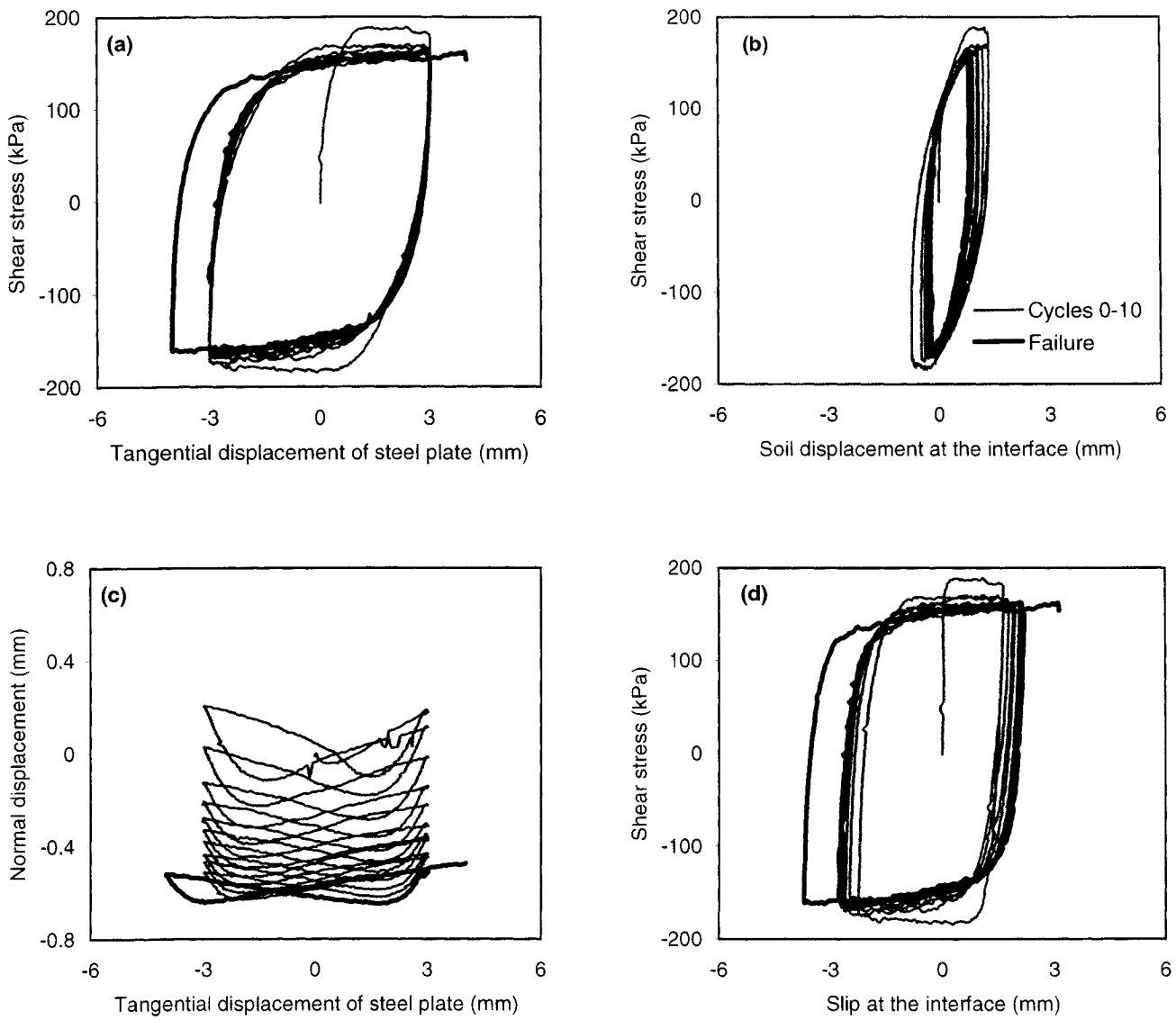

Figure 3.29 Results of the test conducted on dense sand interface with σ_n=300 kPa and A=3 mm

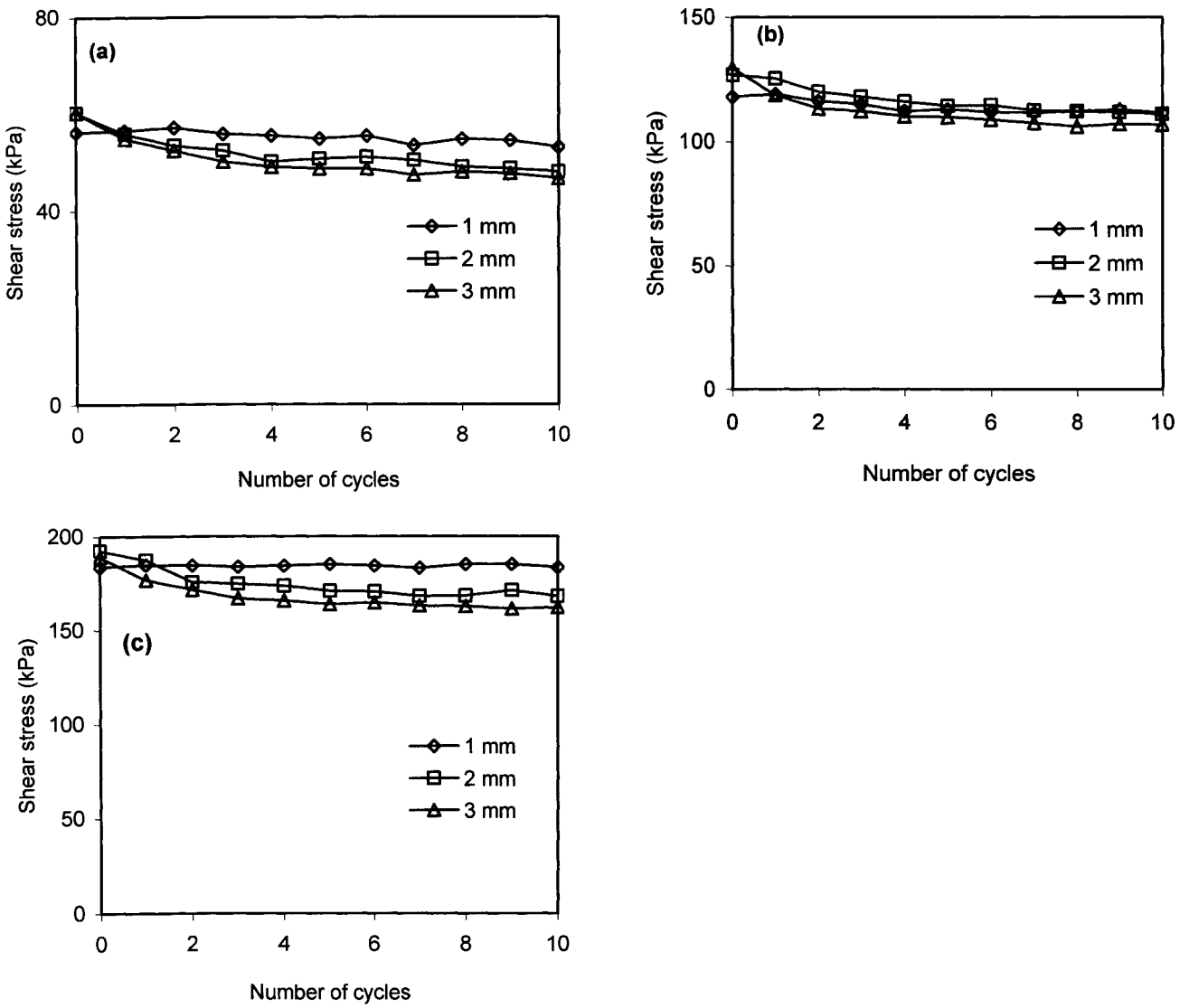

Figure 3.30 Effect of amplitude of tangential displacement and number of cycle on mobilized shear stress for the dense sand-steel plate interface: (a) σ_n=100 kPa, (b) σ_n=200 kPa, (c) σ_n=300 kPa

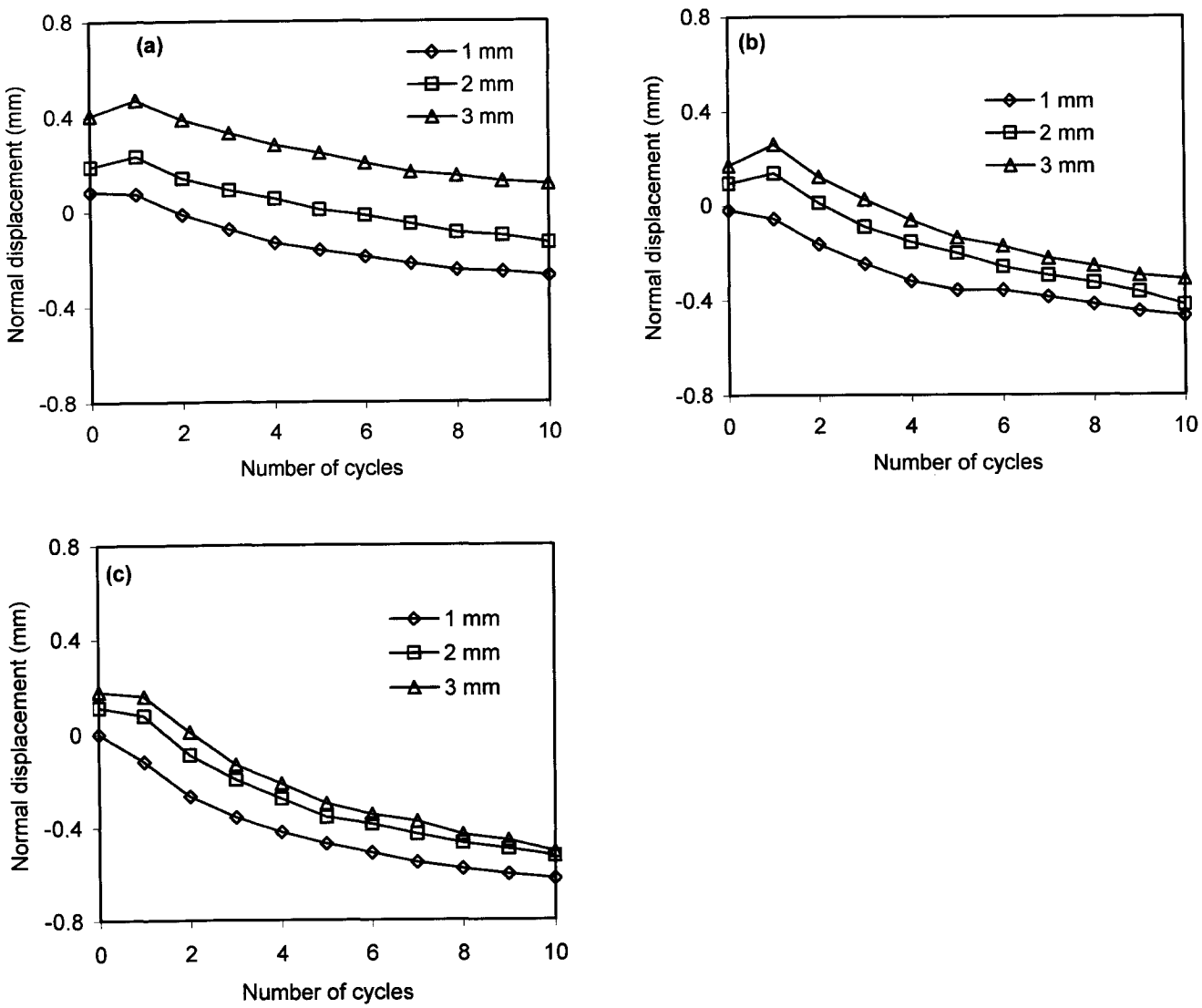

Figure 3.31 Effect of amplitude of tangential displacement and number of cycle on the normal displacement for the dense sand-steel plate interface: (a) σ_n=100 kPa, (b) σ_n=200 kPa, (c) σ_n=300 kPa

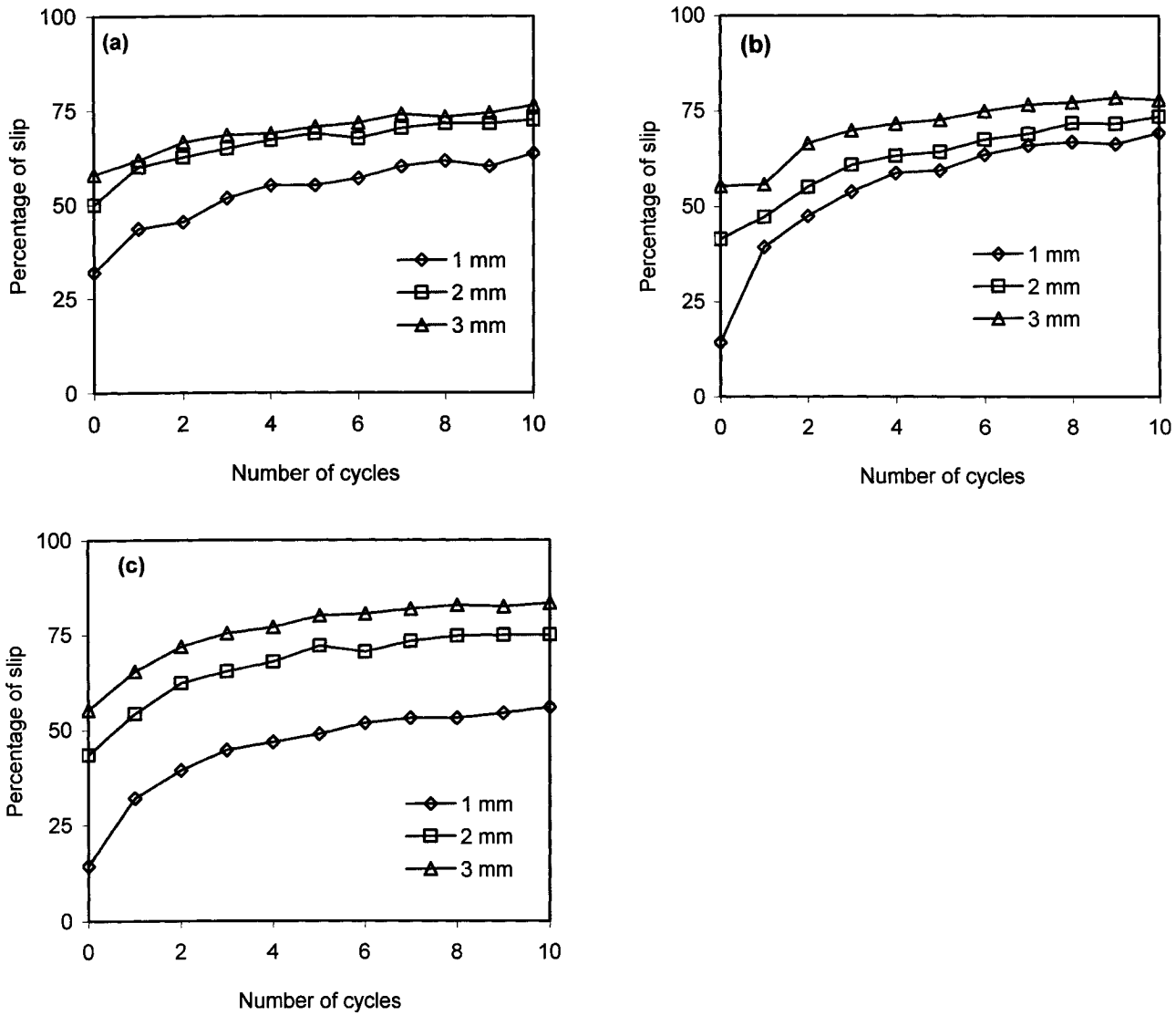

Figure 3.32 Effect of amplitude of tangential displacement and number of cycles on the percentage of slip for the dense sand-steel plate interface: (a) σ_n=100 kPa, (b) σ_n=200 kPa, (c) σ_n=300 kPa

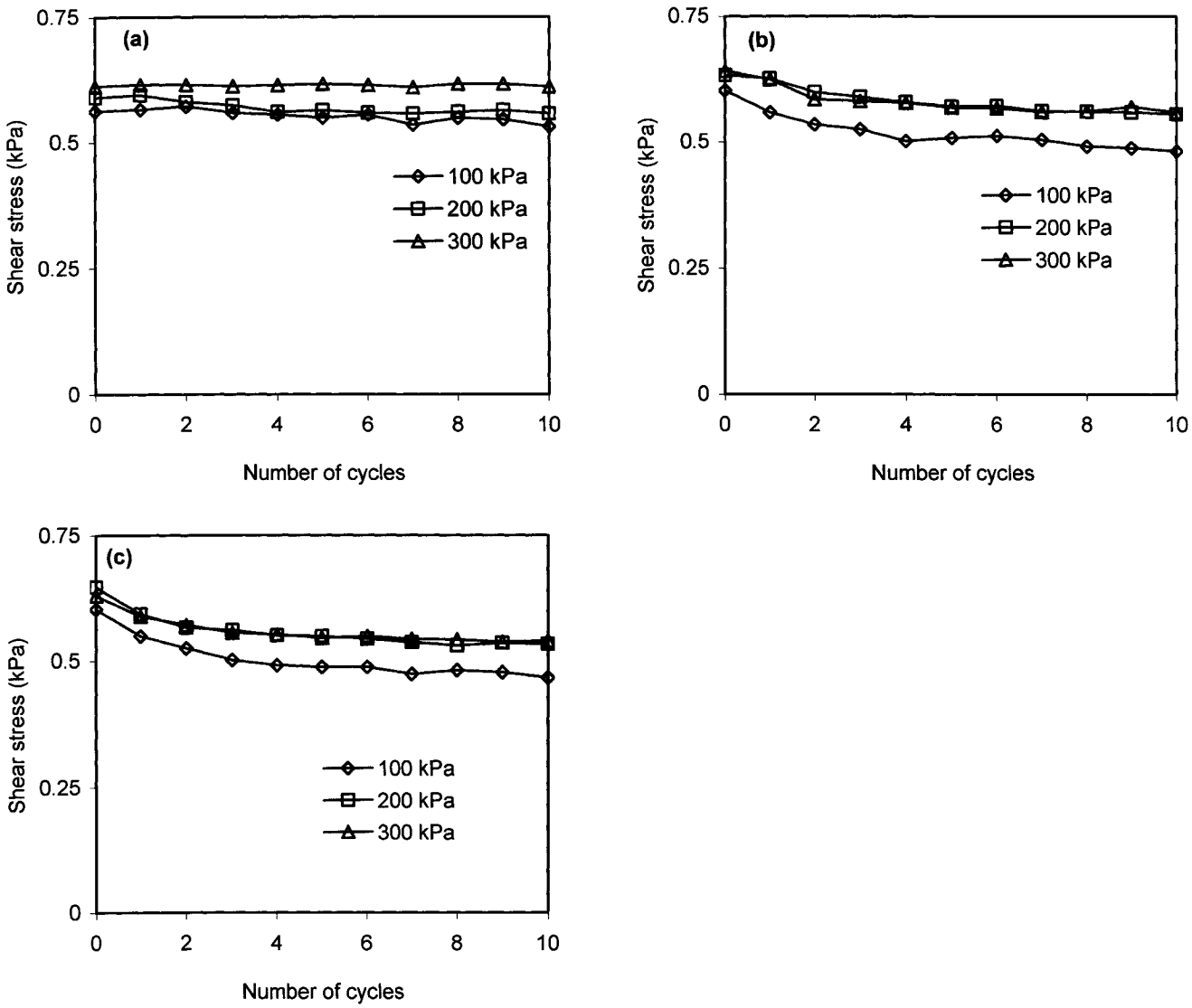

Figure 3.33 Effect of magnitude of normal stress and number of cycles on the stress ratio for the dense sand-steel plate interface: (a) A=1 mm, (b) A=2 mm, (c) A=3 mm

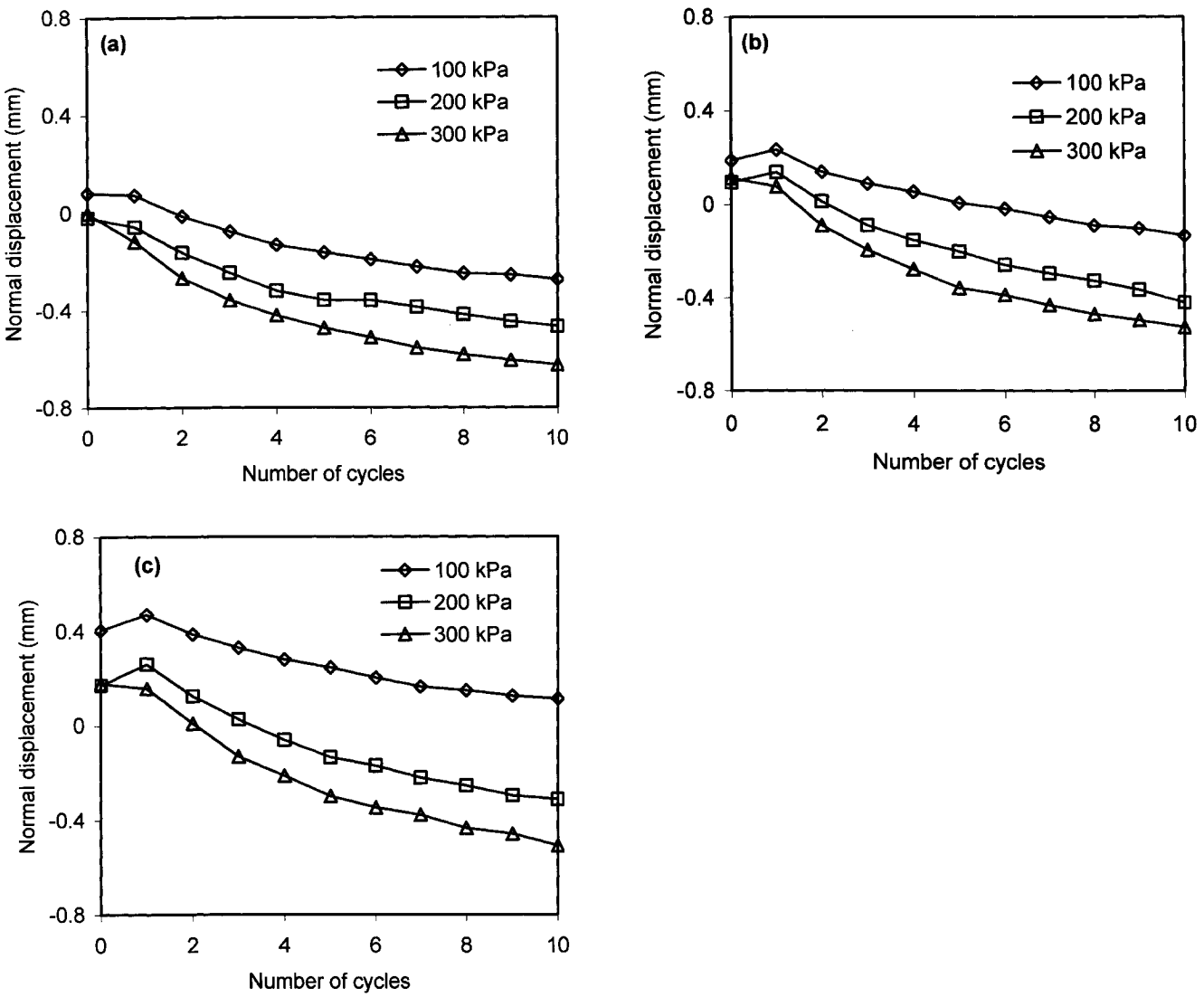

Figure 3.34 Effect of magnitude of normal stress and number of cycles on the normal displacement for the dense sand-steel plate interface: (a) A=1 mm, (b) A=2 mm, (c) A=3 mm

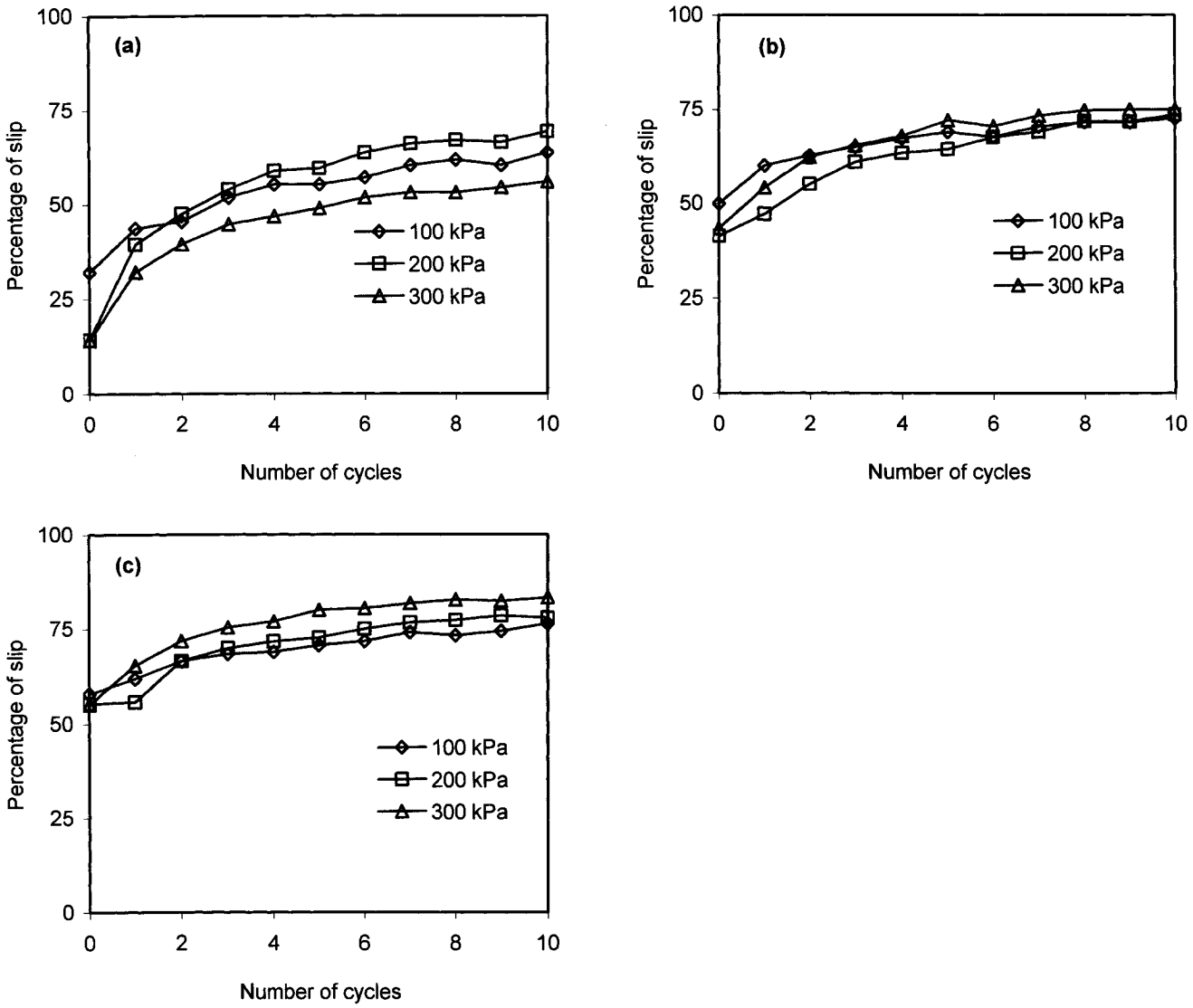

Figure 3.35 Effect of magnitude of normal stress and number of cycles on the normal displacement for the dense sand-steel plate interface: (a) A=1 mm, (b) A=2 mm, (c) A=3 mm

CHAPTER 4

VISUALIZATION OF THE MOVEMENTS OF THE STACK OF PLATES

4.1 Introduction

The interface has been defined as a thin layer of soil next to the contact surface between soil and structural members, which is characterized by strong displacement gradient and significant amount of grain rotation (Kishida and Uesugi 1987; Boulon 1989). While this definition is widely accepted, challenge has always been a determination of the thickness of the interface layer. Due to the difficulties associated with the determination of the thickness of the interface and implementations problems some interface models assumed a zero thickness interface layer. However, studies performed by various investigators (Yoshimi and Kishida, 1981; Uesugi et al. 1988; DeJong et al. 2003) outlined the existence of an interface layer with a finite thickness.

In the first part of this chapter a review of techniques used in the determination of the thickness of the interface layer is provided. In the second part the visualization technique (Li 2001) is used to determine the position of the stack of plates and the thickness of the interface layer during cyclic tests.

4.2 Literature review

A review of the methods used in the determination of the thickness of interface was presented by Uesugi et al. (1988) and Li (2001). The methods have consisted mainly in

tracking the movement of sand particles. Butterfield et al. (1970) and Andrawes and Butterfield (1973) used a stereo-photogrammetric method to measure displacement field in sand and the displacement of sand particles. De Pater and Nieuwenhuis (1986) used the double-exposure photography method to measure the displacement of sand particles. Yoshimi and Kishida (1981) used X-ray photography for measuring deformation of sand mass. They found that the displacement at the interface depended on the roughness of the contact surface. For example, for smooth surfaces the displacement consisted mostly of slip while for rough surfaces the displacement consisted of shear zone distortion. The thickness of the interface was equal to 5 to 8 times the diameter of sand particles. Vardoulakis and Graf (1985) also used the X-ray photography technique and reported a shear band layer equal to 16R where R is the radius of the sand particles.

Uesugi et al. (1988) modified a simple shear soil container by placing a glass window on the front face of the stack of plates. Close-up pictures of the sand particles were taken at several stages in order to determine the movement of the sand particles. Uesugi et al. (1988) confirmed the findings of Yoshimi and Kishida (1981) by reporting that the formation of a shear zone depended on the roughness of the surface. A shear zone formed along a rough interface but for a smooth interface there was no shear zone formation. In addition, their results showed that the thickness of the interface layer was not constant but varied with the amplitude of tangential displacement of the steel plate. The thickness of the interface layer was in general equal to 5 times the diameter of sand particles.

Evgin et al. (2003) used the technique proposed by Uesugi et al. (1988) but the stack of plates was replaced by a rigid box. They measured the translations and rotations of sand particles and they reported that particle movements depended on their position in the soil container and soil fabric. For example, particles located near the contact surface moved more than those away from the contact surface. Particle rotation took place to some extent.

Hu and Pu (2003) used the same technique and reported the existence of a critical relative roughness (R_{cr}) beyond which there is strain localization near the interface and the formation of a shear zone. In their study a value of 0.1 was reported for the critical relative roughness and an interface layer equal to 5 times the mean diameter of sand particles was reported.

The techniques which track the movements of sand particles are complicated and time consuming. Li (2001) proposed instead the visualization of the movement of the stack of plates to provide information related to the interface zone. The thickness of the interface layer increased with the tangential displacement. In addition, the thickness of the interface layer depended on the sand density and the magnitude of normal stress. For medium dense sand the thickness of the interface layer was 7 to 8 times D_{50} while for dense sand the thickness of the interface was 4 to 5 times D_{50}.

DeJong et al. (2003) used a velocity measurement technique known as the Particle Image Velocimetry (PIV) to measure soil deformations. This technique was used to determine the evolution of shear zone in monotonic and cyclic tests. They found that the thickness of the interface layer depended on the type of sand. For tests with uncemented silica sand, the thickness of the shear zone increased with the tangential displacement and reached a maximum value equal to 8 times the mean diameter at high cumulative tangential displacement. The shear zone in the test conducted with Legendre sand, although not well-defined was larger than the shear zone in the tests conducted with uncemented silica sand. As opposed to tests on uncemented silica sand, tests on Legendre sand showed a decrease of the thickness of shear zone with the number of cycles.

4.3 Visualization of the movements of the stack of plates

The procedure used for the visualization of the movements of the stack of plates is similar to that described by Li (2001). The front face of the stack of plates was marked

with two vertical lines. During a test, a digital camera NIKON COOLPIX 5000 was used to take pictures of the stack of plates. The pictures were then transferred in a computer and the software "Digitizer" was used to determine the position of the stack of plates. In this section the positions of the stack of plates in the cyclic tests conducted on loose and dense sand interfaces under a constant normal stress of 300 kPa and amplitude of tangential displacement of 3 mm are presented. Pictures of the stack of plates were taken first before the beginning of the test (Stage 0) and at each reversal of the loading direction (Stages 1 to 21 when the tangential displacement of the steel plate was equal to ± 3 mm). Close-up pictures of a corner of the stack of plates taken during the tests on loose and dense sand interfaces are shown in Figure 4.1 and Figure 4.3, respectively. Figures 4.2 and 4.4 show the digitized positions of selected aluminum plates for the tests on loose and dense sand interfaces, respectively.

Figures 4.2 and 4.3 indicate non-symmetry of the positions of the stack of plates. Further investigation would be necessary to explain this non-symmetry. These figures show that the displacement gradients are higher near the contact surface. Hence it is possible to distinguish two zones: an interface layer and a soil mass. A visual inspection of Figures 4.2 and 4.4 indicates that the interface layer is larger and better-defined for the test on loose sand interface. This observation is in agreement with the results presented by Li (2001). However, the thickness of the interface layer reduces slightly as the number of cycle increased. The thickness of the interface layer varied between 4 and 6 mm (3 to 4.4 D_{50}) for the loose sand interface and 2 and 4 mm (1.5 to 3 D_{50}) for the dense sand interface. The thickness observed in these tests will be used when the experimental results are simulated numerically.

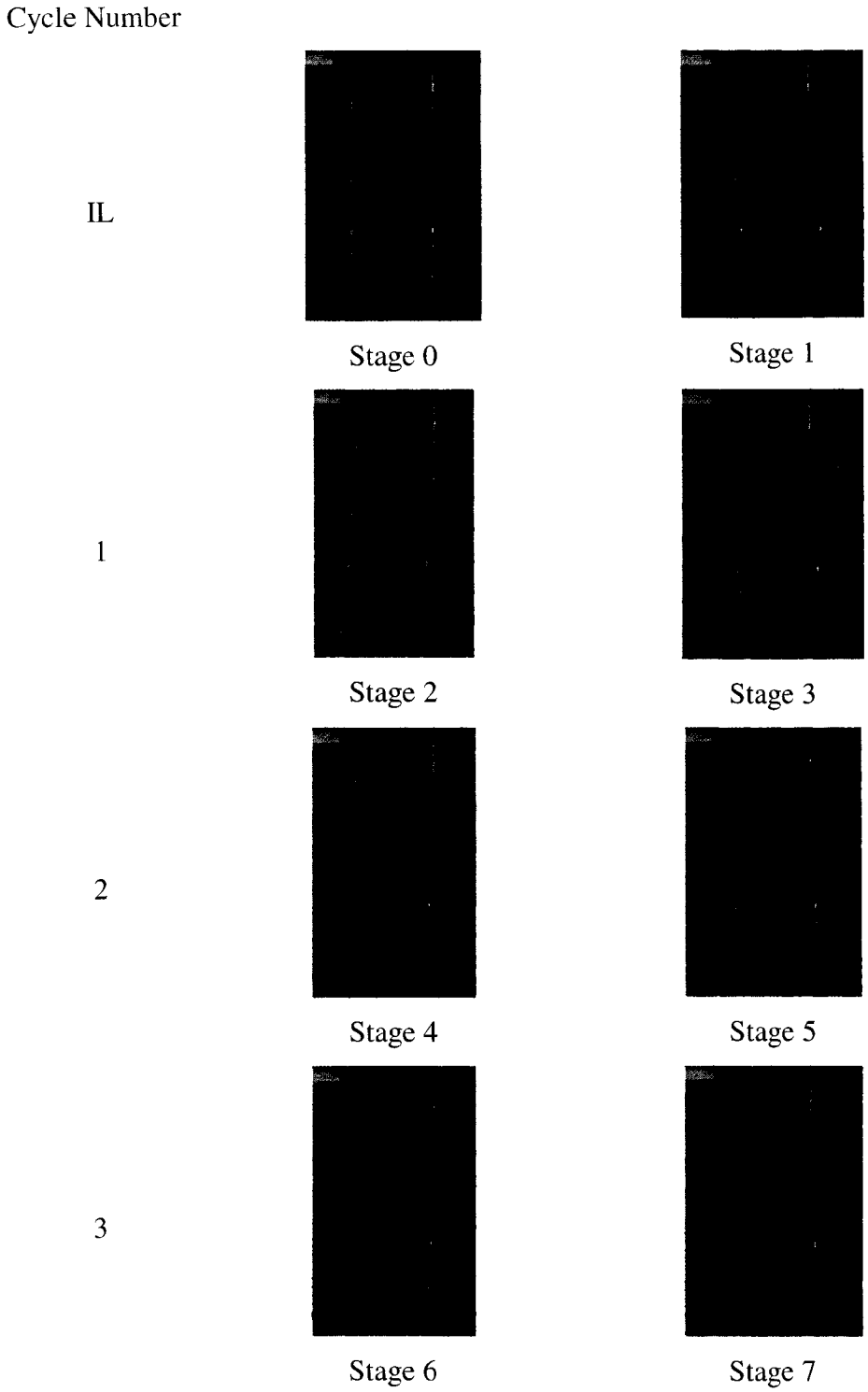

Figure 4.1 Photographs of displacements of stack of plates during cyclic test on loose sand interface σ_n=300 kPa, A=3 mm.

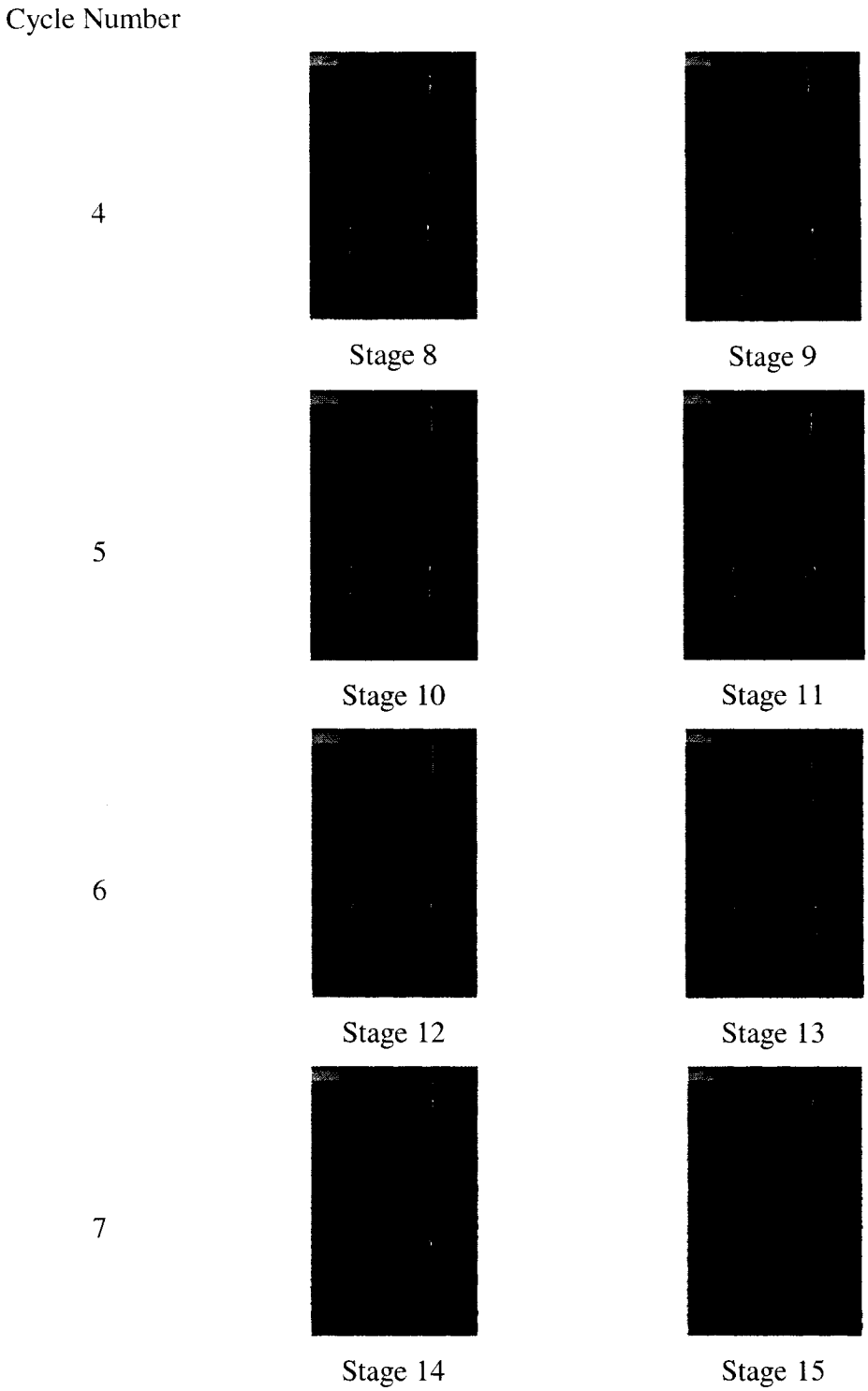

Figure 4.1 (continued) Photographs of displacements of stack of plates during cyclic tests on loose sand interface σ_n =300 kPa, A=3 mm.

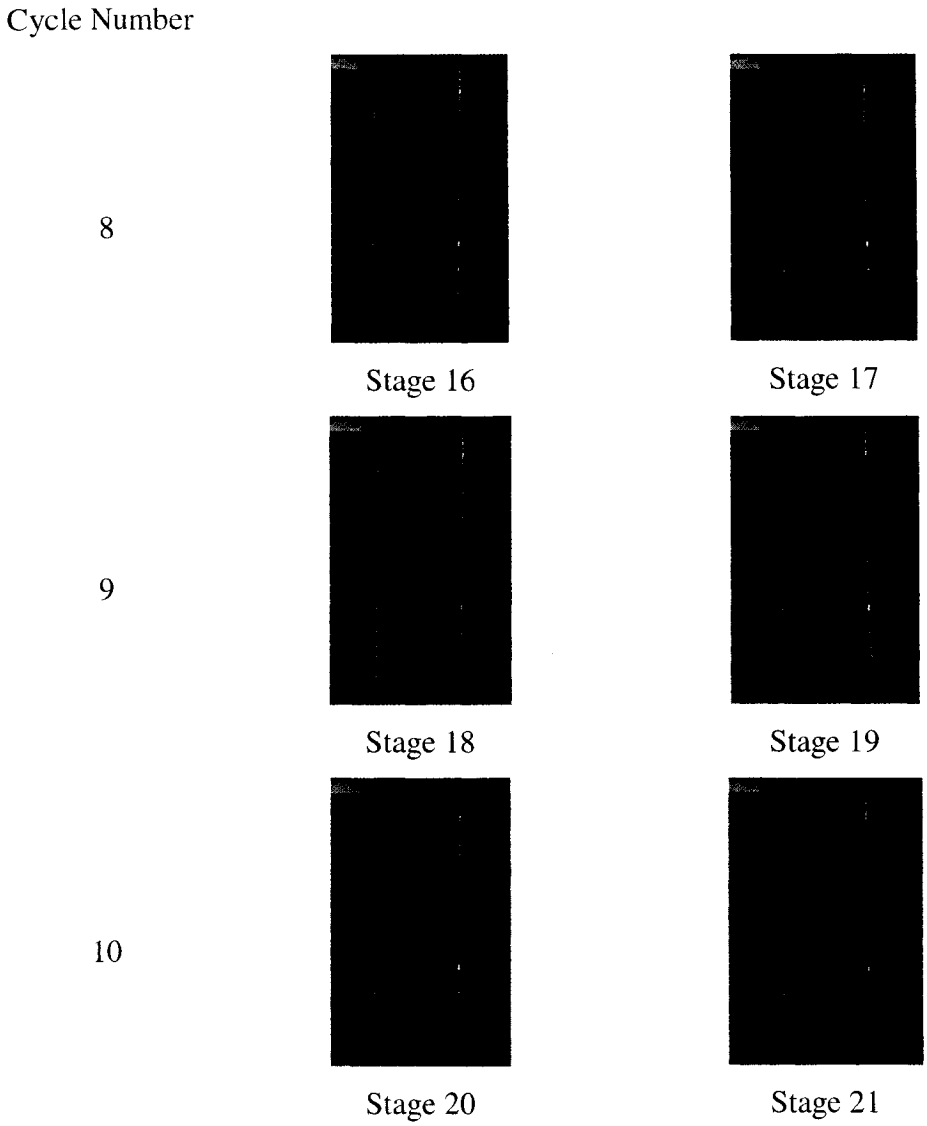

Figure 4.1 (continued) Photographs of displacements of stack of plates during cyclic tests on loose sand interface σ_n=300 kPa, A=3 mm.

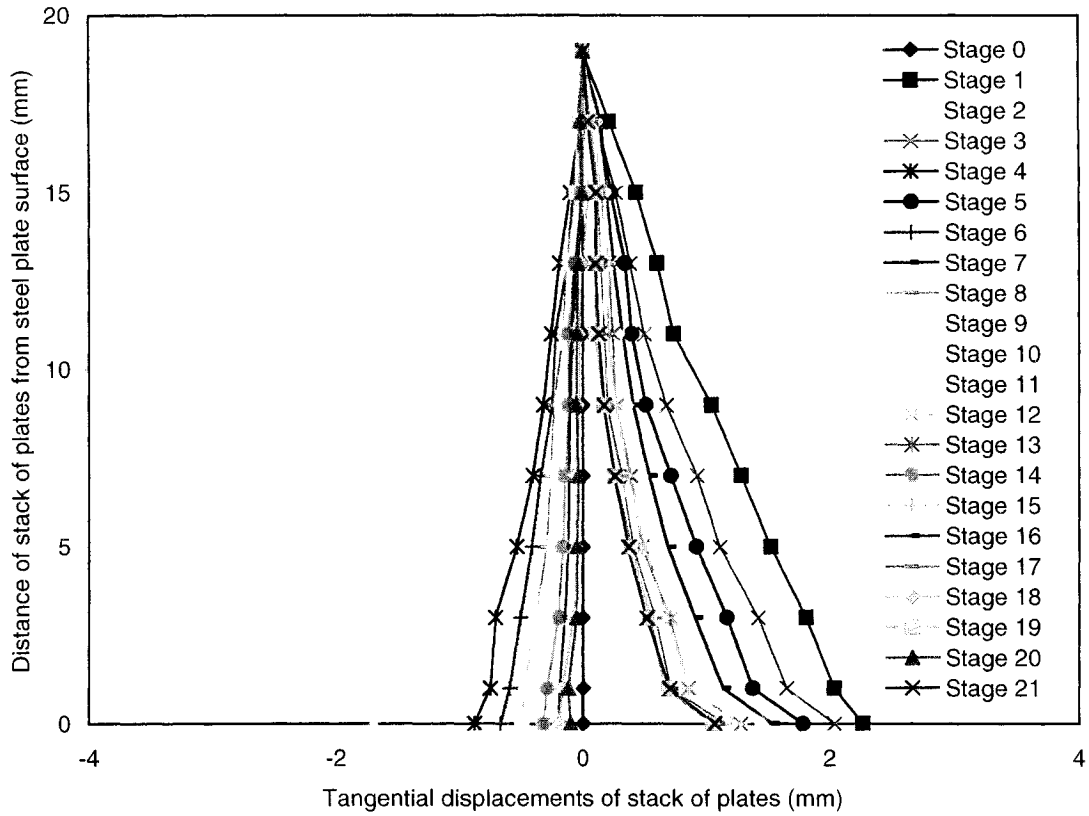

Figure 4.2 Digitized positions of the stack of plates for during cyclic test on loose sand interface σ_n=300 kPa, A=3 mm

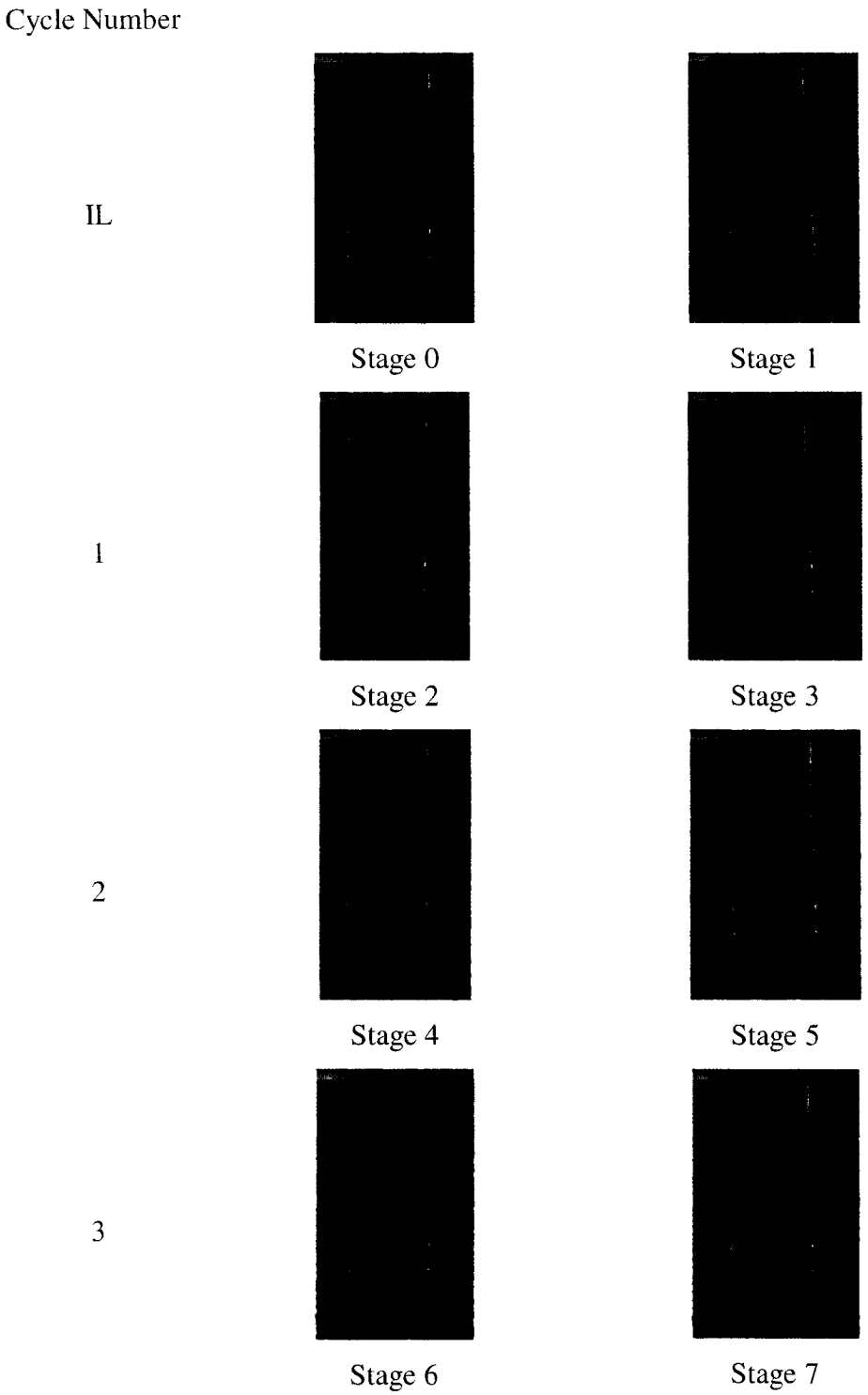

Figure 4.3 Photographs of displacements of stack of plates during cyclic tests on dense sand interface σ_n=300 kPa, A=3 mm.

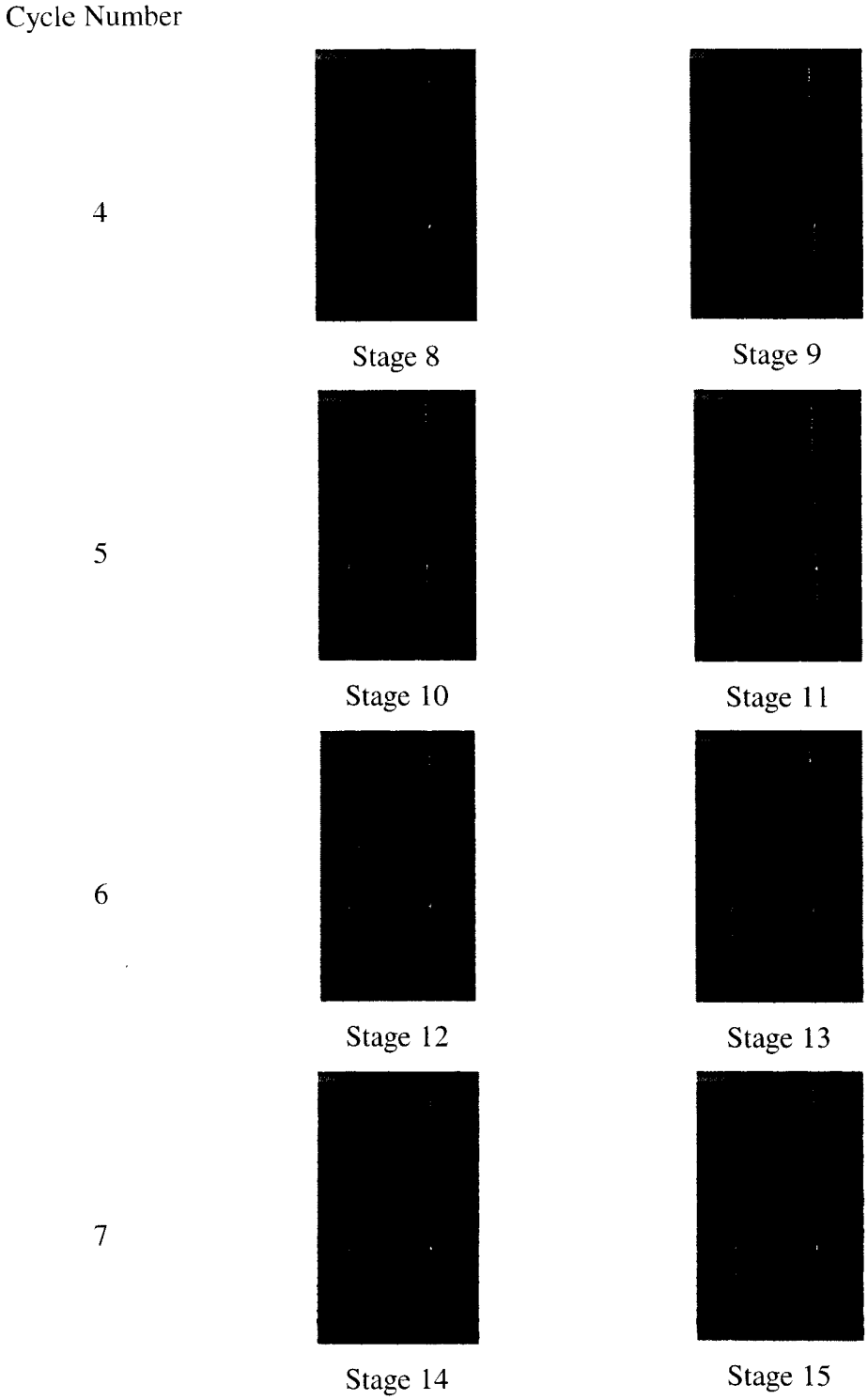

Figure 4.3 (continued) Photographs of displacements of stack of plates during cyclic tests on dense sand interface σ_n=300 kPa, A=3 mm.

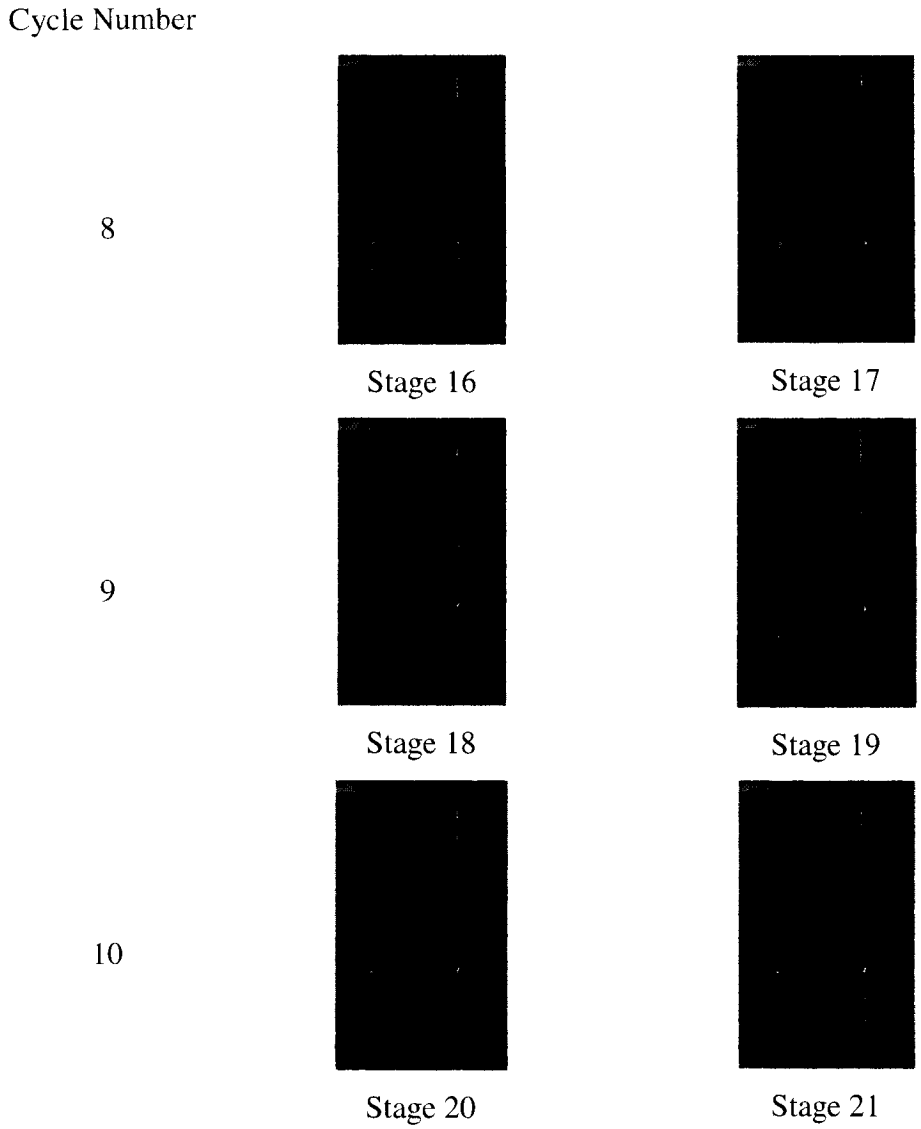

Figure 4.3 (continued) Photographs of displacements of stack of plates during cyclic tests on dense sand interface σ_n=300 kPa, A=3 mm.

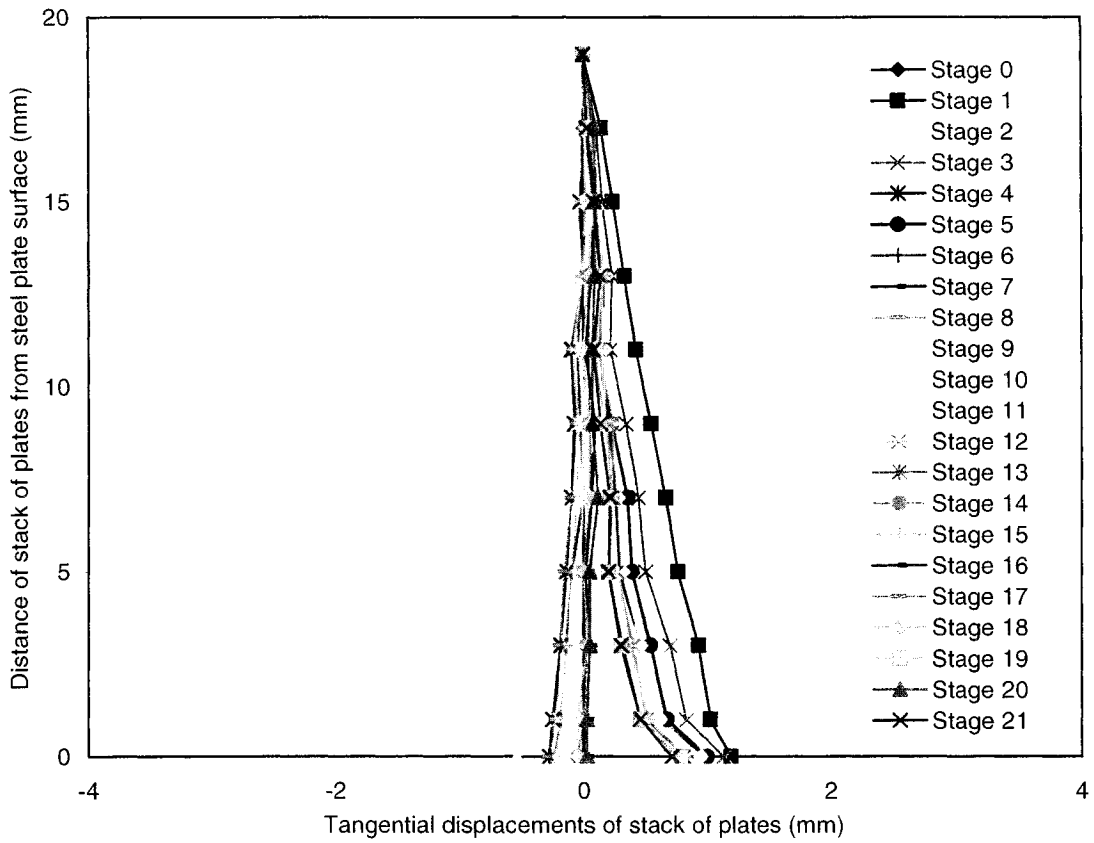

Figure 4.4 Digitized positions of the stack of plates for during cyclic test on dense sand interface σ_n=300 kPa, A=3 mm

PART 2
NUMERICAL SIMULATION
CHAPTERS 5-7

CHAPTER 5

REVIEW OF CYCLIC MODELS FOR THE BEHAVIOUR OF SOILS AND INTERFACES

5.1 Introduction

Several experimental studies on soils and soil-structure interfaces provided valuable information for the development of models to predict the behaviour of soils and interfaces. The earlier models developed for soils were based on the theory of elasticity. However, these models are incapable of reproducing some important features of soil behaviour such as irreversible deformations and path dependent behaviour. Therefore, a theory capable of reproducing these features was necessary. The theory of plasticity provided an answer to many of the shortcomings of the theory of elasticity. The theory of plasticity, devised initially to model the behaviour of metals, was extended by Drucker et al. (1957) to model the behaviour of soils. Owing to this extension and the evolution of the capacities of modern computers, many soil models have emerged: Cam-Clay (Schofield and Wroth, 1968), modified Cam-Clay (Roscoe and Burland, 1968), and Lade and Duncan (1975). These models are often referred to as classical plasticity models. They were used successfully to predict the behaviour of soils subjected to monotonic loads. However, the original versions of these models were not capable of handling the behaviour of soils subjected to cyclic loads.

Modifications were made to the classical theory of plasticity in order to predict the cyclic behaviour of soils. These modifications resulted in the development of models such as the nested surfaces and bounding surface models. This chapter discusses the cyclic models

developed for soils and interfaces. Since most cyclic models were in part based on the theory of plasticity, the salient features of this theory are summarized.

5.2 Theory of Plasticity

In contrast to elastic materials, plastic materials undergo irreversible deformations when they are subjected to external loads. Geological materials (i.e. sands, gravels, clays) are excellent examples of plastic materials which deform plastically even at low load range. In the theory of plasticity, deformations are assumed to be the sum of reversible elastic deformations and irreversible plastic deformations (Equation 5.1).

$$d\boldsymbol{\varepsilon} = d\boldsymbol{\varepsilon}^e + d\boldsymbol{\varepsilon}^p \qquad 5.1$$

where

$\boldsymbol{\varepsilon}$ =total strain, $\boldsymbol{\varepsilon}^e$ =elastic strain, and $\boldsymbol{\varepsilon}^p$ = plastic strain. The superscripts e and p stand for elastic and plastic respectively.

Besides this assumption, models based on the theory of plasticity require the definition of a yield (loading) surface, a hardening rule, and a flow rule.

5.2.1 Yield (loading) surface

A yield surface delimits the region of pure elastic deformation from the region where plastic deformations may occur. In other words, only elastic deformations are allowed inside the yield surface. The yield surface is often expressed mathematically as a function of the stress tensor, $\boldsymbol{\sigma}$, the plastic strain, $\boldsymbol{\varepsilon}^p$, and a hardening parameter, k (Equation 5.2).

$$f = f(\boldsymbol{\sigma}, \boldsymbol{\varepsilon}^p, k) \qquad 5.2$$

Several yield surfaces that are special cases of Equation 5.2 were proposed in the literature. One may list among others the Von Mises, Tresca, Lade, and Mohr Coulomb yield surfaces. The Mohr Coulomb yield surface is often used in soil mechanics. Schofield and Wroth (1968) also proposed as part of the Cam-Clay model a yield surface derived from the concept of critical state.

The yield surface is used to define the loading criterion, which describes the conditions necessary for the occurrence of plastic deformations, and elastic deformations. The loading condition for plastic deformations is described as:

$$f = 0 \text{ and } df = \frac{\partial f}{\partial \boldsymbol{\sigma}} : d\boldsymbol{\sigma} > 0 \qquad 5.3$$

Purely elastic deformations occur when

$$f \leq 0 \text{ and } df = \frac{\partial f}{\partial \boldsymbol{\sigma}} : d\boldsymbol{\sigma} \leq 0 \qquad 5.4$$

5.2.2 Flow rules

Flow rules are used to specify the direction of plastic deformations. The theory of plasticity assumes the existence of a plastic potential function, g, to which the plastic deformations are orthogonal. This assumption is mathematically described by Equation 5.5.

$$d\boldsymbol{\varepsilon}^p = d\lambda \frac{\partial g}{\partial \boldsymbol{\sigma}} \qquad 5.5$$

where

$$d\lambda = \frac{1}{H'}\frac{\partial f}{\partial \boldsymbol{\sigma}} : d\boldsymbol{\sigma} \qquad 5.6$$

g = plastic potential function, $d\lambda$ = scalar factor of proportionality, and H' =hardening (plastic) modulus.

The combination of Equations 5.5 and 5.6 gives:

$$d\boldsymbol{\varepsilon}^p = \frac{1}{H'}\left(\frac{\partial f}{\partial \boldsymbol{\sigma}} : d\boldsymbol{\sigma}\right)\frac{\partial g}{\partial \boldsymbol{\sigma}} \qquad 5.5$$

The flow rule is said to be associated if the plastic potential function is equal to the yield surface, otherwise it is non-associated. The non-associated flow rule is most appropriate for geological materials (Chen and Muzino, 1990). However, the majority of classical plasticity models used an associated flow rule for its simplicity.

5.2.3 Hardening rules

Among the plasticity models, one may distinguish the perfectly plastic (non-hardening) models and the hardening models. Perfectly plastic models are mainly used for materials which do not harden. For these materials the size, shape, and position of the yield surface are constant (Figure 5.1a). Although experimental evidence shows that soils are hardening materials, perfectly plastic material models are often used to provide a first approximation for the behaviour of soils.

In hardening models, three rules are used to define the movement of the yield surface: isotropic hardening, kinematic hardening and mixed hardening rule. For isotropic hardening, the shape of the yield surface does not change, but its size does (Figure 5.1b). For kinematic hardening the shape and size of the yield surface are constant, but, the

surface is allowed to translate without rotation (Figure 5.1c). Mixed hardening (Figure 5.1d) is a combination of isotropic and kinematic hardening.

The hardening rule influences the ability of a model to handle cyclic loading conditions. For example, the majority of classical plasticity models failed to reproduce the cyclic behaviour of soils because they used an isotropic hardening rule instead of a kinematic hardening or mixed hardening rule.

5.3 Cyclic models for soils

5.3.1 Multi-surface models

The framework of the nested surfaces (multi-surfaces) models was independently devised by Iwan (1967) and Mròz (1967) to predict the cyclic behaviour of metals. These models, as implied by their name, used a nest (f_i, i=1...n) of yield surfaces (Figure 5.2a) as opposed to the classical plasticity models which used a single yield surface. Each surface, f_i, was associated with a hardening modulus (H_i') used for the calculation of the plastic deformations. In other words, the plastic modulus was a discrete function of the nested surfaces (Figure 5.2b). The surfaces translated only in a kinematic manner, but, they were not allowed to intersect each other (Figures 5.2c and 5.2d). Prévost (1977, 1978) extended the nested surface concept to model the undrained and drained cyclic behaviour of soils. In this extension the yield surfaces were also allowed to contract or expand (isotropic hardening).

The multi-surface models are powerful for cyclic loading. However, the main limitation of these models is the difficulty to record the size and location of each surface in a numerical analysis (Chen and Mizuno 1990).

5.3.2 Bounding surface models

A bounding surface model was initially developed for metals by Dafalias and Popov (1975) and Krieg (1975) before its extension to soils (Dafalias and Herrmann 1980). A comprehensive description of the model was provided by Dafalias (1986). This model is conceptually a simpler version of the nested surfaces model. Only two surfaces were used, namely, a loading surface and a bounding surface (Figure 5.3). The model used a mixed hardening rule for the loading surface and isotropic hardening rules for the bounding surface. In the first formulations of the model, the loading surface was constrained to remain always inside the bounding surface. It could contact the bounding surface tangentially but would never intersect it. Manzari and Dafalias (1997) departed from this restriction by allowing the yield surface to cross the bounding surface.

A stress state on the loading surface is associated with a stress image on the bounding surface (point B in Figure 5.3) using a mapping rule. Usually, a simple radial mapping rule which defines the stress image as the intersection of the bounding surface and the straight line joining the stress origin and the current state (i.e. line OAB in Figure 5.3) is used. The plastic modulus, used to compute plastic deformations, is not anymore a discrete function but a continuous function of the distance that separates the actual stress state and its stress image. This definition of the plastic modulus constitutes the main difference between the bounding surface model and the multi-surface model. Moreover, the bounding surface model requires an explicit specification of the magnitude and the direction of the plastic deformation.

Another important feature of the bounding surface model is the occurrence of plastic deformations inside the bounding surface. This is a net departure from classical plasticity models where plastic deformations are allowed only on the yield surface. Despite this particularity, the formulation of the bounding surface model is very flexible, and it offers

the possibility of extending a classical plasticity model to a bounding surface model (Dafalias and Herrmann 1982).

Bounding surface models are powerful for modeling cyclic loading (Chen and Muzino, 1990). They have been used by various researchers to predict the monotonic and cyclic behaviour of clay (Dafalias and Herrmann 1982, 1986), and sand (Aboim and Roth 1982; Bardet 1986, 1987; and Wang 1990). Crouch et al. (1994) presented a unified bounding surface model for clay and sand. Manzari and Dafalias (1997), Li and Dafalias (2000, 2002), Li (2002), and Dafalias and Manzari (2004) combined the concepts of critical state soil mechanics and the state parameter (Been and Jefferies 1985) to devise bounding surface models for sand. These models used a unique set of parameters for soils at all density and confining pressures. The model proposed by Dafalias and Manzari (2004) is described in Chapter 6.

5.3.3 Subloading surface models

Hashiguchi and Ueno (1977) proposed the subloading surface model. The model used two surfaces: a normal-yield surface and a subloading surface which is enclosed in the normal yield surface. The two surfaces have the same shape and form. The main difference between the subloading surface model and the bounding surface models resides in the fact that the subloading surface does not translate but expends or contracts with plastic deformations. The subloading surface coincides with the normal-yield surface when the current stress state reaches the normal-yield surface. Hashiguchi (1985, 1989) extended the model to describe the cyclic behaviour of engineering materials. Hashiguchi and Chen (1998) applied the extended model to soils.

5.3.4 Other selected cyclic models

Carter et al. (1982) proposed a cyclic model for saturated clays. The model is based on the modified Cam-Clay model with the addition of a parameter to account for cyclic loading. The motivation for the development of this model is an observation that during unloading-reloading cycles, permanent deformation occurs earlier than predicted by Cam-Clay type models. In order to take into consideration this observation, the model allowed the yield surface to contract in an isotropic manner during unloading. But the yield surface remains stationary during loading or reloading in the elastic domain. A schematic description of the yield surface variation is shown in Figure 5.4. The model gave good predictions for the behaviour of saturated clays under cyclic loading conditions. However, the model predictions are highly influenced by the shapes of the yield surface and the plastic potential.

Pender (1982) presented a cyclic model based on the critical state. The initial version of the model had two problems: a rapid accumulation of strains and a quick build up of pore water pressure for increasing number of cycles. Modifications were made to the initial model so that it handled cyclic loading. First, the yield surface moves with the current stress state during unloading. Second, the two problems mentioned are dealt with by using a cyclic hardening index which increases with the number of cycles. Thus, the material becomes stiffer with increasing number of cycles. Pender mentioned that the model may not be able to handle a monotonic response that follows a set of cyclic loadings.

Ghaboussi and Momen (1982) proposed a cyclic model for sand using a yield surface asymptotic to the failure surface. The model used a mixed hardening rule. During unloading, the plastic modulus was related to the degree of stress reversal which was a function of the stresses at the last unloading and the last reloading process. A non-associated flow rule was used to compute the plastic deviatoric strains. The volumetric strains, determined empirically, were predicted with reasonable accuracy. However, the amount of accumulated irreversible deformations was underestimated. Furthermore, the

model could not reproduce the post-peak softening behaviour observed in dense sand samples because of the asymptotic relation between the yield surface and the failure surface.

Nova (1982) devised a cyclic model which used non-associated flow and mixed hardening rules. The model made use of a hardening function which depended on the volumetric and deviatoric plastic strains. The unloading-reloading behaviour of soil was assumed "paraelastic" (i.e. path independent between suitably defined stress reversal points). For example, during unloading, the bulk and shear modulii were expressed as a function of a paraelastic strain. But, during reloading, the bulk and shear modulii were assigned their initial values. With this feature, the model could predict a monotonic loading response which follows a set of cyclic loading. The main limitation of the model was the treatment of soil as an isotropic material.

5.4 Cyclic models for interfaces

The development of cyclic models for interfaces did not evolve as quickly as the development of cyclic models for soils. This section provides a literature review of the cyclic models formulated for interfaces.

5.4.1 Ramberg-Osgood type models for interfaces

Desai et al. (1985) proposed a non-linear elastic Ramberg-Osgood type model for the cyclic response of interface. The model was based on experimental investigations conducted on soil-structure interfaces. The model reproduced behaviour such as the increase in peak shear stress with density and number of cycles, the hardening of interfaces with the number of cycles, the increase of the stiffness of the interface with normal stress, and the influence of amplitude and rate of displacements on the maximum mobilized shear stresses. In addition, the model allowed slip and no-slip modes of

deformation. However, the normal displacements of interfaces were not predicted. Therefore, the model was extended by Desai and Nagaraj (1988) in order to predict the normal displacement. In the extended model, the normal and the tangential responses were uncoupled. The extended model allowed also debonding and rebonding modes of deformation. In these Ramberg-Osgood type models the inelastic deformation is not included in the sense of the theory of plasticity.

5.4.2 Model based on the Hierarchical Single-Surface models

Navayogarajah et al. (1992) described a cyclic model for sand-structure interfaces based on the Hierarchical Single-Surface model (HISS) and plasticity theory. The HISS model could be used with an associative or a non-associative flow rule. The model assumed an isotropic hardening rule. The model was developed to take into consideration the normal response, the importance of the roughness of interfaces, and the influences of several factors (i.e. type of sand, mean grain size, initial density of soil, interface roughness and normal stress) that affect the behaviour of interfaces.

The cyclic response was handled by taking into consideration the change in loading direction, defining properly a material memory, and using a cyclic parameter. The cyclic parameter permitted for example the simulation of cyclic volumetric response. The model allows strain-softening when the peak stress value is reached during the first cycle.

5.4.3 Bounding surface type models for interfaces

Aubry et al. (1990) proposed a model which used mixed hardening and non-associated flow rules. A yield criterion is defined taking into account the concept of critical state in interfaces, the influence of compressive effective normal stress, and the dilative and contractive behaviour of interfaces. The model introduced a cyclic loading function which had a memory of the last load reversal.

Sharhour and Rezaie (1997) formulated a model which used a bounding surface of Mohr-Coulomb type. The flow rule was non-associated. The constants of the model were derived from the results of constant normal stress tests.

Mortara et al. (2002) proposed a cyclic model for interfaces. This model extended a monotonic interface model (Ghionna and Mortara 2002) by adding a kinematic hardening rule, a moving cyclic yield domain, and a cyclic flow rule. In addition, the model used a non-associated flow rule and a Cam-Clay type plastic potential. An important feature of the model was the use of a double stress-dilatancy relationship derived from experimental observations. The parameters of the model could be obtained from the results of constant normal load tests conducted on interfaces. The model was validated for one-way constant normal load and two-way constant stiffness test results.

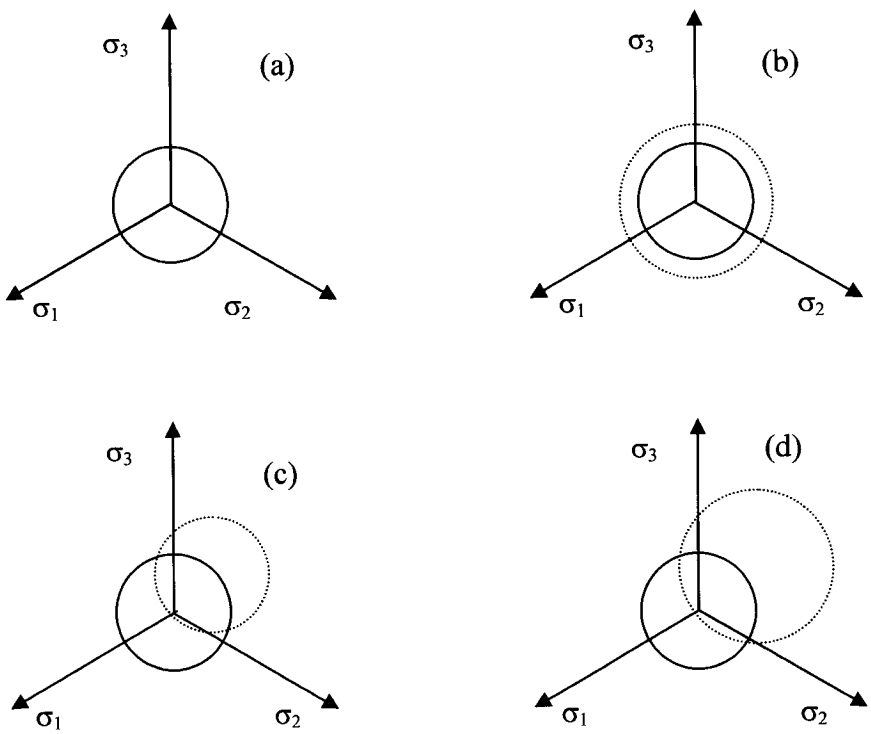

Figure 5.1 Hardening rules in the stress space (a) Perfectly plastic, (b) Isotropic hardening, (c) Kinematic hardening (d) Mixed hardening (after Desai and Siriwardane 1984)

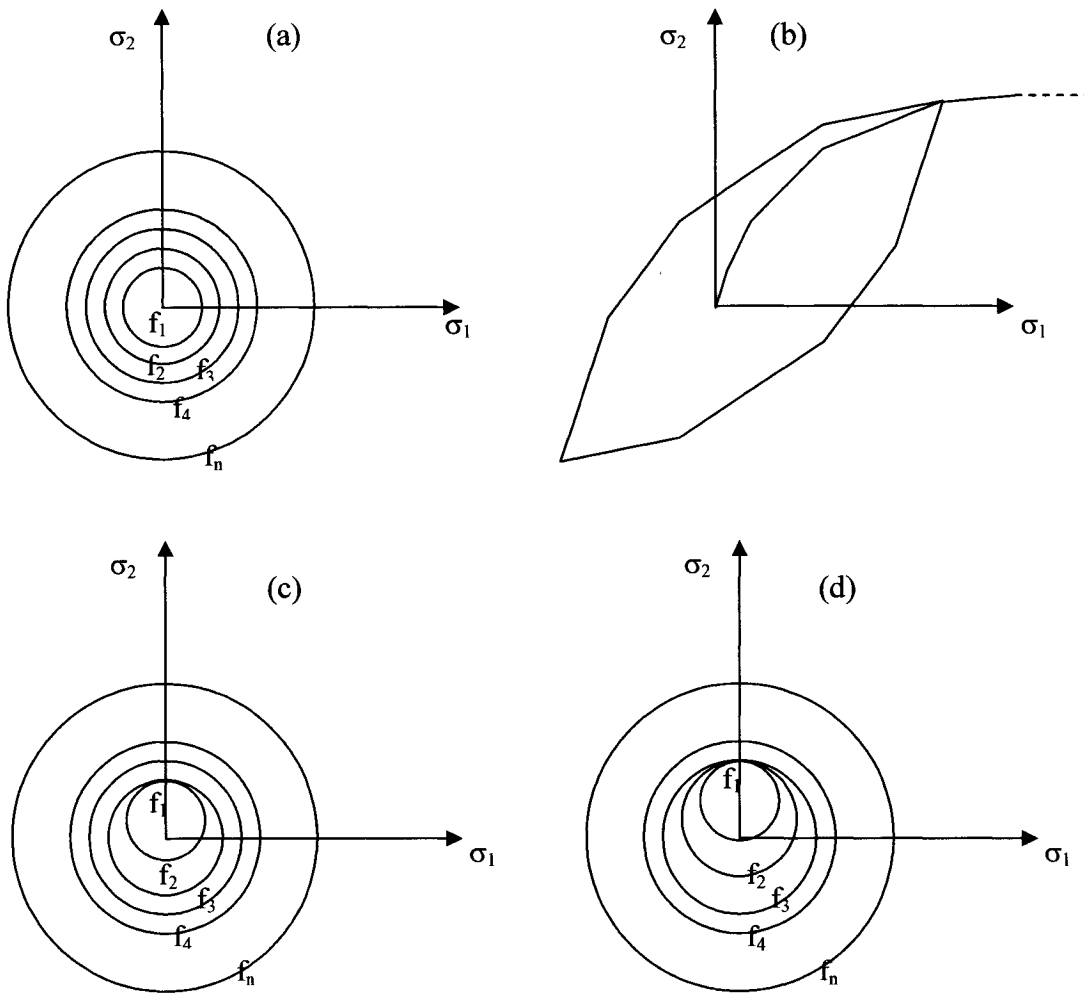

Figure 5.2 Position of yield surface in the multi-surface model. (a) Initial position of the yield surfaces (b) Evolution of plastic modulus (c) Movement of yield surface f_1 (d) Movement of yield surfaces f_1 and f_2 (modified after Desai and Siriwardane 1984)

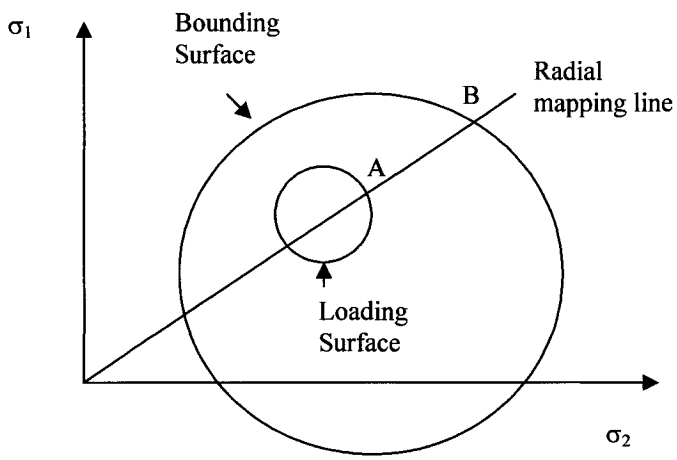

Figure 5.3 Bounding surface, loading surface and radial mapping line (modified after Dafalias and Popov 1975)

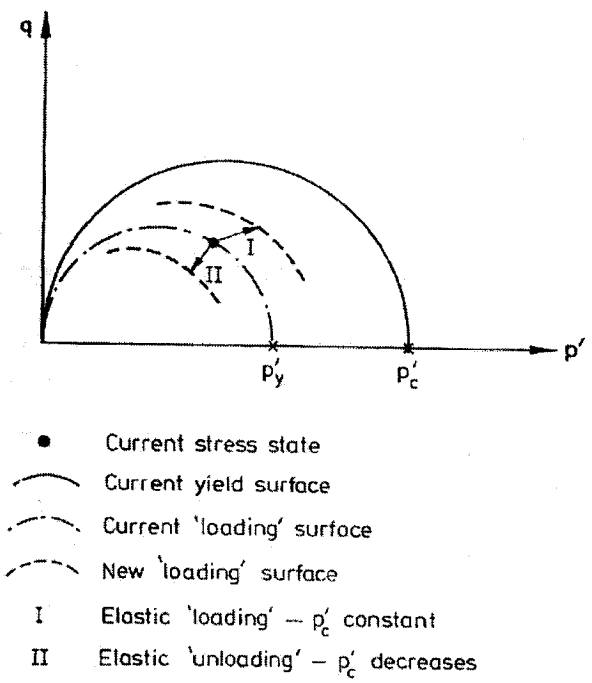

Figure 5.4 The yield surface and the 'loading' surface in p'-q space (after Carter et al. 1982)

CHAPTER 6

BOUNDING SURFACE PLASTICITY: DAFALIAS AND MANZARI'S MODEL

6.1 Introduction

Dafalias and Manzari (2004) formulated a bounding surface model to analyze the monotonic and cyclic behaviour of sand in drained and undrained conditions. The model was built on the framework of former models proposed by Manzari and Dafalias (1997) and Li and Dafalias (2000). The model used the concepts of critical state soil mechanics. Moreover, with a proper insertion of the state parameter (Been and Jefferies 1985), the model can simulate the behaviour of sand at various densities and confining pressure with a single set of model parameters (Manzari and Dafalias 1997).

A comprehensive description of the model in the triaxial stress space and the extention of the model to the generalized stress space were provided by Manzari and Dafalias (1997) and Dafalias and Manzari (2004). Because the triaxial stress space is a special case of the generalized stress space, only the description in the generalized stress space is given in this chapter. The model is integrated using a forward Euler method with return to yield surface, implemented in the object oriented programming language JAVA, and validated by comparing its predictions with those made by Dafalias and Manzari (2004). A parametric study is done to analyze the sensitivity of the model to changes in the model constants. The chapter ends with the predictions of six conventional triaxial tests. The predictions are compared with the experimental results.

6.2 Description of the model

Total strain rate

The total strain rate is decomposed, as commonly done in the theory of plasticity, into two parts: an elastic strain rate and a plastic strain rate.

$$\dot{\boldsymbol{\varepsilon}} = \dot{\boldsymbol{\varepsilon}}^{e} + \dot{\boldsymbol{\varepsilon}}^{p} \qquad 6.1$$

The superscripts e an p stand for elastic and plastic, respectively.

Elastic strain rate

The elastic deviatoric strain rate, $\dot{\mathbf{e}}^{e}$, and the elastic volumetric strain rate, $\dot{\varepsilon}_{v}^{e}$, are given by Equation 6.2a.

$$\dot{\mathbf{e}}^{e} = \frac{\dot{\mathbf{s}}}{2G} \; ; \; \dot{\varepsilon}_{v}^{e} = \frac{\dot{p}}{K} \qquad 6.2a$$

$$G = G_0 p_a \frac{(2.97 - e)^2}{1 + e} \left(\frac{p}{p_a}\right)^{1/2} \; ; K = \frac{2(1+\nu)}{3(1-2\nu)} G \qquad 6.2b$$

$$\mathbf{s} = \boldsymbol{\sigma} - p\mathbf{I} \; ; \; p = \frac{1}{3} \operatorname{tr} \boldsymbol{\sigma} \qquad 6.2c$$

where $\boldsymbol{\sigma}$=stress tensor, $\mathbf{s}$=deviator stress tensor, p=mean effective pressure, $\mathbf{I}$=identity tensor, p_a= atmospheric pressure, G=shear modulus, K=bulk modulus, e=void ratio, ν=Poisson ratio, and G_0 =model constant.

Generalized yield surface

The model uses, as shown on Figure 6.1, a circular yield surface. The yield surface is expressed mathematically as:

$$f = [(\mathbf{s} - p\boldsymbol{\alpha}) : (\mathbf{s} - p\boldsymbol{\alpha})]^{1/2} - \sqrt{2/3}pm = 0 \qquad 6.3$$

where α is the centre of the yield surface and corresponds to a back stress ratio. The term $\sqrt{2/3}m$ represents the radius of the yield surface, where m is a model constant. The gradient of the yield surface is expressed as:

$$\frac{\partial f}{\partial \boldsymbol{\sigma}} = \mathbf{n} - \frac{1}{3}(\mathbf{n} : \mathbf{r})\mathbf{I} \quad \text{where } \mathbf{n} = \frac{\mathbf{r} - \boldsymbol{\alpha}}{\sqrt{2/3}m} \text{ and } \mathbf{r} = \mathbf{s}/p \qquad 6.4$$

In addition to the yield surface, three surfaces, namely, a bounding surface, a dilatancy surface, and critical surface are used in the model (Figure 6.1). These surfaces are expressed mathematically as:

$$\boldsymbol{\alpha}_\theta^a = \sqrt{2/3}\alpha_\theta^a \mathbf{n} \qquad (a=b,c,d) \qquad 6.5a$$

$$\alpha_\theta^b = g(\theta, c)M\exp(-n^b\psi) - m \qquad 6.5b$$

$$\alpha_\theta^d = g(\theta, c)M\exp(n^d\psi) - m \qquad 6.5c$$

$$\alpha_\theta^c = g(\theta, c)M - m \qquad 6.5d$$

$$\psi = e - e_c \qquad 6.5e$$

$$e_c = e_0 - \lambda_c (p_c / p_a)^{\xi} \tag{6.5f}$$

$$g(\theta, c) = \frac{2c}{(1+c) - (1-c)\cos 3\theta} \tag{6.5g}$$

$$c = \frac{M_e}{M_c} \tag{6.5h}$$

$$\cos 3\theta = \sqrt{6}\,\mathrm{tr}\,\mathbf{n}^3 \tag{6.5i}$$

The superscripts b, c, d stand for bounding, critical, and dilatancy surface, respectively. Ψ is the state parameter (Been and Jefferies 1985); e_c is the critical state void ratio associated with a mean pressure p_c; θ is Lode's angle and it varies between 0 and $\pi/3$. The parameters n^b, n^d, M, c, e_0, λ_c, and ξ are all model constants.

Plastic strain rate

The plastic strain obtained from a non-associated flow rule is given by:

$$\dot{\boldsymbol{\varepsilon}}^p = \langle L \rangle \mathbf{R} \tag{6.6a}$$

where

$$\mathbf{R} = \frac{\partial g}{\partial \boldsymbol{\sigma}} = B\mathbf{n} - C(\mathbf{n}^2 - \frac{1}{3}\mathbf{I}) + \frac{1}{3}D\mathbf{I} \tag{6.6b}$$

$$B = 1 + \frac{3}{2}\frac{1-c}{c} g(\theta, c)\cos 3\theta\,;\; C = 3\sqrt{\frac{3}{2}}\frac{1-c}{c} g(\theta, c) \tag{6.6c}$$

$$L = \frac{1}{K_p}\frac{\partial f}{\partial \sigma} : d\sigma = \frac{2G\mathbf{n} : \dot{\mathbf{e}} - \mathbf{n} : \mathbf{r}\dot{\varepsilon}_v}{K_p + 2G(B - C\,tr\,\mathbf{n}^3) - KD\mathbf{n} : \mathbf{r}} \qquad 6.6d$$

$$K_p = \frac{2}{3} ph\mathbf{b} : \mathbf{n} \text{ where } \mathbf{b} = \alpha_\theta^b - \alpha \qquad 6.6e$$

$$h = \frac{b_0}{(\alpha - \alpha_{in}) : \mathbf{n}};\ b_0 = G_0 h_0 (1 - c_h e)(p / p_a)^{-1/2} \qquad 6.6f$$

D is the dilatancy function, L is the loading index; K_p is the plastic modulus; h_0 and c_h are model constants.

The dilatancy function is given by:

$$D = A_d \mathbf{d} : \mathbf{n} \text{ where } \mathbf{d} = \alpha_\theta^d - \alpha \qquad 6.7a$$

$$A_d = A_0 (1 + < \mathbf{z} : \mathbf{n} >);\ \dot{\mathbf{z}} = -c_z < -\varepsilon_v^p > (z_{max}\mathbf{n} + \mathbf{z}) \qquad 6.7b$$

z is a fabric tensor; A_0, c_z, and z_{max} are model constants.

Isotropic and Kinematic hardening

Since the radius of the yield surface is assumed constant in the model (i.e. no isotropic hardening), the consistency condition ($\dot{f} = 0$) is satisfied by expressing the evolution of the back stress ratio as:

$$\dot{\alpha} = \frac{2}{3}\langle L \rangle h\mathbf{b} \qquad 6.8$$

Stress increments

The equations 6.2a and 6.6a give the strain increments as a function of stress increments. These equations are inverted to express the stress increment as a function of the strain increment. Hence, for a given strain increment, the stress increment is expressed as:

$$\dot{\boldsymbol{\sigma}} = 2G\dot{\mathbf{e}} + K\dot{\varepsilon}_v\mathbf{I} - < L > \{2G[\mathbf{Bn} - C(\mathbf{n}^2 - \frac{1}{3}\mathbf{I})] + KD\mathbf{I}\} \qquad 6.9a$$

Equation 6.9a is often written in the following form for a numerical implementation

$$\dot{\boldsymbol{\sigma}} = \mathbf{C}^{ep} : \boldsymbol{\varepsilon} \qquad 6.9b$$

where

$$\mathbf{C}^{ep} = C_{ijkl}^{ep} = \left[C_{ijkl} - \frac{\frac{\partial g}{\partial \sigma_{rs}} C_{ijrs} C_{mnkl} \frac{\partial g}{\partial \sigma_{mn}}}{K_p + \frac{\partial f}{\partial \sigma_{ab}} C_{abcd} \frac{\partial g}{\partial \sigma_{cd}}} \right] \qquad 6.9c$$

$$\mathbf{C}^{e} = C_{ijkl} = (K - \frac{2G}{3})\delta_{ij}\delta_{kl} + G(\delta_{ik}\delta_{jl} + \delta_{il}\delta_{jk}) \qquad 6.9d$$

$\mathbf{C}^{ep}$ is the elastoplastic stiffness tensor and $\mathbf{C}^{e}$ is the tensor of the elastic constant.

6.3 Integration and implementation of the model

The model is integrated using a forward Euler algorithm with a return to the yield surface (Sloan 1987, Jakobsen and Lade 2002). A new stress state is calculated based on the current stress state ($\boldsymbol{\sigma}_A$), the back stress ratio ($\boldsymbol{\alpha}_A$) associated to the current stress state,

the strain increment ($\dot{\boldsymbol{\varepsilon}}$), and the material constants. The integration procedure is shown in Figure 6.2. The first step, known as elastic shooting, consists of calculating a trial elastic stress increment ($\dot{\boldsymbol{\sigma}}^e$) by assuming that the strain increment is purely elastic (Equation 6.10).

$$\dot{\boldsymbol{\sigma}}^e = \mathbf{C}^e_{(\boldsymbol{\sigma}_A)} : \dot{\boldsymbol{\varepsilon}} \qquad 6.10$$

This yields a trial stress $\boldsymbol{\sigma}_B$ at point B (Equation 6.11).

$$\boldsymbol{\sigma}_B = \boldsymbol{\sigma}_A + \dot{\boldsymbol{\sigma}}^e \qquad 6.11$$

The value, f_B, of the yield surface is evaluated at the point B. If $f_B<0$, the assumption that the elastic strain increment is purely elastic is true. However, if $f_B>=0$, it is necessary to examine the value, f_A, of the yield surface at the current stress state. If $f_A<0$ then the point A is inside the yield surface, and it is necessary to find the stress $\boldsymbol{\sigma}_C$ (Equation 6.12) at point C (located on the segment AB) where the value f_C of the yield surface vanishes. In other words it is necessary to find the ratio β=AC/AB. If f_A=0 then A=C and β=0. Knowing that $\beta \in [0, 1]$, it is possible to find β by using the bisection method.

$$\boldsymbol{\sigma}_C = \boldsymbol{\sigma}_A + \beta\dot{\boldsymbol{\sigma}}^e \qquad 6.12$$

The strain rate ($\beta\dot{\boldsymbol{\varepsilon}}$) between A and C is purely elastic, the remaining part ($(1-\beta)\dot{\boldsymbol{\varepsilon}}$) of the strain rate is used to find the stress state $\boldsymbol{\sigma}_E$ at point E (Equation 6.13).

$$\boldsymbol{\sigma}_E = \boldsymbol{\sigma}_C + (1-\beta)\mathbf{C}^{ep}_{(\boldsymbol{\sigma}_C)} : \dot{\boldsymbol{\varepsilon}} \qquad 6.13$$

Usually the stress state $\boldsymbol{\sigma}_E$ drifts off the yield surface. Hence, it is necessary to devise a procedure to return $\boldsymbol{\sigma}_E$ to a stress state $\boldsymbol{\sigma}_D$ on the yield surface. This is achieved by using

the correction method proposed by Gens and Potts (1988). During the correction process the total strain increment remains unaltered and it is necessary to find the variable χ such that

$$f(\boldsymbol{\sigma}_D,\boldsymbol{\alpha}_D) = f(\boldsymbol{\sigma}_E - \chi \mathbf{C}^e : \frac{\partial g}{\partial \boldsymbol{\sigma}}, \boldsymbol{\alpha}_E + \dot{\boldsymbol{\alpha}}) = 0 \qquad 6.14$$

A first estimate of the variable χ is

$$\chi = \frac{f(\boldsymbol{\sigma}_E,\boldsymbol{\alpha}_E)}{K_p + (\frac{\partial f}{\partial \boldsymbol{\sigma}_E})^T : \mathbf{C}^e : (\frac{\partial g}{\partial \boldsymbol{\sigma}_E})} = 0 \qquad 6.15$$

The first estimate is accurate only for small strain increment. Therefore, it is necessary to verify that the stress state D fulfills the yield criterion to some close tolerance (Jakobsen and Lade 2002). If the yield criterion is not satisfied to some close tolerance (TOL), an iterative procedure which starts from the position $\boldsymbol{\sigma}_0 = \boldsymbol{\sigma}_E$ and $\boldsymbol{\alpha}_0 = \boldsymbol{\alpha}_E$ is necessary. The iterative procedure is summarized below:

Initial state $\boldsymbol{\sigma}_0$, $\boldsymbol{\alpha}_0$

If $|f(\boldsymbol{\sigma}_0,\boldsymbol{\alpha}_0)| \le TOL$

Iteration i=1,2,….,imax

$$\chi_{i-1} = \frac{f(\boldsymbol{\sigma}_{i-1},\boldsymbol{\alpha}_{i-1})}{K_{p,i-1} + (\frac{\partial f}{\partial \boldsymbol{\sigma}_{i-1}})^T : \mathbf{C}^e : (\frac{\partial g}{\partial \boldsymbol{\sigma}_{i-1}})} = 0$$

$$\sigma_i = \sigma_{i-1} - \chi_{i-1} Ce \frac{\partial g}{\partial \sigma_{i-1}}$$

$$\dot{\boldsymbol{\alpha}}_{i-1} = \frac{2}{3}\chi_{i-1} h_{i-1} \mathbf{b}_{i-1}$$

$$\boldsymbol{\alpha}_i = \boldsymbol{\alpha}_{i-1} + \dot{\boldsymbol{\alpha}}_{i-1}$$

Stop iteration when $|f(\boldsymbol{\sigma}_i,\boldsymbol{\alpha}_i)| \le TOL$

Final state $\boldsymbol{\sigma}_D = \boldsymbol{\sigma}_i$, $\boldsymbol{\alpha}_D = \boldsymbol{\alpha}_i$

The forward Euler method with a return to the yield surface presented in this section may be combined with a subincrementation of the strain increment (Jakobson and Lade 2002).

6.4 Determination of model constants

A total of fifteen model constants were used in the model. The model constants were divided into six groups according to their functions: Elastic constants (G_0 and ν); Critical state constants (M, c, λc, e_0, and ξ); Yield surface constant (m); Plastic modulus constants (h_0, c_h, and n^b); Dilatancy constant (A_0 and n^d); and Fabric-dilatancy tensor constants (z_{max} and c_z). The process for determining the model constants, explained by Li and Dafalias (2000) and Dafalias and Manzari (2004), is summarized in this section.

The elastic constants G_0 and ν can be obtained by fitting Equation 6.2b into the triaxial data. But if the shear stiffness at small strains is important, experimental data from small strain tests, such as resonant column tests or bender elements tests should be used for the determination of G_0. Li and Dafalias (2000) reported that high G_0 values may yield negative values for Poisson's ratio (ν). In these situations, they proposed an alternative approach which consisted to select first a value for ν before calculating the value of G_0. However, Li and Dafalias (2000) mentioned that this alternative does not guarantee the accuracy of the elastic shear response, and it should be used when the shear stiffness is unimportant in the elastic range or when accurate measurements for G are unavailable. The second approach was used in this research program by selecting Poisson's ratio in the range of values (0.15-0.35) reported by Budhu (1999).

The critical state constant M is the slope of the critical state line in the q-p space. At least two triaxial tests conducted at different confining pressures are necessary for the determination of M. It is important to mention that the value of M obtained from triaxial compression tests (M_c) often differs from the value obtained from triaxial extension tests

(M_e). If the friction angle, ϕ, of the soil is known, M_c and M_e are determined from the following equations.

$$M_c = \frac{6\sin\phi}{3-\sin\phi} \qquad 6.16a$$

$$M_e = \frac{6\sin\phi}{3+\sin\phi} \qquad 6.16a$$

Note that M, used solely without any of the subscripts e or c, refers to M_c. The model constant c is the ratio of M_e and M_c.

$$c = \frac{M_e}{M_c} = \frac{3-\sin\phi}{3+\sin\phi} \qquad 6.17$$

The constants e_0, λ_c, and ξ are obtained by fitting a power function to the critical state (Equation 6.5f). The yield surface constant, m, is typically in the order of M/100. The plastic modulus constant h_0, and c_h are obtained by trial-and-error which consists in performing simulations for different values of the model constant and retaining the value for which the simulations match better the experimental observations. The constant n^b is obtained from conventional triaxial test using the following equation.

$$n^b = \ln(M/M^b)/\psi^b \qquad 6.18$$

where M^b is the peak stress ratio and ψ^b is the value of ψ at the peak stress ratio.

The dilatancy constant A_0 is obtained by trial-and-error; the dilatancy constant n^d is determined with the following equation

$$n^d = \ln(M^d / M) / \psi^d \qquad 6.19$$

where M^d and ψ^d are the stress ratio and the value of ψ, respectively, at the phase transformation point.

Finally, the fabric tensor constants z_{max} and c_z are obtained by trial-and-error fitting of loading-unloading reverse loading, or cyclic data, preferably undrained, where the stress ratio must exceed M^d in order to activate the evolution of **z** (Equation 6.7).

6.5 Verification of the model

The predictions made for sand behaviour in three triaxial tests (Manzari and Dafalias 2004) were repeated (Figure 6.3) in order to verify that the model was correctly programmed in the present study. The model constants used by Dafalias and Manzari (2004) are provided in Table 1. The initial void ratio in the three triaxial tests was 0.996, 0.917, and 0.831, respectively; the initial mean pressure was p_0=100 kPa.

Figure 6.3a gives the evolution of deviatoric stress with axial strain, and Figure 6.3b gives the evolution of volumetric strain with axial strain. The predictions in Figure 6.3a match those reported by Dafalias and Manzari (2004). This indicates that the model was correctly programmed.

6.6 Parametric study

In this section a parametric study is conducted to analyze the sensitivity of the model to changes in the model constants. This parametric study is particularly useful given that five of the fifteen model constants are determined by trial-and-error. The effects of the fifteen model constants on the predictions of conventional triaxial tests (deviatoric stress versus axial strain, and volumetric strain versus axial strain) are shown in Figures 6.4 to

6.18 for loose sand (e_i=0.996) and in Figures 6.19 to 6.23 for dense sand (e_i=0.831). The plots on each figure show the prediction of the model for a base case where the model constants take the values listed in Table 1 and four additional cases where the subject model constant takes the value of the base case decreased or increased by 10% and 30% while the other constants remain unchanged. In other words if the value of the subject model constant is 'y' in the base case, its values in the four additional cases are 0.7y, 0.9y, 1.1y, and 1.3y respectively. The labels "-side" and "+side" appearing in the figures indicate the direction of decreasing and increasing values of the model constant.

6.6.1 Effect of model constant G_0

Figures 6.4a and 6.5a show that as the constant G_0 increases the material response becomes stiffer. However, the changes in G_0 are practically uninfluential at large axial strains. The compressive volumetric strain decreases with increasing values of G_0 for the loose sand (Figure 6.4b). However, the dilative volumetric strain increases with increasing values of G_0 for dense sand (Figure 6.5b).

6.6.2 Effect of model constant ν

Figures 6.6 and 6.7 show that changes in the values of Poisson's ratio (ν) have insignificant effect on the predictions of the model.

6.6.3 Effect of model constant M

Changes in the values of the constant M affect significantly the predictions of the model as illustrated in Figures 6.8 and 6.9. The deviator stress increases with increasing values of M (Figure 6.8a and 6.9a). Moreover, as the value of M becomes large, the compressive volumetric strain increases for loose sand (Figure 6.8b), and the dilative volumetric strain increases for dense sand (Figure 6.9b)

6.6.4 Effect of model constant c

Figures 6.10 and 6.11 show that as expected the changes in the values of the model constant c are uninfluential on the predictions of the model for conventional compression triaxial tests. However, the constant c is expected to influence the predictions in the simulation of extension triaxial tests.

6.6.5 Effect of model constant λ_c

Changes in λ_c affect slightly the deviator stress which decreases for increasing values of λ_c (Figures 6.12a and 6.13a). However, they have a larger effect on the volumetric strain. In fact, as the value of λ_c increases, the compressive volumetric strain increases for loose sand (Figure 6.12b) while the dilative volumetric strain decreases for dense sand (Figure 6.13b).

6.6.6 Effect of model constant e_0

Figures 6.14 and 6.15 show that changes in e_0 affect significantly the model predictions. For example the deviator stress increases with increasing value of e_0 (Figures 6.14a and 6.15a). For the loose sand, the compressive volumetric strain decreases as the value of e_0 increases and the loose sand starts to experience dilation like dense sand (Figure 6.14b). Dense sand experience more dilation for increasing values of e_0. But for decreasing values of e_0, dense sand starts behaving like loose sand (Figure 6.15b). These observations imply that changes of the e_0 values may render a sand sample which is dense (loose) in the base case loose (dense). This occurs because the changes in the values of e_0 modify the critical state position and therefore the loose and dense sand regions.

6.6.7 Effect of model constant ξ

Changes in the value of the constant ξ are uninfluential on the relation of deviator stress versus axial strain (Figure 6.16a and 6.17a). However, they influence to some extend the volumetric strain. For increasing values of ξ, the compressive volumetric strain increases for loose sand (Figure 6.16b) and the dilative volumetric strain decreases for dense sand (Figure 6.17b).

6.6.8 Effect of model constant m

Changes in this model constant are practically uninfluential on the predictions of the model as illustrated in Figures 6.18 and 6.19.

6.6.9 Effect of model constant h_0

The effects of h_0 and G_0 on the model simulations are similar. In fact, increasing values of h_0 yield a stiffer sand response (Figures 6.20a and 6.21a), larger compressive volumetric strain for loose sand (Figure 6.20b) and larger dilative volumetric strain for dense sand (Figure 6.21b).

6.6.10 Effect of model constant c_h

Figures 6.22 and 6.23 show that changes in c_h affect significantly the predictions of the model. It is important to mention that contrary to the study of the other model constants, the values of c_h were increased by 1% and 3% in two cases instead of 10% and 30%. In other words, if 'y' is the value of c_h in the base case the values of c_h in the other four cases are 0.7y, 0.9y, 1.01y and 1.03y respectively instead of 0.7y, 0.9y, 1.1y and 1.3y. Figures 6.22a and 6.23a illustrate that the response of the sand becomes softer as the

value of c_h increases while the compressive volumetric strain increases for loose sand (Figure 6.22b) and the dilative volumetric strain increases for dense sand (Figure 6.23b).

6.6.11 Effect of model constant n^b

Figure 6.24a shows that the response of loose sand becomes softer as the value of n^b increases, but the response of dense sand becomes stiffer (Figure 6.25a). The compressive and the dilative volumetric strain increase with increasing values of n^b for loose sand (Figure 6.24b) and dense sand (Figure 6.25b), respectively.

6.6.12 Effect of model constant A_0

Figure 6.26a shows that the deviator stress increases with increasing values of A_0 for loose sand. The opposite behaviour is observed on dense sand as illustrated in Figure 6.27a. The compressive and dilative volumetric strain increases with increasing values of A_0 for loose sand (Figure 6.26b) and dense sand (Figure 6.27b), respectively.

6.6.13 Effect of model constant n^d

Figures 6.28 and 6.29 show that increasing values of n^d yields similar effect on the model predictions as increasing values of A_0. In other words, the deviator stress increases with increasing values of n^d for loose sand (Figure 6.28a) but it decreases for dense sand (Figure 6.29a). In addition, the compressive and dilative volumetric strain increases with increasing values of n^d for loose sand (Figure 6.28b) and dense sand (Figure 6.29b), respectively.

6.6.14 Effect of model constant z_{max}

Figures 6.30 and 6.31 show that changes in z_{max} are uninfluential on the predictions of the model for conventional triaxial tests.

6.6.15 Effect of model constant c_z

Similar to the changes in z_{max}, the change in c_z are uninfluential on the predictions of the model for conventional compression triaxial tests (Figures 6.32 and 6.33).

Based on the parametric study on the predictions of the model for conventional triaxial tests the model constants can be divided into three categories according to their influences: high influence constants (M, e_0, c_h, A_0), moderate influence constants (G_0, λ_c, ξ, h_0, n^b, n^d), and low influence constants (ν, c, m, z_{max}, c_z)

6.7 Predictions of the model

A total of six conventional compression triaxial tests were conducted on the sand used to study the behaviour of interfaces. Three tests were performed at a confining pressure of 100 kPa (Figure 6.34) and the remaining tests were carried out at confining pressures of 150 kPa, 200 kPa, and 300 kPa (Figure 6.35). After isotropic consolidation the relative density of the tests conducted at a confining pressure of 100 kPa was 36.0%, 57.6%, and 59.6%, respectively, while the relative density of the tests conducted at confining pressures of 150 kPa, 200 kPa, and 300 kPa was 27.3%, 28.3%, and 24.3%, respectively.

These tests were used as described in the Appendix A to determine the model constants which are presented in Table 6.2. Predictions were made for the six triaxial tests using these constants. The predictions are also presented in Figures 6.34 and 6.35. The predictions of the volumetric strains are in reasonably good agreement with the

experimental data although there are some scatters (Figure 6.34b and 6.35b). However the model reproduces well as indicated in Figures 6.34a and 6.35a the relationship between deviator stress and axial strain. This indicates that the model proposed by Dafalias and Manzari (2004) can successfully simulate the monotonic behaviour of the sand used in this research program.

Table 6.1 Model constants (after Dafalias and Manzari, 2004)

Constant	Variable	Value
Elasticity	G_0	125
	ν	0.05
Critical state	M	1.25
	C	0.712
	λ_c	0.019
	e_0	0.934
	ξ	0.7
Yield surface	m	0.01
Plastic modulus	h_0	7.05
	c_h	0.968
	n^b	1.1
Dilatancy	A_0	0.704
	n^d	3.5
Fabric-dilatancy tensor	z_{max}	4
	c_z	600

Table 6.2 Model constants for the sand used in this investigation

Constant	Variable	Value
Elasticity	G_0	142
	ν	0.25
Critical state	M	1.42
	C	0.679
	λ_c	0.019
	e_0	0.938
	ξ	0.65
Yield surface	m	0.01
Plastic modulus	h_0	6.35
	c_h	0.968
	n^b	1.3
Dilatancy	A_0	0.904
	n^d	2.3
Fabric-dilatancy tensor	z_{max}	4
	c_z	600

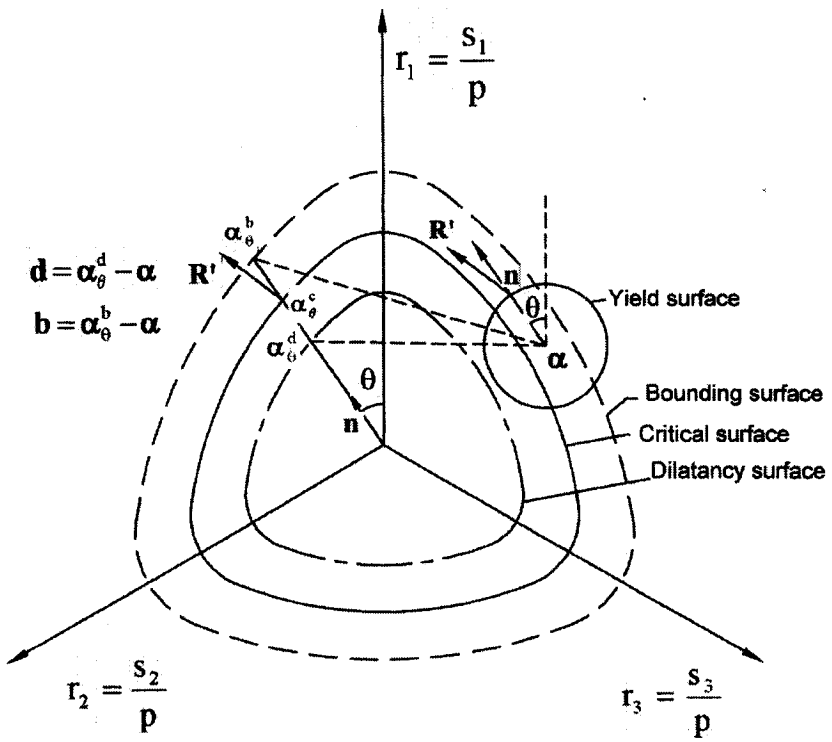

Figure 6.1 Yield, critical, dilatancy, and bounding surfaces on the stress ratio π plane (after Dafalias and Manzari 2004)

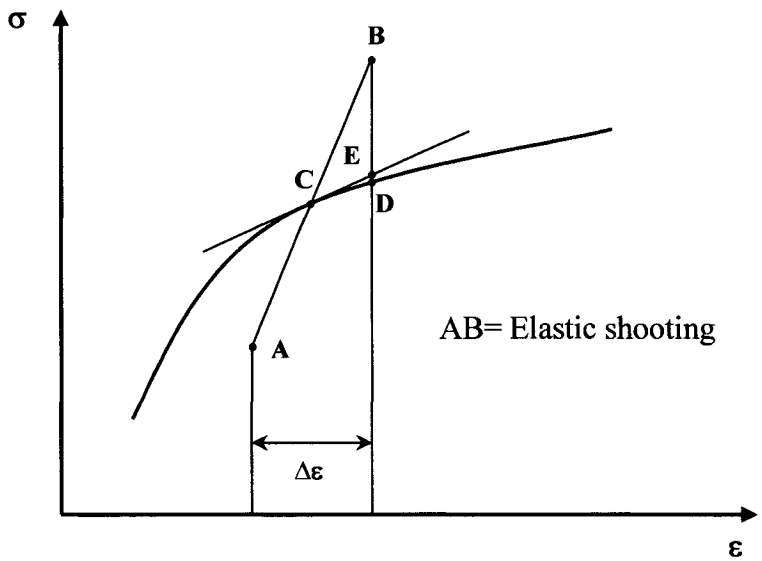

Figure 6.2 Stress-strain relation used to explain the integration procedure (after Jakobsen and Lade, 2002)

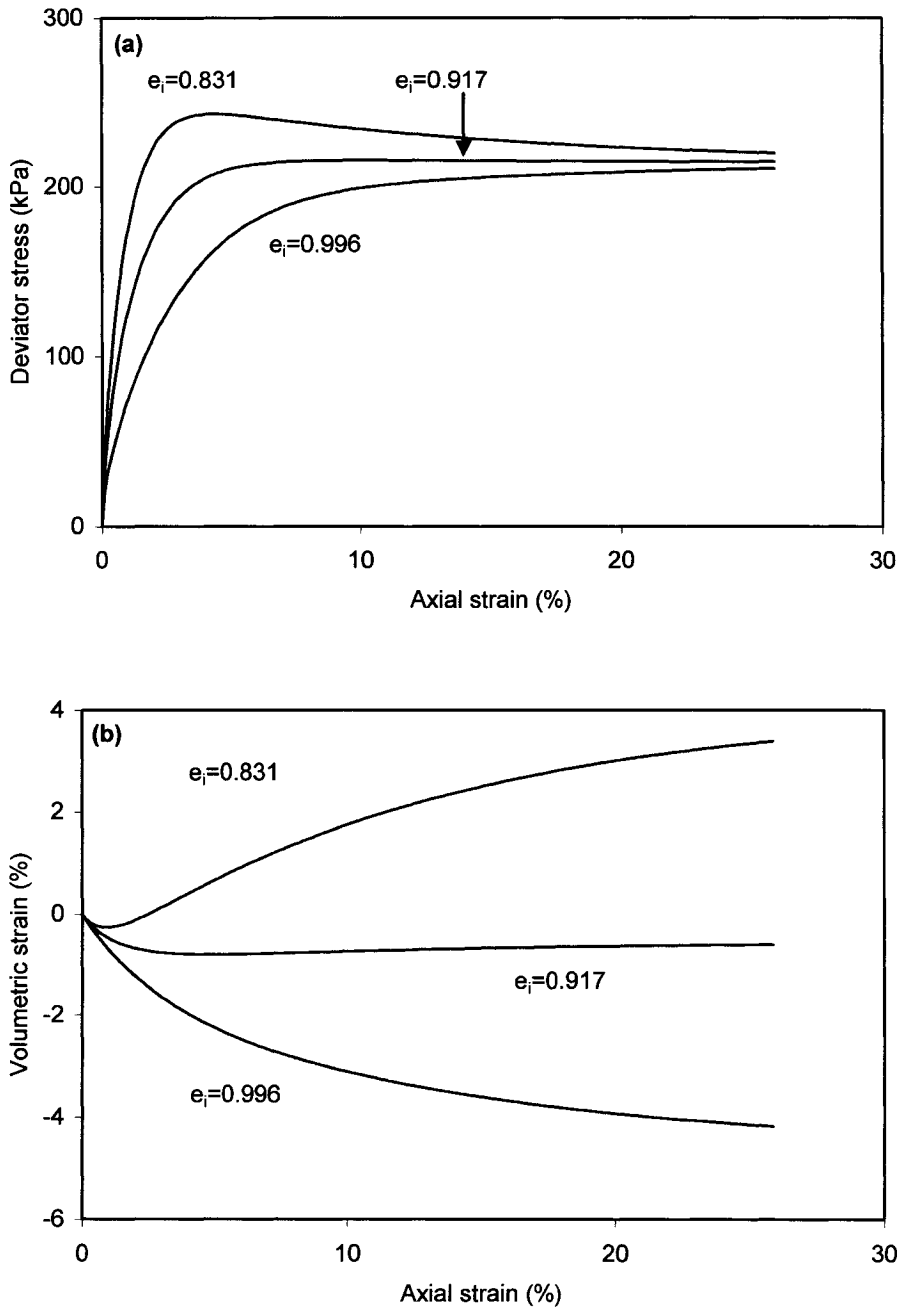

Figure 6.3 Simulation of sand behaviour in triaxial tests (p_0=100 kPa)

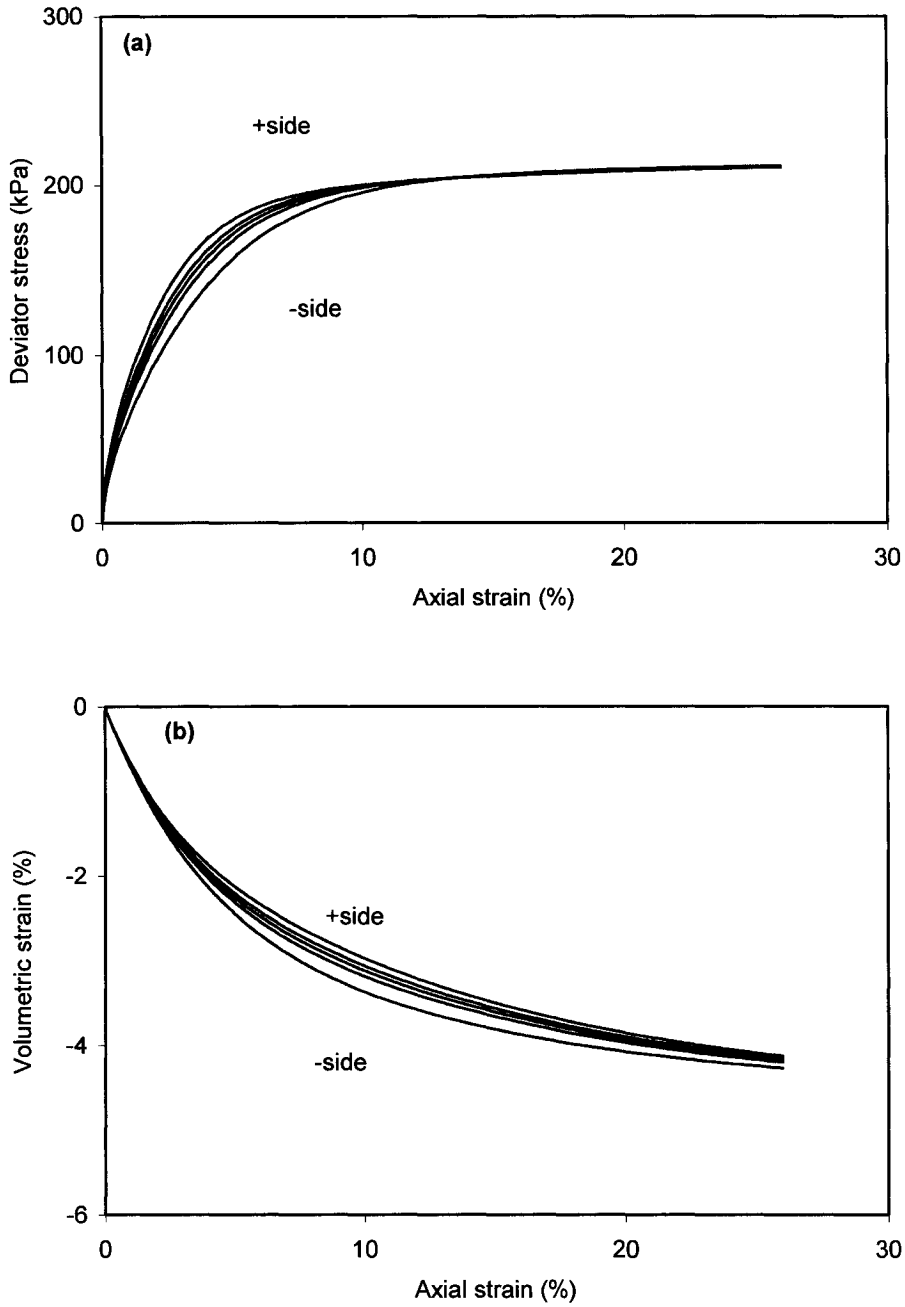

Figure 6.4 Effect of model constant G_0 on the simulations of the behaviour of loose sand

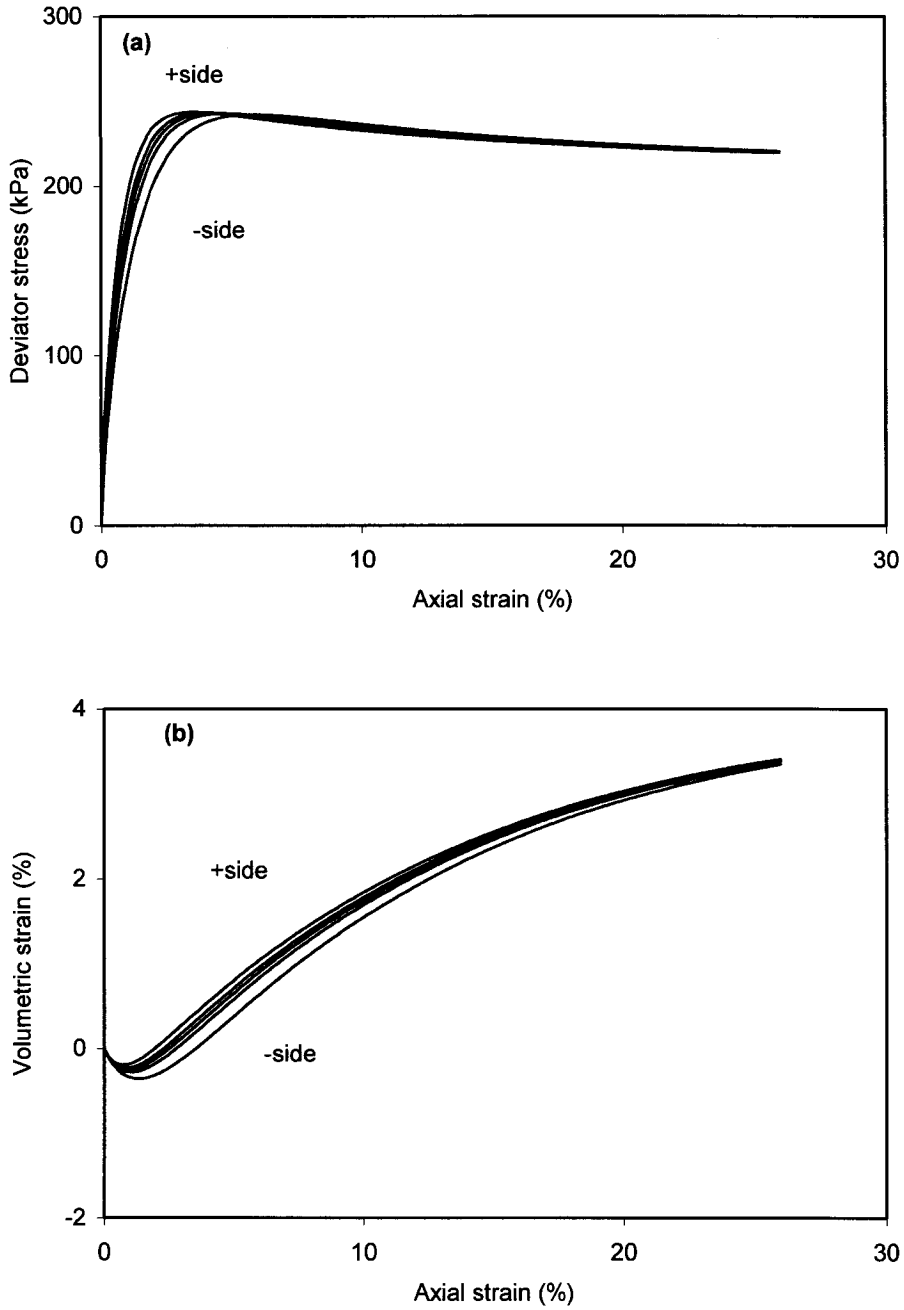

Figure 6.5 Effect of model constant G_0 on the simulations of the behaviour of dense sand

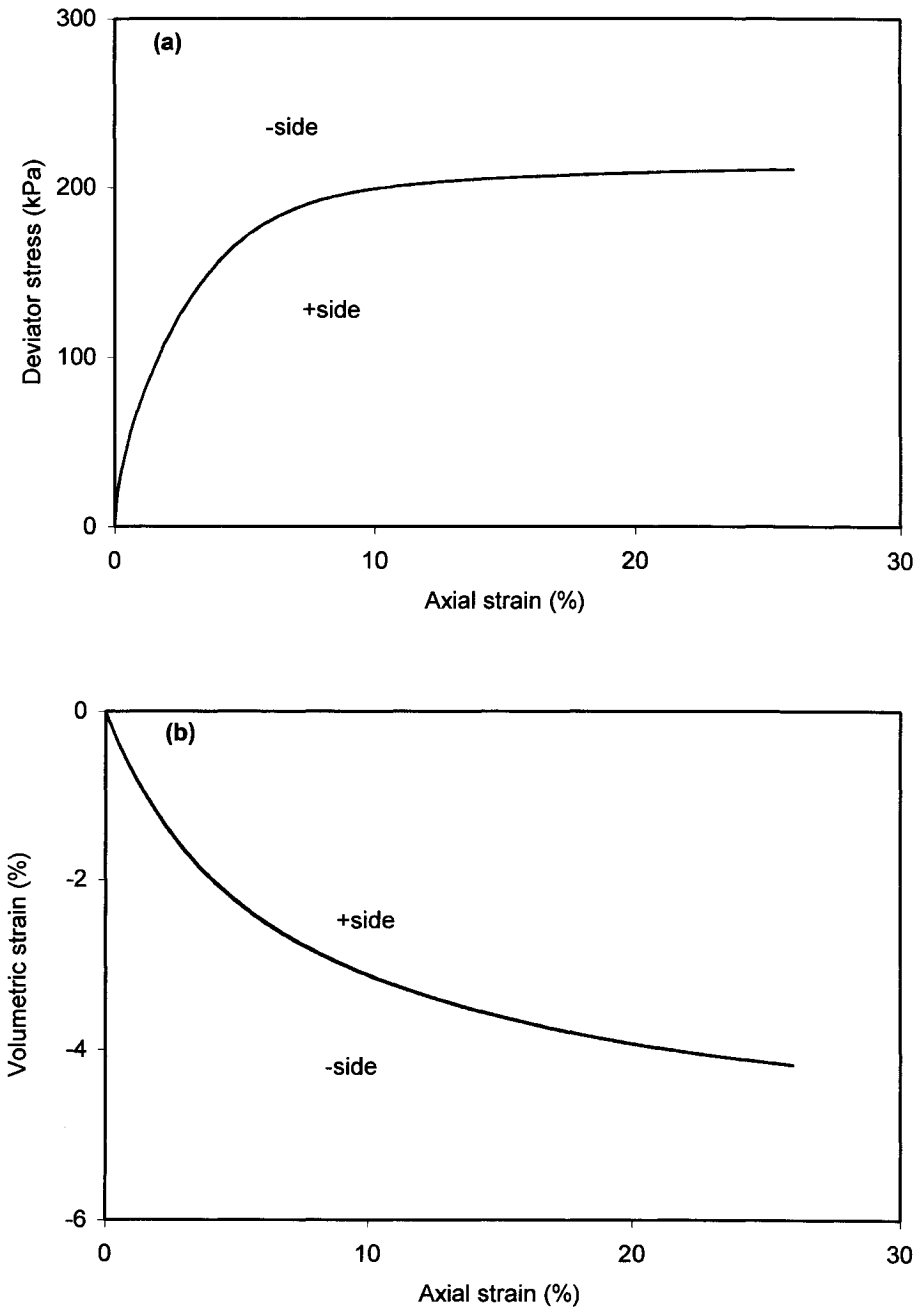

Figure 6.6 Effect of model constant ν on the simulations of the behaviour of loose sand

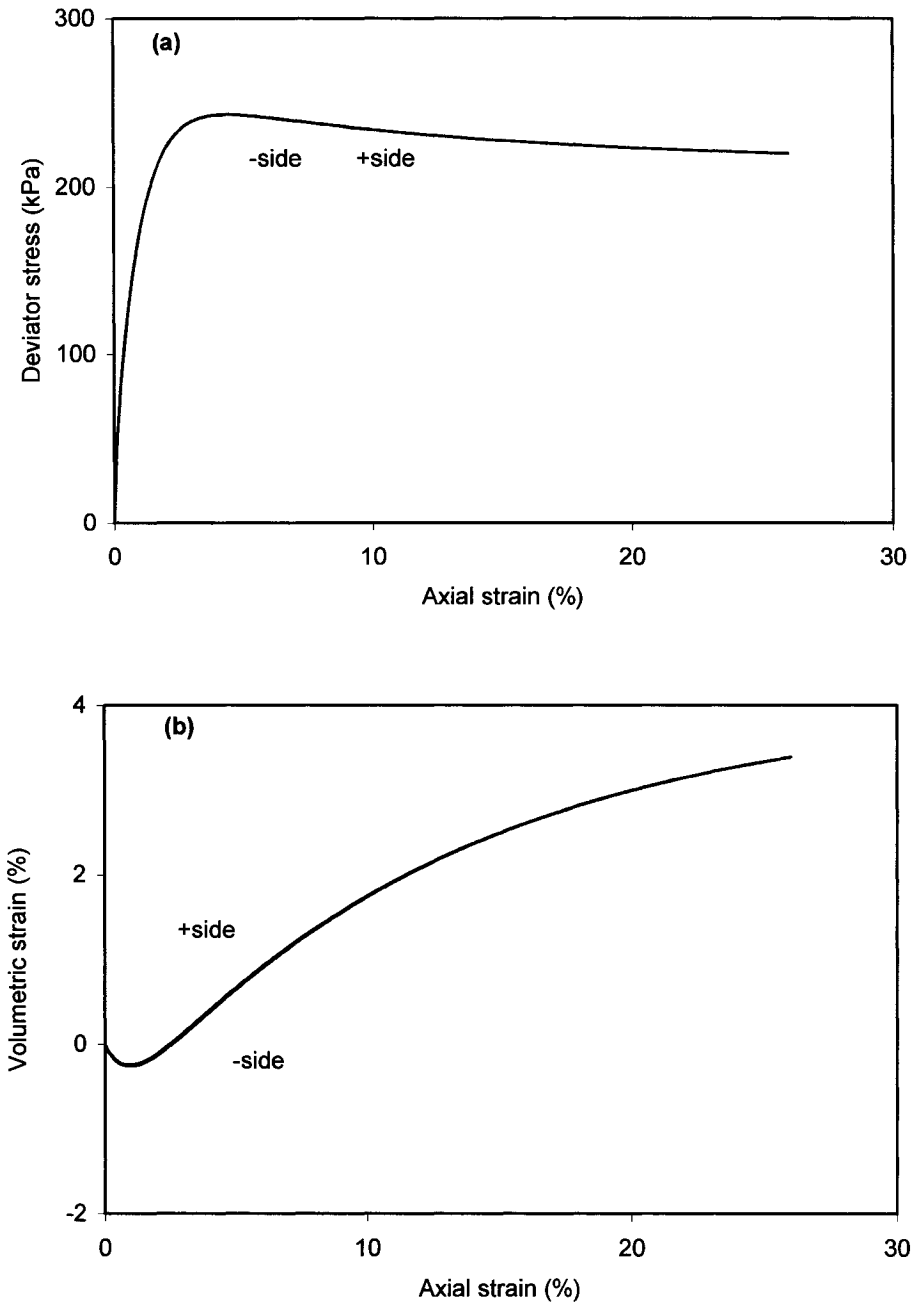

Figure 6.7 Effect of model constant ν on the simulations of the behaviour of dense sand

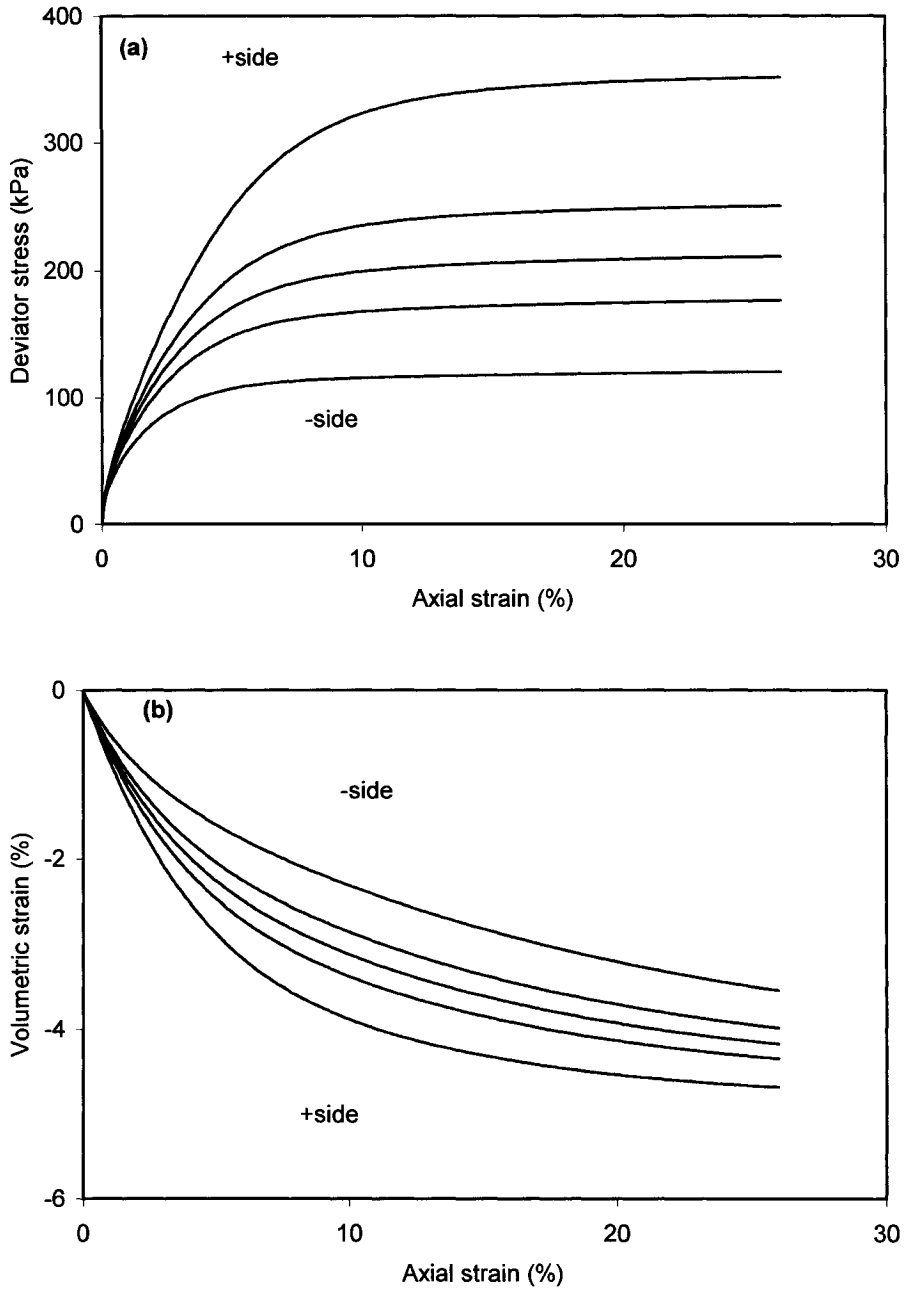

Figure 6.8 Effect of model constant M on the simulations of the behaviour of loose sand

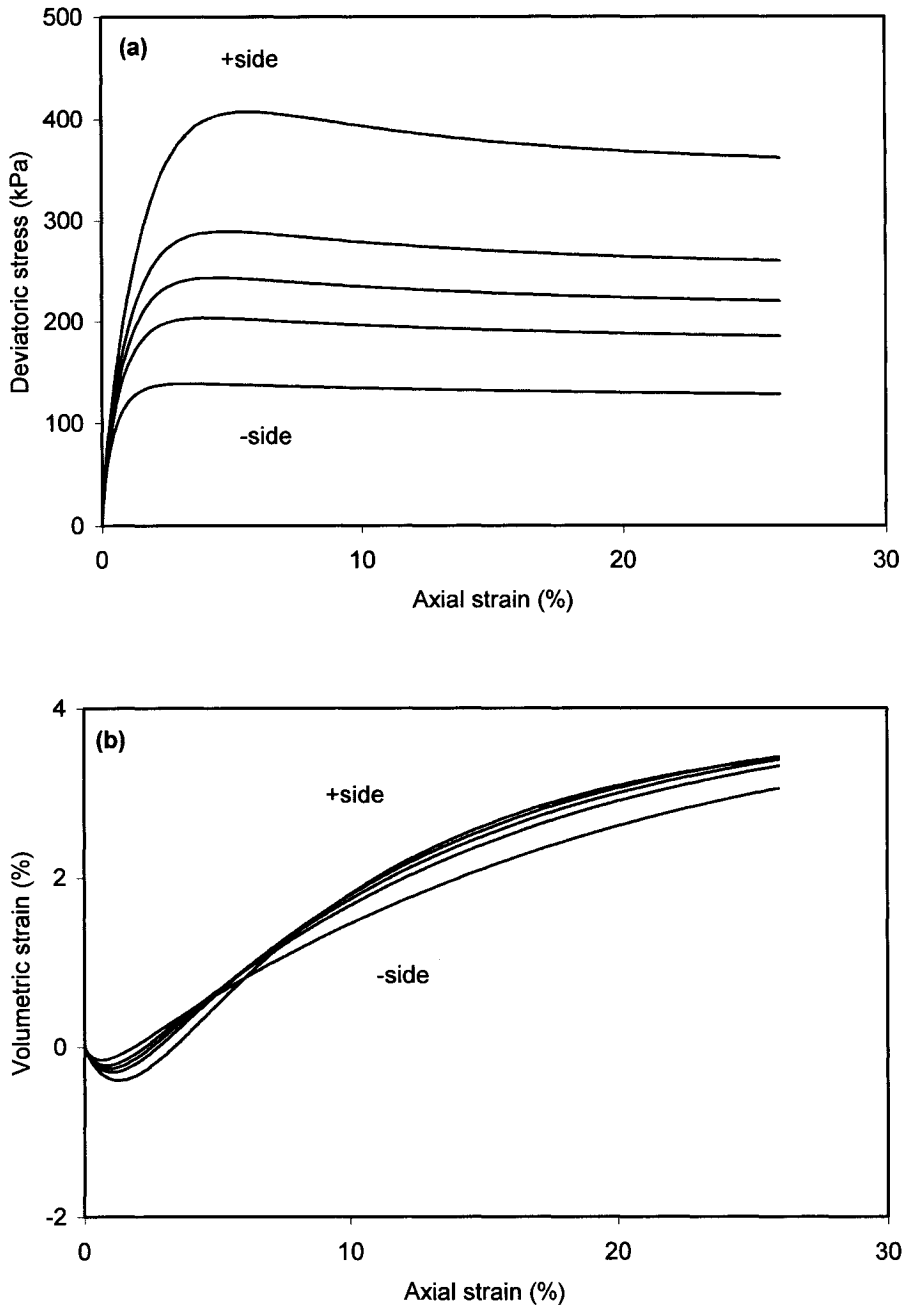

Figure 6.9 Effect of model constant M on the simulations of the behaviour of dense sand

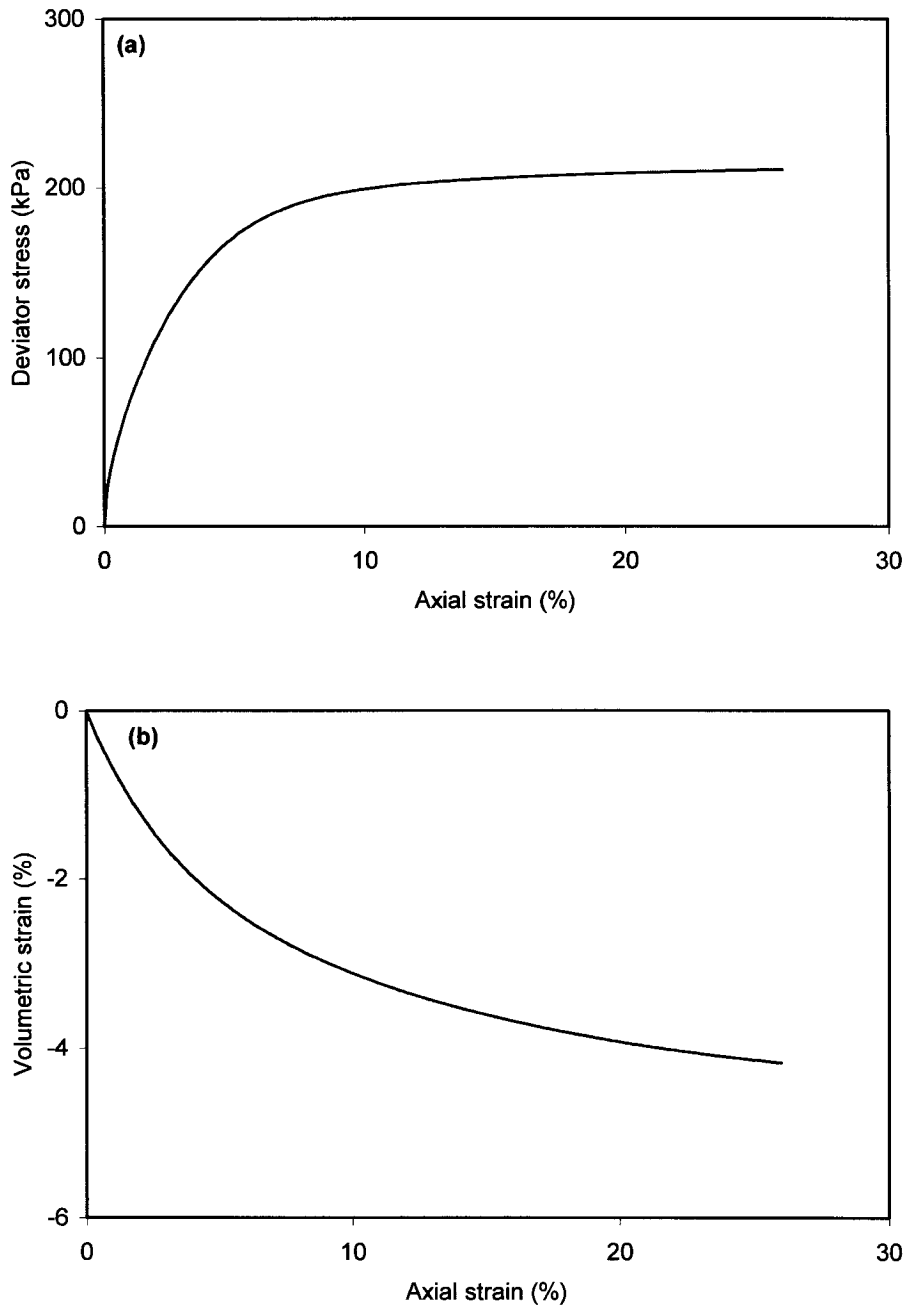

Figure 6.10 Effect of model constant c on the simulations of the behaviour of loose sand

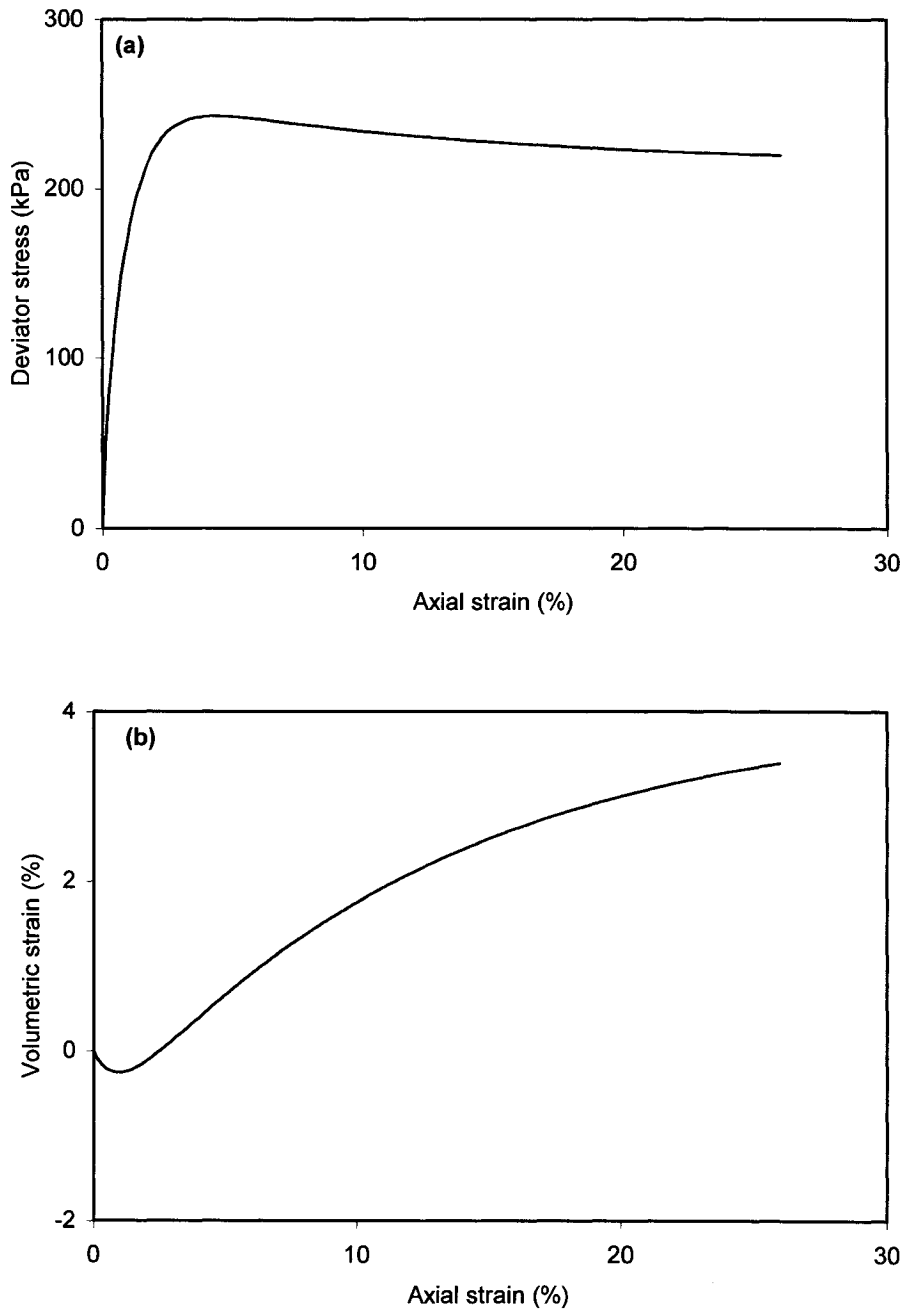

Figure 6.11 Effect of model constant c on the simulations of the behaviour of dense sand

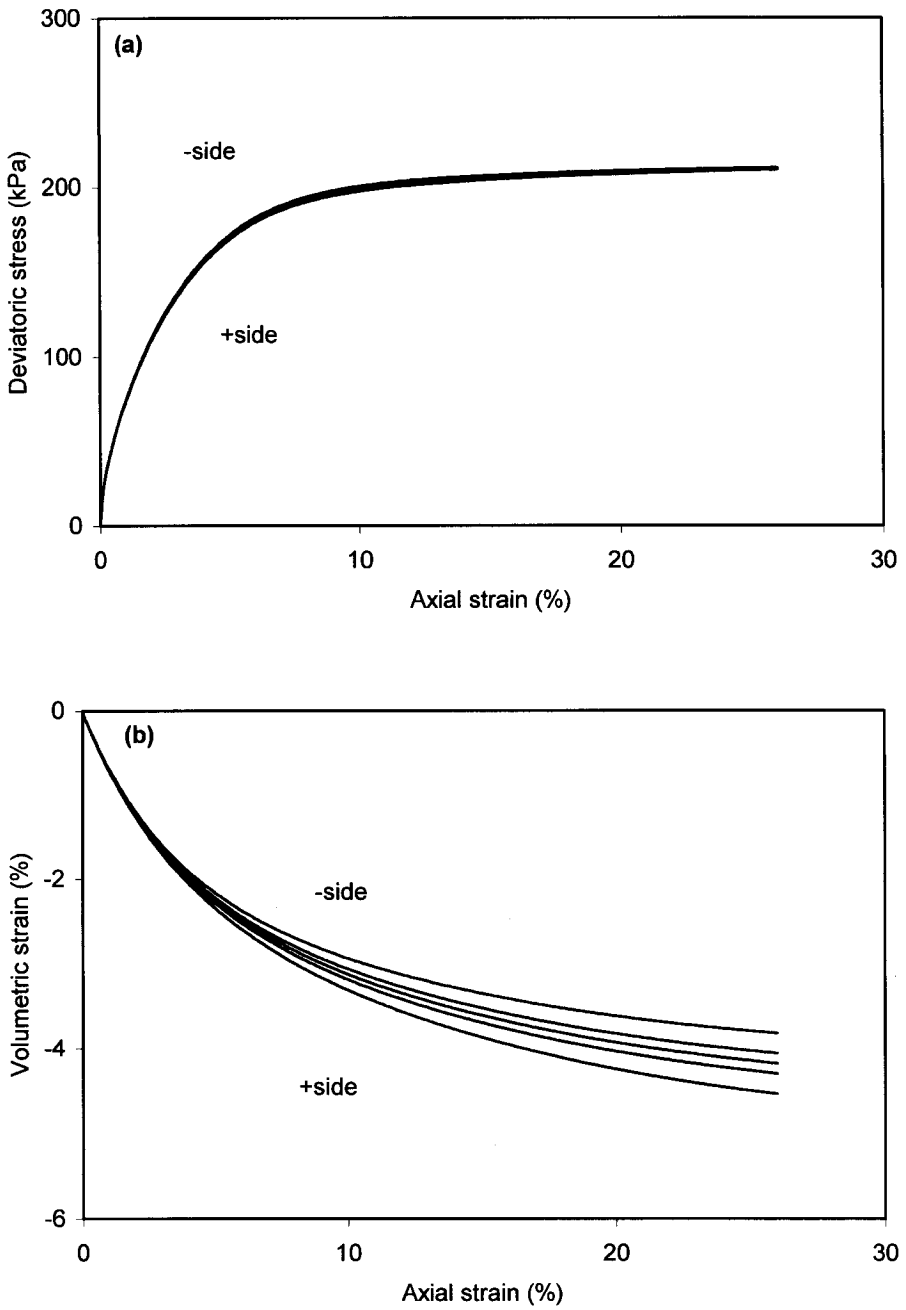

Figure 6.12 Effect of model constant λ_c on the simulations of the behaviour of loose sand

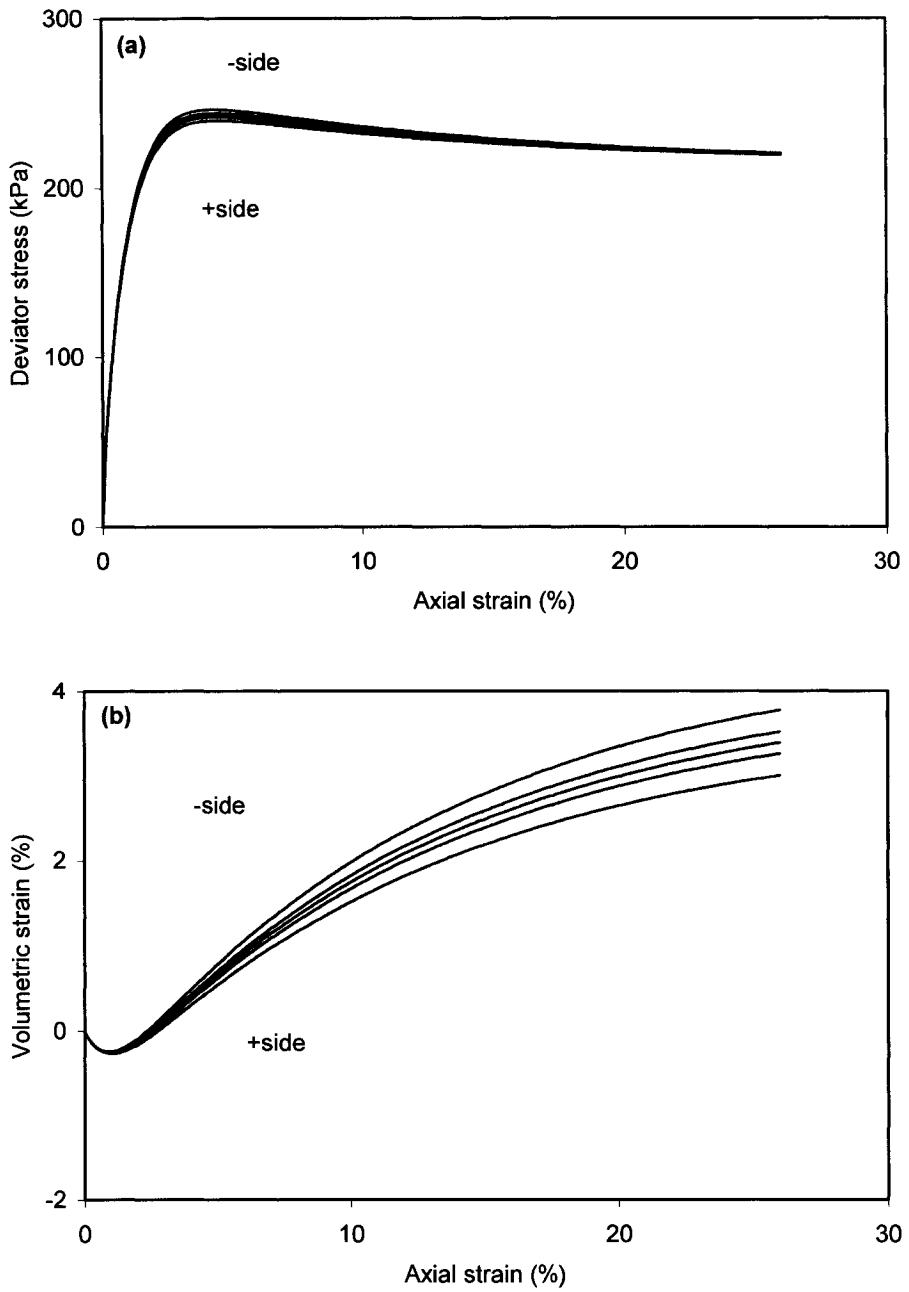

Figure 6.13 Effect of model constant λ_c on the simulations of the behaviour of dense sand

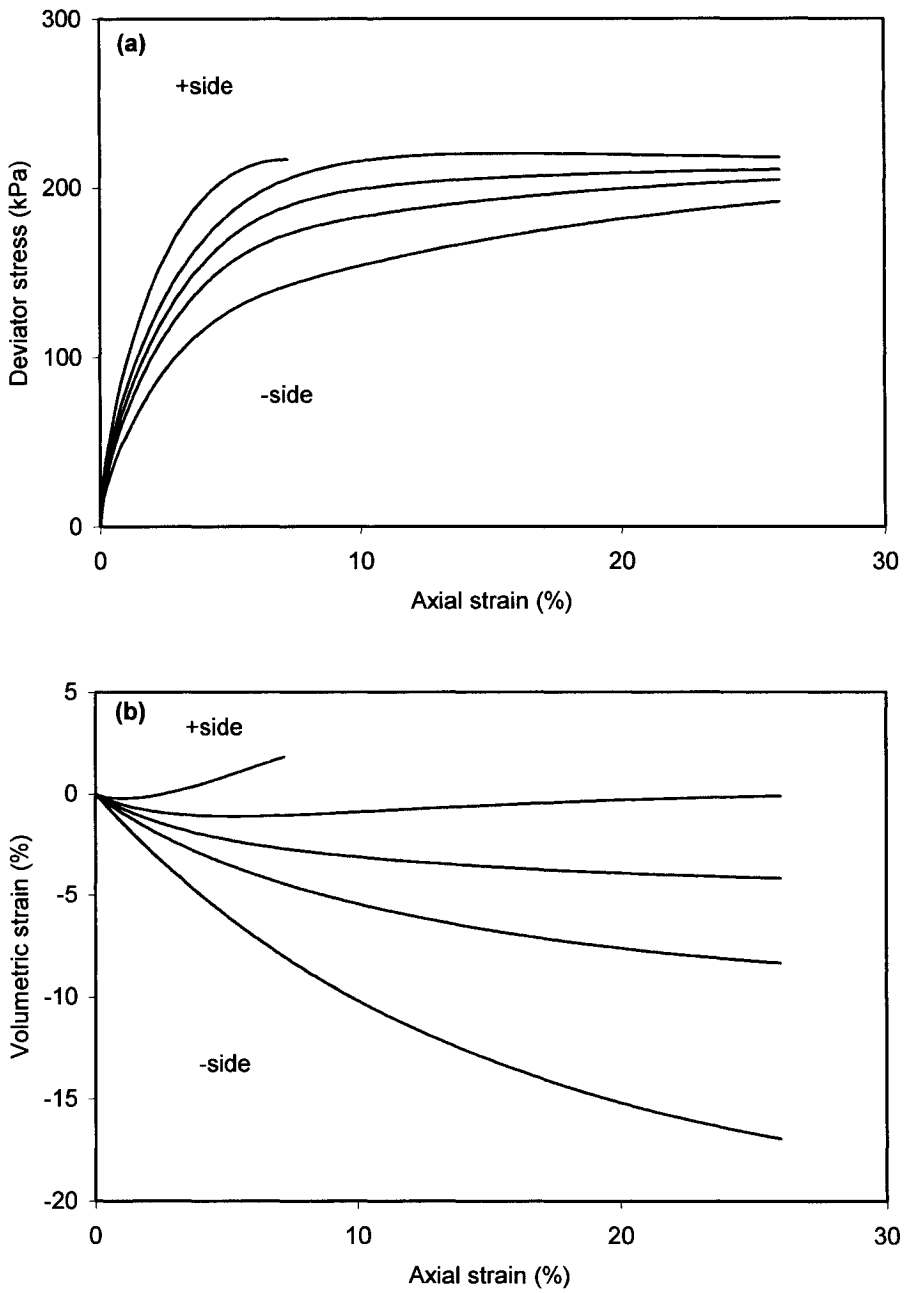

Figure 6.14 Effect of model constant e_0 on the simulations of the behaviour of loose sand

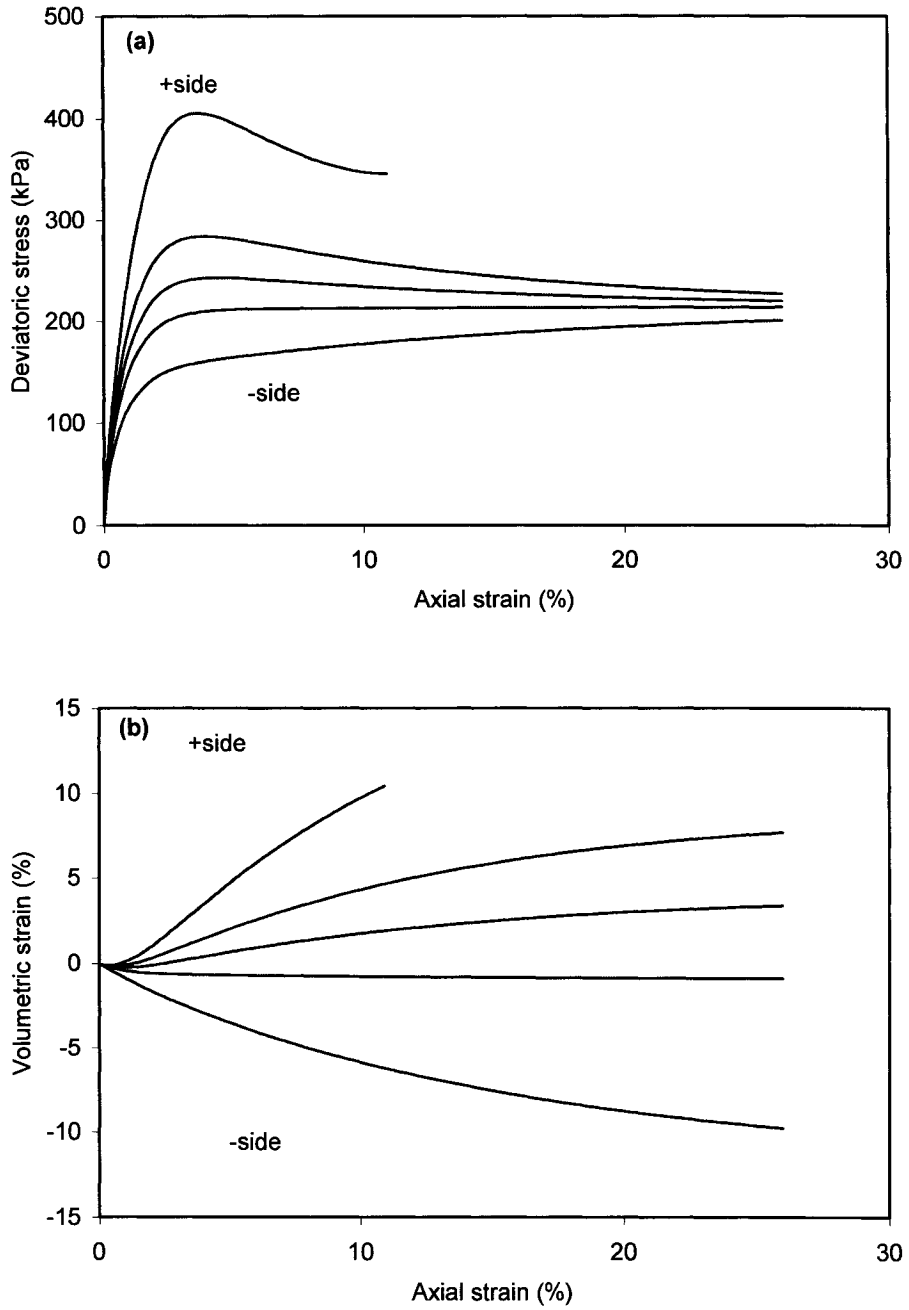

Figure 6.15 Effect of model constant e_0 on the simulations of the behaviour of dense sand

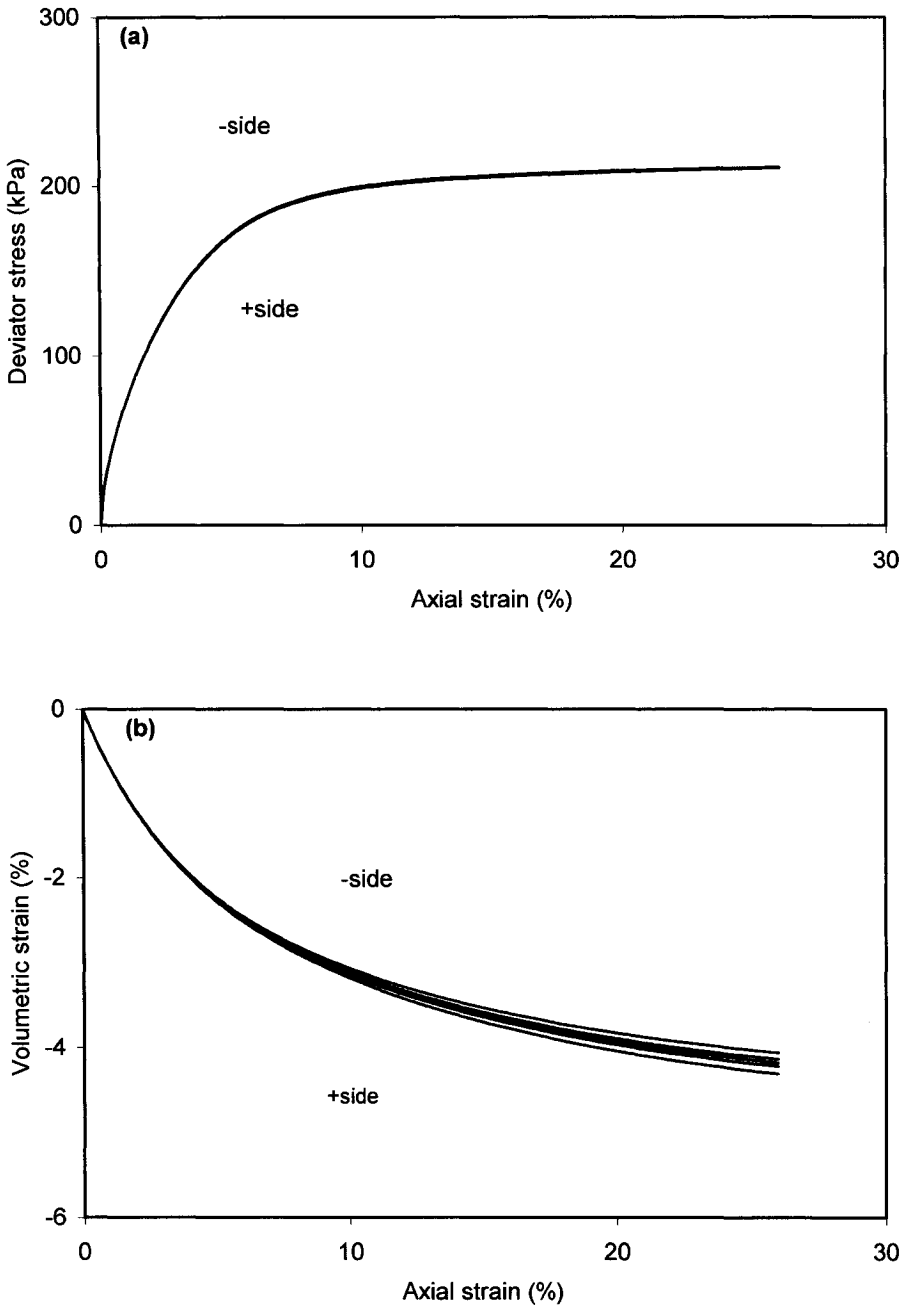

Figure 6.16 Effect of model constant ξ on the simulations of the behaviour of loose sand

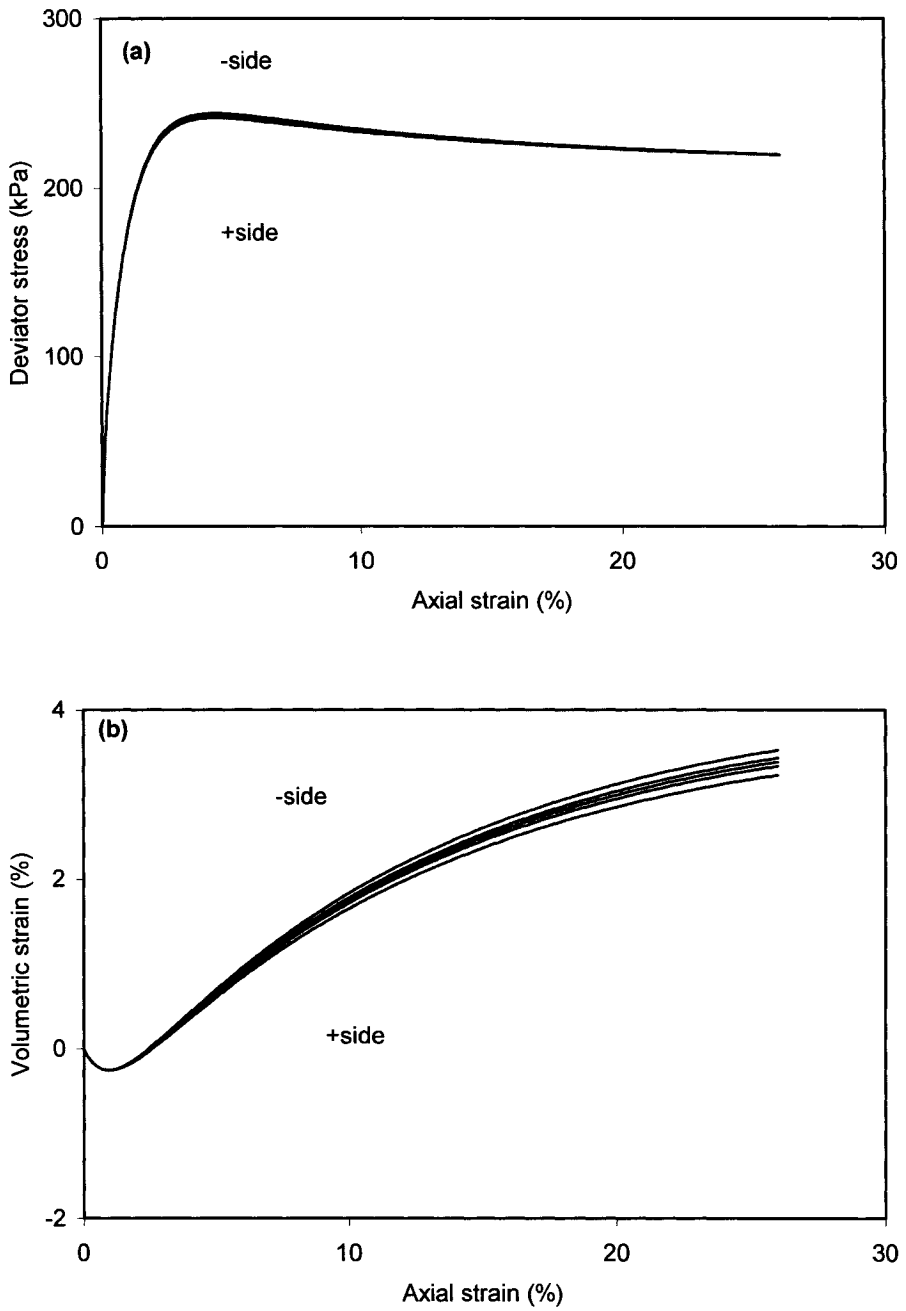

Figure 6.17 Effect of model constant ξ on the simulations of the behaviour of dense sand

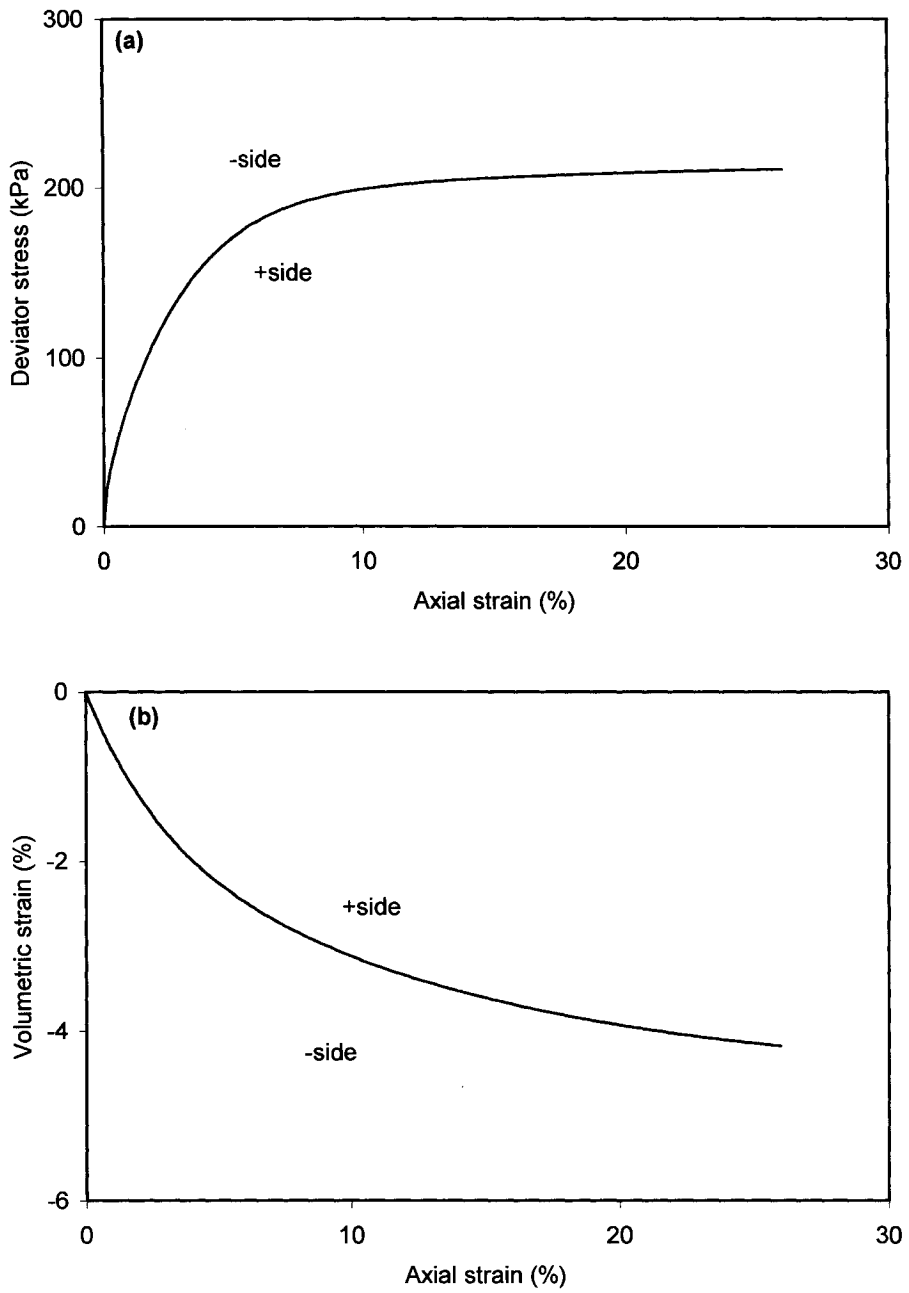

Figure 6.18 Effect of model constant m on the simulations of the behaviour of loose sand

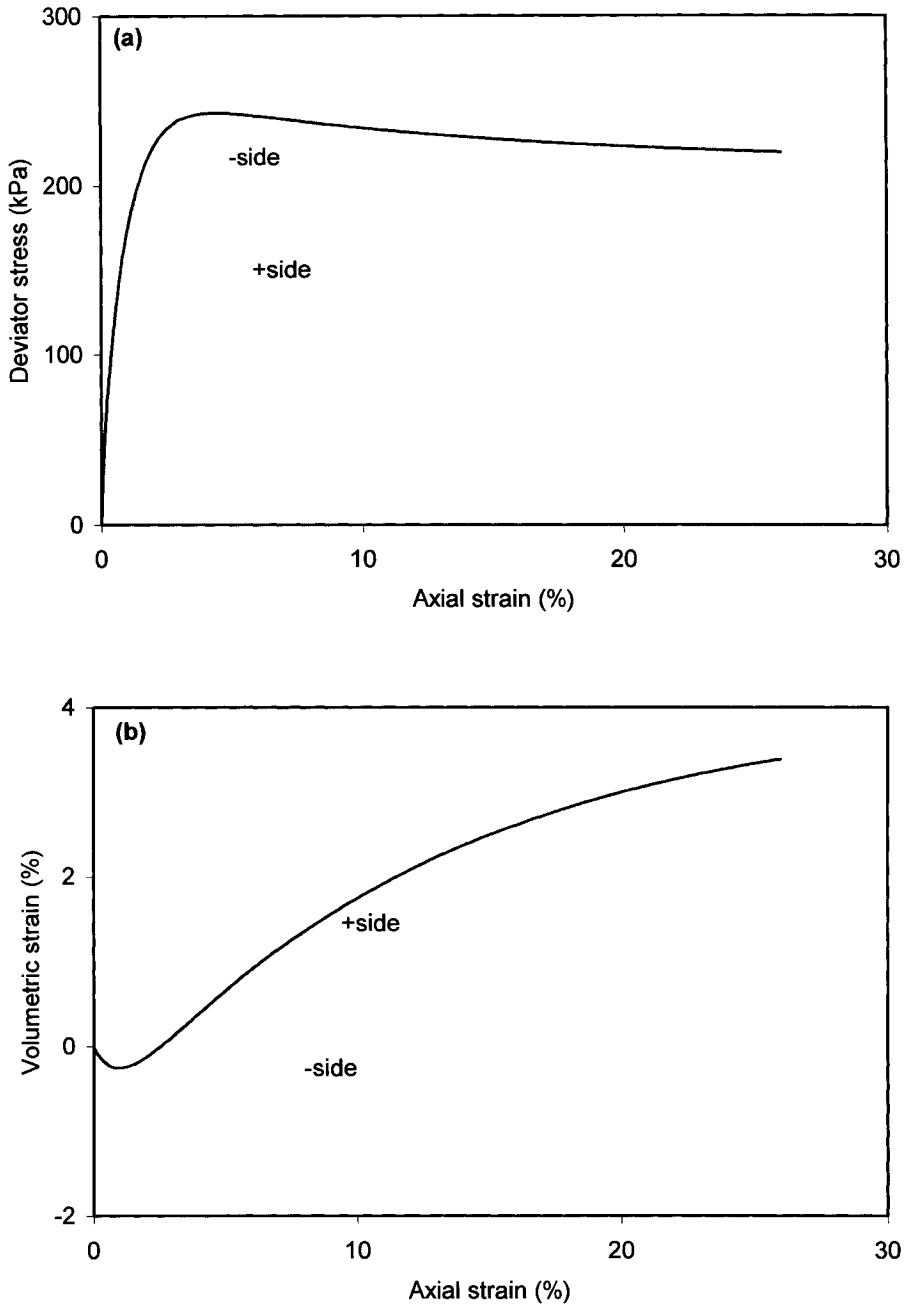

Figure 6.19 Effect of model constant m on the simulations of the behaviour of dense sand

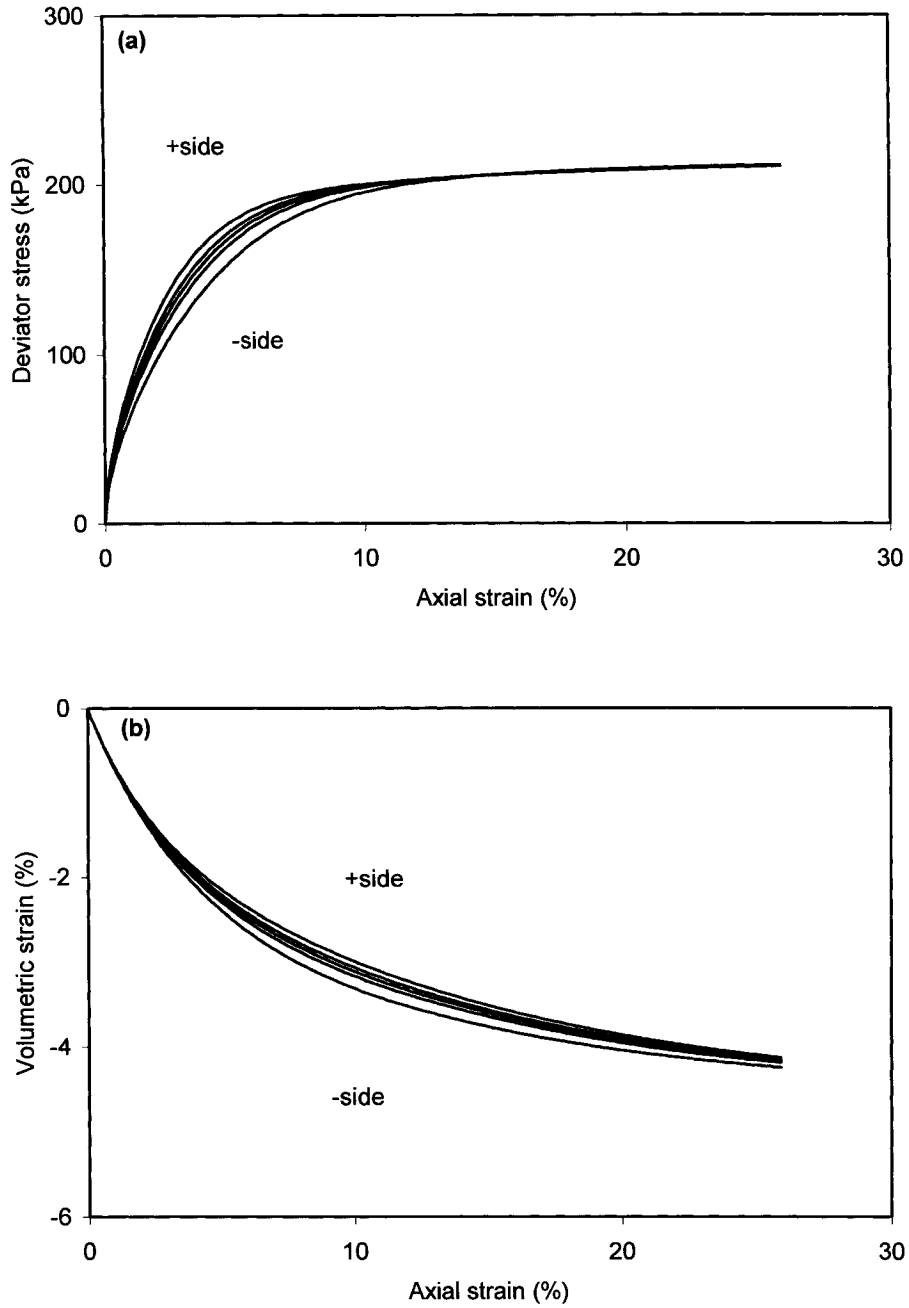

Figure 6.20 Effect of model constant h_0 on the simulations of the behaviour of loose sand

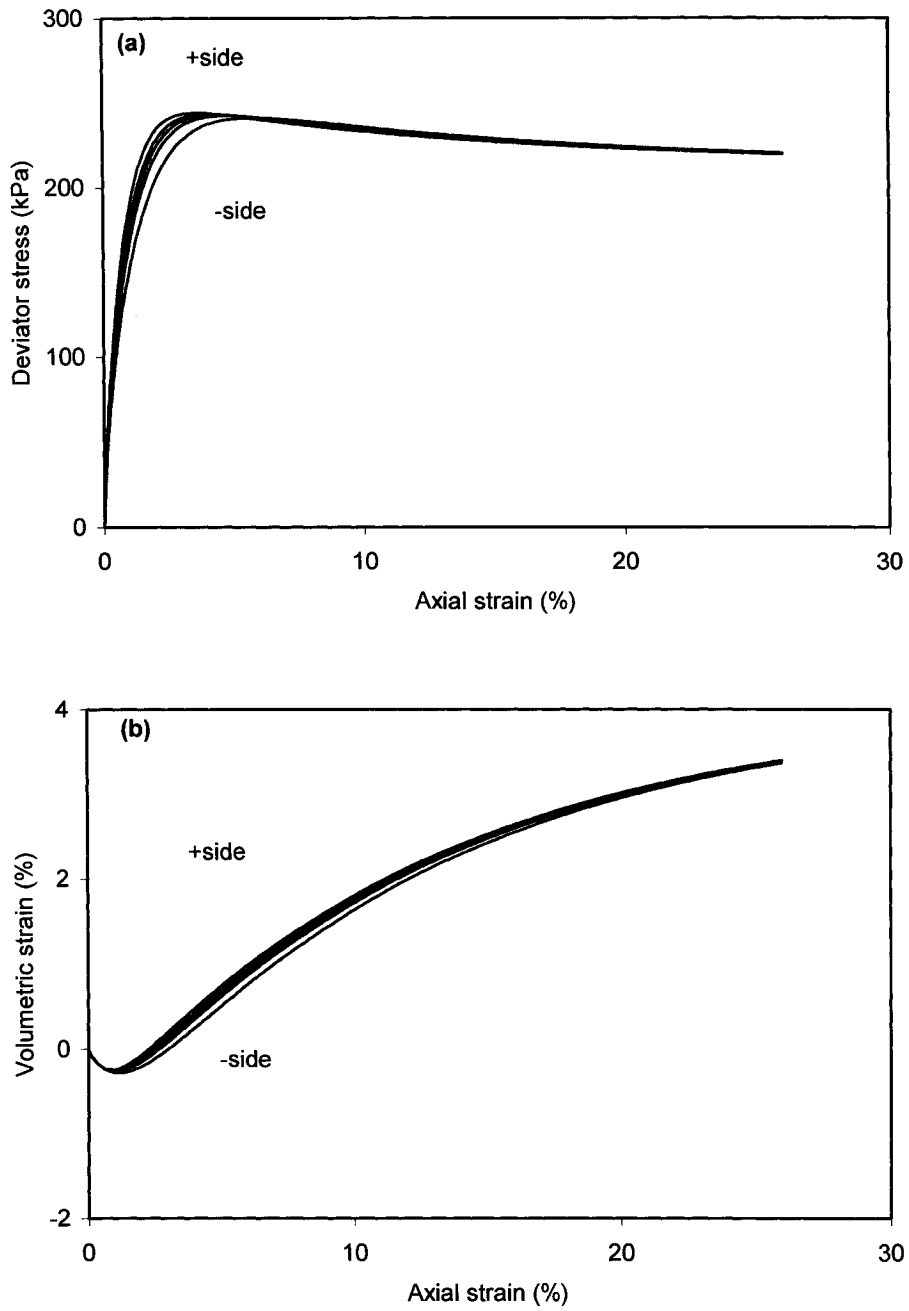

Figure 6.21 Effect of model constant h_0 on the simulations of the behaviour of dense sand

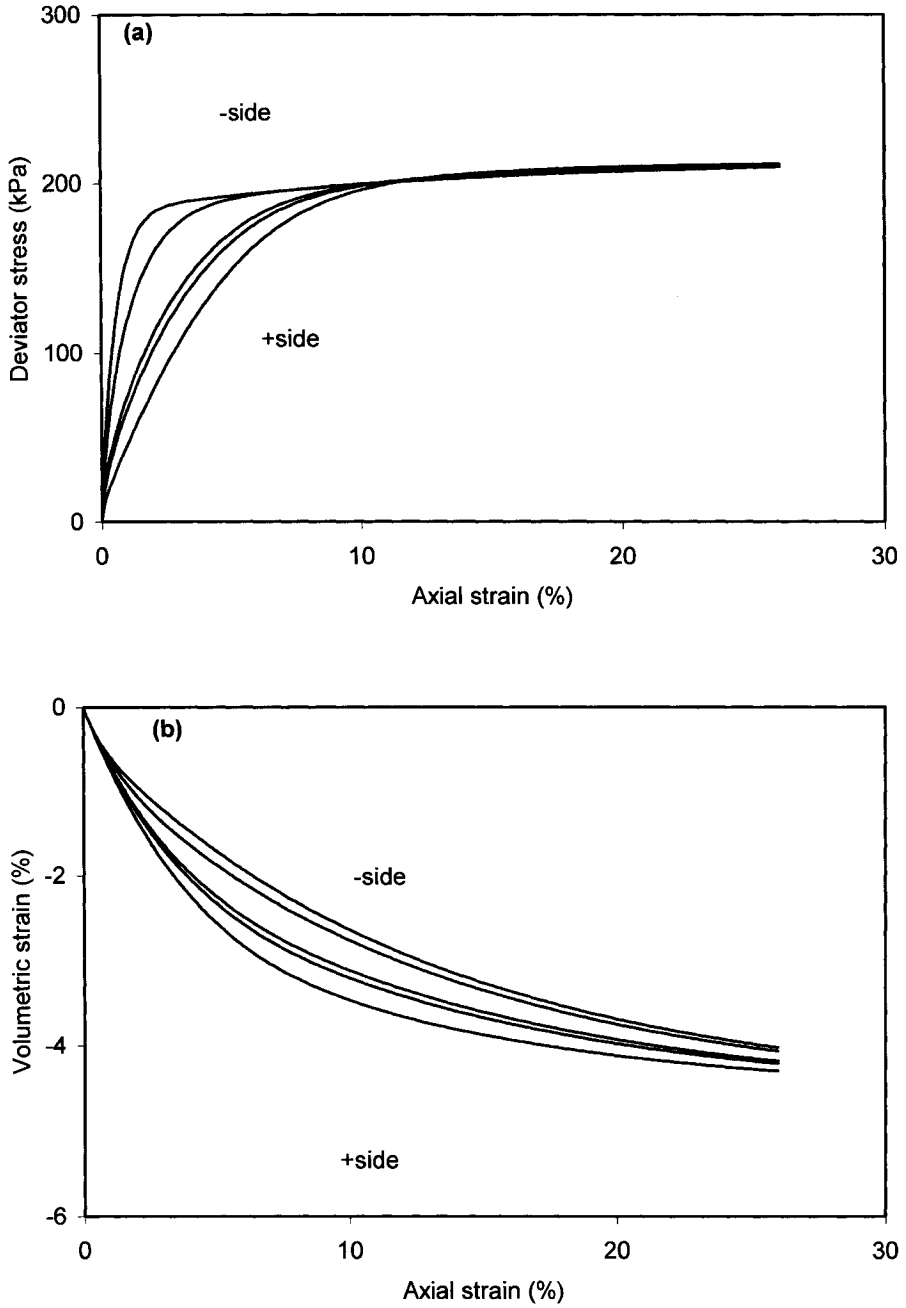

Figure 6.22 Effect of model constant c_h on the simulations of the behaviour of loose sand

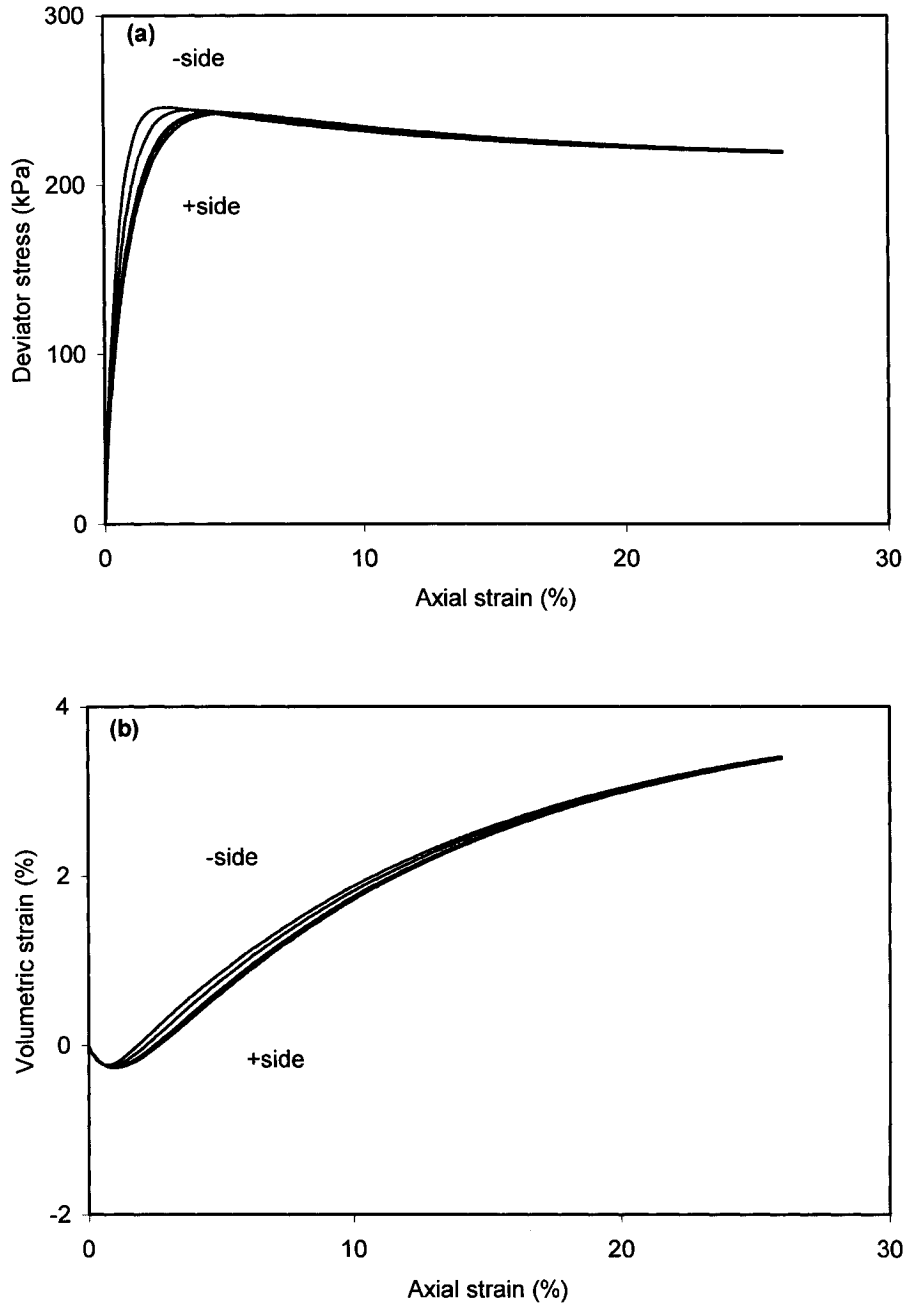

Figure 6.23 Effect of model constant c_h on the simulations of the behaviour of dense sand

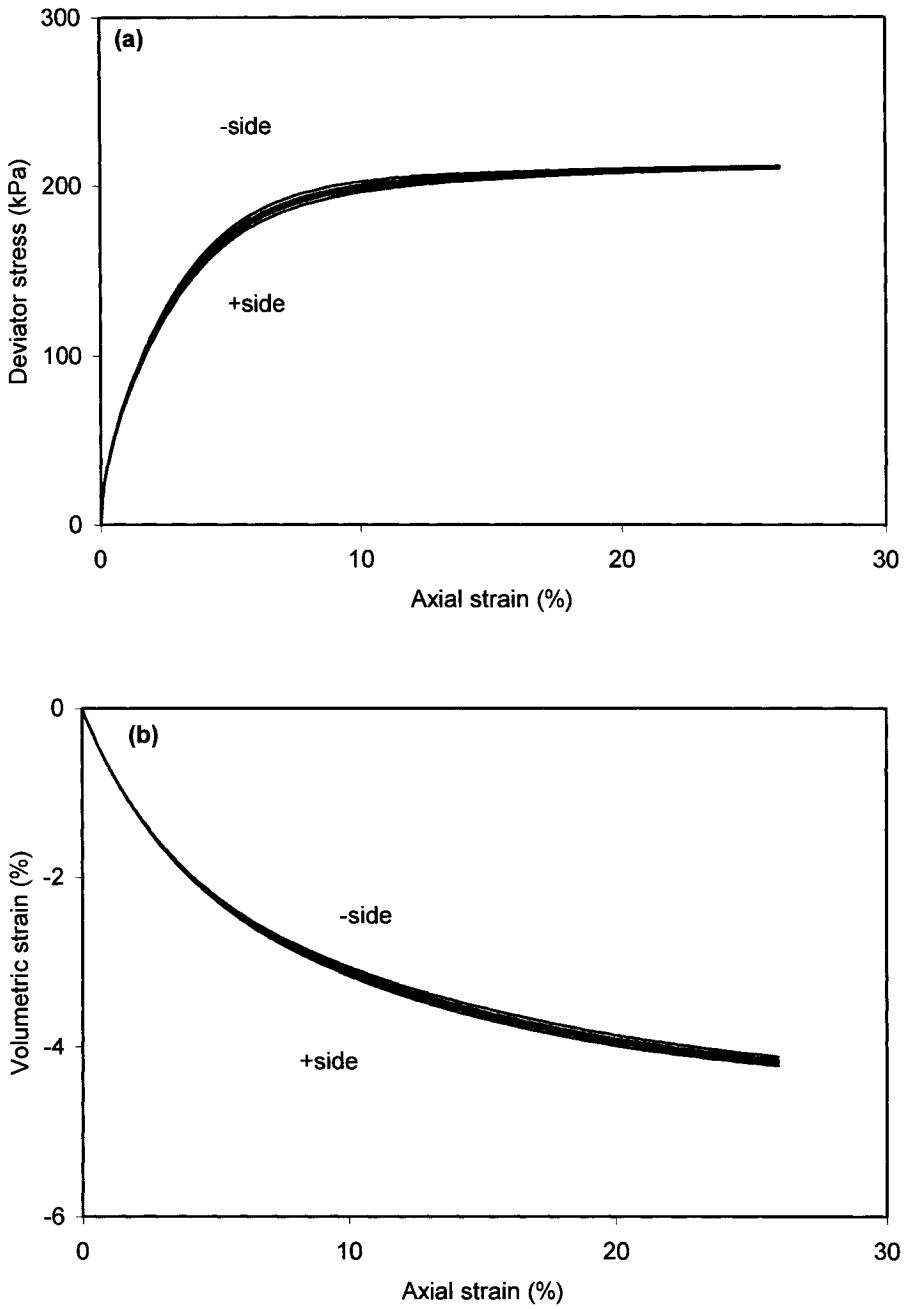

Figure 6.24 Effect of model constant n^b on the simulations of the behaviour of loose sand

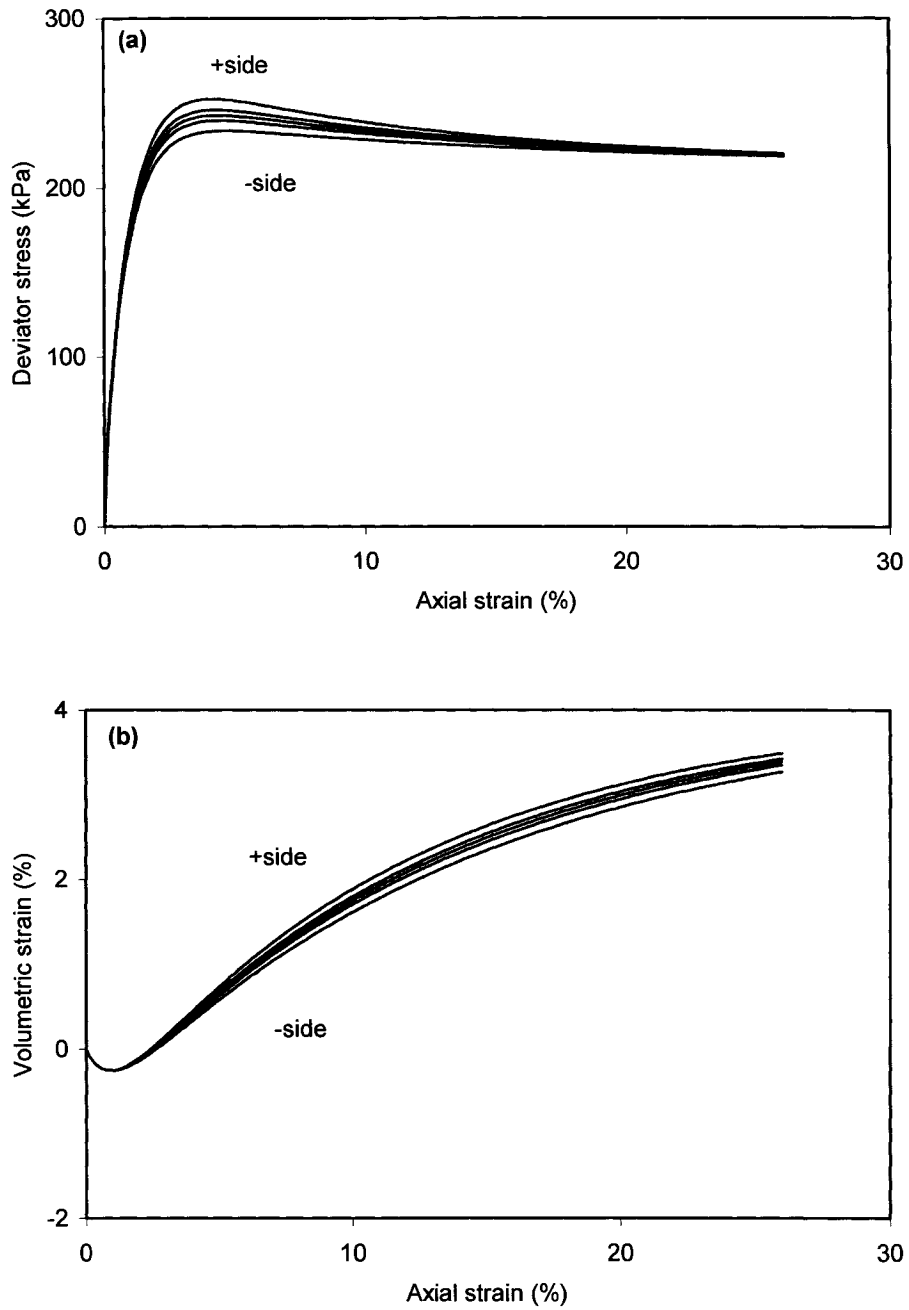

Figure 6.25 Effect of model constant n^b on the simulations of the behaviour of dense sand

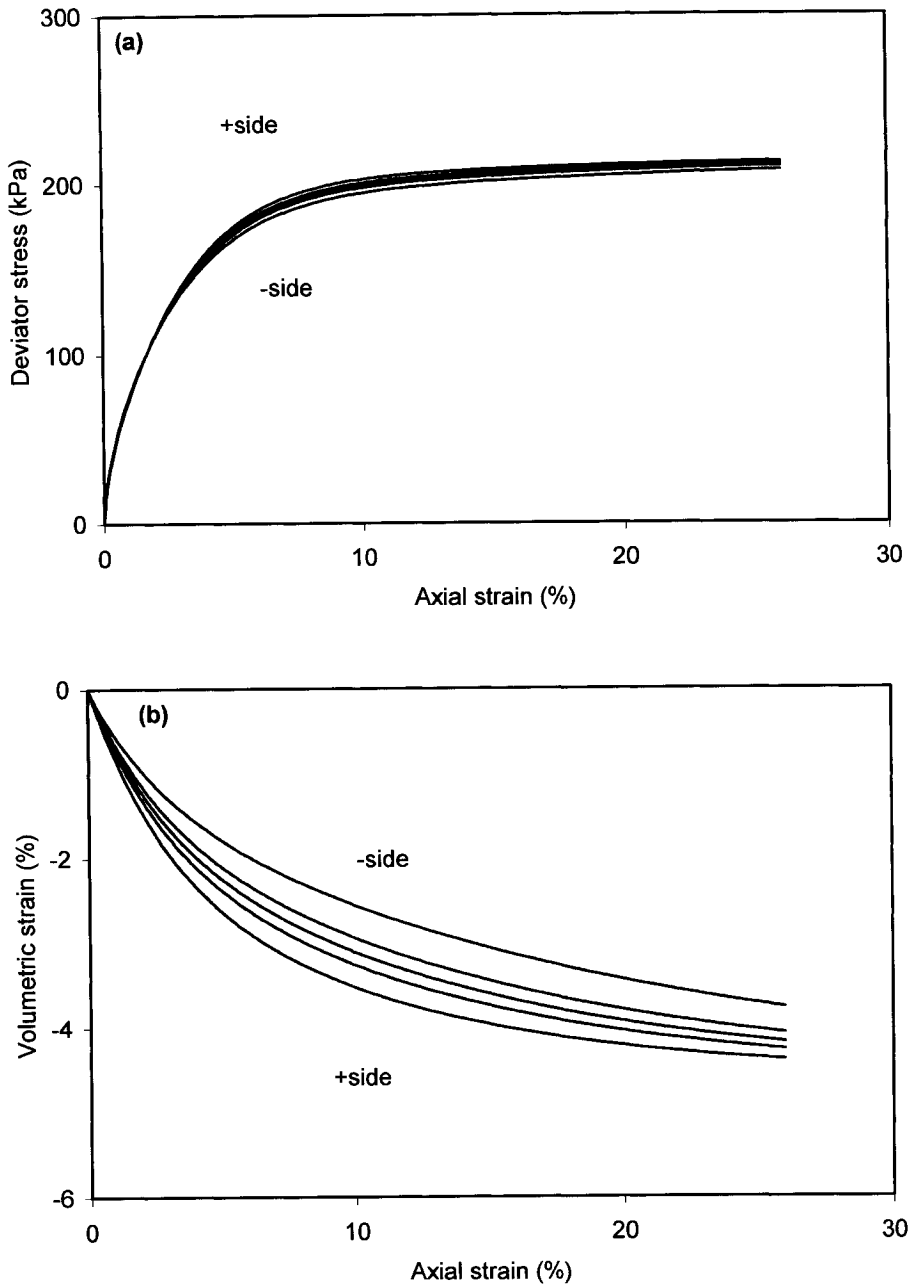

Figure 6.26 Effect of model constant A_0 on the simulations of the behaviour of loose sand

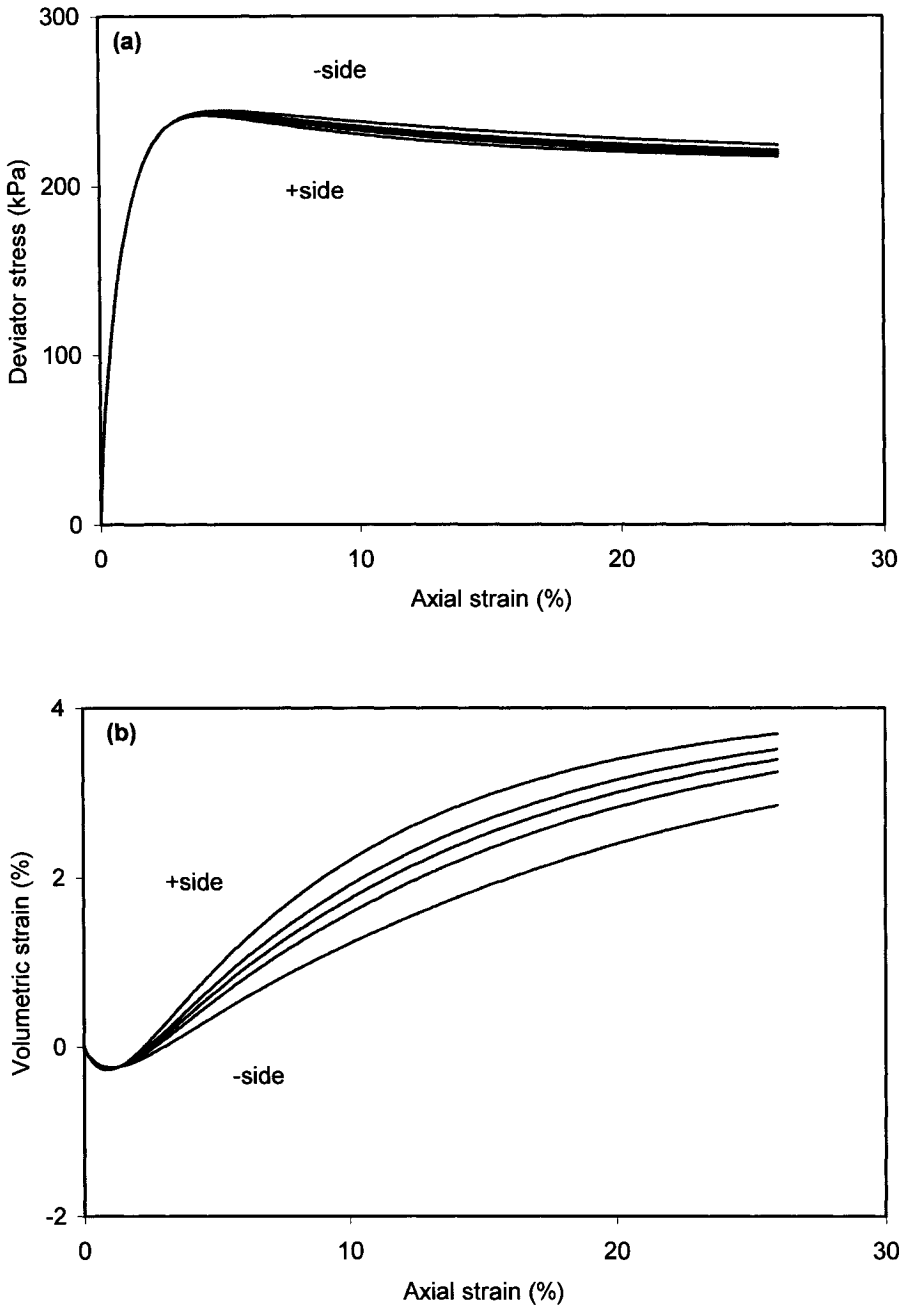

Figure 6.27 Effect of model constant A_0 on the simulations of the behaviour of dense sand

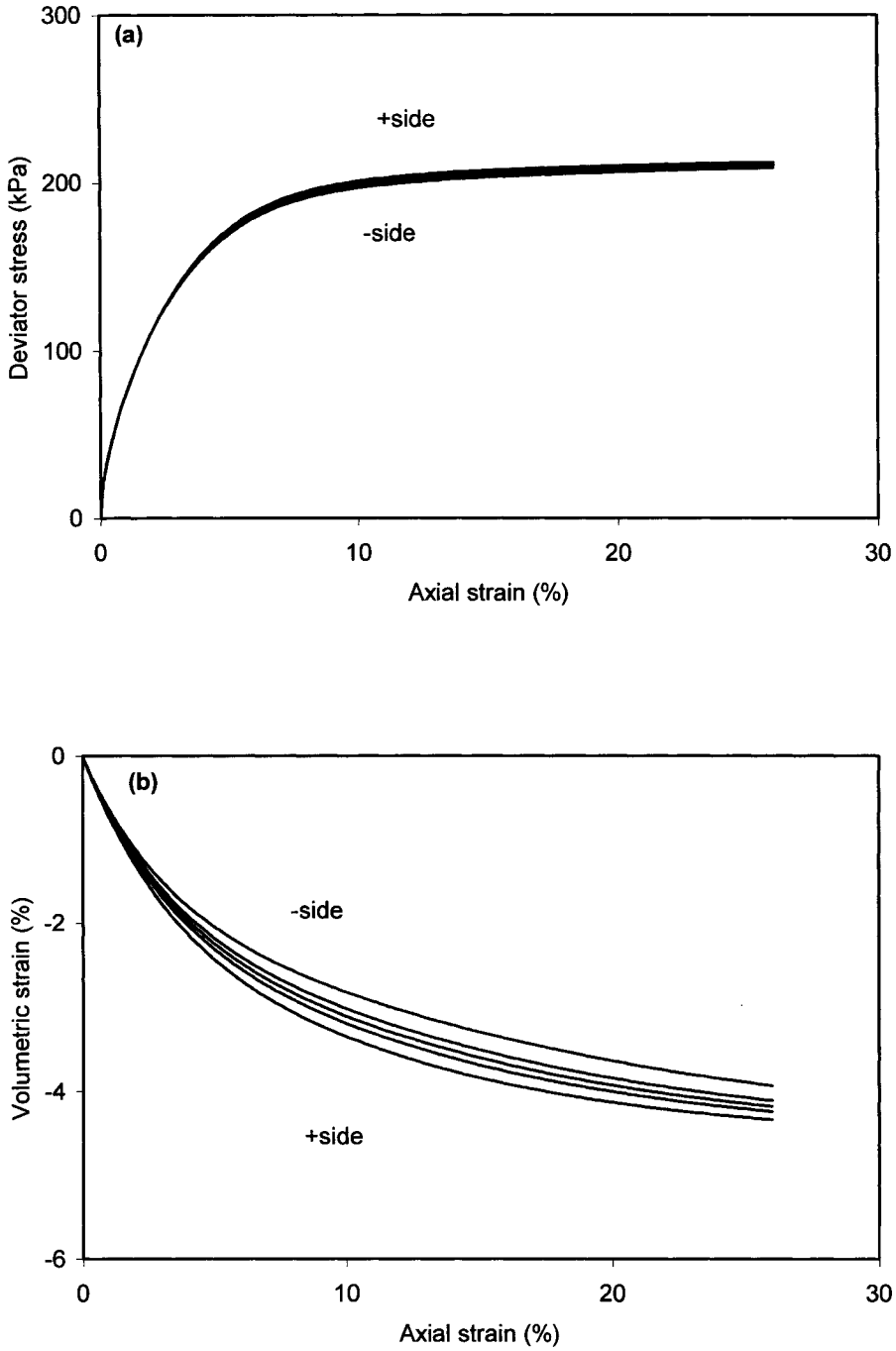

Figure 6.28 Effect of model constant n^d on the simulations of the behaviour of loose sand

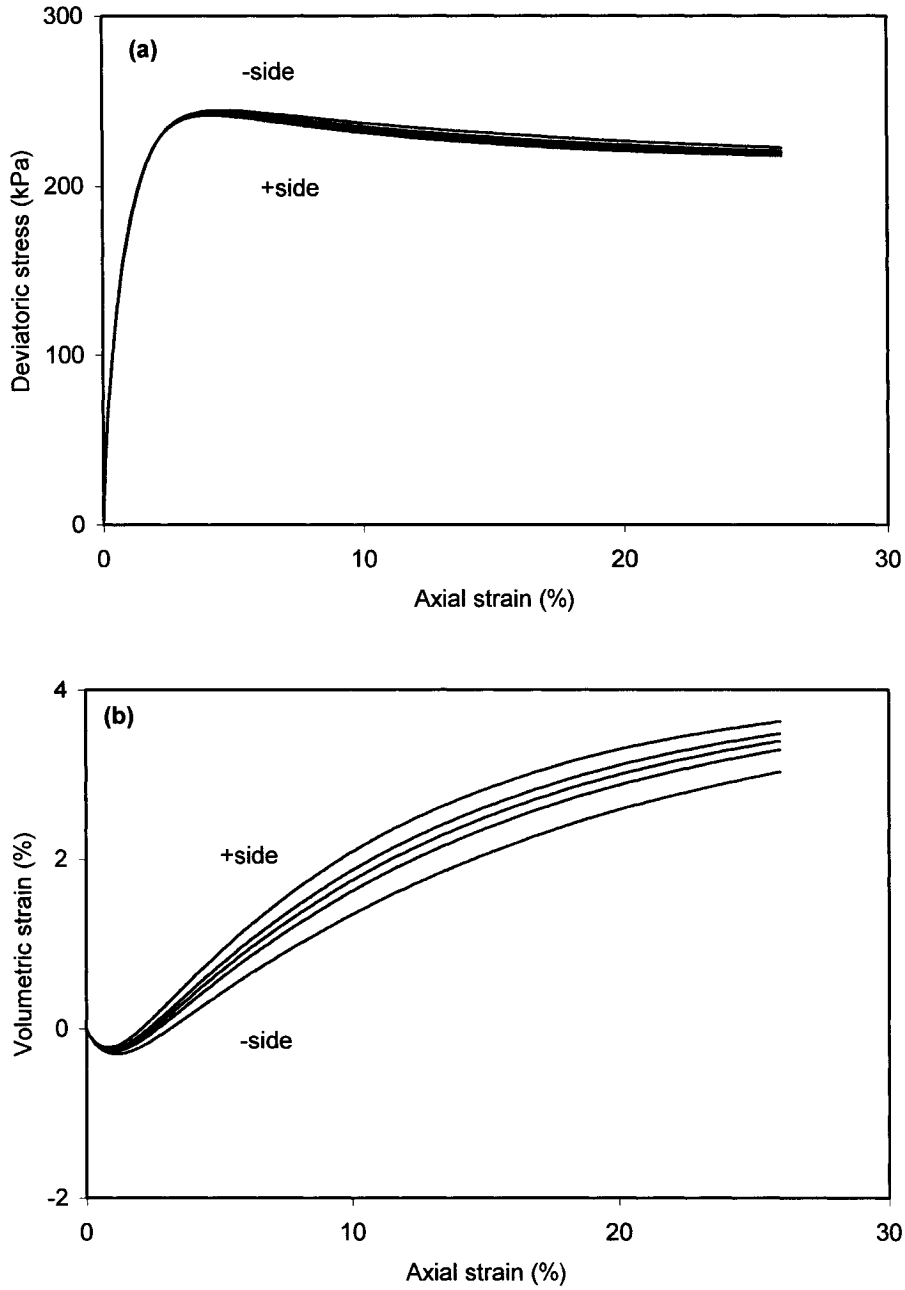

Figure 6.29 Effect of model constant n^d on the simulations of the behaviour of dense sand

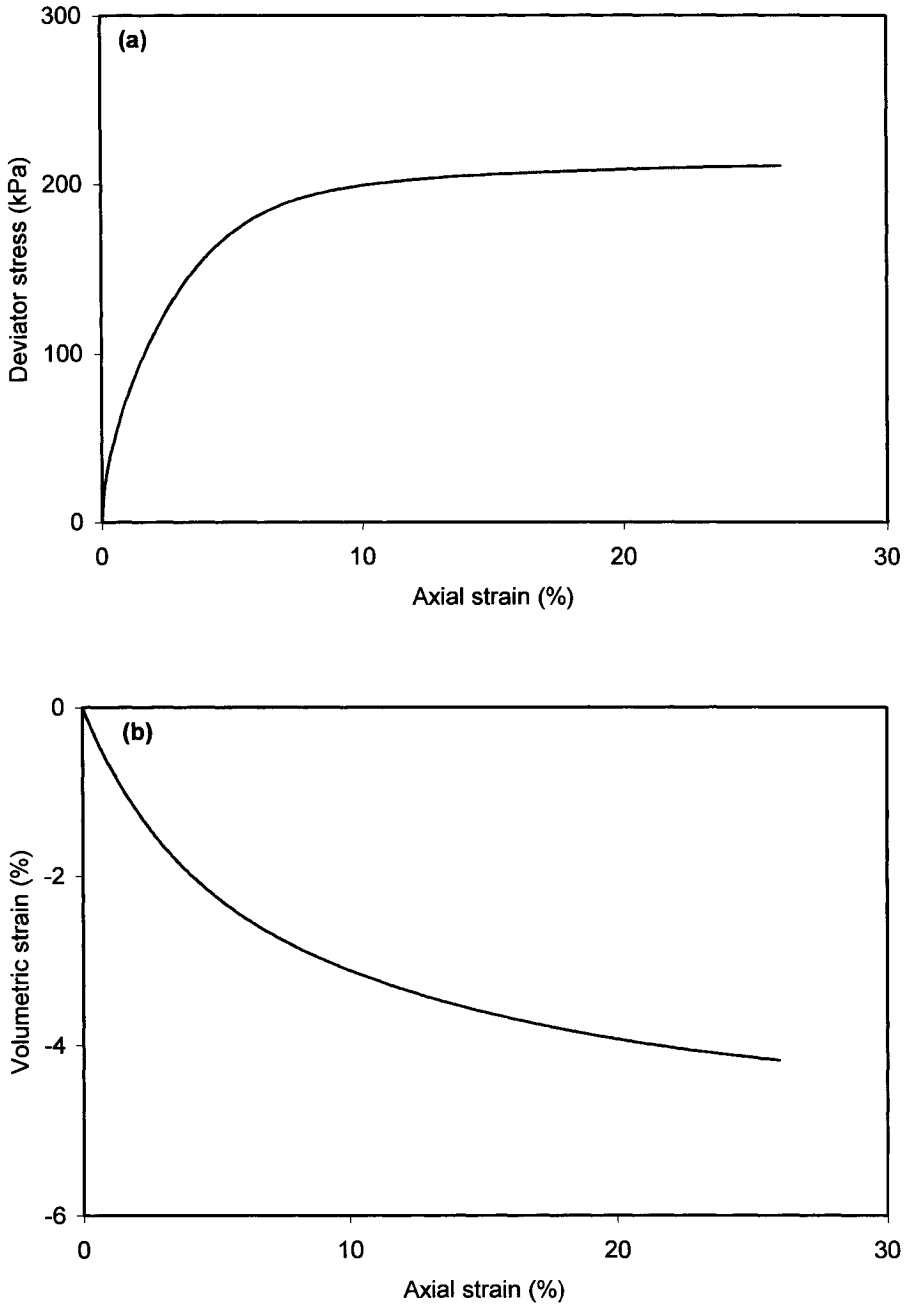

Figure 6.30 Effect of model constant z_{max} on the simulations of the behaviour of loose sand

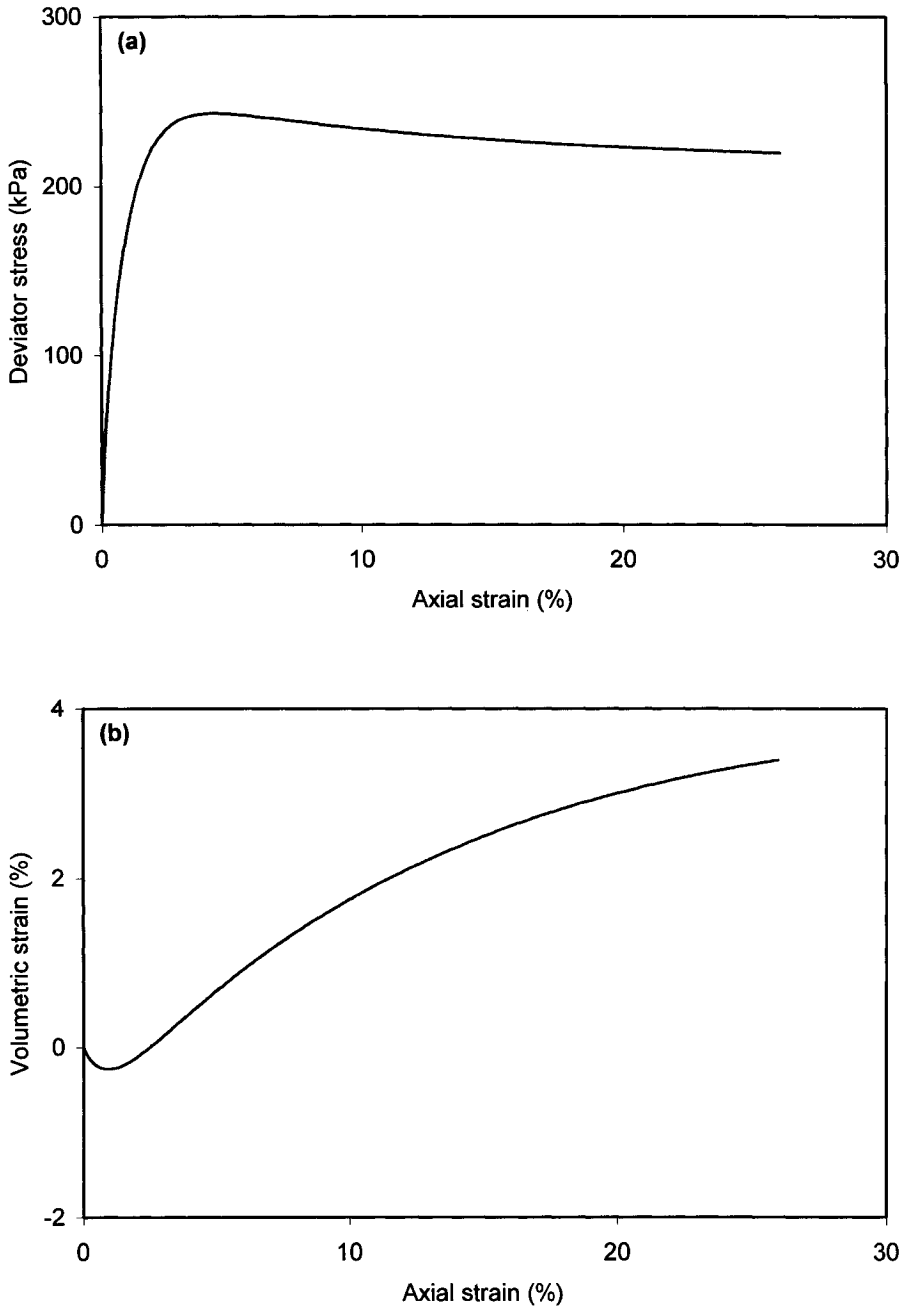

Figure 6.31 Effect of model constant z_{max} on the simulations of the behaviour of dense sand

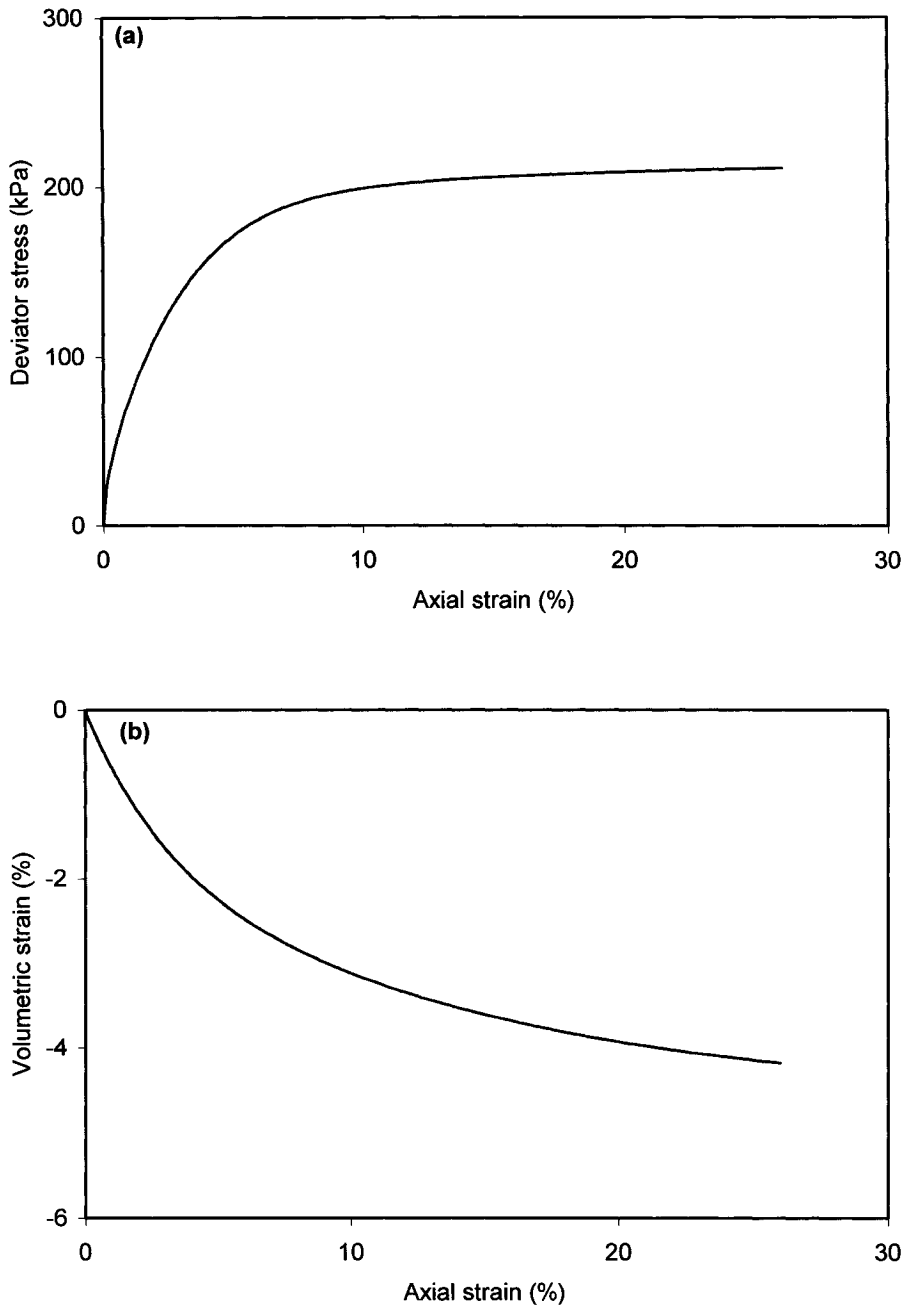

Figure 6.32 Effect of model constant c_z on the simulations of the behaviour of loose sand

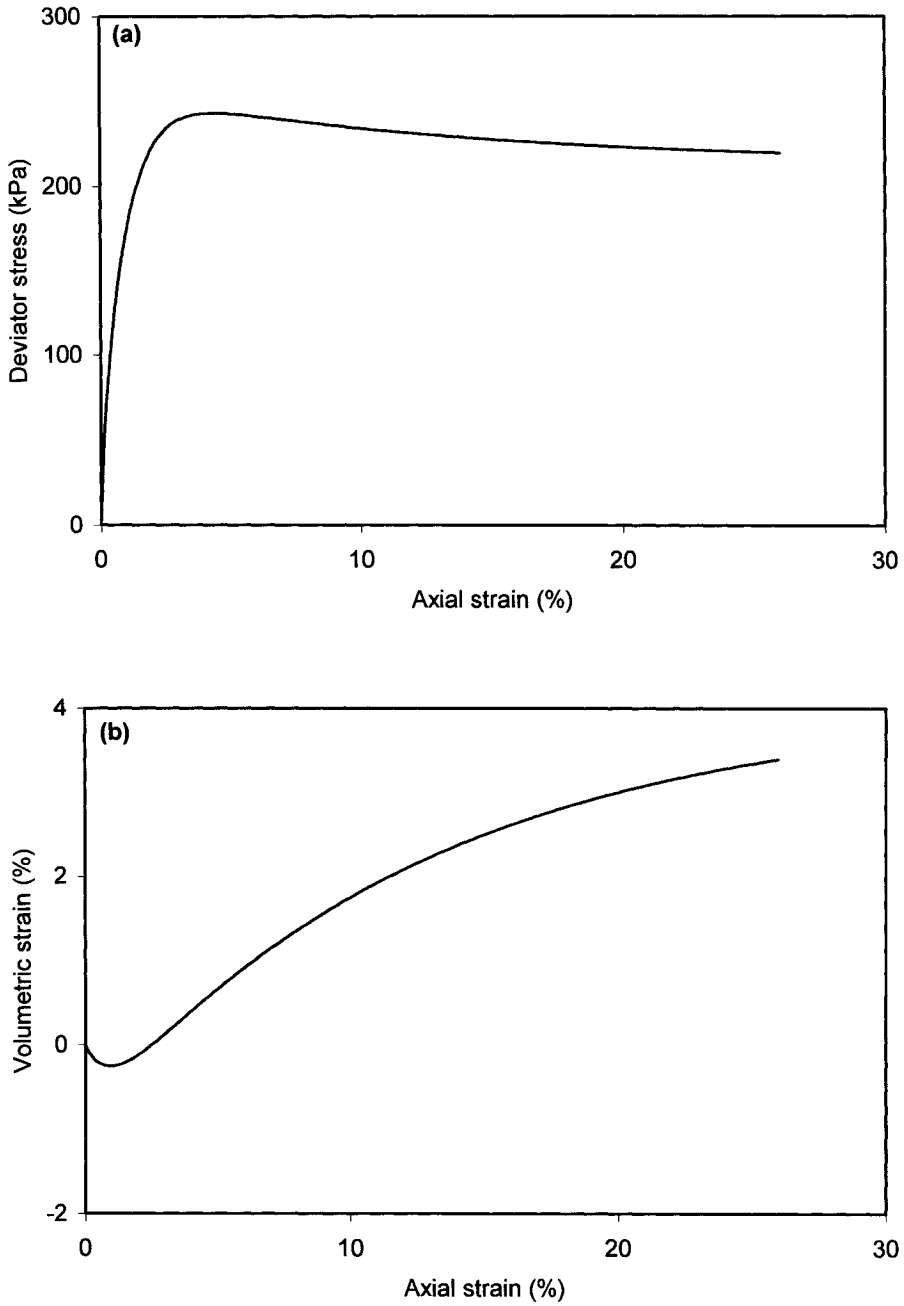

Figure 6.33 Effect of model constant c_z on the simulations of the behaviour of dense sand

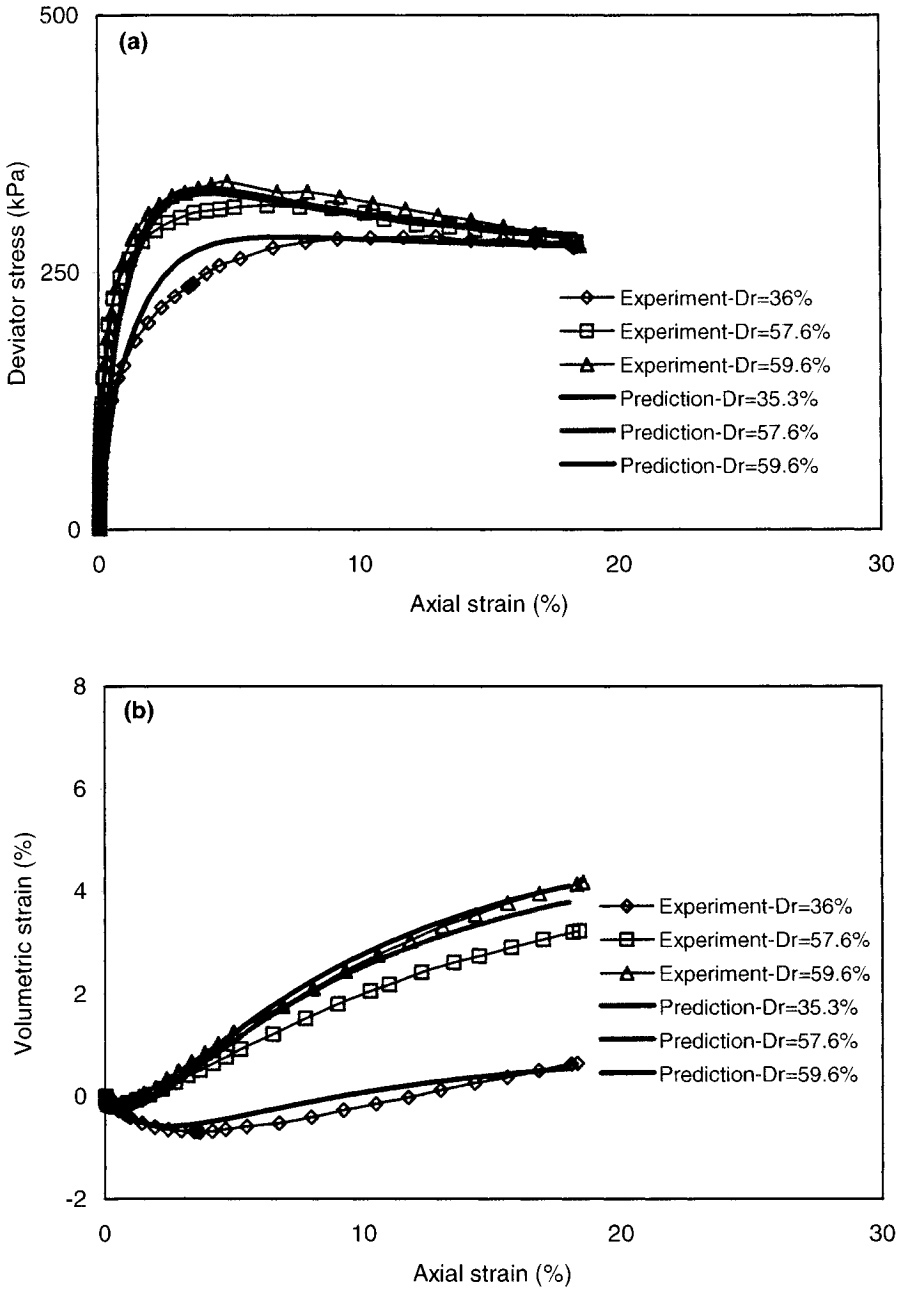

Figure 3.34 Comparison between model simulations and triaxial tests data (confining pressure =100 kPa)

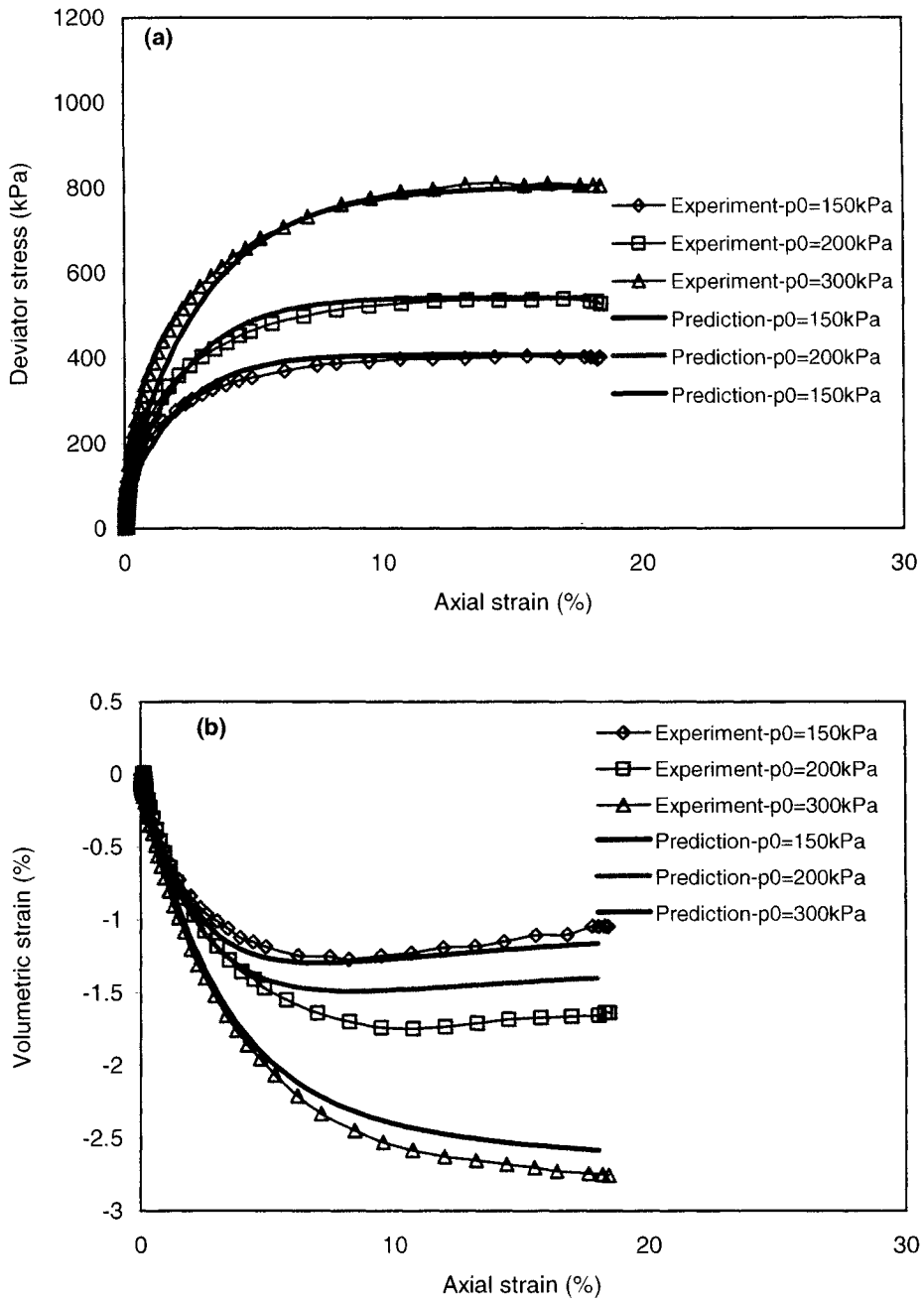

Figure 3.35 Comparison between model simulations and triaxial tests data (confining pressure =150 kPa, 200 kPa, and 300 kPa)

CHAPTER 7

MODELING THE CYCLIC BEHAVIOUR OF SAND-STRUCTURE INTERFACES

7.1 Introduction

The model presented in Chapter 6 is used in this chapter to simulate the cyclic behaviour of loose and dense sand interfaces. The determination of the model parameters is described and then predictions are made for the tests conducted with a normal stress of 300 kPa and an amplitude of tangential displacement of 3 mm.

7.2 Determination of model parameters

The model has fifteen parameters as described in Chapter 6. All model constants, except G_0, M, c, and A_0 are kept the same as those presented in Table 6.2. The model constants G_0 and A_0 are assigned values of 85 and 0.754, respectively.

The constant M is obtained by using the residual friction angle mobilized at the interface (Equation 6.16a). The results of monotonic tests on loose sand interface are used to obtain the friction angle (Figure 7.1). The measured friction angle is δ=26° and the values of M and c corresponding to this friction angle are 1.03 (Equation 6.16a) and 0.745 (Equation 6.17), respectively.

The constants e_0, λ_c, and ξ are obtained from triaxial data (Chapter 6) and they have the same values as those presented in Table 6.2. However, an alternative approach which

used the interface test data was devised to determine the value of these constants. The alternative approach consisted of fitting an equation similar to Equation 6.5f to the void ratio versus normal stress data obtained at the end of the monotonic tests conducted on loose sand interfaces and the normal stress acting on the interface. This was achieved simply by replacing the mean pressure in Equation 6.5f by the normal stress. This approach was used because of the similarities reported by Boulon and Nova (1990) between interface tests and triaxial tests. Figure 7.2 shows that the values 0.938, 0.019, and 0.65 used for e_0, λ_c, and ξ, respectively, fit well the interface test data.

7.3 Model predictions

Before making predictions the initial state of stress and the strains in the interfaces tests are presented.

7.3.1 Initial state of stress

The initial state of stress was taken such that the normal stress in the vertical direction $\sigma_{11}=\sigma_n$, and the normal stresses in two horizontal directions are determined using the well known empirical equation proposed by Jaky (1944) ($\sigma_{22}=\sigma_{33}=\sigma_n(1-\sin\phi)$). The initial values of the shear stress are zero. As a result the initial stress tensor $\boldsymbol{\sigma}$ is:

$$\boldsymbol{\sigma}=\begin{bmatrix}\sigma_n & 0 & 0\\ 0 & \sigma_n(1-\sin\phi) & 0\\ 0 & 0 & \sigma_n(1-\sin\phi)\end{bmatrix} \qquad 7.1$$

7.3.2 Input strains

The strain driven version of the model was used for the simulations (Equation 6.9). Input strain rates representing plane strain conditions were used (i.e. $\varepsilon_{13}=\varepsilon_{23}=\varepsilon_{33}=0$). In

addition, the lateral normal strain is assumed equal to zero ($\varepsilon_{22}=0$). Therefore, the only non-zero components of the strain rate are the vertical normal strain (ε_{11}) and the shear strains ε_{12} and ε_{21}. The shear strains are determined from the digitized positions of the stack of plates shown in Figures 4.2 and 4.3 for loose sand and dense sand interfaces, respectively. As a result the strain tensor $\boldsymbol{\varepsilon}$ is expressed as:

$$\boldsymbol{\varepsilon} = \begin{bmatrix} \varepsilon_{11} & \varepsilon_{12} & 0 \\ \varepsilon_{21} & 0 & 0 \\ 0 & 0 & 0 \end{bmatrix} \qquad 7.2$$

7.3.3 Predictions and discussion

Predictions are made for the first two cycles of the experimental results shown in Figures 3.14 and 3.29. The experimental results and the predictions are shown together in Figures 7.3 and 7.4. A comparison of the test results related to the test on loose sand interface (Figure 7.3a and 7.3c) with the model predictions (Figure 7.3b and 7.3d) shows a good agreement between the predictions and experimental results. The model reproduces qualitatively and quantitatively the increase in shear stress and the increase in normal displacement observed for loose sand interfaces.

With respect to the dense sand interface, there is a good agreement between the shear stress mobilized during the experiment (Figure 7.4a) and the model predictions (Figure 7.4b). However, there is a discrepancy between the experimental normal displacement (Figure 7.4c) and the predicted normal displacement (Figure 7.4d). This discrepancy may be attributed in part to the fact that the experimental normal displacements are average values within the sand sample while the predicted normal displacements are calculated at the interface using average values. The normal displacement at different locations within the sand sample can be obtained by performing a finite element analysis.

One may also refer to the critical state concept to explain this discrepancy. For example, a sample with initial mean pressure (p) and density (e) located below the critical state curve will experience an initial compression phase then it will dilate until it reaches the critical state. This explains the increase in the predicted normal displacement shown in Figure 7.4d. However the experimental data show that the sample is compressing as the number of cycle increases. This may at first seem in contradiction with the critical state concept. However that is not the case because as expected in each cycle the sample experience compression followed by dilation. The contradiction will likely be the uniqueness of the critical state curve. For example if the critical state curve is allowed to change as the number of cycle increases one may be able to observe the overall compression displayed by the experimental results. An argument which favours the change of the critical state curves is particle crushing observed in interface tests (Uesugi and Kishida 1986a, DeJong et al. 2003).

The crushing of particles implies that the fines content of the sample changes during a test. Therefore the grain size distribution of a sample at the beginning of a test is not the same as the grain size distribution at the end of the same test. This opens a window for a change in the position of the critical state curve. As pointed out by Papadimitriou et al. (2005), who studied the effect of sample preparation method on sand response, the relocation of the critical state curve as a function of loading direction and manner and/or sample preparation method is a debatable issue in the literature. Therefore further investigation on the uniqueness of the critical state curve will be necessary to clarify this issue.

7.4 Summary

The simulations presented in this chapter show that it is possible to model successfully the main aspects of the behaviour of interfaces under cyclic loading conditions using the model proposed by Dafalias and Manzari (2004). The model reproduces qualitatively and

quantitatively the shear stress mobilized in loose and dense sand interfaces and the normal displacement in the loose sand interface. However, there is a discrepancy between the observed and predicted normal displacements for the dense sand interface.

Table 7.1 Model constants for interface behaviour simulation

Constant	Variable	Value
Elasticity	G_0	85
	ν	0.25
Critical state	M	1.03
	c	0.745
	λ_c	0.019
	e_0	0.938
	ξ	0.65
Yield surface	m	0.01
Plastic modulus	h_0	6.35
	c_h	0.968
	n^b	1.3
Dilatancy	A_0	0.754
	n^d	2.3
Fabric-dilatancy tensor	z_{max}	4
	c_z	600

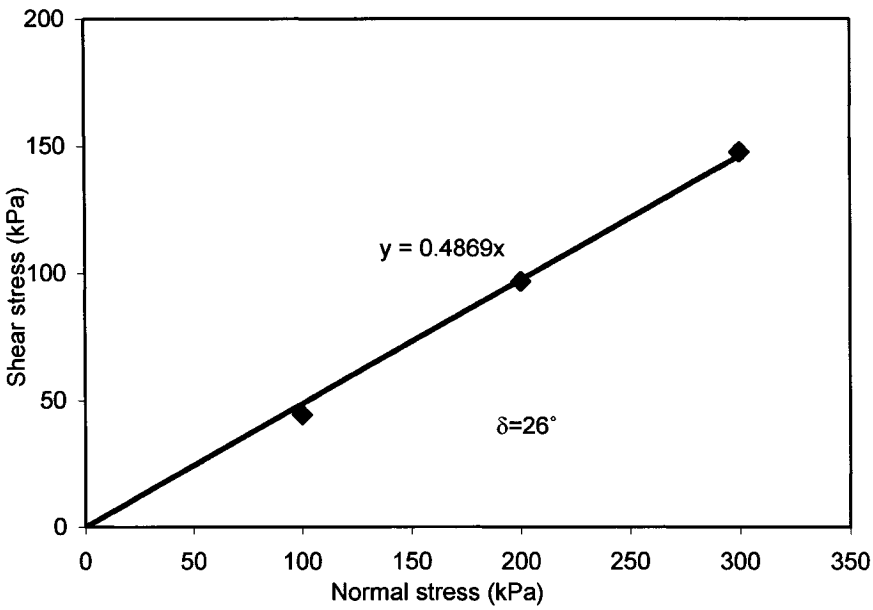

Figure 7.1 Shear stress versus normal stress relation used to find the friction angle

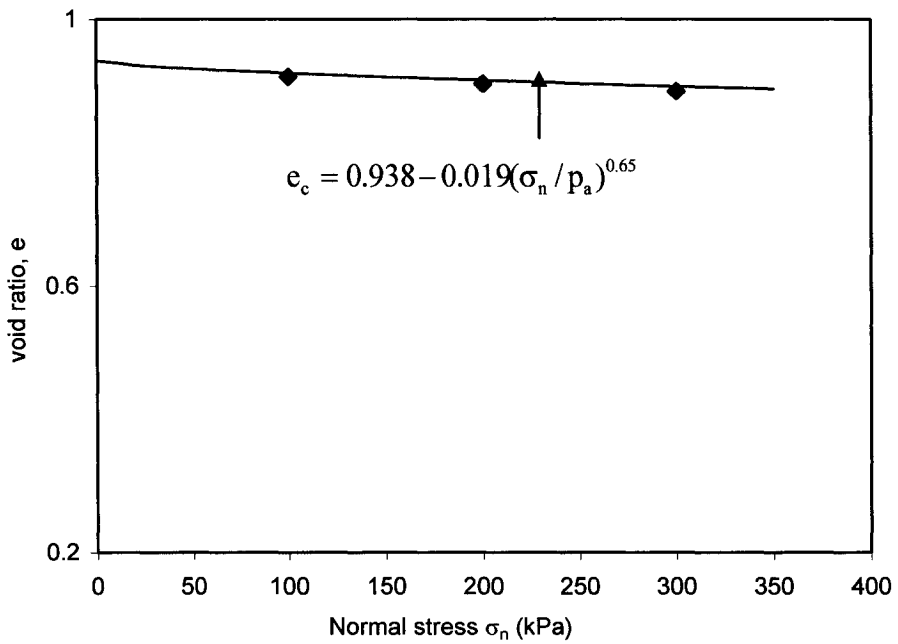

Figure 7.2 Power function fitted to the e-σ_n relation obtained from monotonic tests conducted on loose sand interface

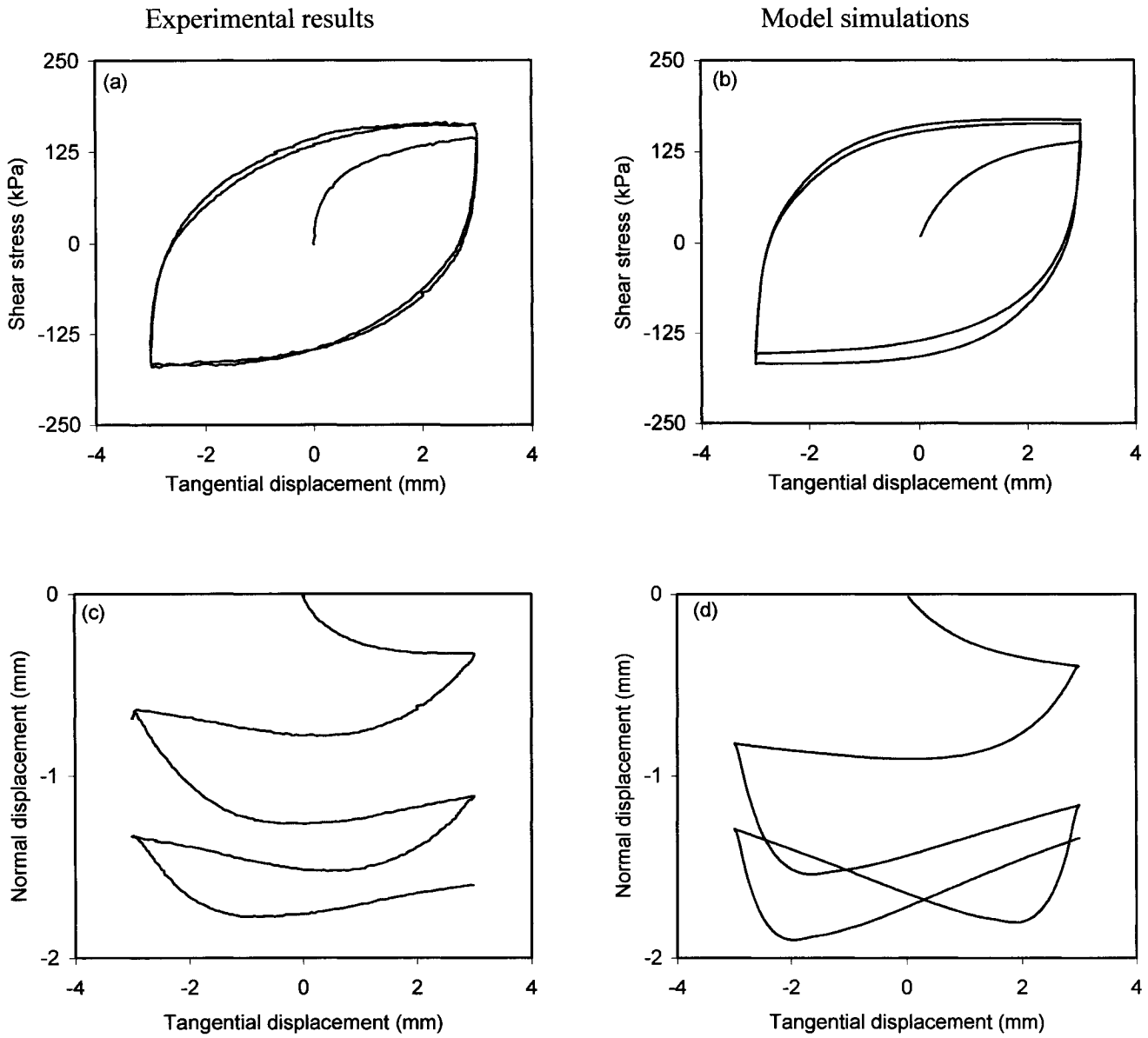

Figure 7.3 Simulation versus experimental results for the loose sand interfaces

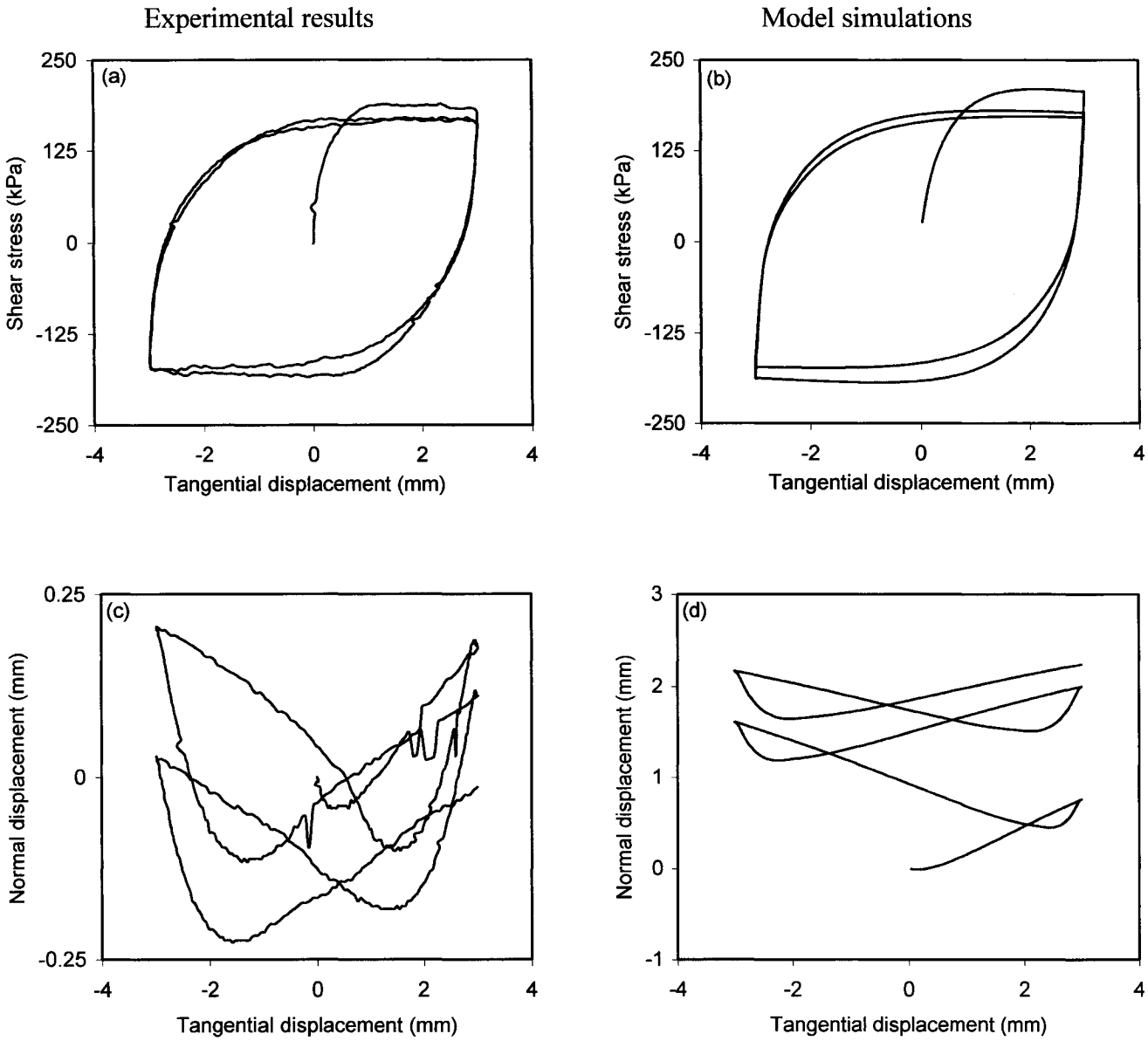

Figure 7.4 Simulation versus experimental results for the dense sand interfaces

CHAPTER 8

CONCLUSIONS AND RECOMMENDATIONS

8.1 Summary

This research program had two main objectives: 1) to achieve a better understanding of the behaviour of interfaces subjected to cyclic loads, 2) to model the cyclic behaviour of interfaces with a bounding surface plasticity model.

The first objective was accomplished by performing a series of cyclic tests on sand-structure interfaces using an apparatus referred to as **C**yclic **3** **D**imensional **S**imple **S**hear testing of **I**nterface (C3DSSI). The effects of the initial sand density, the number of cycles, the magnitude of normal stress, and the amplitude of tangential displacement on the shear stress mobilized at the interface, the normal displacement, and the slip taking place at the interface were investigated. Although the research focused on the cyclic behaviour of interfaces, monotonic tests were also conducted on sand-structure interfaces under constant stress and constant volume conditions because an understanding of the cyclic behaviour requires a prior understanding of the monotonic behaviour.

The second objective was achieved by using the bounding surface model developed by Dafalias and Manzari (2004) to simulate the behaviour of sand. In addition, a parametric study was conducted on the fifteen model constants in order to investigate the model sensitivity to changes in the values of these constants. The model was used to simulate the behaviour of sand in triaxial and interface tests.

8.2 Conclusions

The conclusions of this research program are as follows:

1) The monotonic tests conducted on interfaces under constant volume conditions displayed a behaviour resembling that of sand in undrained triaxial tests. The shear stress versus normal stress relation outlined a phase where deformations continued at a nearly constant stress ratio which was independent of the initial normal stress and the initial sand density.
2) The interface tests highlighted that the density of sand significantly affects the interface response:
    - During the first few cycles, the mobilized shear stress on the interface with dense sand is, as expected, higher than that of the interface with loose sand. However, as the number of cycles increases, the mobilized shear stress on the interface increases for loose sand and decreases for dense sand; and, eventually, the mobilized shear stress becomes almost independent of the initial density.
    - For loose sand, as the number of displacement cycles increases, the contraction of the sand sample increases at a diminishing rate. For dense sand, the vertical displacement, after an initial increase (dilation), decreases at a diminishing rate. However, the amount of contraction is much larger for loose sand.
    - The amount of slip occurring at the interface increases with increasing number of cycles for both densities. Interfaces with dense sand, however, experience a larger amount of slip.
3) The magnitude of normal stress affects the mobilized shear stress, the change in sample height, and the slip occurring at the interface. Increasing values of normal stress yield increasing values in shear stress ratio, larger change in sample height and more slip at the interface.

4) The amplitude of tangential displacement influences the interface response:
    - For loose sand, there is a positive relation between shear stress and amplitude of tangential displacement during the initial cycles. This relation is reversed during the later cycles. In addition, the change in sample height and the portion of sliding displacement at the interface increase with the amplitude of tangential displacement.
    - For dense sand, when the amplitude of tangential displacement is such that the peak stress is not reached during initial loading, the shear stress hardly changes in the subsequent cycles. If, on the other hand, the amplitude of tangential displacement is such that the peak shear stress is reached during initial loading, the shear stress decreases in the subsequent cycles. Furthermore, the cumulative change in sample height is smaller for larger amplitude of tangential displacement; the amount of slip is larger for increasing values of amplitude of tangential displacement.
5) The amount of slip is important in the response of interfaces. In most of the cyclic tests performed, the amount of slip increases with the number of cycles, and becomes larger than the displacement at the interface resulting from shear deformation of soil. Therefore, not making a distinction between the amount of slip and the deformation of soil, as usually done when a direct shear type container is used, would yield incomplete information about the interface behaviour.
6) The bounding surface model proposed by Dafalias and Manzari (2004) was successfully used to simulate the cyclic behaviour of interfaces. The model reproduced qualitatively and quantitatively the shear stress mobilized in loose and dense sand interfaces and the normal displacement in the loose sand interface. However, there was a discrepancy between the observed and predicted normal displacement for the dense sand interface.

8.3 Recommendations for further research

The following topics are recommended for further research:

1) The evaluation of the amount of particle crushing taking place during interface tests and its influence on the behaviour of interfaces.
2) The study of the influence of the surface roughness on the cyclic behaviour of interfaces.
3) The derivation of a relation that links the amount of slip to the tangential displacement of the steel plate, the sand density, the number of cycles, and the amplitude of normal stress.
4) An investigation of the cyclic behaviour of interfaces under constant volume conditions.
5) The incorporation of the model into finite element software to analyze boundary value problems.
6) An investigation of a possible relocation of the critical state curve.

REFERENCES

Aboim, C.A., and Roth, W.H. (1982). Bounding surface plasticity applied to cyclic loading of sand. International Symposium on Numerical Models in Geomechanics, R. Dungar, G.N. Pande, and J.A. Studer (Editors), A.A. Balkema, Zurich, Switzerland, pp. 65-72.

Airey, D.W., Al-Douri, R.H., and Poulos, H.G. (1992). Estimation of pile friction degradation from shearbox tests. Geotechnical Testing Journal, ASTM, Vol. 15, pp. 388-392.

Al-Douri, R.H., and Poulos, H.G. (1992). Static and cyclic direct shear tests on carbonate sands. Geotechnical Testing Journal, ASTM, Vol. 15, pp. 138-157.

Andrawes, K.Z., and Butterfield, R. (1973). The measurement of planar displacements of sand grains. Géotechnique, Vol. 23, No. 4, pp. 571-576.

Aubry D, Modaressi A, Modaressi H. (1990). A constitutive model for cyclic behaviour of interfaces with variable dilatancy. Computers and Geotechnics, Vol. 9, pp. 47-58.

Bardet, J.P. (1986). Bounding surface plasticity model for sands. J. Engrg. Mechanics, Vol. 112, No. 11, pp. 1198-1217.

Bardet, J.P. (1987). Bounding surface modeling of cyclic sand behavior. Proceedings of the Workshop on Constitutive Laws for the Analysis of Fill Retention Structures, E. Evgin (Editor), Ottawa, pp. 1-19.

Been, K., and Jefferies, M.G. (1985). A state parameter for sands. Géotechnique, Vol. 35, No. 2, pp. 99-112.

Boulon, M. (1989). Basic features of soil structure interface behaviour. Computers and Geotechnics, Vol. 7, pp. 115-131.

Boulon, M., Nova, R. (1990). Modeling of soil-structure interface behaviour: A comparison between elastoplastic and rate type laws. Computers and Geotechnics, Vol. 9, pp. 21-46.

Budhu, M. (1999). Soil mechanics and foundations. John Wiley & Sons, Inc, United States of America.

Butterfield, R., Harkness, R.M., and Andrawes, K.Z. (1970). A stereo-photogrammetric method for measuring displacement fields. Géotechnique, Vol. 20, No. 3, pp. 308-314.

Carter, J.R., Booker, J.R., and Wroth, C.P. (1982). A critical state soil model for cyclic loading. *Soil Mechanics – Transient and Cyclic Loads*, G.N. Pande and O.C. Zienkiewicz (Editors), pp. 219–252.

Chen, W.F., and Muzino, E. (1990). Nonlinear analysis in soil mechanics Theory an Implementation. Developments in geotechnical engineering, Vol. 53.

Crouch, R.S., Wolf, J.P.and , Dafalias, Y.F. (1994). Unified critical-state bounding-surface plasticity model for soil. Journal of Engineering Mechanics, Vol. 120, No. 11, pp. 2251-2270.

Dafalias, Y.F. (1986). Bounding surface plasticity. I: Mathematical formulation and hypoplasticity. J. Engrg. Mechanics, ASCE, Vol. 112, No. 12, pp. 966-987.

Dafalias, Y.F. and Herrmann, L.R. (1982). Bounding surface formulation of soil plasticity. *Soil Mechanics – Transient and Cyclic Loads*, G.N. Pande and O.C. Zienkiewicz (Editors), pp. 253–282.

Dafalias, Y.F. and Herrmann, L.R. (1980). A bounding surface plasticity model. Proceedings of the International Symposium on Soils under Cyclic and Transient Loading, Swansea, United Kingdom, Vol. 1, pp. 335-345.

Dafalias, Y.F., and Manzari, M.T. (2004). Simple Plasticity Sand Model Accounting for Fabric Change Effects. J. Eng. Mech., Vol. 130, No. 6, pp. 622-634.

Dafalias,Y.F. and Popov, E.P. (1975). A model of nonlinearly hardening materials for complex loading. Acta Mechanica , Vol. 21, pp. 173-192.

Dafalias, Y.F. and Herrmann, L.R. (1986). Bounding surface plasticity. II: Application to isotropic cohesive soils. J. Engrg. Mechanics, ASCE, Vol. 112, No. 12, pp. 1263-1291.

De Pater, C.J. and Nieuwenhuis, J.D. (1986). Method for measuring the deformation of a sand surface. Géotechnique, Vol. 36, No. 4, pp. 581-585.

DeJong, J.T., Randolph, M.F., and White, D.J. (2003). Interface load transfer degradation during cyclic loading: a microscale investigation. Soils and Foundations, Vol. 43, No. 4, pp. 81-93.

Desai, C.S., Drumm, E.C., and Zaman, M.M. (1985). Cyclic testing and modeling of interfaces. Journal of geotechnical engineering, Vol. 111, No. 6, pp. 793-815.

Desai, C.S., and Nagaraj, B.K. (1988). Modeling for cyclic normal and shear behavior of interfaces. Journal of Engineering Mechanics, Vol. 114, No. 7, pp. 1198-1217.

Desai, C.S, and Siriwardane, H.J. (1984). Constitutive laws for engineering materials with emphasis on geologic materials. Prentice-Hall, Inc., Englewood Cliffs, New Jersey 07632.

Drucker, D.C., Gibson, R.E., and Henkel, D.J. (1957). Soil mechanics and work hardening theories of plasticity. Trans., ASCE, Vol. 122, pp. 338-346.

Evgin, E., Assane O. T., Infantes J. A. (2003). Visualization of movements of particles in an interface test. Proceedings, 56th Canadian Geotechnical Conference,Winnipeg, Manitoba, Canada.

Fakharian, K. and Evgin, E. (1993). A three-dimensional apparatus for cyclic testing of interfaces. 46th Canadian Geotechnical Conference, Saskatoon: pp. 485-493.

Fakharian, K. (1996). Three-dimensional monotonic and cyclic behaviour of sand-steel interfaces: testing and modeling. Ph.D. Thesis, Department of Civil Engineering, University of Ottawa, Ottawa, Ontario, Canada.

Fakharian, K. and Evgin, E. (1996). An automated apparatus for three-dimensional monotonic and cyclic testing of interfaces. Geotechnical Testing Journal, ASTM, Vol. 19, pp. 22-31.

Fakharian, K. and Evgin, E. (1997). Cyclic simple-shear behaviour of sand-steel interfaces under constant normal stiffness condition. Journal of Geotechnical and Geoenvironmental Engineering, ASCE, Vol. 123, No. 12, pp. 1096-1105.

Gens A. and Potts, D.M. (1988). Critical state models in computational geomechanics. Engrg. Comput., Vol. 5, No. 3, pp. 178-197.

Ghionna V.N., Mortara G. (2002). An elastoplastic model for sand-structure interface behaviour. Géotechnique, Vol. 50, No. 1, pp. 41-50.

Hashiguchi, K., and Ueno, M. (1977). Elastoplastic constitutive laws of granular materials. In S. Murayama and A.N. Schofield (Editors), Constitutive equations of soils, Proc. 9th Int. Conf. Soil Mech. Found. Eng., Spec. Session 9, Tokyo, JSSMFE, pp. 73-82.

Hashiguchi, K. (1989). Subloading surface model in unconventional plasticity. Int. J. Solids Struct., Vol. 25, pp. 917-945.

Hashiguchi, K., and Chen, Z.P. (1998). Elastoplastic constitutive equation of soils with the subloading surface and the rotational hardening. Int. J. Numer. Analyt. Meth. Geomech., Vol. 22, pp. 197-227.

Hu, L., and Pu, J.L. (2003). Application of damage model for soil-structure interface. Computers and Geotechnics, Vol. 30, pp. 165-183.

Ishihara, K., Tatsuoka, F., and Yasuda, S. (1975). Undrained deformation and liquefaction of sand under cyclic stresses. Soils and Foundations, Vol. 15, No. 1, pp. 29-44.

Iwan, W.D. (1967). On a class of models for the yielding behavior of continuous and composite systems. J. Appl. Mech. (ASME), Vol. 34, pp. 612-617.

Jakobsen, K.P., and Lade, P.V. (2002). Implementation algorithm for a single hardening constitutive model for frictional materials. Int. J. Numer. Anal. Meth. Geomech., Vol. 26, pp. 661-681.

Jaky, J. (1994). The coefficient of earth pressure at rest. Journal for Society of Hungarian Architects and Engineers, pp. 355-358.

Kishida, H., and Uesugi, M. (1987). Tests of the interface between sand and steel in the simple shear apparatus. Géotechnique, Vol. 37, No. 1, pp. 45-52.

Krieg, R.D. (1975). A practical two surface plasticity theory. J. Appl. Mech. (ASME), Vol. 42, pp. 641-646.

Lade, P.V. and Duncan, J.M. (1975). Elasto-plastic strain-strain theory for cohesionless soil. J. Geotech. Eng. Div., ASCE, Vol. 101 (GT10), pp. 1037-1053.

Li, B. (2001). An experimental study and numerical simulation of sand-steel interface behaviour. Master's Thesis, University of Ottawa, Ontario, Canada.

Li, X.S. (2002). A sand model with state-dependent dilatancy. Géotechnique, Vol. 52, No. 3, pp. 173-186.

Li, X.S., Dafalias, Y.F. (2000). Dilatancy for cohesionless soils. Géotechnique, Vol. 50, No. 4, pp. 449-460.

Li, X.S., Dafalias, Y.F. (2002). Constitutive modeling of inherently anisotropic sand behavior. Journal of Geotechnical and Geoenvironmental Engineering, Vol. 128, No. 10, pp. 868-880.

Manzari, M.T., and Dafalias, Y.F. (1997). A Critical State Two-Surface Plasticity Model for Sand. Géotechnique, Vol. 47, No. 2, pp. 255-272.

Mortara, G., Boulon, M., and Ghionna, V.N. (2002). A 2-D constitutive model for cyclic interface behaviour. Int. J. Numer. Anal. Meth. Geomech., Vol. 26, pp. 1071-1096.

Mròz, Z. (1967). On the description of anisotropic work hardening. J. Mech. Phys. Solids, Vol. 15, pp. 163-175.

Navayogarajah, N., Desai, C. S., Kiousis, P. D. (1992). Hierarchical Single-Surface model for static and cyclic behavior of interfaces. Journal of Engineering Mechanics, Vol. 118, No. 5, pp. 990-1011.

Nova, R. (1982). A constitutive model for soil under monotonic and cyclic loading. . *Soil Mechanics – Transient and Cyclic Loads*, G.N. Pande and O.C. Zienkiewicz (Editors), pp. 343-373.

Paikowsky, S.G., Player, C.M., and Connors, P.J. (1995). A dual interface apparatus for testing unrestricted friction of soil along solid surfaces. Geotechnical Testing Journal, ASTM, Vol. 18, pp. 168-193.

Papadimitriou, A.G., Dafalias, Y.F., and Yoshimine, M. (2005). Plasticity modeling of the effect of sample preparation method on sand response. Soils and Foundations, Vol. 45, No. 2, pp. 109-125.

Pender, M.J. (1982). A model for the cyclic loading of overconsolidated soil. *Soil Mechanics – Transient and Cyclic Loads*, G.N. Pande and O.C. Zienkiewicz (Editors), pp. 283-311.

Porcino, D., Fiovarante, V., Ghionna, V.N., and Pedroni, S. (2003). Interface behaviour of sands from constant normal stiffness direct shear tests. Geotechnical Testing Journal, ASTM, Vol. 26, pp. 289-301.

Potyondy, J.G. (1961). Skin friction between various soils and construction materials. Geotechnique, Vol. 11, pp. 339-355.

Prévost, J.H. (1977). Mathematical modeling of monotonic and cyclic undrained clay behavior. Int. J. Numer. Anal. Meth. Geomech., Vol. 1, pp. 195-216.

Prévost, J.H. (1978). Plasticity theory for soil stress-strain behavior. J. Eng. Mech. Div., ASCE, Vol. 103 (EM5), pp. 1177-1194.

Roscoe, K.H. and Burland, J.B. (1968). On the Generalized Stress-Strain Behaviour of 'Wet' Clay. In: J. Heyman and F.A. Leckie (Editors), Engineering Plasticity. Cambridge University Press, Cambridge, England, pp. 535-609.

Schofield, A.N and Wroth C.P. (1968). Critical State Soil Mechanics. McGraw-Hill, New York, N.Y., 310 pp.

Shahrour I. and Rezaie. F. (1997). An elastoplastic constitutive relation for the soil-structure interface under cyclic loading. Computers and Geotechnics, Vol. 21, pp. 21-39.

Shahrour I. and Rezaie. F. (1999). Experimental study of the behaviour of a calcareous sand: structure interface. Engineering of Calcareous Sediments, Al-Shafei (Editor), pp. 69-77.

Uesugi, M., and Kishida, H. (1986a). Influential factors of friction between steel and dry sands. Soils and Foundations, Vol. 26, No. 2, pp. 33-46.

Uesugi, M., and Kishida, H. (1986b). Frictional resistance at yield between dry sand and mild steel. Soils and Foundations, Vol. 26, No. 4, pp. 139-149.

Uesugi, M., Kishida, H., and Tsubakihara, Y. (1988). Behaviour of sand particles in sand-steel friction. Soils and Foundations, Vol. 28, No. 1, pp. 107-118.

Uesugi, M., Kishida, H., and Tsubakihara, Y. (1989). Friction between sand and steel under repeated loading. Soils and Foundations, Vol. 29, No. 3, pp. 127-137.

Uesugi, M., Kishida, H., and Uchikawa, Y. (1990). Friction between dry sand and concrete under monotonic and repeated loading. Soils and Foundations, Vol. 30, No. 1, pp. 115-128.

Tabucanon, J.T., Airey, D.W., and Poulos, H.G. (1995). Pile skin friction in sands from constant normal stiffness tests. Geotechnical Testing Journal, ASTM, Vol. 18, pp. 350-364.

Tejchman, J., and Bauer, E. (2004). Effect of cyclic shearing on shear localization in granular bodies. Granular Matter, Vol. 5, pp. 200-212.

Vardoulakis, I., and Graf, B. (1985). Calibration of constitutive models for granular materials using data from biaxial experiments. Géotechnique, Vol. 35, No. 3, pp. 299-317.

Wang, Z. L., Dafalias, Y. F., Shen, C. K. (1990). Bounding surface hypoplasticity model for sand. Journal of Engineering Mechanics, Vol. 116, No. 5, pp. 983-1001.

Yoshimi, Y. and Kishida, T. (1981). A ring torsion apparatus for evaluating friction between soil and metal surface. Geotechnical Testing Journal, Vol. 4, No. 4, pp. 145-152.

APPENDIX A

DETERMINATION OF MODEL CONSTANTS FROM EXPERIMENTAL DATA

This appendix deals with the determination of the fifteen constants used in Dafalias and Manzari's (2004) bounding surface model. The model constants are divided into six groups according to their functions (Elastic constants (G_0 and ν); Critical state constants (M, c, λc, e_0, and ξ); Yield surface constant (m); Plastic modulus constants (h_0, c_h, and n^b); Dilatancy constant (A_0 and n^d); and Fabric-dilatancy tensor constants (z_{max} and c_z)). They are determined in this appendix from six triaxial tests data. Three tests were performed at a confining pressure of 100 kPa (Figure A.1) and the remaining tests were carried out at confining pressures of 150 kPa, 200 kPa, and 300 kPa (Figure A.2). After the isotropic consolidation, the relative density of the three samples in the tests conducted at a confining pressure of 100 kPa were 36.0%, 57.6%, and 59.6%, while the relative density in the tests conducted at confining pressures of 150 kPa, 200 kPa, and 300 kPa were 27.3%, 28.3%, and 24.3%, respectively.

Elastic constants ν and G_0

A value of 0.25 was selected for Poisson's ratio (ν). This value was taken from the range of Poisson's ratio used for sand (Budhu 1999).

Due to the lack of small strain test data, G_0 was determined from the triaxial data. First the secant modulus (E) at axial strains of 0.05 % and 0.1% were determined. Then the

shear modulus (G) was related to the secant modulus through Equation A.1. Finally, G_0 is determined with Equation A.3 which was obtained after equaling Equation A.1 and Equation A.2 (Equation used by Dafalias and Manzari (2004) for the calculation of G).

$$G = \frac{E}{2(1+\nu)} \qquad \text{A.1}$$

$$G = G_0 p_a \frac{(2.97-e)^2}{1+e}\left(\frac{p}{p_a}\right)^{1/2} \qquad \text{A.2}$$

$$G_0 = \frac{E(1+e)}{2(1+\nu)p_a(2.97-e)^2\left(\frac{p}{p_a}\right)^{1/2}} \qquad \text{A.3}$$

The values of G_0 for the six tests are summarized in Table A.1. The table shows that G_0 varied between 81 and 255 depending on the test conditions (confining pressure and relative density) and the axial strain level. Nevertheless, the average (i.e. G_0=142) of G_0 values in all six tests at axial strains (ε_a) of 0.05% and 0.1% is used as input for the model.

Table A.1 Model constant G_0 determined from triaxial data

Confining pressure (kPa)	Relative density Dr (%)	G_0 at ε_a=0.05% (kPa)	G_0 at ε_a=0.1% (kPa)	Average G_0
100	36	255	131	193
100	57.6	122	90	106
100	59.6	219	151	185
150	27.3	105	81	93
200	28.3	171	118	145
300	24.3	151	109	130
	Average	171	114	142

Critical state constants M, c, e_0, λ_c, and ξ

The friction angle of the sand is necessary for the determination of M and c. The friction angle is determined from the slope of the line tangent to the Mohr circles corresponding to the end of the six tests (Figure A.3). It has a value of 35°. The values of M and c determined from equations A.4 and A.5 are 1.42 and 0.679 respectively.

$$M_c = \frac{6\sin\phi}{3-\sin\phi} \qquad \text{A.4}$$

$$c = \frac{3-\sin\phi}{3+\sin\phi} \qquad \text{A.5}$$

The constants e_0, λ_c, and ξ are obtained by fitting a power function to the critical state (Equation 6.5f). The void ratios at the end of the triaxial tests are plotted against the mean pressures at the end of the triaxial tests (Figure A.4). The values of e_0, λ_c, and ξ are 0.938, 0.019, and 0.65, respectively. As a result, the equation of the critical state curve is:

$$e_c = 0.938 - 0.019(p_c / p_a)^{0.65} \qquad \text{A.6}$$

Yield surface constant m

The yield surface constant m is assigned the value 0.01 which is approximately equal to M/100.

Plastic modulus constants h_0, c_h, and n^b

The plastic modulus constant h_0, and c_h, obtained by trial-and-error, are 6.35 and 0.968 respectively. Trial-and-error consists in performing simulations for different values of the

model constant and retaining the value for which the simulations match better the experimental observations. The constant n^b is obtained from the following equation:

$$n^b = \ln(M/M^b)/\psi^b \qquad \text{A.7}$$

where M^b is the peak stress ratio and ψ^b is the value of ψ at the peak stress ratio.

Two triaxial tests (i.e. Dr = 57.6% and 59.7%) which exhibit a peak stress ratio are used for the determination of n^b (Table A.2). The average value of n^b (i.e. 1.3) obtained from the two tests is used as input for the model.

Table A.2 Model constant n^b determined from data at peak stress ratio

Confining pressure (kPa)	Relative Density Dr (%)	Mean pressure p^b (kPa)	Deviator stress q^b (kPa)	Peak stress ratio $M^b=q^b/p^b$	Void ratio e^b	e_c	$\psi^b=e_c-e_b$	n^b
100	57.6	204.756	313.636	1.532	0.834	0.908	-0.074	1.1
100	59.6	213.340	338.351	1.586	0.833	0.907	-0.074	1.5
							Average	1.3

Dilatancy constants A_0 and n^d

The dilatancy constant A_0, obtained by trial-and-error, has a value of 0.904. The dilatancy constant n^d is determined with the following equation

$$n^d = \ln(M/M^d)/\psi^d \qquad \text{A.8}$$

where M^d and ψ^d are the stress ratio and the value of ψ, respectively, at the phase transformation point.

The data from four tests which exhibit a well defined phase transformation are used for the determination of n^d (Table A.3). The average value of n^d (i.e. 2.3) obtained from the four tests is used as input for the model.

Fabric-dilatancy tensor constants z_{max} and c_z

The constants z_{max} and c_z are obtained by trial-and-error fitting of loading-unloading reverse loading, or cyclic data, preferably undrained. Since loading-unloading triaxial data for the sand used in this research program are unavailable the values of z_{max} and c_z are assigned the same values as those used by Manzari and Dafalias (2004). Therefore z_{max} and c_z are assigned the values 4 and 600, respectively.

Table A.3 Model constant n^d determined from data at phase transformation point

Confining pressure (kPa)	Relative Density Dr (%)	Mean pressure p^d (kPa)	Deviator stress q^d (kPa)	Stress ratio $M^d=q^d/p^d$	Void ratio e^d	e_c	$\psi^b=e_c-e_d$	n^d
100	36	179.79	239.17	1.330	0.878	0.910	-0.032	1.9
100	57.6	166.54	199.64	1.199	0.814	0.912	-0.098	1.7
100	59.6	170.09	210.46	1.237	0.808	0.911	-0.104	1.3
150	27.3	279.35	387.85	1.388	0.897	0.901	-0.005	4.3
							Average	2.3

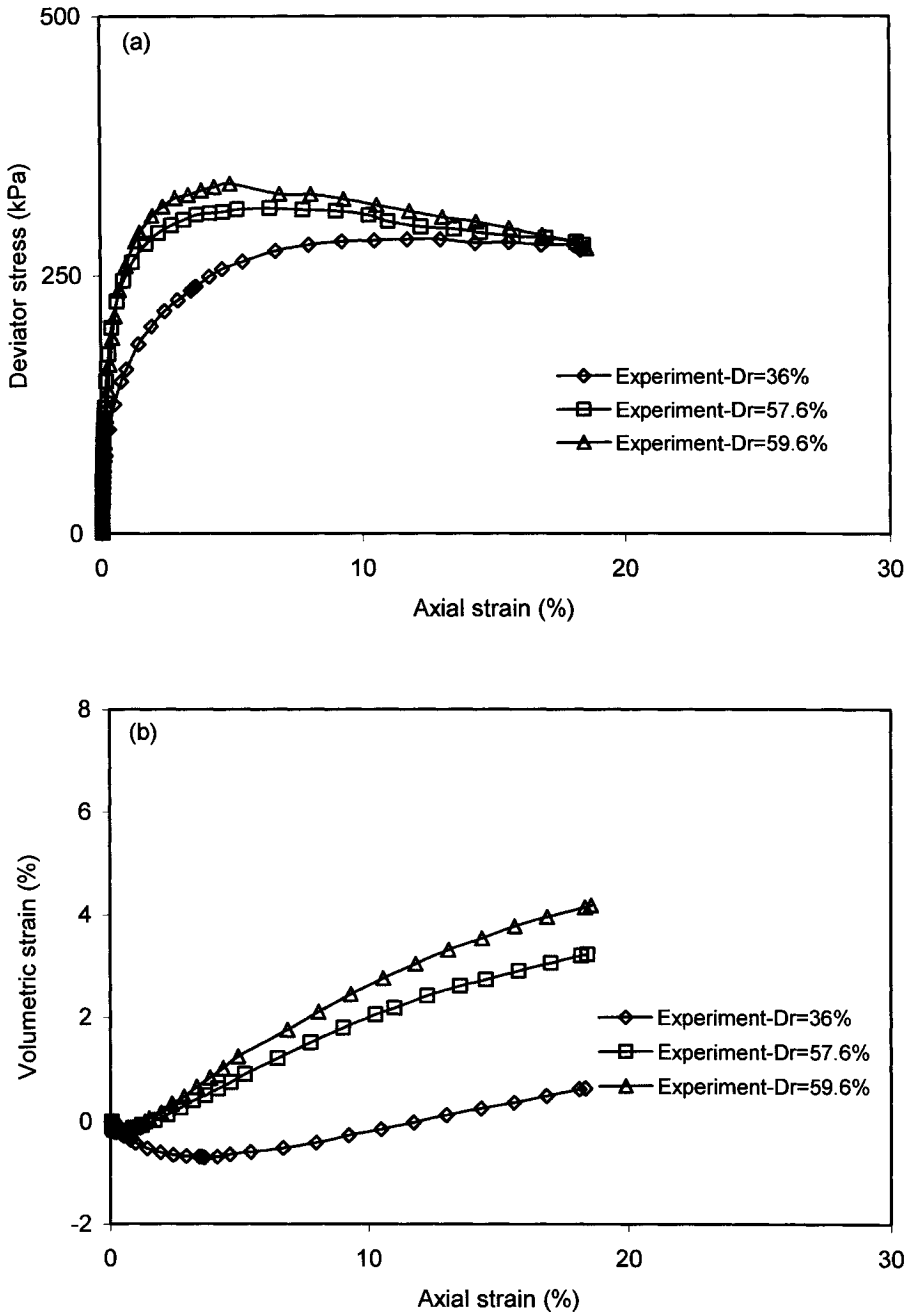

Figure A.1 CD triaxial test data (Confining pressure =100 kPa)

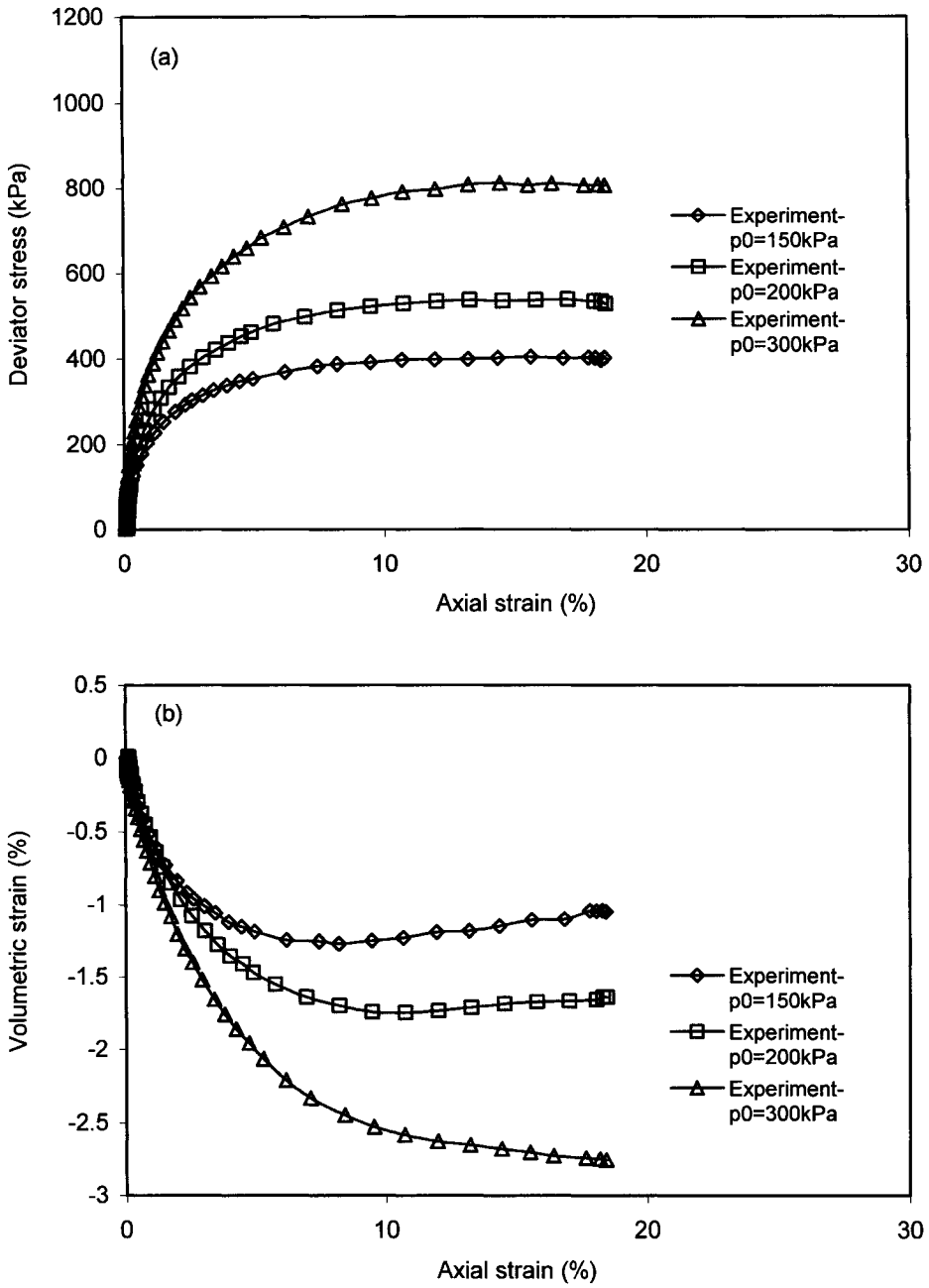

Figure A.2 CD triaxial test data (Confining pressure =150 kPa, 200 kPa, and 300 kPa)

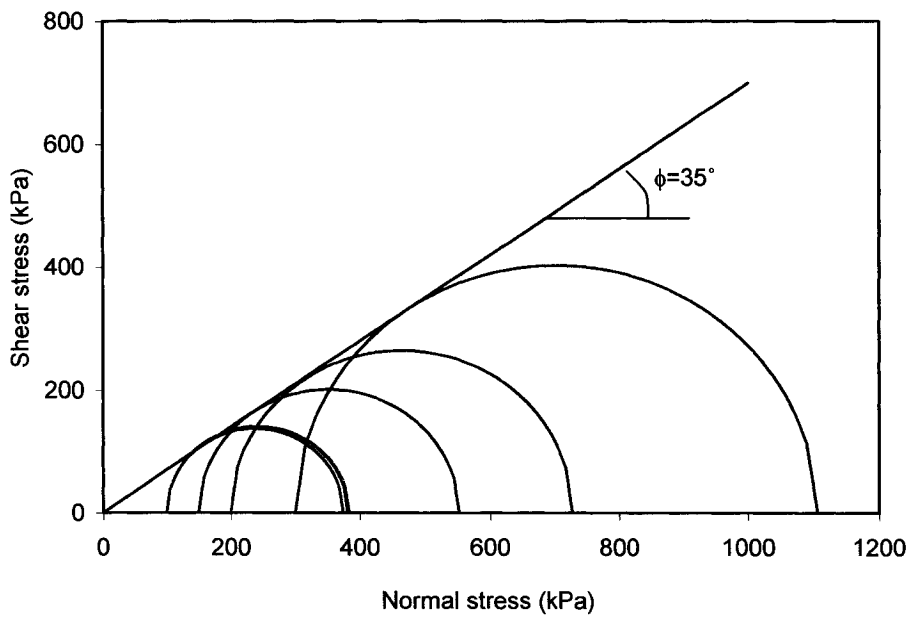

Figure A.3 Friction angle determined and Mohr circles derived from CD triaxial test data

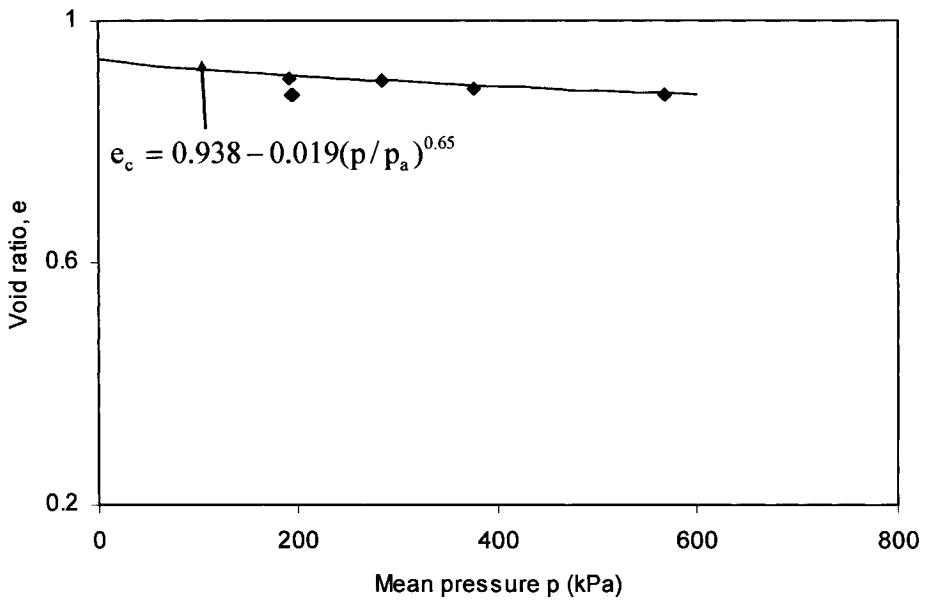

Figure A.4 Power function fitted to the e-p relation obtained from CD triaxial test data